INFORMATION TO USERS

This manuscript has been reproduced from the microfilm master. UMI films the text directly from the original or copy submitted. Thus, some thesis and dissertation copies are in typewriter face, while others may be from any type of computer printer.

The quality of this reproduction is dependent upon the quality of the copy submitted. Broken or indistinct print, colored or poor quality illustrations and photographs, print bleedthrough, substandard margins, and improper alignment can adversely affect reproduction.

In the unlikely event that the author did not send UMI a complete manuscript and there are missing pages, these will be noted. Also, if unauthorized copyright material had to be removed, a note will indicate the deletion.

Oversize materials (e.g., maps, drawings, charts) are reproduced by sectioning the original, beginning at the upper left-hand corner and continuing from left to right in equal sections with small overlaps. Each original is also photographed in one exposure and is included in reduced form at the back of the book.

Photographs included in the original manuscript have been reproduced xerographically in this copy. Higher quality 6" x 9" black and white photographic prints are available for any photographs or illustrations appearing in this copy for an additional charge. Contact UMI directly to order.

UMI

A Bell & Howell Information Company
300 North Zeeb Road, Ann Arbor MI 48106-1346 USA
313/761-4700 800/521-0600

EFFECT OF MYOFIBRIL LENGTH AND TISSUE CONSTITUENTS ON ACOUSTIC PROPAGATION PROPERTIES OF MUSCLE

BY

NADINE BARRIE SMITH

B.S., University of Illinois, 1985
M.S., University of Illinois, 1989

THESIS

Submitted in partial fulfillment of the requirements
for the degree of Doctor of Philosophy in Biophysics
in the Graduate College of the
University of Illinois at Urbana-Champaign, 1996

Urbana, Illinois

UNIVERSITY OF ILLINOIS AT URBANA-CHAMPAIGN

THE GRADUATE COLLEGE

MAY 1996

WE HEREBY RECOMMEND THAT THE THESIS BY

NADINE BARRIE SMITH

ENTITLED EFFECT OF MYOFIBRIL LENGTH AND TISSUE CONSTITUENTS ON ACOUSTIC PROPAGATION PROPERTIES OF MUSCLE

BE ACCEPTED IN PARTIAL FULFILLMENT OF THE REQUIREMENTS FOR THE DEGREE OF DOCTOR OF PHILOSOPHY

W. O'Brien
Director of Thesis Research

Head of Department

Committee on Final Examination†

Albert S Feng
Chairperson

W. O'Brien

† Required for doctor's degree but not for master's.

O-517

EFFECT OF MYOFIBRIL LENGTH AND TISSUE CONSTITUENTS ON ACOUSTIC PROPAGATION PROPERTIES OF MUSCLE

Nadine Barrie Smith, Ph.D.
Graduate Program in Biophysics
University of Illinois at Urbana-Champaign, 1996
Professor William D. O'Brien, Jr., Advisor

The ultrasonic speed and attenuation coefficient of three muscle samples were measured in-vitro as a function of temperature and frequency. The sarcomere length of each of these samples was also determined. The three muscle groups were bovine longissimus dorsi, psoas major and lobster extensor. These were chosen to separately determine the effects of physical components (% water, % fat and % protein) and structural components (sarcomere length) on the ultrasonic propagation properties. The scanning laser acoustic microscope (SLAM) was used to measure the attenuation coefficient, speed and heterogeneity index of all three samples at 100 MHz. The Daedal exposimetry system (DES) was used to determine both of these quantities as a function of frequency over a range 2-7 MHz. In addition, measurements were made at three temperatures, 4, 20 and 37°C. The chemical composition of the muscle groups was determined using wet/dry techniques (% water), ether extraction (% fat) and nitric acid digestion (% protein). The sarcomere length for individual samples was determined using light microscopy of suitable stained slides. Finally, the effect of the sarcomere structure was determined by homogenizing the tissue samples, and measuring ultrasonic propagation. The destruction of the regular myofibril architecture showed that the muscle structure plays a critical role in the propagation of ultrasound through tissue. Using the results from these studies a series of multiple linear regression models was determined, which allowed the physical and structural determination of a fourth muscle type (bovine semitendinosus) based solely on the acoustic properties. Subsequent measurement of the physical and structural properties were made to test the accuracy of the developed models. The prediction model for estimating tissue constituents and sarcomere lengths at 100 MHz is remarkably accurate, with very low errors in estimating the tissue constituents within 5% and sarcomere lengths with an accuracy of less than half a micron. Overall, the empirical model developed using the DES was not as accurate as that of the SLAM. Results at the lower temperature of 4°C were consistently better than those at higher temperatures, with all parameters being predicted within 10% of the measured values.

DEDICATION

To my mother and father.

ACKNOWLEDGEMENTS

I would like to most gratefully thank Professor William D. O'Brien, Jr. for giving me constant encouragement, endless understanding and support over the years. His friendship, belief and patience has enabled me to get this far. I will always be grateful to him for giving me the many opportunities to travel and to present this and other research at many conferences.

This project could not have been completed without the use of the biochemical analysis facilities of Dr. Neal Merchen and the patience and lessons of Laura Bauer. Additionally, I could not have made the sarcomere length measurements without the help and time of my good friend, Dr. Jim Zachary. My gratitude goes out to Dr. Philip Best and Dr. Albert Feng for their helpful comments on my thesis and their willingness to serve on my committee.

Throughout my career at the Bioacoustics Research Laboratory I have benefited from the friendships and camaraderie of many people built on the days of working and struggling together. On many an occasion I have run to others who have helped me out of difficult situations. Those times I will never forget (i.e. laboratory moving, chasing loose chinchillas, bulls chasing me, flooding basements, searching in skids for lost data, etc. etc.). I would like to acknowledge Wanda Elliot for always having an ear that I could bend; to Billy McNeil who would fix everything in a jiffy and always have the best sense of humor; to Bob Cicone who would fix my sick computer and be a friend that I could talk to about fishing. I will always cherish the friendship of Lisa Wilmes who helped me survive the early years of the Ph.D. program. Within my group I would like to recognize my "brothers and sisters" who have been there through thick and thin; Eric Chen, Scott Ellis, Rich Czerwinski, Kate Hillsley and Dudley Swiney.

Special thanks to Amy Anderson for her constant assistance and making this process so much easier by her presence. And finally, I gratefully acknowledge the unfailing aid and constant emotional reassurance of Andrew Webb.

TABLE OF CONTENTS

LIST OF TABLES

TABLE **PAGE**

TABLE **PAGE**

LIST OF FIGURES

FIGURE **PAGE**

FIGURE **PAGE**

1. INTRODUCTION

Acoustic propagation properties of biological tissues such as the attenuation coefficient, absorption coefficient and speed of sound are influenced at the macromolecular level by specific tissue constituents. In the past researchers have only examined the influence of the tissue constituents water, protein (such as collagen) and fat on the propagation properties. Lately researchers have attempted to analyze the propagation properties by examining the anatomy and structure of the muscle itself, for example cardiac muscle [Rose et al, 1995, O'Brien et al., 1995] . At this time there is no agreement on what constituents of muscle tissue are the dominant contributors to attenuation or speed. The goal of this research is to determine the relationship between the acoustic propagation properties of skeletal muscle to both the tissue's composition and structure. The hypothesis is that one can develop a series of mathematical expressions relating the speed and attenuation coefficient at a variety of temperatures and frequencies to the tissue composition and structure. This in turn would allow prediction of these physical and biochemical properties from ultrasonic measurements. The impact of the development of such a model is outlined below.

1.1 Significance

A thorough understanding of the mechanisms of the interaction between acoustic propagation properties and skeletal muscle tissue is required for the clinical application of quantitative tissue characterization. Ideally, empirical mathematical expressions could be developed relating important physiological information to their interaction with ultrasound. Such relationships are possible since the ultrasonic propagation properties of biological material such as attenuation coefficient and speed of sound are determined by interactions at the macromolecular level. The major tissue constituents such as water, protein, fat, glycogen and collagen often correlate with the observed ultrasonic propagation properties as a function of frequency and temperature. [Johnston et al., 1978; Suzuki et al., 1992; Akashi et. al., 1995]. The acoustic impedance and speed are a function of the inertia and restoring parameters (elasticity) of a biological material.

Many pathological conditions exhibit a change in the mechanical and structural properties of tissue, which has previously been shown to be detectable via changes in the attenuation and speed in connective tissue [Hete and Shung, 1994; van der Steen et. al., 1994]. This information could potentially be used to non-invasively detect the progress in wound healing [Olerud et al., 1990]. Ultrasound has also been used to diagnose the extent and progression of dystrophies since an abnormal amount of fat and collagen in muscle is sometimes reflected in increased echogenicity. A study by Reimers et al. (1993) using

ultrasound images to determine the extent of muscular dystrophy suggests that fat replacement causes the increase in muscle echogenicity. However, based on their findings, they also suggest that intramuscular fibrosis did not significantly affect the muscle echogenicity. Yet other studies have correlated increased image echo with an increase in collagen content of a diseased fibrotic muscle [Heckmatt et al., 1982; Lamminen et al., 1988; Hete and Shung, 1993]. Muscular Dystrophy is characterized by infiltration into the muscle structure by fat and/or connective tissue [Lamminen et al., 1988]. The extent of the disease is marked by the extent of muscle replacement by fat or connective tissue. Severe cases result in total atrophy of the muscle by replacement of more than 50% of the muscle structure by fat and connective tissue. Increased areas of connective tissue known as fibrosis are the prominent feature in Duchenne's muscular dystrophy. Another characteristic of this disease is the degeneration of muscle fibers via necrosis and phagocytosis. Dystrophy also shows a prominent increase of endomysial and perimysial connective tissue [Foidart et al., 1981]. Another example is the work which showed that the ultrasonic propagation properties of aging incisional wounds (in dogs) correlated well with the proportions of water and connective tissue [Olerud et al., 1990]. These are examples which demonstrate that with good ultrasonic propagation data, tissue structure and constituents can be determined. The development of global mathematical relationships between the two measurements is key to quantitative assessment of these pathological conditions.

Industrial interest in the structure and constituents of skeletal muscle is concerned with the nutritional value of the tissue. The quality of the meat is related to the marbling or the amount of fat in the tissue. Muscle with a higher percentage of fat are ranked as more tender and favorable. The ability to accurately determine the quality of meat based on tissue composition has great economic value to the meat industry. Acoustic propagation properties have previously been shown to relate to the tissue constituents and ultrasound has been shown to offer an improved method to grade beef over present industrial procedures [Tervola et al.,1985; Hein et al., 1993].

A thorough understanding of the mechanisms and correlation of the interaction between acoustic propagation properties and skeletal muscle tissue offers a promising means for characterizing the physiological state of soft tissues. A biological process such as the mechanical and structural state of connective tissue results in a change in the attenuation coefficient and speed [Olerud et al., 1990; Hete and Shung, 1995]. However, to date, a complete analysis on the role of both muscle composition and structure (including the effects of anisotropy) on the acoustic propagation properties has not been developed. It is the goal of these experiments to elucidate these relationships.

1.2 Specific Aims

The specific aims are carefully designed to test the hypothesis that specific skeletal muscle constituents and structure can be predicted from detailed knowledge of the acoustic propagation properties. In addition, the acoustic propagation properties of the skeletal muscle tissue are found to be a function of factors such as frequency, temperature and anisotropy of the muscle (i.e. direction of the muscle fiber). Additional experiments have therefore been performed to determine the effect of these variables on the propagation properties.

Reported herein are four experiments which use either the scanning laser acoustic microscope (SLAM) or the Daedal exposimetry system (DES) to study the relationship between ultrasonic propagation properties and the tissue constituents and sarcomere length. The SLAM provides high spatial resolution due to the very high operating frequency of 100 MHz. The DES allows measurement of ultrasonic properties as a function of frequency and also temperature. The sarcomere length of skeletal muscle provides valuable information about the structural architecture of the skeletal muscle. The SLAM is used to determine the attenuation coefficient, speed and heterogeneity index of muscle tissue at a frequency of 100 MHz and a temperature of 20°C while the DES is used to determine the attenuation coefficient and speed at frequencies from 2-7 MHz and temperatures of 4, 20 and 37°C.

The first experiment determines if sarcomere length and tissue constituents of bovine semitendinosis can be predicted from attenuation coefficient and speed measurements using the SLAM at 100 MHz. The specific objectives of these experiments are:

1) To measure the propagation properties, tissue constituents and sarcomere length of bovine psoas major, longissimus dorsi and lobster extensor muscle. These particular tissues were chosen to allow ready differentiation between the effects of tissue constituents and sarcomere lengths. The percentage of fat and water is similar for the first two samples, but the fat content of lobster is considerably less. The sarcomere length for the longissimus dorsi is less than for the psoas, in turn less than for the lobster extensor.
2) To determine if the ultrasonic propagation properties are statistically correlated with the tissue constituents and sarcomere length.
3) To develop multiple linear regression equations using the bovine and lobster muscle to predict the tissue constituents and sarcomere length of bovine semitendinosis.
4) To measure the attenuation coefficient and speed of the semitendinosis.

5) To predict the tissue constituents and sarcomere length of bovine semitendinosis using the multiple linear regression equations and compare the actual tissue constituents results to the predicted results.

The second experiment is very similar to the first experiment except the system used to determine the acoustic propagation properties is the DES which operates from 2-7 MHz and 4, 20 and 37°C. This experiment elucidates the relationships between the acoustic propagation properties, tissue constituents and sarcomere length as a function of frequency and temperature for one muscle type. The specific objectives of these experiments are

1) To determine the attenuation coefficient and speed at 2-7 MHz and 4, 20 and 37°C for 20 samples of bovine longissimus dorsi using the DES.
2) To determine the tissue constituents and sarcomere length of the 20 samples.
3) To develop multiple linear regression equations which predict the tissue constituents and sarcomere length from the acoustic propagation properties of the 20 samples.
4) To measure the attenuation coefficient and speed of the 20 different samples of longissimus dorsi.
5) To predict the tissue constituents and sarcomere length of longissimus dorsi using the multiple linear regression equations and compare the actual tissue constituents and sarcomere length results to the predicted results.

The third experiment determines the myofibrilar (structural) contribution to the attenuation coefficient and speed using the SLAM. The specific objectives of these experiments are

1) To measure the acoustic propagation properties of 18 samples of longissimus dorsi samples from an parallel to perpendicular fiber orientation through selected angles.
2) To homogenize the samples and determine the propagation properties of the homogenized samples.
3) To assess the influence of the myofibrilar contribution.

The aim of the last experiment is to predict the angle of the muscle fiber of semitendinosis from the attenuation coefficient and speed. The specific objectives of these experiments are

1) To determine the attenuation coefficient and speed of semitendinosis as a function of the myofibril orientation from 0° to 180° in 5° increments using the DES at 20°C in a tank of degassed ringers.
2) To develop regression equations which predict the fiber angle or orientation based on the attenuation coefficient and speed.

1.3 Thesis Outline

The outline for this dissertation is as follows. Chapter 2 derives many of the fundamental acoustic equations and discusses the mechanisms involved in the attenuation phenomena. The purpose of the third chapter is to discuss skeletal muscle physiology and anatomy to develop a basic knowledge which is necessary before an explanation of the interaction between ultrasound and skeletal muscle can be attempted. Since the cell shape and contractiblilty is either directly or indirectly associated with fibrous proteins which form the cytoskeleton in muscle, the constituents of skeletal muscle are also examined. Chapter 4 is a literature survey of the ultrasonic propagation properties of skeletal muscle tissue. Chapter 5 describes the instrumentation assembled for the ultrasonic tissue measurement systems for the SLAM and the DES and Chapter 6 explains the tissue preparation, biochemical analysis and sarcomere length measurement procedure. Chapter 7 begins by assessing the uncertainty of the SLAM and the DES determining the attenuation and speed of materials with known acoustic properties. The remaining portion of Chapter 7 is devoted to presents the results of the experiment described in the Specific Aims and Chapter 8 is devoted to summarizing and discussing this research.

2. ACOUSTIC THEORY

This chapter presents the mechanisms describing the propagation of ultrasound through both fluids and anisotropic media, summarizes below. Sound waves traveling through a fluid medium cause a periodic change in the density, pressure and temperature as a function of time. The wave equation describes the propagation of a wave in a lossless medium and is developed from the equation of state, the continuity equation and the equation of motion. Changes in density related to changes in pressure are described by the equation of state. The continuity equation is based on the conservation of mass and describes the motion of particles which produces a change in density. Changes in pressure are related to change in particle displacement through the equation of motion. Additionally, the density, pressure and the temperature of a media varies periodically when a sound wave is passed through the fluid, thereby effecting the speed of sound.

Attenuation is comprised of two effects on the propagating wave: absorption and scattering. Development of the lossless wave equation neglects the absorption effects of the medium where acoustic energy is converted into thermal energy. The absorption mechanism consist of viscous losses, heat conduction and relaxation processes. Scattering occurs when acoustic energy is deflected or redirected from its normal propagation.

2.1 Equation of State

The equation of state for a fluid relates deformation in the fluid to internal restoring forces which can be thought of as relating changes in pressure to changes in density. To begin, the following definitions can be used:

$$p = P - P_0 \tag{2.1-1}$$

where $p = p(x,t)$ is the excess or acoustic pressure as a function of space and time, P is the instantaneous pressure at any point and P_o is the constant equilibrium or ambient pressure in the fluid. Similarly the density can be described as

$$\rho = \rho_0 + \rho_e \tag{2.1-2}$$

where ρ is the total density or instantaneous density at any point, ρ_o is the equilibrium or ambient density and ρ_e is the excess density.

For simply linear equations to be developed the amplitude changes of the excess pressure (p) and density (ρ_e) are assumed to be small compared to the ambient pressure (P_o) and density (ρ_o). Also, acoustic disturbances are assumed to be adiabatic, that is

there is no significant exchange of thermal energy from one particle to the next. If a system is adiabatic then the entropy of the system is constant. Therefore the thermal conductivity of the fluid and temperature gradients within the fluid are small due to a wave perturbing the fluid.

The equation of state can be derived by expressing the pressure as a function of the density

$$P = f(\rho). \tag{2.1-3}$$

Similarly under equilibrium or ambient conditions the pressure as a function of the density is expressed as

$$p_0 = f(\rho_0). \tag{2.1-4}$$

Using 2.1-1 & 2.1-2, the expression becomes

$$P_0 + p = f(\rho_0 + \rho_e). \tag{2.1-5}$$

The Taylor series expansion gives

$$P_0 + p = f(\rho_0 + \rho_e) = f(\rho_0) + \rho_e f'(\rho_0) + \frac{\rho_e^2}{2!} f''(\rho_0) + \ldots\ldots \tag{2.1-6}$$

If the assumption that the excess density (ρ_e) is very small is applied then the term in ρ_e^2 and all higher orders can be ignored. Since the ambient pressure is related to the ambient density then the excess or acoustic pressure can be expressed as

$$p = \rho_e f'(\rho_0) = \rho_e \left.\frac{dP}{d\rho}\right|_{\rho_0}. \tag{2.1-7}$$

The units of $\frac{dP}{d\rho}$ are m^2/s^2 which implies that

$$p = \rho_e c^2 \tag{2.1-8}$$

which is the equation of state where c is the speed of sound. More detailed derivation and discussion about the speed of sound will follow is section 2.5.

2.2 The Continuity Equation

The continuity equation is based on the conservation of mass and describes the motion of particles which causes a change in density or condensation. Motion of the fluid is related to the compression or dilation due to a functional relationship between the particle velocity and the instantaneous density. Due to the presence of an acoustic wave the pressure can be introduced by considering a small volume element with volume $dV=dxdydz$. Based on the conservation of mass the net rate at which mass flows into the volume must equal the rate at which mass within the volume increases. If a sound wave passes through or flows into the volume from the x, y and z directions, the net influx of mass into the volume will be

$$-\left[\frac{\partial \rho u_x}{\partial x}+\frac{\partial \rho u_y}{\partial y}+\frac{\partial \rho u_z}{\partial z}\right]dV=-[\nabla\cdot(\rho u)]dV \qquad (2.2\text{-}1)$$

where $\vec{u}=u_x\hat{x}+u_y\hat{y}+u_z\hat{z}$ is the particle displacement velocity and $\nabla\cdot$ is the divergence operator. The continuity equation is obtained by setting the increase in mass in the volume, which is $\left(\frac{\partial \rho}{\partial t}\right)dV$, equal to the net influx:

$$\frac{\partial \rho}{\partial t}+\nabla\cdot(\rho u)=0. \qquad (2.2\text{-}2)$$

At this point the condensation term, s, can be introduced as the fractional increase in the density:

$$s=\frac{\rho-\rho_o}{\rho}=\frac{\rho_e}{\rho} \qquad (2.2\text{-}3)$$

If equation 2.2-3 is rewritten as $\rho=\rho_o(1+s)$ and it is assumed that s is very small, 2.2-2 becomes:

$$\frac{\partial s}{\partial t}+\nabla\bullet u=0. \qquad (2.2\text{-}4)$$

which is the continuity equation.

2.3 The Equation of Motion

The equation of motion relates changes in pressure to changes in motion. Development of the equation of motion begins with considering a small volume element given by $dV=dxdydz$. If a disturbance produced by an acoustic wave acts on the volume from the +x direction, the force exerted on this small volume will be pdA in the x axis. In the x+dx plane, the pressure will be

$$p+\frac{\partial p}{\partial x}dx \tag{2.3-1}$$

and the force exerted on the material by this pressure in the original element is

$$-\left(p+\frac{\partial p}{\partial x}dx\right)dA \tag{2.3-2}$$

The net force on the small volume dV is

$$pdA-pdA-\frac{\partial p}{\partial x}dxdA=-\frac{\partial p}{\partial x}dV. \tag{2.3-3}$$

Using Newton's equation of motion gives

$$-\frac{\partial p}{\partial x}dV=(\rho_o dV)\ddot{\xi} \tag{2.3-4}$$

or

$$\rho_o\ddot{\xi}=-\frac{\partial p}{\partial x} \tag{2.3-5}$$

where ξ is defined as the as particle displacement from the equilibrium position and $\ddot{\xi}=\frac{\partial^2\xi}{\partial t^2}$ is the particle acceleration. If the y and z axes were also considered, the equation of motion would be

$$\rho_o\frac{\partial u}{\partial t}=-\nabla p. \tag{2.3-6}$$

where $\nabla p = \frac{\partial p}{\partial x} + \frac{\partial p}{\partial y} + \frac{\partial p}{\partial z}$ which is called the gradient of the pressure.

2.4 The Linearized Wave Equation

To get one differential equation which describes the propagation of sound with a single dependent variable the equations of state, continuity and motion are combined. Starting with the equation of motion (2.3-6) the divergence of both sides is taken to yield

$$\rho_o \nabla \cdot \frac{\partial u}{\partial t} = -\nabla \cdot (\nabla p) = -\nabla^2 p \qquad (2.4\text{-}1)$$

where ∇^2 is the Laplacian operator. Taking the time derivative of the continuity equation (2.2-4) yields

$$\frac{\partial^2 s}{\partial t^2} + \nabla \cdot \frac{\partial u}{\partial t} = 0. \qquad (2.4\text{-}2)$$

The combination of the two equations above gives

$$\nabla^2 p = \rho_o \frac{\partial^2 s}{\partial t^2} \qquad (2.4\text{-}3)$$

The condensation, s, is eliminated by using the equation of state (2.1-8) to give

$$\nabla^2 p = \frac{1}{c^2} \frac{\partial^2 p}{\partial t^2} \qquad (2.4\text{-}4)$$

which is the linearized wave equation where the speed of sound in fluids, c, is

$$c^2 = \frac{\gamma B_T}{\rho} = \frac{B_s}{\rho} \qquad (2.4\text{-}5)$$

where B_T is defined to be the bulk modulus in Pascals (Pa) and γ is the ratio of specific heats and B_s is the.

2.5 Speed of Sound

The density, pressure and the temperature of an element of a fluid varies periodically when a sound wave is passes through the fluid. The speed of sound in a fluid is determined by its compressibility and the thermodynamic equations of state of the fluid. This section discusses the dependence of the velocity on the pressure and temperature in terms of the equations of state of the fluid. Recall that equation (2.4-5) stated that

$$c^2 = \frac{\gamma B_T}{\rho} = \frac{B_s}{\rho}.$$

This section will derive this relationship by expressing pressure as a function of both the density and temperature, $P = f(\rho, T)$, of the fluid and taking the exact differential. However the expression for the exact differential has derivatives which cannot be reduced immediately and therefore other thermodynamic relationships beginning with state equations of a fluid must first be derived. These thermodynamic relationships for the fluid state equations will first be derived which can later replace expressions in the exact derivative of $P = f(\rho, T)$ will be found and expressed in the exact derivative.

A better understanding of the system is necessary to derive the adiabatic speed of sound. The definition of the adiabatic speed of sound requires that there is no heat flow and the change in entropy is zero. Therefore the best place to begin is to start with the entropy, S. Entropy is defined as a function of the volume, V, temperature, T, and pressure, P. If the entropy is first expressed as a function of only V and T,

$$S = S(V, T) \tag{2.5-1}$$

and taking the exact differential yields,

$$dS = \left(\frac{\partial S}{\partial T}\right)_V dT + \left(\frac{\partial S}{\partial V}\right)_T dV. \tag{2.5-2}$$

Using the Maxwell relation:

$$\left(\frac{\partial S}{\partial V}\right)_T = \left(\frac{\partial P}{\partial T}\right)_V \tag{2.5-3}$$

and the definition of heat capacity, C_V, (J•mol/K) at constant volume:

$$C_v = T\left(\frac{\partial S}{\partial T}\right)_V \tag{2.5-4}$$

then equation (2.5-2) becomes:

$$TdS = C_v dT + T\left(\frac{\partial P}{\partial T}\right)_V dV. \tag{2.5-5}$$

Entropy can also be regarded as a function of the pressure, P, and temperature, T. Therefore entropy is again expressed as

$$S = S(P,T) \tag{2.5-6}$$

and again taking the exact differential yields:

$$dS = \left(\frac{\partial S}{\partial T}\right)_P dT + \left(\frac{\partial S}{\partial P}\right)_T dP \tag{2.5-7}$$

Now using another Maxwell relation

$$-\left(\frac{\partial S}{\partial P}\right)_T = \left(\frac{\partial V}{\partial T}\right)_P \tag{2.5-8}$$

and heat capacity, *Cp*, at constant pressure

$$C_v = T\left(\frac{\partial S}{\partial T}\right)_P \tag{2.5-9}$$

and hence equation (2.5-7) becomes:

$$TdS = C_p dT + T\left(\frac{\partial V}{\partial T}\right)_V dP \tag{2.5-10}$$

To determine the ideal gas constant, $R = C_p - C_v$, one needs to subtract (2.5-5) from (2.5-10) to get

$$0 = (C_P - C_v)dT - T\left(\frac{\partial V}{\partial T}\right)_V dP - T\left(\frac{\partial P}{\partial T}\right)_V dV \qquad (2.5\text{-}11)$$

or

$$(C_P - C_v)dT = T\left(\frac{\partial V}{\partial T}\right)_V dP + T\left(\frac{\partial P}{\partial T}\right)_V dV \qquad (2.5\text{-}12)$$

Using the identity:

$$\left(\frac{\partial P}{\partial T}\right)_V \left(\frac{\partial T}{\partial P}\right)_V = 1 \quad \text{and} \quad \left(\frac{\partial V}{\partial T}\right)_P = 1 \Big/ \left(\frac{\partial T}{\partial V}\right)_P$$

Equation (2.5-12) can be written as:

$$(C_P - C_v)dT = T\frac{\left(\frac{\partial P}{\partial T}\right)_V \left(\frac{\partial T}{\partial P}\right)_V}{\left(\frac{\partial T}{\partial V}\right)_P} dP + T\frac{\left(\frac{\partial P}{\partial T}\right)_V \left(\frac{\partial T}{\partial V}\right)_P}{\left(\frac{\partial T}{\partial V}\right)_P} dV \qquad (2.5\text{-}13)$$

or

$$(C_P - C_v)dT = T\frac{\left(\frac{\partial P}{\partial T}\right)_V}{\left(\frac{\partial T}{\partial V}\right)_P}\left[\left(\frac{\partial T}{\partial P}\right)_V dP + \left(\frac{\partial T}{\partial V}\right)_P dV\right]dP \qquad (2.5\text{-}14).$$

Equation (2.5-14) can be expressed in a more elegant form using the ideal gas law. From the ideal gas law, temperature is a function of both pressure and volume and can be written as $T = f(P,V)$. Taking the exact differential

$$dT = \left[\left(\frac{\partial T}{\partial P}\right)_V dP + \left(\frac{\partial T}{\partial V}\right)_P dV\right] \qquad (2.5\text{-}15)$$

will reduce (2.5-14) to

$$(C_P - C_v) = T\frac{\left(\frac{\partial P}{\partial T}\right)_V}{\left(\frac{\partial T}{\partial V}\right)_P} \qquad (2.5\text{-}16)$$

Multiplying the numerator and denominator by $\left(\frac{\partial P}{\partial T}\right)_V$ yields

$$(C_P - C_v) = T\frac{\left(\frac{\partial P}{\partial T}\right)_V^2}{\left(\frac{\partial T}{\partial V}\right)_P\left(\frac{\partial P}{\partial T}\right)_V}. \qquad (2.5\text{-}17)$$

Making use of the identity

$$\left(\frac{\partial T}{\partial V}\right)_P\left(\frac{\partial P}{\partial T}\right)_V\left(\frac{\partial V}{\partial P}\right)_T = -1 \qquad (2.5\text{-}18)$$

to get and expression for the R, the ideal gas constant.

$$R = C_P - C_v = -T\frac{\left(\frac{\partial P}{\partial T}\right)_V^2}{\left(\frac{\partial P}{\partial V}\right)_T} \qquad (2.5\text{-}19)$$

Using the identities again gives:

$$R = C_P - C_v = -T\frac{\left(\frac{\partial V}{\partial T}\right)_P\left(\frac{\partial P}{\partial V}\right)_T\left(\frac{\partial V}{\partial T}\right)_P\left(\frac{\partial P}{\partial V}\right)_T}{\left(\frac{\partial P}{\partial V}\right)_T} \qquad (2.5\text{-}20)$$

Regroup and multiply by V^2/V^2 yields

$$R = C_P - C_v = -TV\left[\frac{1}{V^2}\left(\frac{\partial V}{\partial T}\right)_P\left(\frac{\partial V}{\partial T}\right)_P\right]\cdot -V\left(\frac{\partial P}{\partial V}\right)_T. \qquad (2.5\text{-}21)$$

The coefficient of volume expansion, β, (1/Pa), is defined as

$$\beta = \frac{1}{V}\left(\frac{\partial V}{\partial T}\right)_P \qquad (2.5\text{-}22)$$

and the isothermal bulk modulus, B_T, (Pa), is defined as

$$B_T = -V\left(\frac{\partial P}{\partial V}\right)_T \tag{2.5-23}$$

Thus equation (2.5-21) becomes

$$R = C_P - C_v = TV\beta^2 B_T = \frac{-T\left(\frac{\partial P}{\partial T}\right)_V^2}{\left(\frac{\partial P}{\partial V}\right)_T} \tag{2.5-24}$$

Again using (2.5-5)

$$TdS = C_v dT + T\left(\frac{\partial P}{\partial T}\right)_V dV$$

and deriving the following relation

$$V = \frac{M}{\rho}$$

$$\frac{dV}{d\rho} = \frac{d}{d\rho}\left(\frac{M}{\rho}\right) = -\frac{M}{\rho^2}$$

gives

$$dV = -\frac{M}{\rho^2}dp \tag{2.5-25}$$

$$\left(\frac{dP}{dV}\right)_T = -\frac{\rho^2}{M}\left(\frac{dP}{d\rho}\right)_T \tag{2.5-26}$$

Using equation (2.5-25), equation (2.5-5) can be re-written as

$$TdS = C_v dT - \frac{TM}{\rho^2}\left(\frac{\partial P}{\partial T}\right)_V d\rho \tag{2.5-27}$$

which can be substituted into (2.5-24) to yield

$$R = TV\beta^2 B_T = \frac{-T\left(\frac{\partial P}{\partial T}\right)_v}{-\frac{\rho^2}{M}\frac{\partial P}{\partial \rho}} \tag{2.5-28}$$

$$R = \frac{\frac{TM}{\rho^2}\left(\frac{\partial P}{\partial T}\right)^2}{\left(\frac{\partial P}{\partial \rho}\right)_T} \tag{2.5-29}$$

which can be re written as

$$\left(\frac{\partial P}{\partial \rho}\right)_T R = \frac{TM}{\rho^2}\left(\frac{\partial P}{\partial T}\right) \tag{2.5-30}$$

Recall that for an adiabatic process there is no gain or loss of heat or heat flow, ($\Delta q=0$) therefore the change in entropy is zero ($dS=0$). In (2.5-27) we define $dS=0$, therefore

$$C_v dT = \frac{TM}{\rho^2}\left(\frac{\partial P}{\partial T}\right)_\rho d\rho \Rightarrow \frac{dT}{d\rho} = \frac{TM}{C_v\rho^2}\left(\frac{\partial P}{\partial T}\right)_\rho \tag{2.5-31}$$

Now, to actually derive $\frac{dP}{d\rho}$ which is defined to be equal to c^2, one starts with the pressure as a function of both the density and temperature, or $P = f(\rho, T)$, and takes the exact differential.

$$dP = \left(\frac{\partial P}{\partial \rho}\right)_T d\rho + \left(\frac{\partial P}{\partial T}\right)_\rho dT \tag{2.5-32}$$

divide through by $d\rho$ and substitute in equation (2.5-29)

$$\frac{dP}{d\rho} = \left(\frac{\partial P}{\partial \rho}\right)_T + \left(\frac{\partial P}{\partial T}\right)_\rho \frac{dT}{d\rho} = \left(\frac{\partial P}{\partial \rho}\right)_T + \left(\frac{\partial P}{\partial T}\right)_\rho^2 \frac{TM}{C_v\rho^2} \tag{2.5-33}$$

and substitute in equation (2.5-28)

$$\frac{dP}{d\rho}=\left(\frac{\partial P}{\partial \rho}\right)_T+\frac{R}{C_v}\left(\frac{\partial P}{\partial \rho}\right)_T \tag{2.5-34}$$

and recall that $R=C_p-C_v$ so (2.5-32) becomes

$$\frac{dP}{d\rho}=\left(\frac{\partial P}{\partial \rho}\right)_T+\frac{C_p-C_v}{C_v}\left(\frac{\partial P}{\partial \rho}\right)_T$$

$$\frac{dP}{d\rho}=\left(\frac{\partial P}{\partial \rho}\right)_T+(\gamma-1)\left(\frac{\partial P}{\partial \rho}\right)_T=\left(\frac{\partial P}{\partial \rho}\right)_T+\gamma\left(\frac{\partial P}{\partial \rho}\right)_T-\left(\frac{\partial P}{\partial \rho}\right)_T$$

$$\frac{dP}{d\rho}=\gamma\left(\frac{\partial P}{\partial \rho}\right)_T \tag{2.5-35}$$

where $\gamma=\frac{C_P}{C_V}$ or the ratio of specific heats. And recall from (2.5-26) that

$$\left(\frac{dP}{dV}\right)_T=-\frac{\rho^2}{M}\left(\frac{dP}{d\rho}\right)_T$$

thus (2.5-35) becomes

$$\frac{dP}{d\rho}=\gamma\left[-\frac{M}{\rho\cdot\rho}\left(\frac{dP}{dV}\right)_T\right]. \tag{2.5-36}$$

And recall that the isothermal bulk modulus in (2.5-23) defined as

$$B_T=-V\left(\frac{\partial P}{\partial V}\right)_T$$

can be substituted into equation (2.5-36) as follows. Thus

$$\frac{dP}{d\rho}=\gamma\left[-\frac{M}{\rho\cdot\rho}\left(\frac{dP}{dV}\right)_T\right]$$

$$c^2 = \frac{dP}{d\rho} = \frac{\gamma B_T}{\cdot \rho} \qquad (2.5\text{-}37)$$

and since $\gamma B_T = B_s$, the adiabatic bulk modulus, then one can also write.

$$c^2 = \frac{\gamma B_T}{\rho} = \frac{B_s}{\rho} \qquad (2.5\text{-}38)$$

The reciprocal of B_s is the adiabatic compressibility, $1/K_S$. Whether sound disturbances are considered to be adiabatic or isothermal depends on the system under investigation. The adiabatic assumption ($\Delta q=0$) is better at lower frequencies that at higher frequencies because heat production due to conduction is weaker when the wavelengths are longer (Pierce, 1989). One of the essential characteristics of the speed is that, along with the density of the material, the characteristic impedance of the material can be calculated. Also, the elasticity of a material can be determined from the speed thus making it an essential quantity in investigating the mechanical properties of a biological tissue.

Ultrasonic wave propagation in biological soft tissue has usually employed an isotropic model. i.e. having properties that are the same in all directions. However, the speed of sound in muscle has been found to vary with the direction of propagation. Recall that the propagation speed depends on tissue density and elasticity and thus provides quantitative information about muscle's mechanical properties. The use of the linear elastic theory applied to soft tissues has been used to determine mechanical properties and assumes a systemic structure for an anisotropic tensor [Levinson, 1987]. Velocity of ultrasound through the anisotropic soft tissue can be used to determine the elastic stiffness constants C_{33} and C_{11}. C_{33} is the elastic stiffness constant associated with velocity propagation along the longitudinal mode of the acoustic wave or parallel to the muscle fiber ($C_{33} = \rho V_{para}^2$) and C_{11} is the elastic stiffness constant associated with the velocity propagation along the transverse mode of the acoustic wave or perpendicular to the muscle fiber ($C_{11} = \rho V_{perp}^2$) [Hoffmeister et al., 1994].

2.6. Classical Absorption Mechanisms

Development of the wave equation in the previous section neglected absorption effects of the medium. This section considers the influence of absorption, or more specifically absorption, on sound propagation. Ultrasonic attenuation is the loss of acoustic energy from a propagating sound beam. Attenuation is composed of two loss mechanisms known as absorption and scattering. Absorption mechanisms convert acoustic energy into

thermal energy. Scattering refers to acoustic energy being deflected out of the beam. Absorption mechanisms can in turn be divided into three categories: viscous losses, heat or thermal conduction losses and losses due to molecular exchanges of energy. [Kinsler, et al., 1982].

Sound waves in a medium cause expansions and contractions. Fluids will exhibit resistance to the distortion, which is known as viscosity. The relative motion between adjacent parts of the medium caused by expansions and compressions due to a sound wave leads to a viscous loss or frictional loss. The one dimensional lossy wave equation is developed by considering the viscosity of the fluid. Taking into account that a fluid is viscous, the one dimensional lossy wave equation would then be derived as

$$\frac{\partial^2 \xi}{\partial t^2} = c^2 \frac{\partial^2 \xi}{\partial x^2} + R \frac{\partial^3 \xi}{\partial x^2 \partial t} \qquad (2.6\text{-}1)$$

where R is a constant describing a resistive term representing a viscosity factor [Mason and Thurston, 1982]. Equation (2.6-1) is satisfied by a damped harmonic wave of the form

$$\xi = \xi_0 e^{j(\omega t - \bar{k}x)} \qquad (2.6\text{-}2)$$

where $\omega=2\pi f$ is the angular frequency (f is the frequency in Hz) and $\bar{k}$=(k-ja) is the complex wave number. The real wave number, k, is defined as $k=\omega/c=2\pi/\lambda$ (λ is the wavelength) α is the absorption coefficient. The solution to equation 2.6-2 is given by

$$\alpha = \frac{\omega}{c}\frac{1}{\sqrt{2}}\left[\frac{\sqrt{1+(\omega\tau)^2}-1}{1+(\omega\tau)^2}\right]^{1/2} \qquad (2.6\text{-}3)$$

$$c_p = c\sqrt{2}\left[\frac{1+(\omega\tau)^2}{\sqrt{1+(\omega\tau)^2}+1}\right]^{1/2} \qquad (2.6\text{-}4)$$

where c_p is the phase speed and τ is the relaxation time. The dependence of the phase speed, c_p, on frequency indicates that the dissipative medium is dispersive. Each absorption process is characterized by a relaxation time. An example of how a wave is attenuated and the importance of the relaxation time is demonstrated when the period of the acoustic cycle is greater than the time required for a portion of the compression energy of the fluid to be converted into internal energy of molecular vibration. During the expansion

cycle some of this energy will be delayed in its restoration, resulting in a tendency toward pressure equalization and an attenuation of the wave.

There exist two types of viscosity in a fluid, shear and bulk, which need to be distinguished. Shear viscosity (η) is a measure of the diffusing momentum of molecules from regions of fluid possessing higher velocities to regions of lower velocities. Bulk viscosity (η_B) is defined as compression volume or bulk changes with respect to time and mediums resistance to these expansions and contractions. In Stoke's 1845 memoir "On the Theories of the Internal Friction of Fluids in Motion, and of the Equilibrium and Motion of Elastic Solids", he assumed that a fluid possessed only shear viscosity and no bulk viscosity. Under these conditions the relaxation time due to the shear viscosity (t_S) was found to be

$$\tau_s = \frac{4\eta}{3\rho_o c^2}. \qquad (2.6\text{-}5)$$

If the relaxation time is very small compared to the period of the sound wave, (i.e. $\omega\tau << 1$) the absorption coefficient (α_S) due to the shear viscosity would be

$$\alpha_s = \frac{2\eta\omega^2}{3\rho_o c^3}. \qquad (2.6\text{-}6)$$

Another mechanism of absorption is thermal conduction. In 1868 Kirchhoff worked out the influence of heat conduction on the propagation of sound (Lindsay, 1982) through a fluid. When the thermal conductivity, k, is due to the heat flow in a fluid, then the absorption coefficient (α_K) associated with thermal conductivity alone is

$$\alpha_\kappa = \frac{1}{2}\frac{\omega^2}{\rho_o c^3}(\gamma - 1)\frac{\kappa}{C_p} \qquad (2.6\text{-}7)$$

where $\gamma = \frac{C_p}{C_v}$. The quantity C_p is the molar heat capacity at constant pressure and the quantity C_v is the molar heat capacity at constant pressure.

The classical absorption coefficient is the sum of the absorption coefficient terms developed by Stokes and Kirchoff by taking into account the viscous and thermal conductivity losses of the media. The classical absorption coefficient is

$$\alpha(classical) = \frac{\omega^2}{2\rho c^3}\left[\frac{4}{3}\eta + (\gamma - 1)\frac{\kappa}{Cp}\right] \qquad (2.6\text{-}8)$$

However the classical absorption coefficient does not totally account for values of the absorption coefficient which are experimentally measured in fluids. The difference between the calculated classical absorption coefficient and the observed absorption coefficient can differ by as much as a factor of 4.3 in acetone [Kinsler et al., 1982]. This disagreement suggests that there are other factors leading to absorption which need to be examined.

2.7. Molecular Mechanisms of Ultrasound Absorption

Any delay in the restoration of the propagating wave corresponds to a conversion into either heat and/or internal energy. Losses associated with molecular exchange are due to relaxation processes. A molecular process whose characteristic relaxation time determines the rate at which equilibrium is restored after the perturbation, is referred to as a relaxation process. Much of the excess absorption beyond the classical absorption is accounted for by three processes known as structural, thermal and chemical relaxation.

2.7.1 Structural Relaxation

Disturbance to the structure of a fluid due to a propagating wave changes the molecular structure equilibrium. The energy going into rearranging the molecular structure, thereby causing the structure to be more closely packed, causes energy to be removed from the wave. One of the early explanations of the structural relaxation phenomenon considers what happens to a molecule of water [Hall, 1948]. Hall's theory suggests that the excess absorption in water results from a structural relaxation directly related to volume change. Water is assumed to be a two-state liquid with the lower energy state considered as the normal state. The higher energy state is the one in which the molecules have a more closely packed structure. At equilibrium, most of the molecules are in the first state. The passage of a compressional wave is assumed to promote the transfer of molecules from the first, low energy, more open state to the more closely packed, high energy, second state. The time delays in this process and in its reversal lead to a relaxation dissipation of acoustic energy.

When a biomacromolecule, like hemoglobin, is in solution, a certain amount of solvent becomes associated with the molecule since the hemoglobin has polar side chains. Entropic considerations suggest that the water molecules order themselves about the non-polar molecule and are interconnected by hydrogen bonds. This forms a structured

hydration layer about the macromolecule. Propagating acoustic energy acts to disrupt the structured or low entropy state and absorption of the acoustic wave occurs.

2.7.2 Thermal Relaxation

Another mechanism for acoustic absorption can be predicted by taking into account the internal structure of the molecules and the interaction between the molecules that lead to internal vibrations, rotations and translations. The molecular thermal relaxation theory begin by stating that each molecule possesses 3 degrees of translational freedom. In addition there are also internal degrees of freedom associated with the rotation and vibration of these molecules. The time necessary for the transfer of the translational motion in the molecule into internal states compared to the period of the acoustic process determines how much acoustic energy is converted into thermal energy. The temperature exchange process associated with the energy exchange between the vibrational and rotational modes in the molecule gives rise to the relaxation process. Absorption arising from perturbations in molecular equilibrium due to temperature alterations in the compressional wave is considered to be due to thermal relaxation mechanisms.

Hence molecular thermal relaxation is characterized as a single relaxation process and is one in which the propagation of an acoustic wave perturbs the system between only 2 energy states. However thermal relaxation has not been successful in accounting for the observed excess absorption associated with polar liquids like alcohol or water. The thermal relaxation time is very short due to the strong intermolecular forces of these liquids and the magnitude of the absorption is proportional to the relaxation time. The fact that excess absorption in water is not due to thermal relaxation is demonstrated by making absorption measurements at 4.0^{o}C. The thermal relaxation process can be accounted for in these experiments due to the fact that the coefficient of thermal expansion is zero at 4.0 ^{o}C. At this temperature fluctuations of temperature cannot be varied as the pressure is varied.

2.7.3 Chemical Relaxation

The volume change which results from the perturbation of a chemical reaction from equilibrium by the pressure disturbance when an acoustic wave is propagated through a liquid medium, is considered to be a chemical relaxation mechanism. Another example is the conversion of the kinetic energy of the molecule into energies of association and dissociation between the different ionic species. The chemical relaxation mechanism has been used to explain the high value of ultrasonic absorption by proteins. For example, the mechanism for absorption at extremes of pH is the relaxation of proton-transfer equilibrium occurring at ionizable residues [Strom-Jensen and Dunn, 1984]. It is

considered that the propagating acoustic wave disturbance perturbs the protons from the solvent (water) to the solute. The energy necessary to drive this reaction is extracted from the acoustic wave.

2.8 Scattering

When a sound wave encounters a solid obstacle, a fraction of the wave is redirected or scattered. Scattering can be defined as the change of amplitude, frequency, phase velocity or direction of propagation as the result of an obstacle or non-uniformity in the medium. The scattering of a plane wave by an obstacle excludes the absorption process by which part of the energy of the wave is absorbed by mechanisms discussed in previous sections. The focus of this section will be to discuss the complexities behind scattering, to introduce basic scattering theory and examine attenuation in muscle with respect to scattering.

A rigorous explanation of scattering theory has been covered in several outstanding texts [Pierce, 1981, Morse & Ingard, 1968; Skudrzyk, 1971]. The basic concept introduces the scattered pressure wave composed of the actual pressure wave minus the undisturbed wave i.e. with the obstacle absent. From this point the discussion can take several directions.

One of the first distinctions that should be made is whether the scattering volume consists of a single scatterer or a statistical distribution of scatterers. The complication caused by a distribution of scatterers is the re-radiation and interaction of the wave with other single bodies. Thus, single scatterers are usually considered where interaction occurs between only the incident wave and a single scatterer. Also the physical properties of the scatterer such as the density, compressibility, roughness and thermal conductivity should be taken into consideration.

In a distribution of scatterers, the problem becomes complicated by the fact that the sound radiated by single bodies can interact with the incident wave and the sound scattered by other single bodies. Therefore the distribution in the medium must be known to calculate how these scatters interact with each other. The bodies may be arranged in a pattern that resembles simple shapes. For example, the scattering caused by a large number of closely spaced small spheres arranged with spherical symmetry may simply resemble the sound scattered by an equivalent larger sphere. If there is a reasonably fixed order of alignment in the distribution of the objects then diffraction effects may become important. When the scattering body is large compared with the wavelength, sound is considered to be reflected and diffracted rather than scattered; however the effects are generally the same [Morse and Ingard, 1968]. Finally statistical techniques that describe

the overall pattern of scatterer such as the inhomogeneous continuum model have been developed.

The next level of complexity deals with the shape of the single scatterer. The scatterer can be shaped as a cylinder, ellipsoid, sphere, knife edge, disk or some other inhomogeneous geometry. Each of these shapes leads to a different pressure field. Often equations for single scatters are developed considering only one scatterer and therefore interaction occurs only between the incident wave and one body.

The size of the obstacle is also important. Generally, if the object is large (i.e. $a >> 1$ or $ka >> 1$ where a is the radius and k the wave number, $k=\omega/c$) then half the scattered wave spreads out approximately uniformly in all directions from the obstacle and half the scattered wave is concentrated behind the obstacle or interferes destructively with the plane wave. If the obstacle is small (i.e. $a << 1$ or $ka << 1$) then the scattered wave spreads out approximately uniformly in all directions from the obstacle. Finally if the object is of intermediate size (i.e. $a \approx 1$ or $ka \approx 1$) then a variety of interference patterns occur.[Morse & Ingard, 1968]

At the moment the discussion of the energy lost from an incident wave due to absorption and scattering considers only a non-rigid object of radius a. For an incident plane wave the amount of energy lost divided the wave's intensity which is defined as the cross section of the object, S [Morse & Ingard, 1968]. Energy can be lost from the incident beam from absorption by the sphere, which is called the absorption cross section S_α, or from deflection by the sphere called the scattering cross section S_S. The total power withdrawn from the beam is the sum of the absorption cross section S_α, and the scattering cross section, S_S, and is called the total cross section, $S = S_S + S_\alpha$.

A simplified derivation of the total cross section of a scatterer is developed in the following discussion [Chivers, 1977]. Using Figure 2.8-1, a single discrete scatterer irradiated by an incident plane wave p_i will give rise to a scattered wave p_s of the form

$$p_i = gp_s \qquad (2.8\text{-}1)$$

where p_s is the scattered wave, p_i is the incident wave and g is a function of frequency and scatter parameters such as size, shape and density. The total wave at point r due to the object at r_1 is

$$p(r) = p_i(r) + E(r, r_1)gp \qquad (2.8\text{-}2)$$

where the function E describes the propagation of the wave from r_1 to r. If scattering is spherically symmetrical and propagation is in a homogeneous medium then the function E will be of the form

$$E(r,r_1)=e^{\left[\frac{-jk|r-r_1|}{|r-r_1|}\right]} \tag{2.8-3}$$

The incident wave will be

$$p_i = Ae^{-jkr} \tag{2.8-4}$$

where A is the amplitude of the incident wave. The net flux is found by integrating equation 2.8-2 over the area of the sphere to obtain

$$4\pi A^2(g_1. - g_1) - 4\pi A^2 jk|g_1^*|^2 \tag{2.8-5}$$

where the first term is the flux of the wave entering the sphere, the second term is the flux of the scattering coming out of the sphere and g_1^* indicates a complex conjugate. Dividing equation 2.8-5 by the flux per unit area in the incident wave, A^2jk, gives the total attenuation cross section,

$$\Sigma = \Sigma_\alpha + \Sigma_s = -\frac{8\pi}{k}\mathrm{Im}(g_1) \tag{2.8-5}$$

The total cross section measures the total loss due to the presence of a scatterer.

Specific acoustic scattering problems can be quite complex. In many instances there are no exact solutions to the scattering problems. As a result researchers attempt to get around this problem by making simplifying assumptions or approximations about the scattering volume or its interaction with the incident sound volume. While an approximation is convenient it does not accurately describe the scattered acoustic field. Therefore when proposing an equation which describes a scattered acoustic field it is important that the limitations of the scattering equation be presented. For biological media scattering volumes are considered to vary internally, and therefore the scattering can take on a very complex form. One limitation of statistical models of scattering in biological media requires that the medium does not contain large acoustic interference (i.e. bone and tissue).

One of the most useful models used to describe the interaction between an acoustic plane wave and scattering in cardiac muscle is the Born approximation [Mottley and Miller, 1988; Verdonk et al., 1992; Kumar and Mottley, 1994; Rose et al., 1995]. Simply stated, the Born approximation computes the scatter pressure by first assuming that multiple scattering does not occurs. Therefore, the total scattering pressure is the sum of the scattering pressures from each body [Rose and Richardson, 1982]. With respect to biological scatterers, the time domain Born approximation is used to describe the interaction of an acoustic plane wave impulse on an arbitrarily shaped inhomogeneity embedded in a homogeneous medium. Thus the time domain Born approximation provides a way of describing the scatter field from different shaped scatterers such as a large globular protein or cylinder shaped myofibril. The relationship between the shape of the scatterer fields and the scatter shape enables one to Fourier transform the resulting equation.

The time domain Born approximation has been used to describe the anisotropy of ultrasonic backscatter measured in canine and human myocardium . The myocardium is modeled as a group of cylindrically shaped scatters or prolate spheroids uniformly distributed in a homogeneous medium. The Born approximation predicts that the maximal backscatter occurs when insonifying perpendicular to the fibers, and minimal backscatter parallel to the fibers [Mottley and Miller, 1988; Verdonk et al., 1992].

Rose et al, (1995) have recently used the Born approximation to propose a microscopic elastic wave theory for ultrasonic frequency dependent backscatter from myocardium tissue. The Born approximation assumes that the power received at the transducer is the sum of the scatter power in the direction of the transducer from each individual scatter located in the volume of the beam. The model used for the scatterer in this application of the Born approximation is an ellipsoidal shell with the properties of wet collagen imbedded in a medium with the properties of myocardium.

While these empirical results indicate the validity of the Born approximation in the literature, it should be noted that there are some limitations on the assumptions used. First, calculations of the backscatter assume that scattering from the tissue is weak. This is not always true as indicated from the strong speckle regions from liver which indicate strong scatter. Second, the Born approximation fails when either the phase or amplitude of the wave inside the scattering volume varies substantially from the incident pressure wave. A phase difference of $\pi/2$ radius has been demonstrated to be the maximum limit of the Born approximation acceptability [Segal and Greenleaf, 1984]. Lastly, the Born approximation discounts multiple reflections from within a scatterer and ignores incoherent summation due to multiple scattering. In this case the Born approximation will only be valid only if scattering is weak.

3. SKELETAL MUSCLE PHYSIOLOGY

The purpose of this chapter is to present a discussion of skeletal muscle physiology, anatomy and chemical constituents to develop a knowledge base which is necessary for an explanation of the interaction between ultrasound and skeletal muscle.

3.1 Skeletal Muscle Structure

A muscle fiber is a single skeletal-muscle cell with the nuclei of the cell just beneath the plasma membrane. Muscle fibers can be as long as 20 cm and have a diameter between 10 and 150 μm, although some species like the crab *Maia squinado* or the barnacle *Balanus nubilus* have been found to have diameters in the order of 1-2 mm [Huxley, 1973]. A muscle is actually a number of muscle fibers bound together by connective tissue and is attached to bones at each end of the muscle by tendons which are bundles of collagen fibers. Skeletal muscle has a characteristic banding pattern, thereby the term striated muscle. The thin and thick filaments are organized into cylindrical bundles known as myofibrils which give rise to the striated pattern. A sarcomere is the repeating unit of the myofibril. The contractile protein myosin makes up the thick filament. The proteins actin, troponin and tropomyosin comprise the thin filaments (Figure 3.1-1).

The dark area of the A band is produced from the thick filaments. A sarcomere contain two set of thin filaments anchored to a network of interconnecting proteins known as the Z line (or Z disk) or *zwischenscheibe* which means inverted disk [Gould, 1973]. The diameter of the Z disk is on the order of 1-2 μm. A sarcomere is defined by two successive Z lines. In bovine skeletal muscles, sarcomere lengths at rest are 1.82-3.46 μm. In the extensor muscle of the crayfish the sarcomere length is in the region of 10 μm while the sarcomere length for the crab *Cancer* is 10-15 μm [Huxley, 1973].

Anchored to each Z line are thin filaments (50-70 Å diameter) from two adjacent sarcomeres. The area which lies between the ends of the A bands of two adjacent sarcomeres is known as the I band and is bisected by the Z line. A relatively light band in the center of the A band is known as the H zone or *heller* , meaning clearer or brighter. The H zone corresponds to the space between the ends of the two sets of thin filaments in each sarcomere and therefore only the central portions of the thick filaments are found in the H zone. Thick filaments are approximately 100-120 Å in diameter and approximately 1.5 μm in length. The M line (*mittelschribe*, meaning middle) is a dark band in the center of the H zone consisting of proteins which link together the central region of the thick filaments. Filaments composed of the protein titin extend from the Z lines and are linked to the ends of the thick filaments. Since the thick filaments are

anchored together by the M line neither the thick nor the thin filaments are free-floating. If a myofibril contained a chain of 20,000 sacromeres and the length of each sarcomere decreases from 2.5 μm to 2.0 μm the muscle would contract from 5 cm to 4 cm or 20% of its length.

Projections, which are portions of myosin molecules that extend from the surface of the thick filaments toward the thin filaments, are known as cross bridges. The cross bridges are the force-generating structures in muscle cells since, during muscle contraction, these cross bridges make contact with the thin filaments and exert force on them. Contraction occurs when the sarcomere shortens, which is caused by the thick filaments sliding past the thin filaments (Figure 3.1-2). A cross section through the A band of adjacent myofibrils show the regular arrangement of the thick and thin filaments. Each thick filament is surrounded by a hexagonal array of six thin filaments. Altogether there are twice as many thin filaments as thick filaments.

Connective tissue binds together the muscle fibers into bundles (Figure 3.1-3). The myofibrils are surrounded by a plasma membrane known as the sarcolemma (0.009 μm thick). Around the sarcolemma is a 0.05 μm thick protein polysaccahride cover known as the basal lamina. The 0.20-1.0 μm thick endomysium surrounds the basal lamina. The endomysium surrounds each myofibril with a connective tissue matrix. Approximately 20 to 40 myofibrils along with their endomysium are bundled together into primary bundles, which are in turn grouped into secondary bundles (Figure 3.1-4). These secondary bundles are surrounded in another connective matrix called the perimysium. Nerves and blood vessels run along the interior of the muscle through the perimysium. Fat cells also accumulate along within the perimysium. Surrounding the entire muscle is the connective tissue matrix known as the epimysium. Thus the connective tissue associated with skeletal muscle is divided into three levels of organization: the epimysium, the perimysium and the endomysium.

3.2 Molecular Mechanism of Contraction

Muscle contraction takes place when force is produced by the shortening of a skeletal muscle fiber. This force, propelled by movements of the cross bridges, arises from the overlapping thick and thin filaments in each sarcomere moving past each other. During this motion, known as the sliding-filament mechanism of muscle contraction, the lengths of the thick or thin filaments do not change. The myosin cross bridge attaches to a thin filament which moves in an arc during shortening. Shortening of the sarcomere occurs when the thin filaments at either end of the A band move toward the center of the sarcomere. The cross bridges repeat their swiveling motion many times resulting in

large displacements of the filaments, with each displacement being made up of a series of the small steps. The interactions of the two contractile proteins myosin and actin along with the energy provided from ATP produce the muscle fiber's ability to generate force and movement. Two intertwined helical chains of the polymerized globular protein actin makes up the thin filament. Myosin is made up of a globular heads attached to a long tail. These tails lie along the axis of the thick filament and the globular heads extend out to the sides forming the cross bridges. The cross bridges are formed from the myosin tails which lie along the axis of the thick filament and the globular heads which extend out to the sides. The myosin globular head contains a binding site for actin and an ATPase. This ATPase catalyzes the hydrolysis of ATP to ADP and inorganic phosphate (P_i) thereby releasing the chemical energy stored in ATP. Each cross-bridge cycle consists of four steps:

- Attachment of the cross bridge to a thin filament
- Movement of the cross bridge(i.e. movement of the thin filament)
- Detachment of the cross bridge
- Reattach to a thin filament and repeat the cycle.

During contraction only about 50 percent of the cross bridges of a thick filament are attached to the thin filaments and are producing movement, since each cross bridge undergoes its own cycle of motion independent of the other cross bridges.

Figure 3.2-1 illustrates the chemical and physical events that occur during the four steps of a cross-bridge cycle. Starting with Step 4, the ATP bound to myosin is split releasing chemical energy. This energy is transferred to myosin (M), producing an energized form of myosin (M*) to which the products of ATP hydrolysis, ADP and inorganic phosphate (P_i), are still bound.

Step 4:

$M \bullet ATP$ -- ATP hydrolysis -----> $M^* \bullet ADP \bullet P_i$

In Step 1 a new cross-bridge cycle begins with the binding of an energized myosin cross bridge to actin (A) in a thin-filament :

Step 1:

$A + M^* \bullet ADP \bullet P_i$ -- actin binding ---> $A \bullet M^* \bullet ADP \bullet P_i$

In step 2 a discharge of energy stored in energized myosin binding the myosin to actin triggers resulting motion of the bound cross bridge and the release of ADP and P_i.

Step 2:

$A \bullet M^* \bullet ADP \bullet P_i$ -- cross bridge movement --> $A \bullet M + ADP + P_i$

Myosin binds very firmly to actin and this linkage must be broken in order to allow the cross bridge to reattach to a new actin site and repeat the cycle. ATP binding to myosin is responsible for breaking the link between actin and myosin in step 3. Thus, ATP controls the binding of actin to myosin.

Step 3:

$A \bullet M + ADP + P_i$ -- cross bridge disassociation from actin ----> $A + M \bullet ATP$

Following the disassociation of actin and myosin in step 3, the ATP bound to myosin is split in step 4, thus forming the energized state of myosin (M*), which can now reattach to a new site on the actin filament and repeat the cycle.

Rigor mortis, the stiffening of skeletal muscles that begins several hours after death, illustrates the importance of ATP in dissociating actin and myosin during step 3 of a cross-bridge cycle. The nutrients and oxygen required by the metabolic pathways to form ATP decline after death and therefore the ATP concentration in muscle cells decreases. The myosin cross bridges can bind to actin in the absence of ATP but the resulting breakage of the link between actin and myosin can not occur because these events require the binding of ATP. Immobilized, rigid cross bridges bind the thick and thin filaments. Disintegration of muscle tissue and denatured proteins cause the stiffness of rigor mortis disappears about 48 to 60 hours after death.

Troponin and tropomyosin, located on the thin filaments, are two regulator proteins which prevent the cross bridges from interacting with actin. Two intertwined polypeptides which are arranged end to end along the actin double helix make up the rod-shaped tropomyosin molecule. The cross bridges are prevented from making contact with the myosin-binding site on each actin with the tropomyosin molecule partially covering the binding site. The smaller globular protein troponin binds to both tropomyosin and actin thereby holding the tropomyosin in this blocking position.

The skeletal-muscle plasma membrane is an excitable membrane capable of generating and propagating action potentials. The concentration of Ca^{+2} in the cytosol surrounding the thick and thin filaments is very low in a resting muscle fiber. In this

resting stage very few of the calcium binding sites on troponin are occupied due to the low Ca^{+2} concentration (Figure 3.2-2). Following an action potential, removal of the blocking effect of tropomyosin and cross-bridge cycling occurs due to a rapid increase in cytosolic Ca^{+2} concentration. Ca^{+2} binds to troponin which changes the shape of troponin and allows tropomyosin to expose the myosin binding site on each actin molecule.

The sarcoplasmic reticulum is the source of the increased Ca^{+2} within the muscle fiber. The sarcoplasmic reticulum forms a series of sleeve like structures around each myofibril. The lateral sacs store Ca^{+2}, which is then released following membrane excitation. Two enlarged regions at each end of the sarcoplasmic reticulum are known as lateral sacs which store Ca^{+2} which is released following an action potential. Contraction will not cease until calcium is removed from troponin, and this is achieved by a lowering of the calcium concentration in the cytosol. The membranes of the sarcoplasmic reticulum contain primary active-transport proteins (Ca-ATPases) that pump calcium ions from the cytosol back into the lumen of the reticulum.

3.3 Tissue Constituents of Bovine Skeletal Muscle

Muscle contains water, protein, lipid (fat), carbohydrate, minerals, organic extractives and nucleic acids [Person and Young, 1989]. About 30-40% of the weight of a living mammal consists of skeletal muscle which provides the capacity for movement. Adipose tissue, which is a form of connective tissue, is important to the living muscle system by providing an energy storage site in the form of fat (lipid). Because collagen has such different acoustic properties from those of other tissue constituents it is of particular interest. For example, the elastic properties of soft tissue, largely determined by their collagen concentration, have been suggested to be responsible for the echographic visualizability [Fields and Dunn, 1973]. Therefore the collagen concentration in skeletal muscle has been the subject of much investigation. Since ultrasonic interaction with tissue occurs on the macromolecular level this research will examine the bovine tissue constituents of water, lipid (fat) and protein, particularly collagen.

3.3.1 Water

The size and space available between the molecules in the tissue is determined by the degree of water binding by water-protein and protein-protein interactions. The polar structure of the water molecule causes it to be attracted by both positive and negative charges. The positive and negative charges of glutamic acid and lysine residues of

muscle proteins attract the polar water molecules. By attracting themselves to the polar and charged groups on the muscle, the water molecules stabilize the water-protein interface by lowering the free energy of the system. The muscle proteins with non-polar side chains (e.g. alanine, leucine, valine) repel the water as do the triglycerides of adipose tissue, which explains the low water content of adipose tissue [Price and Schweigert, 1987]. Thus, charged and polar side groups of the muscle protein tend to be on the outside, and in contact with the water. Non-polar side groups tend to be on the hydrophobic interior of the protein [Stryer, 1988].

The myofibrillar proteins are the main water binding components in muscle. Muscle proteins are considered to be hydrophobic since they bind 300-360 g of water per 100 g of protein. Myofibrils bind 70% of the free water, the sarcomplasm contains 20% and 10% is bound by the connective tissue [Price and Schweigert, 1987].

Water is immobilized by the 3-dimensional myofilament network and the amount of water is dependent on the amount of space in the myofilament network [Person and Young, 1989]. Gains and losses of water are due to the swelling and shrinking of the myofilament lattice. When the muscle is contracted and the actin and myosin overlap, the space diminishes.

The water holding capacity of post-rigor muscle is poorly understood [Person and Young, 1989]. During post-rigor, immobilized water is bound in varying degrees with part of the water bound so tightly that it can only be driven off by heating at 100°C for several hours. Alteration in pH has a great influence on the water holding capacity of post-rigor muscle. The water holding capacity is at a minimum at pH 5.0 which is the isoelectric point of myosin and actin. Bovine muscle has a pH of 6.99 at initial postmortem, 5.74 at 24 hours, 5.57 at 48 hours, 5.46 at 72 hours and 5.36 at 96 hours [Person and Young, 1989].

3.3.2 Lipid

Fat and water content of muscles are inversely related [Person and Young, 1989]. It has been suggested that a good measure of either of these two components can be used for estimating the other. Animal fat is insoluble but extractable by non-polar solvents. Lipids have four functions in the living animal: (1) membrane structural component, (2) source of energy, (3) protective component and (4) involvement in cellular recognition.

Lipids are found in the plasma membrane. The structure of the membrane consists of 2 molecular layers of lipid molecules (mostly phospholipids) such that the hydrophobic, non-polar, fatty acid tails (fatty acid moieties) are aligned together, leaving the hydrophilic, polar, head groups facing outward [Alberts et al., 1989].

Lipids in adipose tissue contain a large amount of triglyceride (98-99%) [Garton, 1976]. The triglyceride consists of all 3 hydroxyl groups on the glycerol molecule being esterified with a fatty acid chain. The fatty acids of the triglyceride are mainly palmitic acid, palmitoleic acid, stearic acid or oleic acid. However, the fatty acid composition of the triglyceride of adipose tissue can vary considerably between anatomical sites, for example, between internal and external tissue.

3.3.3 Collagen

Collagen is a fibrous protein present in multicellular organisms. Collagen is known for it high tensile strength due to its forming insoluble fibers. Skin, bone, tendon, cartilage, cornea, blood vessels and muscle all contain collagen; these organs or tissues constitute a quarter of mammalian weight. Collagen's structural motif allows for modification to meet specialized needs for different tissues and to hold cells together in discrete structures. A collagen fiber of 1 mm diameter is estimated to be able to suspend a 20 lb. weight.

The building block of collagen is a monomer which is constructed into polymers. Each monomer is made of three long, helical polypeptide chains known as α–chains. Hydrogen bonding holds the α–chains together. A list of the different types of collagen is identified in Table 3.3.3-1 [Karp, 1984; Kühn, 1987]. Collagen molecules known as procollagen are helical and form a super helix of the subunits. Procollagen is the precursor of collagen. The molecule is about 2900 Å long and has a diameter of 17 Å making for a thin elongated structure. Each α-chain has a length of approximately 1000 amino acids. It is interesting to note that every third residue is a glycine which occurs where the helix turns inside the procollagen such that there is very little room for amino acid side chains. Glysine is the only residue that can fit in the interior of the procollagen. Proline also makes up a large portion of the amino acid residues which, along with lysine, become hydroxylated. Stability of the triple helix comes from the hydrogen bonds that occur from the hydroxylated amino acids [Karp, 1984].

The hydroxlylation of proline and lysine occurs in a postsynthetic (posttranslational) modification which means that hydroxlyation of proline and lysine occurs after the amino acids have been formed into peptide chains. The collagen triple helix structure becomes unstable and denatured at 25°C if the hydroxlylation event is blocked. A consequence of blocking hydroxlylation of an a chain of collagen is the exhibition of the symptoms of vitamin C deficiency or scurvy. Vitamin C or ascorbic acid is required in the collagen hydroxylation reaction. Without this enzymatic process the collagen structure lacks sufficient hydroxyl groups to have its necessary structure.

The α–chains of collagen are synthesized as long molecules known as pro-a chains [Karp, 1984; Stryer, 1988]. At the N-terminal end is an additional fragment of 20,000 molecular weight; at the C-terminal end there is a fragment of 35000 molecular weight. These fragments are later removed. The procollagen is converted into troprocollagen by the enzyme procollagen pepidase. The extra pieces are involved in getting the a chains to align and bind together in a tropocollagen. Disulfide bonds link the pro-α chains together between the cystine residues and the additional terminal fragments. Procollagen then forms the collagen molecule outside the cell by protolytic enzymes. Additional amino acids are removed; certain cogenitial diseases characterized by connective tissue problems are brought on by failure to remove these amino acids.

Collagen molecules are then organized into collagen fibers as they are found in connective tissue. Extracellular enzymes cause collagen to be covalently cross-linked within the collagen molecule and between collagen chains. Collagen fibers become more insoluble as cross-linking increases until the collagen fiber can not be removed even in acidic conditions.

Composition of collagen depends on the type of collagen (Table 3.3.3-1). The most prevalent species is type I collagen which consists of two chains of α1(I) and one of α2(I). Collagen type II consists of three identical chains of collagen α1(III). In the beginning stages of forming the collagen chain the proline residues are converted into hydroxylproline by the enzyme proly-hydroxylase which acts as a dioxygenase [Stryer, 1988]. The C-4 of proline gets attached to the O_2, creating an additional molecule which goes to form succinate from α-ketoglutarate. If, and only if, the proline is located on the amino acid side of a glycine residue will it be hydroxylated on the C-4 position. Lysine residues become hydroxylated in a similar manner by lysyl hydroxylase except at the C-5 position.

A disaccharide of glucose and galactose is covalently bound to the hydroxylysine residue [Stryer, 1988]. The enzymes galactosyl transferase and glucosyl transferase are responsible for the attachment to the carbohydrate units. The number of carbohydrate units per tropocollagen (collagen without the covalent cross-links) depends on the type of collagen. Sheets of collagen (type IV) are rich in carbohydrates while fibrils (type I) have little carbohydrates.

Collagen fibers are formed from row-arrays of the 3000 Å tropocollagen separated by 680 Å between rows. Within a row-array each tropocollagen is sequentially separated by a 400 Å gap or hole which is important in cross-linking. These gaps are suggested to be important in bone formation. Bone consists of two phases; one phase is an inorganic phase, calcium phosphate, the other is an organic phase, collagen. Collagen

is needed for the deposition of calcium phosphate crystals to form bone. The holes or gaps are nucleation site for calcium deposits.

Covalent cross-links are formed by lysine and hydroxylysine residues. The enzyme lysyl oxidase is involved in the process of converting the e-amino of the residue to an aldehyde. Lysine side chains are precursors for inter-molecular cross-links in collagen. Aldehyde derivatives of the lysine residues undergo an aldol condensation. The carboxyl group of the aldehyde is combined with the enolated ion of the other aldehyde. Joining of one lysine residue and two hydroxylysine residues forms the intermolecular process which is called a hydroxypyridinium cross-link. Four residues in a tropocollagen are involved in the cross-link. These are two lysines, one near the amino terminus and one near the carboxyl terminus, and hydroxylysines in helical regions by the end of the molecule. The physiological function and tissue age is responsible for the extent of cross-linking. The Achilles tendon has highly cross-linked collagen. In contrast, a rat's flexible tail has much less.

Type I, II and III collagen is found in muscle in varying levels depending on the muscle classification. Divalent and trivalent cross-links are at intermolecular and intramolecular locations. Generally there is an increasing total collagen cross-linking with increasing age in bovines.

There is evidence that there are age related changes of collagen in slow, fast, and cardiac muscle of rats [Mohan and Radha, 1980]. Working with an age range of albino rats from 5 to 25 months it was found that collagen levels increased 30% in slow muscle, 40% in fast muscle and 50% in cardiac muscle with increasing age. The collagen from the muscles of older animals was found to be less sensitive to collagenases than the younger animal muscle.

3.3.4 Muscle Proteins

With intact skeletal muscle, 75% of the volume is made up by myofibrils with the remaining volume consisting of stromal and sarcoplasmic proteins flowing around and through the skeletal muscle fibers and connective tissue. The muscle can be considered to have two distinct sets of cytoskeletal filaments which are continuous and extensible. One set consists of the thick and thin filaments within the sarcomere which is considered to be the endosarcomeric lattice. The other network enveloping each sarcomere and connecting other cell muscle organelles is called the exosarcomeric lattice. The major protein components of vertebrate skeletal myofibrils are identified in Table 3.3.4-1.

Both the endosarcomeric and exosarcomeric lattice offer the role of structural scaffolding and contribute to the elastic properties of tension and compliance. The

structural purpose of the endosarcomeric lattice is to supply scaffolding for the thick and thin filaments along with modulation of the thin filament arrangement. The exosarcomeric lattice supplies scaffolding for the sarcomere. Mechanically both the endosarcomeric and exosarcomeric lattice offer elastic properties and resting tension. A model of the organization of the filaments in skeletal muscle cells is shown in Figure 3.3.4-1 [Wang, 1985].

Four individual proteins make up almost 80% of the total myofibril content. Myosin and actin are the structural proteins that make up the myofibrils. The major function of myosin and actin is contraction of the sarcomere of the myofibril. These myofibrillar proteins are responsible for contraction in the living muscle and rigor mortis in the postmortem muscle. The function and physical size of actin, myosin, troponin and tropomyosin were discussed in previous section and Table 3.3.4-1 lists the known molecular weights of these proteins.

The actin binding protein, α-actin, is a binding protein is found in the Z-disks. Actin filaments are anchored by their ends to the Z disk where they are held in a square lattice arrangement by their proteins. Purified α-actin is a rod shaped molecule which can bundle actin filaments together into parallel arrays. A similar function may be performed by myomesin which cross-links adjacent myosin filaments at the M-Line. Filamin is a large structural protein (500 kDa) isolated from the Z-disk with a diameter of 4 nm. Unfortunately this protein has not been well characterized [Wang, 1985].

Myofibrils also contain a system of highly insoluble protein filaments which can be isolated after all the actin and myosin has been actively extracted from the sarcomere. One set of these filaments is a large protein called titin once thought to be connectin. Titin run parallel to the thick and thin filaments in the sarcomere and attaches the think filaments to the Z disks. These titin filaments are very elastic and are hypothesized to act as springs to help keep the think filaments centered in the Z disks.

3.3.5 Tissue Constituents based on Muscle Group

The discussion of muscle thus far has given general numerical values of the percentage of water, fat, protein and collagen in bovine skeletal muscle. However these values vary for different muscle groups. Specific collagen content plays an important role in affecting the ultrasonic attenuation and backscatter of the tissues [Mimbs et al., 1981; O'Donnell et al., 1979]. Since each skeletal muscle type has a different total collagen content, percent water and percent fat, it would not be surprising to find differing acoustic properties related to the tissue content. Also, similar tissue types will produce different acoustic signatures depending on whether the muscle is in a diseased

state. The high fat content of dystrophic muscle gives rise to echographic visibility of ultrasonic images [Lamminen et al., 1988; Heckmatt et al., 1982; Dock et al., 1990]. There are also indications that the sarcomere length affects the scattering of the tissue [Glueck et al., 1985; O'Brien et al, 1995].

Based on this information it is important to know a value for the percentage of water, fat and collagen of the skeletal muscle under investigation. Table 3.3.5-1 lists 13 different bovine skeletal muscles types by their anatomical, wholesale and retail cut names since an element of familiarity can be gained by associating the well known commerical names with the anatomical name. Yet with respect to this research, it would be functional to rank the muscle groups by percentage of water, fat, collagen and sarcomere length listed in Table3.3.5-2 [McKeith et al., 1985; Brackebusch, 1988]. The longissimus dorsi is abbreviated LD and the psoas major and the LD-Loin are highlighted in the table for comparison since these are the skeletal groups used in this research. What should be pointed out in the table is that the psoas major and the LD-Loin are very similar in the tissue constituents of collagen content, percent water and percent fat. Moreover, the psoas major (3.46 μm) has almost twice the sarcomere length of the LD-Loin (1.84 μm). These similarities and variances in the psoas major and the LD-Loin will be examined in more detail in a later section.

4. ULTRASONIC PROPAGATION PROPERTIES OF SKELETAL MUSCLE: PREVIOUS RESULTS

Ultrasonic propagation properties such as attenuation and speed correlate well with the constituents of skeletal muscle. This section is a literature survey of the ultrasonic propagation properties of muscle tissue with the emphasis on skeletal muscle. To get a clear understanding of the interaction between ultrasound and skeletal muscle it is important to first see how ultrasound interacts with the constituents of the muscle. This discussion begins by examining the acoustic properties of water, fat, protein and collagen. Section 4.2 is a literature survey and review of acoustic properties of bovine skeletal muscle. A review of past research will present a history of what problems and questions have been answered about the interaction of sound and tissue but point out what problems are still unsolved.

4.1 Constituents of Muscle

Ultrasonic propagation properties of tissue are largely determined at the molecular level i.e. basic tissue constituents such as water, fat and protein (particularly collagen).. Attenuation as a function of frequency and temperature in tissue was determined many years ago [Dunn, 1969]. Carstensen et al. (1953) determined that the total protein content of blood was proportional to the attenuation.

Of all the tissue constituents, water is the most abundant making up about 70%-80% of all tissue. The general trend for the attenuation coefficient is that it decreases for an increasing percentage of water. Since water is both isotropic and homogeneous, the ultrasonic absorption is considered to be equal to the attenuation. The absorption of water is below that of tissue but the values for the ultrasonic speed are comparable to those of tissue [Johnston et al., 1979]. There exists many theoretical predictions for the temperature dependence of the speed of sound in water based on empirical data [Bhatia, 1967; Miller and Kubinski, 1975]. For example, from Kinsler et al. (1989), the numerical formula for the speed of sound in water is

$$c(P,t) = 1402.7 + 488t - 482t^2 + 135^3 + (15.9 + 2.8t + 2.4t^2)(Pg/100) \qquad (4.1\text{-}1)$$

where Pg is the gauge pressure in bars and t =T/100, with T in °C. Equation 4.1-1 is suggested to be accurate to within 0.05% for $0 \le T \le 100$°C and $0 \le Pg \le 200$ bar (1 bar = 10^5 Pa). Figure 4.1-1 displays the temperature dependency of water from empirical data; the graph plots the speed of sound of distilled, degassed water versus temperature at a pressure of 1.013 x 10^5 Pa [Dunn et al., 1969]. These results agrees with equation 4.1-1

to within 0.04%. The measured ultrasonic absorption of water is proportional to the square of the frequency. At 37°C, the frequency-free absorption coefficient, a/f^2 has a value of 15.7×10^{-17} s^2/cm [Pinkerton, 1949].

Based on studies which have examined attenuation characteristics of proteins in solution, proteins seem to be largely responsible for tissue attenuation [Dunn and O'Brien, 1977]. With proteins in solution a certain amount of water becomes associated with the protein and the perturbation of the hydration layer between the water and the protein gives rise to the attenuation. Also, increasing protein content in tissue exhibits an increase in the attenuation coefficient. At a frequency of 1 MHz tendon was found to differ from testis in attenuation by one order in magnitude [Johnston et al, 1979]. In accounting for the ultrasonic attenuation exhibited by soft tissue several types of mechanisms have been considered. These mechanisms involve structural and chemical relaxation of the macromolecular constituents and processes arising from the inhomogeneous nature of the tissue including scattering, viscous relative motion and thermal losses [O'Donnell and Miller, 1979]. There also exists a trend of increasing absorption versus increasing molecular weight of the protein [Kessler et al., 1970]. It was found that the attenuation coefficient increases as a function of molecular weight for a solution of polyethylene glycol up to a molecular weight of 10,000.

Collagen is one of the most abundant proteins in the body giving the tissue strength, elasticity and structure. The ultrasonic propagation properties of tissue are affected by the collagen content because of its high Young's Modulus. Hence the ultrasonic speed increases with increasing collagen content since the speed is proportional to the square root of the modulus of the material [Fields and Dunn, 1973; Kinsler et al., 1982; Agemura et al., 1990]. In general, high collagen content tissues such as tendon or articular cartilage have the highest attenuation coefficient values. Table 4.1-1 lists the collagen content for various collagen containing tissues compared to the attenuation (at 1 MHz) and speed [Johnston et al., 1979]. The attenuation and speed are found to increase for increasing collagen content. The suggested mechanism for attenuation is due to structural relaxation.

Figure 4.1-2 is a graph of the attenuation coefficient versus frequency (0.5-7 MHz) for tendon, heart and liver [Goss et al., 1979]. The purpose of introducing this graph is to show the general trend of attenuation versus frequency for biological tissues of varying constituents. Tendon, which has a high protein content (35-40%), high collagen content (32%), low lipid content (1%), and low water content (63%) also has a higher attenuation than heart muscle and liver. A middle range attenuation coefficient is found for heart muscle which has a total protein content of 16.5%, collagen content of 1.7%, lipid content

of 2.6% and water content of 72%. Liver which has the lowest attenuation also has a total protein content of 18%, collagen content of 0.4%, and water content of 71%. These data indicate that high collagen content (tendon) exhibits a high attenuation coefficient and low collagen content (liver) exhibits a low attenuation coefficient [Goss et al., 1979].

Fat is a water free tissue (adipose tissue contains about 10% water) and the amount of body water is inversely proportional to the total amount of body fat [Haney and O'Brien, 1986]. The ultrasonic propagation properties show that fat increases in attenuation over a frequency range of 1-10 MHz although it is about a magnitude lower than muscle. At 100 MHz, for increasing percentage of fat the attenuation increases while the ultrasonic speed decreases for fatty rat liver [Tervola et al., 1985].

For bovine peritoneal fat (consisting of mesothelium and a thin layer of irregular connective tissue that lines the abdominal cavity and covers most of the viscera), Bamber and Hill (1979) found a decrease in the ultrasonic speed with increasing temperature. Figure 4.1-3 is plot of the Bamber and Hill ultrasonic speed versus temperature (10, 20, 30, 44 and 60°C) for bovine peritoneal fat. The error in the speed data was reported to be no greater than 1%. Bamber and Hill also measured the attenuation as a function of frequency (1-7 MHz) and temperature (10, 20, 30, 37 and 60°C) of bovine peritoneal fat (Figure 4.1-4). Attenuation was measured by spectrum analysis technique and the error in the data was reported to be 10%. Examining the attenuation as a function of frequency at one temperature (e.g. 30°C), the attenuation increases with increasing frequency. In contrast, when examining the attenuation as a function of temperature at one temperature (e.g. 1 MHz), the attenuation is 6 dB/cm at 10°C, decreases to around 2 dB/cm for 30-37°C and then increases to 3 dB/cm at a higher temperature of 60°C. Bamber and Hill noted that this reversal occurs at roughly the temperature at which large biological molecules become denatured. Another explanation suggested by Bamber and Hill is that the effect is the result of gas produced, during the experiment by decaying tissues. This reversal is exhibited for all the attenuation measurements as a function of temperature at one particular frequency.

4.2 Skeletal Muscle

Ultrasonic attenuation in muscle varies depending on a number of factors such as frequency, temperature, time of excision, type of muscle, insonification angle and state of contraction. The purpose of this section is to survey and review the literature of all known attenuation coefficient and speed data for bovine skeletal muscle. A review of past research will furnish a history of what problems and questions have been answered about the interaction of sound and tissue but also point out what problems are still unsolved.

Table 4.2-1 lists all the attenuation coefficient and speed data for bovine skeletal muscle starting from Hueter's research on bovine tongue in 1948. The table also lists the type of skeletal muscle used (i.e. longissimus dorsi, semitendinosis) if known and the method by which the measurements were made. Since this is also a review of the literature, there is an additional column for comments by this author since some results have not been successfully reproduced but are listed for completeness. The following paragraphs highlight and review pertinent results pertaining to this research and point out efficacy and inadequacies in the quest for understanding ultrasonic propagation properties.

Some of the earliest work examining attenuation as a function of fiber orientation angle was performed by Colombati and Petralia, 1950. They measured the attenuation of fresh bovine gluteal (related to the gluteus maximus) muscle over a temperature range of 15-18°C using the total acoustic power technique at frequencies of 0.3, 0.87, 1.7 and 3.4 MHz. Their results are plotted in Figure 4.2-1. Other research examining the attenuation as a function of fiber orientation angle was done by Dussick and Fritch, 1956. They measured attenuation of fresh bovine striated muscle using the pulsed transmission technique in a temperature range of 26-28°C for frequencies of 1, 3 and 5 MHz parallel and perpendicular to the muscle fiber. The Dussick and Fritch results are also plotted in Figure 4.2-1 for the purpose of comparing them to the Colombati and Petralia results. Both research demonstrate a higher attenuation for ultrasound insonification parallel to the muscle fiber as compared to perpendicular. The research by these investigators, albeit interesting, did not report the type of skeletal muscle used in their experiments and did not explain the source of the large standard error in their attenuation results.

The variance in ultrasonic attenuation in different muscle type was demonstrated by Marcus, 1973. Marcus measured the attenuation of three different muscle types using the pulse transmission technique at 2.1 MHz. The commercial name of these 3 muscle types are the sirloin tip, center cut and porterhouse. The sirloin tip contained slight fat marbling, the center cut was marbled and banded with fat and the porterhouse was heavily marbled. The results are graphed in Figure 4.2-2. These data seem to suggest that there is a difference in attenuation for different muscle types. However, the results lack other important information such as fiber orientation, error information of attenuation results and information on the number of samples run. Also the porterhouse and sirloin attenuation versus temperature results are in opposite directions from each other.

Other research demonstrating the variance in ultrasonic attenuation in different muscle types has been performed by Dussick and Fritch, 1955. Dussick and Fritch measured the attenuation of bovine diaphragm, thigh (adductor) and thigh (quadriceps) muscles. The results are listed are part of Table 4.2-1. Again the results suggest that there

is a difference in attenuation for different muscle types; however this research did not report any information about temperature or frequency.

Work done by Shore et al. (1986) examined the attenuation coefficient of post-rigor bovine skeletal muscle (semitendinosus) using a pulse transmission method. For the attenuation measurements, Shore, et al. measured the attenuation with the ultrasound beam parallel to the muscle fibers and used temperatures of -20, 0, 20 and 40°C and frequencies of 2, 3, 4, 5, 6 and 7 MHz. Figure 4.2-3 graphs the data listed in paper. The error in the attenuation measurements ranges from 0.128-0.15 dB/cm. However only 7 different muscle samples were measured for each temperature. This same paper, Shore et al. reports the attenuation of ultrasound parallel and perpendicular to the muscle fibers at 20°C for frequencies of 2, 4 and 7 MHz. A graph of these data are plotted in Figure 4.2-4. No error is reported for these data and only 2 muscle samples were used for this experiment.

Woods and Miles (1986) measured the ultrasonic speed in fat trimmed homogenates of bovine skeletal muscle, (*musculus longissimus thoracis et lumborum)*) which typically have a low connective tissue content with a collagen content of 0.6%. The ultrasonic speed versus temperature at 0, 20 and 37°C is plotted in Figure 4.2-5 from the data listed in the report [Woods and Miles, 1986]. These data do not report the number of muscle samples measured at each temperature.

With respect to anisotropy, the work by Shore and Miles (1988) used homogenized muscle of instead of intact muscle bovine muscle and suspensions of myofibrils to measure the attenuation coefficient. Although this research did not directly address the issue of anisotropy, Shore and Miles found that when the myofibrils were exposed to a high concentration of KCl the thick filaments of the sliding lattice dissolved releasing myosin into solution. Myofibrils treated in this manner had a slightly lower attenuation which suggested that the myosin filaments had an attenuation effect.

The research by May, 1986 correlated anisotropy of *M. sternomandibularis* with a stretched and cold shortened muscle. Cold-shortened muscle is skeletal muscle which is exposed to temperatures of 0°-15°C before the onset of rigor which results in the myofibrils shortening 60% of its rest length. Cold-shortened muscle enter rigor sooner than non cold-shortened muscle and the high degree of overlap causes the muscle to be tough. In contrast, muscle stretched using weights is found to be more tender. May (1986) found that the cold-shortened muscle (shorter myofibril length) had a higher attenuation coefficient than the stretched muscle (longer myofibril length). Although these results were not found to be significant and sarcomere length after stretching is unknown the general relation between the attenuation and myofibril length is consistent with the

results in this dissertation which determines the effect of sarcomere length on the acoustic attenuation coefficient.

The ultrasonic speed of sound also seems to vary with different muscle types and temperature as suggested by a compilation of speed results listed in Table 4.2-1. Table 4.2-1 is used in conjunction with Figure 4.2-6 to distinguish the different velocity values used for each muscle type. Much of the reported tissue type is unspecified [Lidwig and Struthers, 1949; Hara et al., 1979] and only one speed value reports whether the ultrasound measurement was performed parallel or perpendicular to the muscle fiber [Dussick and Fitch, 1956]. The muscle samples used for the speed measurements performed by Marcus (1973) are the same as the attenuation measurements described early in this section. Speed measurements by Rich et al., did not report exposure temperature. Since the acoustic speed is known to vary as a function of orientation and temperature which yields information about the structure, density and other physical parameters of the muscle it seems natural that this body of knowledge has been neglected from the acoustic propagation research.

In summary research examining the attenuation coefficient and speed of sound of bovine skeletal tissue is sparse and incomplete. Some work [Dussik and Fritch, 1956; Colobati and Pertlia, 1950] reports fiber orientation but does not report the type of muscle used. This information is important since tissue constituents vary in different muscle types which can lead to different attenuation coefficient values. For example, the work of Marcus examining the different tissue types is somewhat contradictory. Most relevant to this research is the work investigated by May (1986) which indicates that myofibril length effects the acoustic propagation properties. The incompleteness of previous investigations provides the major impetus for this research thesis.

5. INSTRUMENTATION

This chapter describes the instrumentation of the scanning laser acoustic microscope (SLAM) which is used for determining the attenuation coefficient, speed of sound and heterogeneity index in tissue at 100 MHz and the Daedal exposimetry system (DES) which has been developed for characterizing the tissue over a frequency range of 2-7 MHz and temperatures of 4, 20 and 37°C.

5.1 SLAM

The SLAM, which operates at a frequency of 100 MHz, is used to determine the attenuation coefficient, propagation speed and heterogeneity index of the skeletal muscle. Over the past several years the SLAM (Sonomicroscope 100, Sonoscan Inc., Bensenville, IL) has been successfully used in determining the propagation properties in studies of wound healing [Olerud et al., 1990], fatty liver [Tervola et al., 1985a] and ischemic myocardium [Sagar et al., 1990]. Details of the operation of the SLAM have been published previously [Tervola et al., 1985b, Tervola et al., 1985c, Steiger, 1986, Agemura, 1986, Nicozisin, 1989] and will be described briefly in this section.

Figure 5.1-1 shows a block diagram of the SLAM. Operating at a frequency of 100 MHz, a piezoelectric transducer produces sound which propagates through the fused silica stage. The muscle tissue sample is placed on the ultrasonically activated stage supported by a 25 μm sheet of mylar. The sample rests in a thin layer of normal saline and is covered with a semireflective coverslip. A dynamic ripple or surface displacement from the reflection from the coverslip surface, whose amplitude is proportional to the transmitted acoustic pressure, is detected from a focused scanning laser beam probe. The laser light transmitted through the muscle sample and coverslip is processed to produce an acoustic image and an interference image. The acoustic image is used in determining the attenuation coefficient and the interference image is used in calculating the speed. A video monitor displays both images of the tissue specimen area measuring approximately 3 x 2 mm at approximately 100x.

The amplitude of the dynamic ripple at any given position is dependent on the reflection angle of the laser light. The light falling on the photodiode is partially blocked by a knife edge which is placed in the path of the reflected light. The amount of light blocked depends on the angle of the reflected laser light which allows the angular modulation to be converted to light intensity modulation. An electrical signal, proportional to the ripple amplitude, is then produced from the light intensity modulation.

To determine the attenuation coefficient, the acoustic amplitude image displays the spatial amplitude of the acoustic field after passing through the tissue sample (Figure 5.1-

2a). Dark areas on the video monitor represent areas of low ultrasonic energy while bright areas correspond to high ultrasonic energy. The spatial resolution, which is approximately 20 μm, is limited by the acoustic wavelength and laser beam size.

The interference-mode image is produced by adding a reference signal, phase coherent with the transmitted acoustic wave, to the received signal with the transmitted acoustic wave (Figure 5.1-2b). The interferogram consists of 39 vertical interference lines which are equally spaced at 85 μm. The interference-mode image consists of alternating light and dark vertical bands or fringes which correspond to equal phase wavefronts of the ultrasonic field. Bending of the vertical bands to the right or left correspond to increasing or decreasing speeds in the sample relative to the reference medium.

A fraction of the laser beam penetrates the sample through a semitransparent coverslip. The transmitted laser beam is collected by a separate photodiode and is processed and displayed on a second video monitor as the optical image. Acoustic energy is coupled to the tissue sample by the stage which also mechanically supports and illuminates the specimen at the desired angle. The construction of the stage is such that the gold-plated surface of the coverslip rests within the near field of the sound image. The sound beam strikes the quartz surface at an angle of 45° and refracts into the water at 10°.

The acoustic and interference images are digitized by a Data Translation DT2851 high resolution frame grabber which includes software (DT-IRIS) that performs frame averaging, convolutions for filtering and histograms for determining dynamic range. The software utilizes the digitized video images for calculating the attenuation coefficient, speed and heterogeneity index. A more detailed description of the SLAM data acquisition system can be found elsewhere [Nicozisin, 1989].

5.2 DES

The DES has been developed in the Bioacoustics Research Laboratory for determining ultrasonic propagation properties of biological and non-biological materials. This system has also been used for accurate and precise quantification of the acoustic field characteristics of ultrasonic transducers for either medical or scientific purposes. The purpose of this section is to describe the ultrasonic, electrical and mechanical equipment used for the measurement. Basically, ultrasonic propagation property information is derived from placing a tissue sample between a transmitting transducer and a receiving hydrophone as seen in Figure 5.2-1. Waveforms received by the hydrophone on an oscilloscope from a pulse transmitted through the tissue are stored and processed by a computer. The tissue sample is automatically moved through the ultrasound field for multiple measurements by a computer controlled motion system.

A single-cycle gated sine wave is supplied to the transducer by a series of three electronic instruments shown in Figure 5.2-2. Due to limitations of the equipment, a single-cycle square wave could not be used. The first instrument is a device built at the Bioacoustics Research Laboratory which supplies a pulse or gated signal to the HP 8116A pulse/function generator. The time length of the gated sine wave produced by the signal generator is controlled by this variable pulse device. The second instrument is the HP 8116A pulse/function generator. A continuous wave, low level, RF signal is supplied by the HP 8116A pulse/function generator. The HP 8116A is a multiwave programmable 50 MHz generator with a minimum amplitude of 10 mV peak-to-peak. Operation of the HP 8116A can be regulated manually or by the HP-IB computer control (HP8116A Function Generator Service Manual, 1984). The last instrument which amplifies the tone burst signal to the transducer is the ENI A150 Power Amplifier. The ENI A150 Power Amplifier is a 55 dB gain, RF power amplifier which operates over a frequency range of 0.3 to 35 MHz with a maximum power output of 150 watts (Broadband Power Amplifier Instruction Manual Model A150, 1987). The amplifier is not programmable and, therefore, cannot be controlled by the computer.

The basic experimental set-up for determining the acoustic propagation properties of a sample is shown in Figure 5.2-1. A 5 MHz, 1.905 cm diameter, unfocused Panametrics transducer (Model No. A308, Serial No. 4688, Panametrics, Inc. Waltman, MA) is shock excited by the voltage pulse from the ENI A150 Power Amplifier. The transducer produces a pulsed ultrasound signal at a frequency specified by the size of the transducer ceramic. The center frequency of the transducer at the axial maximum of 6.5 cm is approximately 4.5 MHz and has a 6 dB bandwidth of approximately 3 MHz.

Before a sample can be examined the hydrophone must be placed in the axial and lateral maximum of the propagating ultrasound field. Ultrasound signals can be detected by a polyvinyl difluoride bilaminar (PVDF) shielded membrane hydrophone manufactured by Sonic Technologies (Serial Number S/N:804-010, Hatboro, PA). The hydrophone has an active element of diameter 1 mm and cable length 70 cm. A signal detected by the hydrophone is recorded by the Tektronix 11400K Digitizing oscilloscope. Positioning of the hydrophone is performed by the Daedal Positioning System (Parker Daedal, Inc., Harrison, PA).

A block diagram connecting the mechanical and electrical devices used in the experiment is shown in Figure 5.2-2. The positioning system has 5 degrees of freedom made up of three linear and two rotational travels. Movement can be either be manually or computer controlled. The system consists of a superstructure, motors, shaft encoders, limit switches and an electromechanical brake. The rail tables of the superstructure for

linear or long travel have a scanning volume of 60.9 x 45.7 x 45.7 cm. Each English stainless steel leadscrew for linear travel in any direction has a 5 pitch resolution. The rail table incorporates 0.51 cm lead precision-ground ball screws to provide repeatability of +/- 1.27 μm. The base axis is made of two pieces which are 15.24 cm wide x 81.28 cm long with a 3.18 cm leadscrew diameter. The vertical axis consists of two pieces of 15.24 cm wide x 66.1 cm long, and a lead screw 1.59 cm in diameter. Both the base and vertical axis hold a 45.7 cm travel rail with the right linear table following the left table to within 76.2 mm. The horizontal axis is actuated by a rail table with 60.9 cm of travel. Full 360° and partial (10 or -10°) rotational motion make up the final two degrees of freedom.

The five axis motor control system consist of 4 motor drivers (115 VAC / 1 AMP) for microstepping motor control. The base and vertical axes have drivers for synchronized operation. The base axis travel is propelled by a standard NEMA 34 frame size flange mount motor while all other axis are powered by a NEMA 23 size motor. The NEMA 34 motors for the base axis each has a static torque of 380 oz-in. The NEMA 23 motors which actuate the remaining linear and rotational axis each has a static torque of 80 oz-in and a rotational inertia of 1.28 $(\text{oz-in})^2$. Each motor operates at 20,000 motor steps/revolution.

The motors which control travel run in a closed feedback loop. Position information is read by linear and rotary encoders rather than angular displacement of the motor shaft. Resolution linear encoders provide position information of 1 micrometer with a +/-0.005 mm accuracy. Rotary encoders have a 0.01 degree resolution. Two motor controllers for all of the axes are made up of a motor indexer and IEEE-488 interface communications. The indexer is a microprocessor based programmable pulse generator for control of pulse rates and total pulse count for conversion to motor power, and displays the encoder position for each axis. IEEE-488 communication allows movements of the system to be programmed from a PC, and the controller has the capability to generate interrupts on the GPIB bus. Limit and home/zero information is also handled through the controller.

The signals from the hydrophone are recorded and digitized by the 11401 oscilloscope. The Tektronix 11401 features precise signal acquisition circuitry, high resolution digitizer, and local intelligence. The digitizer allows for measurement of a wide variety of pulse and signal parameters automatically. The digitizing oscilloscope can amplify and measure twelve separate signal input channels and acquire and display eight signal input channels simultaneously. Waveform record lengths of 1024 bits to 10,240 bits can be stored for each displayed channel. The bandwidth of the oscilloscope is 1 GHz with 10 bits vertical resolution. The oscilloscope has a vertical accuracy of 2% and time base accuracy to within 100 ps + 0.001% of measurement interval.

The oscilloscope communicates using a GPIB-IEEE 488 industrial standard remote-control interface. The GPIB control software written by National Instruments is programmed in Microsoft C6.0. The host computer used to control the system and acquire data is a Tandy 4000 computer based on a 16 MHz Intel 80386 processor. This computer has two math coprocessors, one an Intel 80387 processor and the other a Weitek 1167 processor. This computer has 4 megabytes of core memory (expandable to 16 megabytes), 71 megabytes of hard drive storage, SuperVGA graphics, and is connected to the university network.

The ultrasound transducer, hydrophone and samples to be tested are submerged in a water tank (51 x 33 x 71 cm) filled with distilled, degassed water. The tank is made almost anechoic by placing 2.54 cm thick SOAB, sound absorbing material around the wall of the tank. To achieve the water temperatures of 4, 20 and 37°C for the surrounding medium of the tissue the temperature of the water is maintained by a Neslab RTE-110 (Neslab, Instruments, Inc. Newington, NH., 03801) water temperature controller which circulates water at a precise temperature through tubes in the tank. The degassed water is stirred occasionally to equilibrate the water temperature throughout the tank with a T-line Laboratory Stirrer (Talboys Engineering Corp., Emerson, NJ.). However the stirrer is not operated during data acquisition since it introduces unwanted electrical noise to the acquired waveform.

The instrumentation for determining the attenuation coefficient and speed and consists of a transmitting ultrasonic transducer (Panametrics 5 MHz, Model Number A308, Serial 4688) immersed in the 51 x 33 x 71 cm tank filled with degassed water, aligned axially with the receiving Sonic Technologies hydrophone (Serial Number S/N:804-010, Hatboro, PA). An amplified single cycle sine wave is supplied to the transducer by an HP 8116A pulse/function generator connected in series to a ENI A150 Power Amplifier which provides a pulse to the transducer and triggers the sweep of the Tektronix 11401 oscilloscope. The scope is used to display the received signal from the hydrophone. The displayed pulse waveform displayed on the oscilloscope is digitally recorded with 32 bit resolution and saved in a 2048 byte file.

6. METHODS

This chapter describes the methodology for determining the ultrasonic propagation properties for the SLAM and DES. A fundamental feature of any measurement is the knowledge of its uncertainty. Thus, the uncertainty of the acoustic properties determined using the SLAM and DES is assessed using materials with known acoustic properties. A series of 4 experiments described in the Specific Aims are required to carry out the goals of this research. Considerable care was taken to obtain and prepare the skeletal muscle samples used in the experiments with the SLAM or the DES. The following sections describe the methods for operating the SLAM and DES and describe the techniques for preparing the tissue sample for each experiment.

- (§6.1) Determination of the propagation properties using the SLAM. Estimation of the uncertainty.
- (§6.1) Determination of the propagation properties using the DES. Estimation of the uncertainty.
- (§6.3) Experiment #1: Determination of the constituents/myofibril length from the acoustic propagation properties using the SLAM.
- (§6.4) Experiment #2: Temperature-frequency dependence of the acoustic propagation properties: Constituents/Myofibril predictions using the DES.
- (§6.5) Experiment #3: Myofibrilar contribution to the acoustic propagation properties using the SLAM.
- (§6.6) Experiment #4: Anisotropy of the acoustic propagation properties of muscle using the SLAM and DES.

6.1 Acoustic Propagation Property Determination using the SLAM

This section describes the methodology for determining the attenuation coefficient, speed of sound and heterogeneity index using the SLAM. Also described in this section is the method for determining the uncertainty of speed and attenuation coefficient using homogeneous liquids with known acoustic properties.

6.1.1 Attenuation Coefficient

The estimation of the attenuation coefficient uses the insertion loss procedure which compares the received signal amplitude of the specimen of known thickness in the sound path with that of a reference medium (saline) [Tervola et al., 1985b]. For determining the insertion loss, a subimage area (the brightest, most uniform) of approximately 400 x 250 μm is chosen which minimizes the effects of the ultrasonic field nonuniforminity over the whole image area. The sample is placed on a mylar sheet (25 μm thick) that is coupled to

the acoustic wave of the SLAM stage using degassed, distilled water. The subimage area is acquired using the DT2851 frame grabber and digitized to yield an average amplitude value (V), that is, the average of these subimage areas mathematically described in the following equation.

$$V = 10\log\left\{\frac{1}{n}\sum_{i}^{n}\left[\left(\frac{1}{3072}\right)\sum_{i=y}^{y+31}\sum_{j=x}^{x+95}\left(v_{ij} - r_i\right)\right]\right\} \qquad (6.1.1\text{-}1)$$

where V = the mean of the image area averages expressed in dB,
n = the number of times the imaging area is averaged,
i = image row index,
j = image column index,
y = starting row number of image area,
x = starting row number of image area,
V_{ij} = digitized value of the pixel at the i^{th} row and j^{th} column and
r_i = average reference level of the i^{th} row (raster line).

The signals received from the subimaged area are digitized to yield an average amplitude value recorded for the tissue sample (V_S) and the saline reference medium (V_r). The insertion loss (IL), in dB, is determined using

$$IL = V_S - V_r \qquad (6.1.1\text{-}2)$$

where V_r is the average of the recorded values for the normal saline and V_S is the individual values from the sample, each in dB.

Five insertion loss values are obtained for each specimen thickness. The insertion loss for three different thicknesses are used for determining the attenuation coefficient. A linear least-squares fit utilizing all of the insertion loss and thickness values is used to determine the slope of insertion loss versus specimen thickness yielding the attenuation coefficient (Figure 6.1.1-1).

6.1.2 Speed

Speed is determined from the interference image using a spatial frequency domain technique [Tervola and O'Brien, 1985]. The field of view (3 mm horizontal and 2 mm vertical) displays approximately 39 equally spaced (by 85 μm) vertical interference lines which covers the specimen and the reference medium of known speed. The phase shift of

the vertical interference lines due to the muscle sample is used to estimate the propagation speed according to Equation 6.1.2-1.

$$C_x = \left(\frac{C_o}{\sin\theta_o}\right)\sin\left\{\tan^{-1}\left[\frac{1}{\left(\frac{1}{\tan\theta_o}\right)-\left(\frac{N\lambda_o}{T\sin\theta_o}\right)}\right]\right\} \qquad (6.1.2\text{-}1)$$

where C_x = speed of sound in the specimen of interest,

C_o = speed of sound in the reference medium,

θ_o = angle of the sound from the normal in the reference medium,

$\lambda_o = C_o/f$, (f = 100MHz)

N = normalized fringe shift and

T = specimen thickness.

The value for θ_o can be determined from Snell's Law using,

$$\theta_o = \sin^{-1}\left[\frac{C_o}{C_s}\sin\theta_s\right] \qquad (6.1.2\text{-}2)$$

where C_S = speed of sound in the fused silica stage (5968 m/s),

θ_S = angle at which the sound waves are traveling through the stage (45°) and

C_O = speed of sound in saline at 30° (1520 m/s).

Using these values, Equation 6.1.2-2 yields $\theta_O = 10.4°$.

The spatial frequency domain technique is used to determine N, the normalized fringe shift (i.e. the amount of lateral fringe shift relative to fringe spacing) in the frequency domain rather than the spatial domain since the spatial frequency spectrum is the Fourier transform of a horizontal raster line. If the phase component of the Fourier transforms of two raster signals, one shifted relative to the other, are evaluated at the frequency at which the spectrum is maximum, the phase difference, $\Delta\varphi(\zeta_o)$, is defined by

$$\Delta\varphi(\zeta_o) = \frac{2\pi y_o}{\lambda_y} = 2\pi N \qquad (6.1.2\text{-}3)$$

where ξ_o = spatial frequency at which the spectrum is a maximum,

y_O = amount of horizontal shift in the signal,

λ_y = fringe line spacing and

N = normalized fringe shift.

Thus the normalized fringe shift, N, indicates the change in phase between two raster lines. The difference between the phase for each raster line in the sample and the average phase determined for the reference medium raster lines is $\Delta\varphi(\xi_o)$. The modulo 2π ambiguity of the phase due to the cyclic nature of the Fourier transform is solved using a phase unwrapping algorithm.

Determination of the ultrasonic speed using the spatial frequency domain technique is represented in Figure 6.1.2-1. The tissue sample is centered in the frame such that the frame contains the sample region and the reference medium above and below the sample. An interference line with no discontinuity is chosen from the interferogram for calculating the speed profile. The ultrasonic speed of that sample is calculated from the mean speed value within the sample region.

6.1.3 Heterogeneity Index

The heterogeneity index is a measure of the acoustic heterogeneity of the muscle's propagation speed. The variation in the spatial speed distribution indicates the acoustic heterogeneity of the tissue. From the interferogram, corrugation of the interference lines in the region of the specimen reflect the heterogeneity of the sample. The standard deviation of the speed values is the statistical measure of the heterogeneity.

6.1.4 Uncertainty Assessment

Dow Corning 710 (Dow Corning, Midland, MI.), a phenylated silicone oil, is often used as reference material for ultrasonic propagation properties such as the attenuation coefficient and speed because it is well characterized acoustically and often referenced in the literature [Dunn et al., 1969; Żeqiri, 1989]. This reference material, used for the calibration and evaluation of ultrasonic instruments, has known and stable characteristic acoustic properties. One of the reasons why Dow Corning 710 is chosen is because of its similar acoustic properties to tissue, especially tissue with lipids (fat) [Fyke et al., 1978]. However, due to the acoustically lossy nature of Dow Corning 710 at high frequencies, an aqueous solution of bovine serum albumin (BSA), which is well characterized at high frequencies, is used for assessing the attenuation coefficient for the SLAM [O'Brien, 1969].

A thermocouple junction of a digital microprocessor thermometer (Omega Engineering Inc., Model HH21) was used to measure the specimen temperature of a drop of oil, saline or BSA which was placed on the stage of the SLAM. The Dow Corning 710, saline and BSA reached a equilibrium temperature of 26.5, 24.8 and 24.9°C, respectively,

in approximately 9 minutes. An equilibrium temperature of 24.8°C (saline) was used for the speed assessment since only a drop of oil was placed on the stage surrounded by the saline.

6.1.4.1 Attenuation Coefficient

The accuracy and precision of the attenuation coefficient were determined using a 10% solution of BSA (Sigma Chemical Co., A-7030). Layers of BSA with varying thicknesses were used to measure the insertion loss for determining the attenuation coefficient on the SLAM. BSA layers were obtained by placing the 10% BSA solution in metal spacers (washers) with thicknesses of 545, 666 and 1063 μm. A zero insertion loss reference was obtained by using a very thin layer of less than 10 μm of BSA using washers cut from mylar plastic. The thickness of the spacers was measured with a calibrated digital micrometer caliper to within ±1 μm (Fowler Electronic Digital Caliper Co.). Since the thickness accuracy, which was assessed to be ±1 μm, contributes to less than 0.1% error for the attenuation coefficient, this uncertainty was ignored.

6.1.4.2 Speed

To determine the accuracy and precision of the modified spatial frequency domain technique (SFDT), the speed of sound was assessed in Dow Corning 710. Since saline does not mix with the silicone oil, saline can be used as a reference. The reported speed of sound values for normal saline and Dow Corning 710 at 24.8°C are 1520 and 1365 m/s, respectively [Dunn et al., 1969]. Although the reported values are for an ultrasonic frequency of 1 MHz, these values are valid since dispersion is negligible.

Using the interference image of the SLAM, the speed of sound for the varying oil thicknesses was determined using the modified SFDT. Within a metal spacer (washer), a drop of Dow Corning 710, surrounded by normal saline, was placed on the SLAM stage. A coverslip was then placed on top of the washer. The thickness of the spacer was measured with a calibrated digital micrometer caliper to within ±1 μm.

6.2 Acoustic Propagation Property Determination using the DES

Frequency and temperature dependent ultrasonic propagation properties of skeletal were determined using the DES. Basically, ultrasonic propagation properties are determined by placing a tissue sample in a water bath between a transmitting transducer and a receiving hydrophone. Waveforms received by a hydrophone are from an ultrasonic pulse transmitted through the tissue or calibration material. The attenuation coefficient is determined using an insertion loss technique. The speed of sound in the material is

calculated from measuring the time shift due to the sample via a correlation technique. Both of these measurements are made when a digitized waveform is acquired with and without a sample in the path of a propagating ultrasound signal. The ultrasonic propagation properties as a function of temperature are derived from placing a tissue sample in a temperature controlled water bath. Waveforms received by the hydrophone are displayed on a digitizing oscilloscope and are stored and processed by a computer. Over one hundred measurements are made by moving the muscle sample in the ultrasound field for acquiring a pulse at distinct locations by an automated computer controlled motion system.

6.2.1 Attenuation Coefficient

The attenuation coefficient is determined by the spectral analysis technique [Madson et al., 1982; Dunn and Goss, 1986]. Determining the attenuation coefficient utilizes a transmitting ultrasonic transducer immersed tank filled with degassed water, aligned axially with the receiving hydrophone. The scope is used to display the received signal from the hydrophone. A typical displayed pulse waveform (Figure 6.2.1-1) displayed on the oscilloscope is digitally recorded with 32 bit resolution and saved in a 2048 byte file.

The waveform received from the hydrophone is a digitally sampled analog signal in the time domain. This digitally acquired waveform $f(n)$ is used to provide details of the insertion loss as a function of frequency by calculating the Fourier transform from the discretely sampled data:

$$F(e^{j\omega}) = \sum_{n=0}^{N-1} f(n) e^{\left(-j\frac{2\pi}{N}nk\right)} \qquad (6.2.1\text{-}1)$$

where $F(e^{j\omega})$ is the discrete time Fourier transform, ω is the radian frequency, $\omega = 2\pi f$, and N is the total number of digital points used in the Fourier calculation [Press et al, 1988].

The power spectrum of the acquired pulse with and without the sample interposed between the transducer and hydrophone is used to calculate the insertion loss of the tissue sample. The tissue is attached to the mechanical arm of the positioning system which allows the sample to be moved in the ultrasound field in an automated and precise manner. An area of 2 x 2 cm in 2 mm steps is scanned for each tissue sample giving rise to 121 different locations for which a waveform is recorded and stored. The 2 x 2 cm area was chosen based on the physical limitation of the longissimus dorsi tissue sample obtained and the size of the scanning tank. The 2 mm step was chosen since 4 mm is the 3dB bandwidth so 2 mm is used to make independent acoustic measurements.

The file which contains the 121 waveforms is processed off-line after the waveforms are acquired. Calculation of the Fourier transform is performed off-line since processing each waveform would require an additional 8 seconds to the actual waveform acquisition experimental time due to the speed of the 16 MHz PC. Figure 6.2.1-2 is a typical power spectrum of a pulse waveform.

The insertion loss at each frequency of interest (2-7 MHz), for temperatures, (4, 20 or 37°C) are stored in a file which contains the 121 insertion loss values. The ultrasonic attenuation coefficient is determined via a linear regression from the slope of the insertion loss versus specimen thickness data at each frequency. Three thicknesses of 0.5, 1.0 and 1.5 cm were used for the insertion loss measurement. Figure 6.2.1-3 is a typical plot of the attenuation coefficient, graphed as a function of frequency and temperature, which is determined from the insertion loss of the 3 different thicknesses.

6.2.2 Slope of the Attenuation Coefficient

One way to describe the attenuation coefficient over the range of 2-7 MHz is to use a best fit line for calculating the slope of the attenuation coefficient (SAC) in dB/cm/MHz for each temperature and fiber orientation. Additionally, the DES can characterize tissue over a large range of temperatures, specifically at 4, 20 and 37°C for this study. This information will elucidate the relationship between the acoustic propagation properties (slope of the attenuation coefficient, and speed) as a function of frequency and temperature and the structure and constituents of muscle.

6.2.3 Ultrasonic Speed

The acoustic speed in tissue is found based on a cross correlation function to determine the time-of-flight in the material. The cross correlation method is a robust method of measuring the time of flight of a heterogeneous and anisotropic material [Maroili et al., 1992]. A second method of measuring the time-of-flight in the material is called the zero-cross technique [Madson et al., 1982]. The zero-crossing technique measures the time-of-flight of a sample by detecting the time shift of an acoustic pulse due to a sample placed the path of the sound. However the zero-crossing technique only is reliably for homogeneous material.

The speed is calculated using the time-of-flight, $\Delta\tau$, is determined from the cross correlation of two acquired pulses. The first pulse, $x(t)$, is the waveform of an acoustic signal without a sample in the path of the propagating ultrasound. The second pulse, $y(t+\tau)$, is the waveform of an acoustic pulse with a delay, τ, due to the interposing sample. The cross correlation is defined as

$$Corr(x,y) = \int_{+\infty}^{+\infty} x(t)y(t+\tau) \qquad (6.2.3\text{-}1)$$

[Press et al., 1988]. The cross correlation is performed by the cross correlation function in MATLAB® (The Math Works, Natick, MA) which returns a value corresponding to the shift due the sample which is used to determine the time-of-flight, Δt. The speed of sound in the sample, c in m/s, is then calculated from

$$c = \frac{c_{H_2O}}{1 + c_{H_2O}\frac{\Delta t}{d}} \qquad (6.2.3\text{-}2)$$

where d is the thickness of the sample in meters and c_{H_2O}=1481 m/s is the speed of sound in water at 20°C [Dunn et al., 1969].

6.2.3 Uncertainty Assessment

Before an experimental system can be used to characterize tissue, the system must first be calibrated using materials with known acoustic properties. The attenuation coefficient and speed of Dow Corning 710 are well characterized for the frequencies and temperatures of interest. A special holder was built to place the Dow Corning 710 fluid sample in the path of the ultrasound beam between the transducer and the hydrophone (Figure 6.2.3-1). One open end of the sample holder cylinder is sealed off using Saran Wrap and held in place with a rubber band. Trapped air bubbles are removed from the Dow Corning 710 using a vacuum pump. The Dow Corning 710 fluid sample is poured into the sample holder cylinder and the open end of the cylinder is sealed with Reynolds 914 film (Reynolds Food Service Packaging, Grottoes, VA) and held in place with a rubber band. Care is taken to remove all trapped air from the Dow Corning 710 in the cylinders. The test cylinder is then placed in the ultrasonic beam path and both the Sonic Technologies hydrophone and the transducer are held stationary within the bath. The Plexiglas rod of the sample holder is attached to the DES positioning system such that the sample can be adjusted in lateral, axial and rotational motion with respect to the propagating beam path between the transducer and hydrophone.

The DES positioning system moves the sample holder cylinder containing Dow Corning 710 in a 1 x 1 cm square taking 1 mm steps. At each step, the digital oscilloscope records the waveform for 100 total measurements for each sample. The ultrasonic

propagation properties of the Dow Corning 710 are measured as described above with the additional variable of making the measurements at different temperatures. The temperature of the water in which the hydrophone, transducer and sample are submerged is changed to determine the ultrasonic propagation properties of the tissue and sample as a function of temperature. Measurements are made at 4, 20 and 37 °C.

6.2.3.1 Attenuation Coefficient

The attenuation coefficient of Dow Corning 710 is determined using three test cylinders (which contain the oil), with thicknesses of 1.0, 1.5 and 2.0 cm, which are used to determine the insertion loss of the ultrasound as a function of thickness. The oil was separated from the water environment of the DES tank by sealing the oil within the test cylinders with Reynolds 914 film. A test cylinder was then placed in the path of the propagating ultrasound. Several experiments using the oil were conducted to measure the insertion loss, as a function of the thickness, which was then used to determine the attenuation coefficient. The thickness of the test cylinders was measured with a calibrated digital micrometer caliper to within ± 1 μm.

6.2.3.2 Speed

To determine the accuracy and precision of DES using the correlation technique, the speed of sound was assessed for Dow Corning 710. Dunn et al., 1973 reports the speed of sound as a function of temperature at 0, 10, 20, 30 and 40°C . The relationship between the speed of sound and temperature is linear and has a negative thermal dependency on speed. Therefore the speed of sound can be calculated at other temperatures using a linear regression of the data. Although the reported values are for an ultrasonic frequency of 1 MHz, these values are valid for the range of 2-7 MHz since dispersion is assumed to be negligible [Dunn et al., 1973].

6.3 Experiment #1: Acoustic Propagation Properties using the SLAM

The purpose of the first experiment was to predict the tissue constituents and sarcomere length of bovine semitendinosis from the attenuation coefficient and speed at 100 MHz using the multilinear regression equations developed from detailed analysis of the ultrasonic propagation properties, tissue constituents and sarcomere length of bovine longissimus dorsi, psoas major and lobster extensor.

For this experiment, 5 samples of longissimus dorsi, 5 samples of psoas major, 5 samples of lobster extensor and 8 samples of semitendinosis were used for the determination of the propagation properties, tissue constituents and sarcomere length using

the SLAM. Figure 6.3-1 indicates that each sample was divided for determination of the tissue constituents, sarcomere length and propagation properties. Bovine muscle samples were obtained from the Meat Science Lab at the University of Illinois within 24 hours after the animal had been slaughtered. Extensor muscles were obtained from individual lobsters which were commercially obtained and handled in a similar procedure to the bovine muscle. All samples were stored in a -70°C Revco freezer pending analysis.

6.3.1 Tissue Preparation

For each muscle sample the acoustic propagation properties were analyzed by the SLAM. Two types of sample orientations were defined according to the relationship between the muscle fiber orientation and the sound beam.

- parallel : ultrasound beam propagating parallel to the muscle fibers.
- perpendicular : ultrasound beam traveling perpendicular to the muscle fibers.

From each sample, two 1 x 1 cm cubes were removed and mounted on cork using Ames Tissue-Tek® O.C.T (optimal cutting temperature, a polyvinyl alcohol, benzalkonium chloride and polyethylene glycol gel). The samples were mounted such that muscle fibers were parallel or perpendicular to the cork surface. For acoustic evaluation by the SLAM, the cork was mounted for sectioning in a Lipshaw Cryostat Microtome (Lipshaw Manufacturing Company, Detroit, MI) at -10°C at the blade edge. Each parallel or perpendicular sample was sectioned into three thicknesses of 60, 100 and 140 μm. The Ames Tissue-Tek® O.C.T was removed from the sliced sample to reveal a rectangular piece of 4 x 1 mm and then placed on the microscope stage for measurement of ultrasonic propagation properties.

Perpendicular slices adjacent to samples used on the SLAM were immediately cut (6 μm) and placed on a slide and stained for sarcomere length measurements which will be described in Section 6.3.3. Cubes of bovine muscle (approximately 3 x 3 x 3 cm) and lobster extensor (approximately 1 x 1 x 1cm) adjacent to the samples used for acoustic evaluation were obtained for tissue characterization.

6.3.2 Analysis Procedure for %Water, %Fat and %Protein

The biochemical analysis was performed at the Animal Science Laboratory in Dr. Neal Merchen's Nutritional Sciences Lab at the University of Illinois according to the Official Methods of Analysis of the Association of Official Analytical Chemists (AOAC). The AOAC is an annual peer reviewed journal which provides the standard method accepted within the Nutritional Sciences Community for determining the proper method for determining the tissue constituents of food products. Dr. Neal Merchen's Nutritional Sciences Lab, which also commercially determines the constituents of food products,

asserts an accuracy of 2% and a precision of 5%, when determining the %water, %fat and %protein of skeletal muscle [Merchen, 1995].

The %water of the muscle sample is determined by the following procedure. First the sample is weighed and placed in a vacuum dryer for 3-4 days. A porcelain crucible is then placed in an oven at 105°C overnight. The crucible is removed from the oven with tongs and placed in a desiccator and then allowed to cool to room temperature. Using tongs to prevent wetness from skin contact, the crucible is removed from the desiccator and weighed. Approximately 0.5-1.0 g of ground sample is placed in the crucible and weighed and allowed to dry overnight in a 105°C oven. The crucible and sample are removed from the oven with tongs, placed in a desiccator and allowed to cool to room temperature. The crucible and sample are removed from the desiccator and weighed. The %dry-matter is determined from the following calculation:

$$\%dry\text{-}matter = \frac{(dry\ crucible\ weight + sample\ weight) - dry\ crucible\ weight}{sample\ weight} x100.$$

(6.3.2-1)

The %water is reported as 100% minus %dry-matter.

The %fat in the samples is determined by ether extraction. The freeze dried sample is ground using a commercial coffee grinder. One gram of ground sample is placed into a Whatman cellulose extraction thimble (27 x 80 mm) which has previously been dried at 105°C, desiccated and weighed. A small piece of cotton in placed on top of the thimble to prevent splattering during extraction. The extraction setup consists of a round bottom flask with a soxhlet at the top and a condenser over the soxhlet. The entire apparatus is placed in a hood. The round bottom flask is filled 3/4 full with petroleum ether with a heating mantle under the flask. The assembled glassware contains the thimbles in the soxhlet and the flask is on the heating mantle. Cold water is run through the condenser to keep the ether evaporation to a minimum. The ether is kept at a constant boil during the 6 hour extraction. When finished, the thimbles are removed and the samples are allowed to dry under the hood until all scent of ether is gone. The thimbles are then dried in an oven at 105°C, desiccated for 20 minutes and weighed. The loss in weight is the ether extracted material or the %fat. The % fat is calculated as

$$\%fat = \left(1 - \frac{sample\ weight}{sample\ weight\ after\ ether\ extraction}\right) x\ \%dry\text{-}matter$$

(6.3.2-2).

The %protein in the sample is determined by nitrogen titration by first weighing out 2g of a well ground sample and transferring it to a 250 mL digestion tube. The tubes are placed in a fume hood and a catalyst is added with 15 mL of H_2SO_4. The tubes are placed in a block and the samples digested at 410.0°F for 45 minutes. Approximately 50-75 mL of water are then added. A solution of NaOH-$Na_2S_2O_3$ is placed in the alkali tank of a steam unit. The digestion tube is attached to the steam unit. A 250 mL receiving flask is placed on the receiving platform containing 25mL H_3BO_4 solution with mixed indicator. Steam is distilled until an absorbing solution of 100-125 mL collects. The absorbing solution is tritrated with 0.2N HCl and the volume required to make up 0.01 mL is recorded. The %protein is recorded by

$$\%protein = (Va - Vb) \times 1.4007 \times N \times 6.25 / g\ sample \qquad (6.3.2\text{-}3)$$

where Va and Vb are the volumes of acid required for the sample and blank, respectively, 6.25 is the protein to nitrogen ratio, 1.4007 is mL to mg conversion for nitrogen, N is the normality of standard acid.

6.3.3 Sarcomere Length Measurements

Muscle samples are mounted on cork using Ames Tissue-Tek® O.C.T. Slices of the samples were cut using a Lipshaw Electric Cyrostat Microtome to thicknesses of 10 μm, placed on a Fisherbrand Superfrost Microscope Slide and stained using the Baxter Diff-Quick® Stain Set. The sarcomere lengths were determined using a Nikon Labophot microscope equipped with a JVC CCD video camera at 100 x 2.5 using Nikon magnifying immersion oil. With the guidance of Dr. James Zachary, a veterinary pathologist at the College of Veterinary Medicine and Editor of Veterinary Pathology, myofibrils were selected from the slides and accurate sarcomere lengths were determined with the microscope. Images of selected myofibrils were acquired using Adobe Photoshop and sarcomere lengths were determined from myofibrils with several clearly defined sarcomeres using a calibrated micrometer. Using an image from a calibrated slide the accuracy and precision were determined to be 5% and 3%, respectively. Only clearly defined Z-Lines, A bands and I bands were counted with a minimum of 5 myofibrils and a total of 50 sarcomeres per sample. Figure 6.3.3-1 displays a typical image of a skeletal muscle fiber.

6.4 Experiment #2: Temperature-Frequency Dependent Acoustic Propagation Properties using the DES

The purpose of the second experiment is to determine the influence of temperature on the acoustic propagation properties and determine the relationship between the tissue constituents and sarcomere length of bovine longissimus dorsi from the acoustic propagation properties using the DES as a function of frequency and temperature. This experiment uses 30 samples of longissimus dorsi for determination of the temperature-frequency dependent acoustic propagation properties and Figure 6.4-1 indicates the procedure for dividing the tissue for tissue constituents, sarcomere length and propagation properties determination.

6.4.1 Tissue Preparation

For this experiment, 30 samples of longissimus dorsi were used for the determination of the propagation properties, tissue constituents and sarcomere length using the DES. Muscle samples of longissimus dorsi from a freshly slaughtered bovines are obtained from the abattoir of the Animal Science Department at the University of Illinois. For determination of the acoustic propagation properties each muscle sample is cut in approximately 10 x 10 cm squares both parallel and perpendicular to the muscle fibers. For each orientation, three samples are cut into thicknesses of 0.5, 1.0 and 1.5 cm for determination of the insertion loss for each thickness. Each sample is vacuum sealed using a commercial meat packaging vacuum sealer.

From each muscle sample, a 1 x 1 cm cube was removed and mounted on cork using Ames Tissue-Tek® O.C.T and used for determination of the sarcomere length for that particular sample. A larger (approximately) 3 x 3 cm cube was obtain from the same sample and used for the determination of the tissue constituents.

6.4.2 Analysis Procedure for %Water, %Fat and %Protein and Sarcomere Length Measurements

The methods for determining the tissue constituents and sarcomere length for this experiment are identical to the procedures described in Section 6.3.2 and 6.3.3, respectively.

6.5 Experiment #3: Myofibrilar Contribution to the Acoustic Propagation Properties at 100 MHz

The purpose of the third experiment is to determine the myofibrilar contribution to the acoustic propagation properties from intact and homogenized tissue. For this experiment, 18 samples of longissimus dorsi were used for the determination of the

propagation properties using the SLAM. Each sample was divided into 3 sections and exposed to the ultrasound with the following orientation.

- parallel : ultrasound beam propagating parallel to the muscle fibers.
- perpendicular : ultrasound beam traveling perpendicular to the muscle fibers.
- homogenized : ultrasound beam propagating through muscle samples in which the fiber orientation had been totally disrupted by the homogenization process.

Each parallel, perpendicular or homogenized sample was sectioned into three thicknesses of 80, 100 and 120 μm. For each thickness the insertion loss, speed and heterogeneity index were determined. Figure 6.5-1 indicates the steps for dividing the sample into 3 sections for the parallel, perpendicular and homogeneous orientation for propagation property determination.

6.5.1 Tissue Homogenization

Eighteen samples of longissimus dorsi were homogenized to determine the structural contribution to the acoustic propagation properties. The skeletal muscle was initially placed into a commercial coffee grinder (Grindmaster Coffee Mill) for 2-5 seconds to destroy the gross structure due to the collagen matrix of the skeletal muscle. From physically handling the tissue, no perceivable temperature increase was noticed due to the grinder. The ground up sample was placed into a test tube and homogenized with a laboratory tissue homogenizer (Motor One) using a fine pestle to destroy any remaining structure. The tissue homogenizer and coffee grinder were carefully cleaned between each sample to prevent contamination between the samples. The homogenized sample was then placed on a cork and embedded in O.C.T., frozen and stored in a -70°C freezer.

6.6 Experiment #4: Anisotropy of the acoustic propagation properties of muscle using the SLAM and DES

Eight samples of semitendinosis were used with the SLAM and the DES to determine the effect of anisotropy on the acoustic propagation properties. The DES is capable of rotating a sample in the ultrasound field by 180° in 5° steps in an automated fashion. Unfortunately multiple fiber orientation angles are harder to obtain since the rotation of the fibers are manual. Figure 6.6-1 indicates the procedure for dividing sample for acoustic determination using the SLAM and the DES.

6.6.1 Tissue Orientation for the SLAM

Eight samples of semitendinosis were used with the SLAM to determine the effect of anisotropy on the attenuation coefficient and speed at 100 MHz. Figure 6.6.1-1

demonstrates the proper technique for obtaining the angles with respect to the ultrasound on the SLAM stage. From each sample three 1 x 1 cm cubes were removed and mounted on cork using Ames Tissue-Tek® O.C.T. For each cube, the fibers were mounted such that muscle fibers were parallel, perpendicular or 45° to the cork surface. Each corked sample was sectioned into three thicknesses of 60, 100 and 140 μm. To determine anisotropic effects on the ultrasonic propagation properties, the muscle fiber was oriented on the SLAM stage at varying angles with respect to the propagating ultrasound through the fused silica stage. From Figure 6.6.1-1 (a) through (e), angles of (a) 90° through (b) 80°, (c) 35° through (d) 55°, and (e) 10° could be obtained.

6.6.2 Tissue Orientation for the DES

The DES is used to rotate a cylindrical plug of bovine semitendinosus in an ultrasound field to determine the ultrasonic propagation properties as a function of the angle of insonification. A cylinder was cored from a sample of semitendinosis in such a manner that as the cylinder rotates the fibers are exposed to the ultrasound from a parallel to perpendicular orientation. Eight samples of semitendinosis were used with the DES at 3 MHz to determine the effect of anisotropy on the attenuation coefficient and speed.

Three cylindrical plugs were cored from the each muscle sample with the plug perpendicular to the fiber axis of the tissue. Commercial cutting tools were obtained which consisted of a hardened steel tube with thin walls and a sharpened saw tooth edge. For smooth cuts into the tissue, frozen (-70°C) chunks (approximately 20 x 20 x 10 cm) of semitendinosis were used. The tool was drilled into the tissue sample to produce a smooth, straight cut through the tissue. The resulting cylinders had diameters of 25.4, 19 and 12.5 mm and a length of 10 mm and were mounted to a rod which provided a means of connecting the sample to the rotational axis of the DES. The angle of insonification is from 0° to 180° in 5° steps.

6.7 Statistical Analysis

Statistical analysis of the results was performed using Microsoft EXCEL 4.0 and SPSS Version. 6.1. (SPSS Inc., Chicago, IL). Acoustic propagation property, tissue constituent and sarcomere length results are reported as a mean ± standard deviation. Several data analysis and statistical inference techniques are applied to the data and are described here.

The accuracy and precision with respect to a measurement technique can be described in statistical terms. The accuracy of a measurement describes the proximity of the measurement to the true value while the precision describes the reproducibility of

successive, independent measures irrespective of how close the measurements are to the true value.

Linear regressions are performed on the data to mathematically determine if there is a relationship between two sets of data. The ultimate purpose of the regression equation is to use one variable to predict another. The linear regression equations can be used to predict how changes in the %water, %fat, %protein and sarcomere length effect the attenuation coefficient or speed. The correlation coefficient (r), indicates the strength of the linear regression model.

ANOVA is a method to analyze the statistical significance of the differences among the means of groups. ANOVA examines the amount of variability (the differences) between the means of a group, compared with the amount of variability among the results within each group; that is, the variance between groups versus the variance within groups. The F-value is used to determine if the between-group differences are significantly greater than chance. If the F-value is greater than the F_{crit} value then the null hypothesis, which says that the results come from the same group, is rejected. For all the data presented, an asterisk is placed next to the F value if it exceeds the 0.05 level of significance and a double asterisk is used if the F value exceeds the 0.01 level of significance.

The interaction between variables is evaluated by the Pearson product-moment coefficient (ρ) with an inclusive range ± 1. Values of +1, 0 and -1 signify a positive relationship, no relationship and negative relationship respectively among the variables. The t-test is a commonly used inferential statistic. Its primary purpose is to determine whether the means of two groups differ to a statistically significant degree. Comparisons between the variables (such as sarcomere lengths, tissue constituents and propagation properties) are performed with a paired Student t-test. The comparisons were considered significantly different when p-values were less than 0.05.

Multivariable linear regressions determine the relationship between a dependent variable and several independent variables. The beta values are indicators of the relative importance of the independent variables to the dependent variable. The F-value and its probability level (F_{sig}) for a given multivariable linear regressions equation are listed to the right of each equation. Below each beta coefficient is the T_{sig} value which indicates the significance of that coefficient to the dependent variable.

Reporting of the percent error is determined using

$$\%error = \left(\frac{actual\ value - measured\ value}{actual\ value} \right) x\ 100 \quad (6.7\text{-}1).$$

The results will often indicate the acoustic propagation properties for the parallel muscle to be different than the perpendicular muscle due to the anisotropy of the muscle. A measure of the effect of anisotropy is the anisotropy index which is defined as,

$$anisotropy\ index = \frac{parallel\ result}{perpendicular\ result} \qquad (6.7\text{-}2)$$

where *parallel result* is the acoustic propagation property determined for the parallel fiber orientation and *perpendicular result* is the acoustic propagation property determined for the perpendicular fiber orientation.

7. RESULTS

The results presented in this chapter are divided into 6 sections corresponding to the following experiments described in the Specific Aims.

- (§7.1) Measurement uncertainty assessment of the SLAM.
- (§7.2) Measurement uncertainty assessment of the DES.
- (§7.3) Predict the tissue constituents and sarcomere length of bovine semitendinosis from the attenuation coefficient and speed at 100 MHz (20°C) using the SLAM.
- (§7.4) Develop multivariable linear regression equations which predict the tissue constituents and sarcomere length of bovine longissimus dorsi from the attenuation coefficient and speed at 2-7 MHz and at 4, 20 and 37°C using the DES.
- (§7.5) Determine the myofibril (structural) contribution to the attenuation coefficient and speed.
- (§7.6) Resolve the effect of anisotropy on the attenuation coefficient and speed using the SLAM and the DES.

7.1 Uncertainty Assessment for the SLAM

Fundamental to any measurement is the knowledge of its uncertainty and the consideration of both the accuracy and precision of the measurement. Dow Corning 710 is often used as reference material for ultrasonic propagation properties such as the attenuation coefficient and speed because it is well characterized acoustically and often referenced in the literature [Dunn et al., 1969; Zeqiri, 1989]. This reference material, used for the calibration and evaluation of ultrasonic instruments, has known and stable characteristics. Due to the acoustically lossy nature of Dow Corning 710 at high frequencies such as 100 MHz, an aqueous solution of bovine serum albumin (BSA), which is also well characterized at high frequencies, is used for assessing the attenuation coefficient for the SLAM. Error assessment is performed in the same manner as a previously published uncertainty assessment for the SLAM [Steiger, 1986].

7.1.1 Attenuation Coefficient Uncertainty for the SLAM

The accuracy and precision of the attenuation coefficient was determined using a 10% solution of BSA. Kessler (1968) independently determined the absorption coefficient at 100 MHz for a 10% BSA (10 gm of BSA per 100 mL distilled water). Since scattering is negligible in homogenous liquids like BSA, the attenuation coefficient is assumed to equal the absorption coefficient. Kessler reported an absorption coefficient of 5.8 dB/mm for BSA at 24.8°C and 100 MHz with an overall uncertainty of ±5%.

For each thickness, six independent insertion loss measurements were determined. A least square regression analysis was used to fit the insertion loss versus thickness data to yield the slope (attenuation coefficient in dB/mm) and the 95% confidence interval. The slope or attenuation coefficient was determined to be 5.5 dB/mm and the 95% confidence interval was determined to be ±6% (from 5.8 to 5.2 dB/mm). Based on the known value of the attenuation coefficient of 5.8 dB/mm, the error was 7.4%. The accuracy uncertainty was determined to be approximately 12.4 % (sum of ±7.4% and ±5% uncertainty in the literature value). Since the 95% confidence interval was ±6%, the precision was ±6%.

7.1.2 Speed Uncertainty for the SLAM

In Table 7.1.2-1 are the mean speed and standard deviation from 10 independent experiments using Dow Corning 710 for each thickness. From the table, the worst-case error for the speed measurements was 1.2%. An error of ±1.0% is assumed for the uncertainty of the literature values for Dow Corning 710 since this value was not reported. Since the worst-case error for the speed measurements was 1.2%, then an approximately ±2.2% (sum of ±1.0% and ±1.2%) worst case assumption was obtained for the accuracy at the speed measurement.

The precision of the speed measurement for Dow Corning 710 is determined from the standard deviation calculated as the average absolute difference between each speed value and the mean speed is expressed as a percentage of the mean value. The precision of the speed measurement was determined to be ±1.4%.

7.2 Uncertainty Assessment for the DES

The accuracy and precision for the attenuation coefficient and speed were determined as a function of frequency and temperature for the DES. The DES will compare the attenuation coefficient and speed of sound measurements of Dow Corning 710 against the values published in the literature [Dunn et al., 1969; Zeqiri, 1989].

7.2.1 Attenuation Coefficient Uncertainty for the DES

The accuracy and precision of the attenuation coefficient were determined from 2-7 MHz (1 MHz steps) and at 4, 20 and 37°C using Dow Corning 710. Attenuation coefficient versus frequency of Dow 710 at 20°C is plotted in Figure 7.2.1-1 from the literature values determined by Zeqiri (1989). The purpose of Zeqiri's work with Dow Corning 710 was to assess the long term stability of the fluid as an attenuation coefficient reference material. Zeqiri's measurements of the attenuation coefficient made at a frequency of 5 MHz over a period of 3 years deviated no greater than 0.5 dB/cm from the

initial measurement. Scattering is absent and therefore the absorption coefficient and the attenuation coefficient are the same [Madson et al., 1982]. Zeqiri's reported a range of the attenuation coefficient as a function of frequency from 0.07 dB/cm at 1 MHz up to 39.3 dB/cm at 10 MHz for Dow Corning 710 at 20°C with an uncertainty of ±5%. There is no existing attenuation coefficient data for Dow Corning 710 at exactly 4 and 37°C published in the literature. However the attenuation coefficient at 4 and 37°C can be calculated from data and information published in Dunn et al. (1969) which reports that the attenuation coefficient is proportional to f^2 up to 20 MHz. Thus, the attenuation coefficient versus frequency of Dow 710 at 4 and 37°C is also plotted in Figure 7.2.1-1 from the literature values determined from Dunn et al. (1969) ; the uncertainty of these values was not reported.

A least square regression analysis was used to fit the insertion loss versus thickness data to yield the slope or attenuation coefficient in dB/cm. The results from 20 independent experiments are plotted against the reported literature values in Figure 7.2.1-1. Table 7.2.1-1 lists the mean attenuation coefficient and standard deviation results along with the %error which is determined using the literature values.

An error of ±1.0% is assumed for the uncertainty of the literature values for Dow Corning 710 at 4 and 37°C since this value was not reported. Zeqiri's reported an uncertainty of ±5% for the oil at 20°C. Since the worst-case error for the attenuation coefficient measurements was 17% (at 4°C and 6 MHz), then an approximate ±18% (sum of ±1% and ±17%) worst case assumption was obtained for the accuracy of the attenuation coefficient measurement. The precision of the speed measurement was determined to be ±5% based on the worst case standard deviation measurement of the attenuation coefficient.

7.2.2 Speed Uncertainty for the DES

To determine the accuracy and precision of DES using the correlation technique described in Chapter 5.2, the speed of sound was assessed in Dow Corning 710. Dunn et al. (1969) reports the speed of sound as a function of temperature at 0, 10, 20, 30 and 40°C which is graphed on Figure 7.2.2-1. As seen in Figure 7.2.2-1 the relationship between the speed of sound and temperature is linear and has a negative thermal dependency for velocity. Therefore the speed of sound can be calculated at other temperatures using a linear regression of the data. Although the reported values are for an ultrasonic frequency of 1 MHz, these values are valid for the range of 2-7 MHz since dispersion is assumed to be negligible [Dunn et al., 1969].

Figure 7.2.2-1 also displays the speed results and standard deviation bars from 20 independent experiments at 4, 20 and 37°C from this investigation. Table 7.1-3 lists the mean speed and standard deviation of Dow Corning 710. From the table, the worst-case error for the speed measurements was 0.4%. An error of ±1.0% is assumed for the uncertainty of the literature values for Dow Corning 710 since this value was not reported. Since the worst-case error for the speed measurements was 0.4%, then an approximately ±1.4% (sum of ±1.0% and ±0.4%) worst case assumption was obtained for the accuracy at the speed measurement.

The precision of the speed measurement for Dow Corning 710 is determined from the standard deviation calculated as the average absolute difference between each speed value and the mean speed and expressed as a percentage of the mean value. The precision of the speed measurement was determined to be ±8%. Table 7.2.2-2 lists a summary of the uncertainty assessment for the SLAM and the DES.

7.3 Tissue Constituents and Sarcomere Length Predictions using the SLAM

The aim of this section is to predict the tissue constituents and sarcomere length of bovine semitendinosis from the attenuation coefficient and speed at 100 MHz using the multilinear regression equations developed from detailed analysis of the ultrasonic propagation properties, tissue constituents and sarcomere length of bovine longissimus dorsi, psoas major and lobster extensor. Sections 7.3.1-7.3.4 develop an empirical mathematical model of the tissue's composition and structure based on the acoustic propagation properties of skeletal muscle, while Section 7.3.5 tests the mathematical model using the attenuation coefficient and speed results from samples of semitendinosis tissue. The mathematical model is a simplified or idealized description of the constituents and physical properties of the muscle that is put forward on the basis of the determination of the acoustic propagation properties.

7.3.1 Generation of the Predictive Model Data Set

The acoustic propagation properties, tissue constituents and sarcomere lengths were determined for a total of 15 muscle samples from individual bovines and lobsters. For each muscle sample the attenuation coefficient, speed and heterogeneity index were determined using the SLAM with the ultrasound propagating parallel and perpendicular to the muscle fiber. Each parallel and perpendicular oriented sample was sectioned into three thicknesses of 60, 100 and 140 μm. For each thickness the insertion loss, speed and heterogeneity

index was determined. The attenuation coefficient was determined from the insertion loss for all three sample thicknesses.

7.3.2 Ultrasonic Propagation Properties of Tissues used for Prediction Model

For this study the experimental design is a randomized block design. This design is chosen because in some experiments the background may lack homogeneity such that complete randomization of the whole background at once would introduce unnecessary error. Randomizing one block of the background at a time will explicitly introduce its effect into the results obtained. Here, the blocks are the muscle samples from individual animals. The response variable attenuation coefficient depends on only the factor muscle fiber orientation. However the speed and heterogeneity index depends on two factors: fiber orientation and sample thickness. The factor level for each factor, orientation and thickness, is listed in Table 7.3.2-1.

7.3.2.1 Attenuation Coefficient

An ANOVA was performed to determine if the attenuation coefficient of the three muscle types was effected by the orientation of the muscle fibers. A significant effect is indicated by the results in Table 7.3.2.1-1. The mean attenuation coefficient and standard deviation both parallel and perpendicular to the muscle fiber were determined for the three types of muscle (longissimus dorsi, psoas major and lobster extensor) and are listed in Table 7.3.2.1-2. The ANOVA of the results in Table 7.3.2.1-2 indicates that the attenuation coefficient was significantly different for ultrasound parallel to the muscle fibers than perpendicular to the muscle fibers. The attenuation coefficient for the parallel orientation was consistently larger than the perpendicular oriented samples for all muscle types, with longissimus dorsi having the largest attenuation coefficient and lobster extensor having the smallest. The anisotropy index for the attenuation coefficient results for longissimus dorsi, psoas major and lobster extensor were 1.82, 1.56 and 1.73, respectively.

7.3.2.2 Ultrasonic Speed

An ANOVA was performed to determine the effect of sample orientation and thickness on the speed for the three muscle types. The ANOVA results in Table 7.3.2.2-1 indicate that there was no overall variation due to specimen thickness for the three types of muscle. Therefore the data for all three sample thicknesses for three muscle types can be pooled without affecting the speed results. The ANOVA of the results in Table 7.3.2.2-2

indicates that the speed was significantly different for ultrasound parallel to the muscle fibers than perpendicular to the muscle fibers. Speed results listed in Table 7.3.2.2-2 were consistently higher in the parallel samples than the perpendicular samples and the highest value was detected in the longissimus dorsi and lowest in the lobster extensor. The anisotropy effect of the pooled speed results for longissimus dorsi, psoas major and lobster extensor was assessed to be 1.01, 1.02 and 1.02%, respectively.

7.3.2.3 Acoustic Heterogeneity

The effects of sample orientation and thickness were determined for the three muscle types by an ANOVA for the heterogeneity index. The results of the ANOVA are shown in Table 7.3.2.3-1 The results in Table 7.3.2.3-1 indicate that both sample orientation and thickness have a significant effect on the heterogeneity index for the longissimus dorsi and psoas major muscle. However sample orientation and thickness have no effect on the lobster extensor. For further analysis the mean and standard deviation of the heterogeneity index are listed in Table 7.3.2.3-2. Table 7.3.2.3-2 illustrates that the heterogeneity index was correlated with the thickness for both the parallel and perpendicular orientation and for all muscle types.

7.3.3 Biochemical Properties & Sarcomere Length

Table 7.3.3-1 lists the average and standard deviation of the measurements of the tissue constituents and sarcomere lengths for each type of muscle used. Water made up the most abundant portion of the tissue types with lobster muscle having almost 9% more water than bovine muscle. Note that the psoas major had the largest amount of fat with twice the amount of fat of the longissimus dorsi and approximately 75% more fat than lobster muscle. (Commercially the psoas major is better known as the filet mignon and its high fat content suggests the reason for its high desirability). The percentage of protein between the different muscle types remained relatively constant in a range of 22.83% - 18.83%. The sum of the %water, %fat and %protein any individual muscle sample totaled to within 1% of 100% with the remaining 1% attributed to ash. The sarcomere lengths for the longissimus dorsi, psoas major and lobster extensor were determined to be 2.10 ± 0.23, 2.98 ± 0.24 and 3.81 ± 0.60 μm, respectively.

The interaction between sarcomere length and tissue constituents was evaluated by the Pearson coefficient (ρ) with an inclusive range ± 1. Values of +1, 0 and -1 signify a positive relationship, no relationship and negative relationship, respectively, among the variables. The Pearson coefficient (ρ) and its level of significance are reported in Table 7.3.3-2. Water and fat exhibited a strong negative interaction ($\rho = -0.81$, Fsig < 0.01)

between the tissue constituents indicating an almost one-to-one replacement between water and fat. In contrast water and sarcomere length exhibited a strong positive interaction (ρ= 0.86, Fsig < 0.001).

Comparisons between the sarcomere lengths, tissue constituents and propagation properties are performed with a paired Student t-test. The comparisons were considered significantly different when p-values were less than 0.05. Table 7.3.3-3. lists the p-values from the comparisons. The tissue constituents of %water and %fat were found to be significantly correlated for the longissimus dorsi and psoas major. However, for the %water and %fat, both the longissimus dorsi and psoas major were found to be significantly different from the lobster extensor. The p-values for the sarcomere lengths indicate significant difference for all three muscle types. Comparison of the acoustic propagation results for the three tissues indicate significant differences except for the comparisons between the attenuation coefficient (perpendicular) for the longissimus dorsi and psoas major (p-value = 0.128).

7.3.4 Correlation Between Ultrasonic, Biochemical and Structural Properties

Figures 7.3.4-1 and 7.3.4-2 graphically display the relationship between propagation properties (attenuation coefficient and speed) versus the tissue constituents (%water, %fat and %protein) and myofibril length for parallel and perpendicular muscle samples.

A simple linear regression was performed on the data to mathematically describe the relationship between the acoustic propagation properties and both the tissue constituents and the sarcomere lengths. Table 7.3.4-1 lists the linear regression equations which relates one acoustic property (i.e. speed, parallel muscle) to either a tissue constituent or sarcomere length. The linear regression equations can be used to predict how changes in the %water, %fat, %protein and sarcomere length can affect the attenuation coefficient or speed. The correlation coefficient (r), which indicates the strength of the linear regression model, and the significance of the relationship, is also reported. The results indicate that changes in the %water (significance < 0.05) have the strongest effect on both the attenuation and speed.

The significance levels in Table 7.3.4-1 indicate that the relations between the acoustic properties and the constituents and physical characteristics (tissue constituents and sarcomere length) of the three types of muscle under parallel and perpendicular orientation are statistically significant. When the results of the three muscle types are pooled and a linear regression is performed on all the pooled data, the correlation coefficient and the

significance of the regression becomes stronger due to the larger data set. The linear regression of the pooled data are listed in Table 7.3.4-2.

7.3.5 The Prediction Model

The results presented in Sections 7.3.1-4 indicate that the propagation properties are influenced by both tissue constituent and sarcomere length of the tissue. This experiment has been structured to develop an empirical mathematical model which can predict specific skeletal muscle constituents and structure from detailed knowledge of the acoustic propagation properties. Table 7.3.5-1 lists multiple linear regression equations (the empirical mathematical model or prediction model) for the estimating tissue constituents and the sarcomere length based on the acoustic propagation properties of longissimus dorsi, psoas major and extensor muscles under parallel and perpendicular orientation. The F-value and its probability level (F_{sig}) for each equation are listed at the right of each equation. Below each coefficient of the equation is the T_{sig} value which indicates the significance of that coefficients to the dependent variable.

To test the prediction model, the ultrasonic propagation properties of bovine semitendinosis were determined and used to predict the tissue constituents and sarcomere length of semitendinosis using the model. Furthermore, the actual tissue constituents and sarcomere lengths were determined and compared to the predicted values.

7.3.5.1 Ultrasonic Propagation Properties of Semitendinosis

The acoustic propagation properties, tissue constituents and sarcomere lengths were determined for 8 samples bovine semitendinosis and handled in the same manner as the samples for the prediction model. For each muscle sample the attenuation coefficient, speed and heterogeneity index were determined using the SLAM with the ultrasound propagating parallel and perpendicular to the muscle fiber. Each parallel and perpendicular oriented sample was sectioned into three thicknesses of 60, 100 and 140 μm. For each thickness the insertion loss, speed and heterogeneity index were determined.

Although the muscle samples used to developed the prediction model previously indicated that orientation has a significant effect on the attenuation coefficient, an ANOVA was nevertheless performed to determine if the attenuation coefficient of semitendinosis was effected by orientation. Once more, a significant effect of orientation is indicated by the results in Table 7.3.5.1-1 where the attenuation coefficient was significantly higher for ultrasound parallel to the muscle fibers than perpendicular. The mean attenuation coefficient and standard deviation both parallel and perpendicular to the muscle fiber were determined for semitendinosis and are listed in Table 7.3.5.1-2. The attenuation coefficient

for the parallel orientation was larger than the perpendicular oriented samples and the anisotropic effect of the attenuation coefficient for semitendinosis was 1.33.

An ANOVA was performed to determine the effect of sample orientation and thickness on the speed for semitendinosis. The ANOVA results in Table 7.3.5.1-3 indicates that there was no overall variation due to specimen thickness for semitendinosis. Therefore the data for all three sample thicknesses for semitendinosis can be pooled without affecting the speed results. The ANOVA of the results in Table 7.3.5.1-3 indicates that the speed was significantly higher for ultrasound parallel to the muscle fibers than perpendicular. Speed results listed in Table 7.3.5.1-4 were consistently higher in the parallel samples than in the perpendicular samples and the highest value was detected in the longissimus dorsi and lowest in the lobster extensor. The effect of anisotropy was determined to be 1.02.

For the semitendinosis, the effects of sample orientation and thickness were determined ANOVA for the heterogeneity index with the results shown in Table 7.3.5.1-5 The results indicate that both sample orientation and thickness have a significant effect on the heterogeneity index for semitendinosis. From further analysis, the mean and standard deviation of the heterogeneity index, listed in Table 7.3.5.1-6., indicate that the heterogeneity index was decreasing with the increasing thickness for both the parallel and perpendicular orientation.

7.3.5.2 Biochemical Properties & Sarcomere Length of Semitendinosis

For semitendinosis, Table 7.3.5.2-1 lists the average and standard deviation of the tissue constituents and sarcomere length. The interaction between sarcomere length and tissue constituents was evaluated by the Pearson coefficient (ρ) reported in Table 7.3.3-2. The interaction between water and fat was the strongest with a negative interaction of ρ= -0.9 which indicates an almost one-to-one replacement between water and fat.

7.3.5.3 Comparison of the Prediction Model and Actual Results

The acoustic, biochemical and sarcomere length results of semitendinosis are compared against the results of the muscle used to develop the multiple linear regression equations (i.e. longissimus dorsi, psoas major and lobster extensor) to determine if semitendinosis comes from the same group using the Student t-test. Table 7.3.5.3-1 list the p-values of the acoustic, biochemical and sarcomere length results of semitendinosis compared with longissimus dorsi, psoas major and lobster extensor results. The comparisons were considered significantly different when p-values were less than 0.05.

Using the multilinear regression equations in Table 7.3.5-1, the predicted tissue constituents and sarcomere length are calculated based on the acoustic propagation properties results of semitendinosis. Table 7.3.5.3-1 lists the means and standard deviation of the parallel and perpendicular model results along with the actual biochemical and sarcomere length results for semitendinosis. Table 7.3.5.3-1 lists the %error for the parallel and perpendicular prediction model compared against the actual biochemical and sarcomere length results.

7.4 Temperature-Frequency Dependent Acoustic Propagation Properties: Tissue Constituents and Sarcomere Length Predictions using the DES

The aim of this section is to determine the influence of temperature on the acoustic propagation properties and determine the relationship between the tissue constituents and sarcomere length of bovine longissimus dorsi from the acoustic propagation properties using the DES. In contrast to the SLAM which operates at 100 MHz and approximately 20°C, the DES determines the ultrasonic propagation properties of tissues in the frequency range of 2-7 MHz and temperatures of 4, 20 and 37°C. This information will enable the relationship between the acoustic propagation properties (slope of the attenuation coefficient and speed) to be determined as a function of frequency and temperature and the structure and constituents of muscle.

Multilinear regression equations are developed from detailed analysis of the ultrasonic propagation properties, tissue constituents and sarcomere length of bovine longissimus dorsi. The procedure for developing and testing the regression equations are as follows:

- (§7.4.2) Determine and analyze the propagation properties for 30 samples of longissimus dorsi for various frequencies and temperatures.
- (§7.4.3) Determine and analyze the sarcomere length and tissue constituents for the samples.
- (§7.4.4) Determine if there is a correlation between ultrasonic, biochemical and structural properties.
- (§7.4.5) Randomly split the 30 samples into two groups of 15 and use one group to develop the empirical model.
- (§7.4.6) Test the predictive ability of the empirical model on the second group.

7.4.1 Generation of the Data Set

The acoustic propagation properties, tissue constituents and sarcomere lengths were determined for a total of 30 muscle samples of longissimus dorsi. For each sample the

attenuation coefficient and speed were analyzed by the DES with the ultrasound propagating parallel and perpendicular to the muscle fiber. Each parallel and perpendicular oriented sample was sectioned into three thicknesses of 0.5, 1.0 and 1.5 cm. For each thickness the insertion loss and speed was determined. The attenuation coefficient was determined from the insertion loss from the three sample thicknesses.

7.4.2 Ultrasonic Propagation Properties of Tissues used for Prediction Model

A randomized block design is used for this experiment. The response variable, the slope of the attenuation coefficient, depends on two factors: fiber orientation and temperature. The speed depends on three factors: fiber orientation, sample thickness and temperature. The factor level for each of these parameters, orientation, thickness and temperature, are listed in Table 7.4.2-1. An analysis of variance (ANOVA) was performed to determine the effects on the propagation measurements on each factor.

7.4.2.1 Slope of the Attenuation Coefficient

The slope of the attenuation coefficient in dB/cm/MHz is determined from a best fit line of the attenuation coefficient over the range of 2-7 MHz for each temperature and fiber orientation. The Pearson product-moment, r, was calculated for each slope. The mean and standard deviation of the Pearson product-moment for all samples was $r = 0.9 \pm 0.1$ which indicates a strong linear relationship between the attenuation coefficient and frequency.

An ANOVA was performed to determine if the slope of the attenuation coefficient was effected by fiber orientation and temperature. A significant effect due to the orientation and temperature is indicated by the F and p-value in Table 7.4.2.1-1. Table 7.4.2.1-2. lists the mean slope of the attenuation coefficient and standard deviation both parallel and perpendicular at 4, 20 and 37°C while Figure 7.4.2.1-2 is a graphical representation of these data. The slope of the attenuation coefficient for the parallel orientation was consistently larger than the perpendicular oriented samples. Ranking the effect of the temperature on the slope of the attenuation coefficient from largest to smallest followed 4, 20 and 37°C, respectively. The anisotropy index for the slope of the attenuation coefficient at 4, 20 and 37°C were 1.82, 1.56 and 1.73, respectively.

7.4.2.2 Ultrasonic Speed

An ANOVA was performed to determine the effect of thickness, sample orientation and temperature on the speed. The ANOVA results in Table 7.4.2.2-1 indicate that there

was no overall variation due to specimen thickness as expected. Therefore these data for all three sample thicknesses can be pooled without affecting the speed results.

With respect to fiber orientation, the ANOVA of the results in Table 7.4.2.2-1 indicate that the speed was significantly higher for ultrasound parallel to the muscle fibers than perpendicular to the muscle fibers. Speed results listed in Table 7.4.2.2-2 were consistently higher in the parallel samples than in the perpendicular samples. As well, the ANOVA of the temperature factor indicated that there were significant variations in the speed due to specimen temperature. With regard to temperature, ranking the speed results from largest to smallest followed 4, 20 and 37°C. A plot of the pooled mean speed and standard deviation as a function of orientation and temperature is shown in Figure 7.4.2.2-1. The anisotropy index for the speed at 4, 20 and 37°C were 1.01, 1.03 and 1.11, respectively.

7.4.3 Biochemical Properties and Sarcomere Length

Table 7.4.3-1 lists the mean and standard deviation of the measurements of the tissue constituents and sarcomere lengths for the 30 samples of longissimus dorsi. Water made up the most abundant portion of the tissue followed by protein and fat, respectively. The interaction between sarcomere length and tissue constituents was evaluated by the Pearson coefficient (ρ) and the level of significance (Fsig) reported in Table 7.4.3-2. The interaction between water and fat was the strongest with a negative interaction of $\rho = -0.91$ which indicates an almost one-to-one replacement between water & fat. Additionally there was significant negative interaction between water & protein ($\rho = -0.50$, Fsig < 0.01) and protein & fat ($\rho = -0.64$, Fsig < 0.01).

7.4.4 Correlation Between Ultrasonic, Biochemical and Structural Properties

A simple linear regression was performed on the data to mathematically describe the relationship between the acoustic propagation properties to the tissue constituents and the sarcomere lengths. Table 7.4.4-1 lists the linear regression equations which relate the acoustic properties at either 4, 20 or 37°C for parallel or perpendicular orientation to the tissue constituent or sarcomere length. The linear regression equations can be used to predict how changes in the %water, %fat, %protein and sarcomere length can effect the attenuation coefficient or speed. The correlation coefficient (r), which indicates the strength of the linear regression model (1 = perfect correlation, 0 = no correlation, -1 = negative correlation), and the significance of the relationship, is also reported. The significance levels in Table 7.4.4-1 indicate that the relations between the slope of the

attenuation coefficient and the tissue constituents (%water and %fat) and under parallel and perpendicular orientation are statistically significant.

7.4.5 The Prediction Model

This experiment has been structured to determine if an empirical mathematical model can predict specific skeletal muscle constituents and structure from detailed knowledge of the acoustic propagation properties. The empirical model is developed by randomly splitting the 30 longissimus dorsi samples into 2 groups of 15 and use one group to develop the empirical model and the second group to test the model. The results presented in the previous section indicate that propagation properties from 2-7 MHz are predominately influenced by the tissue constituents. Table 7.4.5-1 lists multiple linear regression equations for the estimating tissue constituents and the sarcomere length based on the acoustic propagation properties for parallel and perpendicular orientation and temperatures of 4, 20 and 37°C. The F-value and its probability level (F_{sig}) for each equation are listed at the right of each equation. Below each coefficient of the equation is the T_{sig} value which indicates the significance of that coefficient to the dependent variable.

7.4.6 Comparison of the Prediction Model and Actual Results

To test the prediction model, the ultrasonic propagation properties of the second group of 15 samples of longissimus dorsi were used to predict the tissue constituents and sarcomere length based in the prediction equations developed from the first group of 15 samples. Using the multilinear regression equations in Table 7.4.5-1, the predicted tissue constituents and sarcomere length are calculated based on the slope of the attenuation coefficient and speed for the 3 temperatures. Table 7.4.6-1 lists the means and standard deviation of the parallel and perpendicular model results along with the actual results for the tissue constituents and sarcomere length. Table 7.4.6-2 lists the %error for the parallel and perpendicular prediction model compared against the actual biochemical and sarcomere length results.

7.5 Structural Contribution to the Acoustic Propagation Properties

The objective of this section is to determine the structural contribution to the ultrasonic propagation properties using the SLAM which operates at 100 MHz. To determine the degrees to which the structure and architecture contribute to the acoustic propagation properties the following procedure has been developed.

- (§7.5.2) Determine the ultrasonic propagation properties (attenuation coefficient, speed and heterogeneity index) for 18 samples of bovine longissimus dorsi using the SLAM for homogenized and intact muscle.

- (§7.5.3 & 7.5.4) Determine the effects of the homogenization process through visual and biochemical analysis.
- (§7.5.5) Quantify the effects of the ultrasonic propagation properties of homogenized muscle to the intact muscle.

7.5.1 Generation of the Data Set

The attenuation coefficient, speed and heterogeneity index were determined for a total of 18 longissimus dorsi muscle samples from individual bovines. For each sample the acoustic propagation properties were analyzed by the SLAM. Three types of sample orientations were defined according to the relationship between the muscle fiber orientation and the sound beam.

- parallel : ultrasound beam propagating parallel to the muscle fibers.
- perpendicular : ultrasound beam traveling perpendicular to the muscle fibers.
- homogenized : ultrasound beam propagating through muscle samples in which the fiber orientation had been totally disrupted by the homogenization process.

Each parallel, perpendicular or homogenized samples were sliced into three thicknesses of 80, 100 and 120 μm. For each thickness the insertion loss, speed and heterogeneity index was determined. The attenuation coefficient was determined from the least-squares fit of the insertion loss from the three sample thicknesses.

7.5.2 Ultrasonic Propagation Properties

A randomized block design is for this experiment. The response variable attenuation coefficient depends on the factor fiber orientation. However the speed and heterogeneity index depends on the factors fiber orientation and sample thickness. The factor level for orientation and thickness, are listed in Table 7.5.2-1. An ANOVA was performed to determine the effects of the propagation measurements on each factor.

7.5.2.1 Attenuation Coefficient

An ANOVA was performed to determine the effect of fiber orientation. A significant effect is indicated by the results in Table 7.5.2.1-1. The mean attenuation coefficient and standard deviation for parallel, perpendicular and homogenized samples are listed in Table 7.5.2.1-2 and graphed in Figure 7.5.2.1-1. The ANOVA of the results in Table 8.1.2.1-2 reveals that the attenuation coefficient was significantly different depending on the orientation. Ranking the attenuation coefficient results from largest to smallest followed parallel (87 ± 23 dB/mm), perpendicular (45 ± 14 dB/mm) and homogenized (28 ± 14 dB/mm), respectively. The anisotropy index was 3.1.

7.5.2.2 Speed

An ANOVA was performed to determine the effect of sample orientation and thickness on the speed of the samples. The ANOVA results in Table 7.5.2.2-1 indicate that there was no overall variation due to specimen thickness. Therefore the data for all three sample thicknesses can be pooled without affecting the speed results. In contrast, the ANOVA of the results in Table 7.5.2.2-1 indicate that the speed was significantly effected by orientation being higher for ultrasound parallel to the muscle fibers than perpendicular to the muscle fibers. Speed results listed in Table 7.5.2.2-2 and graphed in Figure 7.5.2.2-1. were consistently highest for the ultrasound traveling in the parallel orientation to the muscle fiber and lowest for the ultrasound traveling through the homogenized samples. The mean speed and standard deviation was 1619±16 m/s for parallel, 1599 ± 14 m/s for perpendicular and 1582 ± 18 m/s for homogenized samples. The effect of anisotropy of the tissue was measured as the ratio of the parallel to perpendicular orientation. With respect to the speed results the anisotropic effect value of 1.3%.

7.5.2.3 Heterogeneity Index

The effects of sample orientation and thickness were determined for the samples by an ANOVA for the heterogeneity index. The results of the ANOVA are shown in Table 7.5.2.3-1 and indicate that sample orientation has a significant effect on the heterogeneity index. There is some effect of sample thickness but the p-value (p-value 0.067) is slightly above the significance level of 0.05. Therefore the data for the sample thicknesses can be pooled without affecting the heterogeneity index results. For further analysis the mean and standard deviation of the heterogeneity index for the orientations are listed in Table 7.5.2.3-2 and graphed in Figure 7.5.2.3-1. These results clearly indicate that the homogenized samples are significantly more acoustically homogeneous than the parallel and perpendicular samples and affirm the quality of the homogenization process.

7.5.3 Biochemical Properties

It is important that the homogenization process does not significantly alter the chemical composition of the samples so that the ultrasonic properties of homogenization and intact tissue can be compared directly. A detailed biochemical analysis of the 18 samples of intact longissimus dorsi was determined in another study [Yao, 1995]. A tissue constituents percentage range of 72.5±2.6 for water, 5.5±2.9 for fat and 22.0±1.0 for protein was reported for the 18 samples. After homogenization, respective random samples were selected as a representation of the intact samples and analyzed again for %water, %fat and %protein and compared to their original constituent measurements. The

comparison between the constituents of the intact muscle and the homogenized muscle revealed no greater than a 2% variation in the values. This result indicates the similarity in the constituents of the intact and homogenized samples and moreover indicates no noticeable loss of water due to the homogenization process which would affect the ultrasonic propagation properties.

7.5.4 Sample Homogeneity

In addition to the biochemical analysis and the heterogeneity index, intact and homogenized samples from adjacent tissue from the same animal were microscopically inspected to determine the extent to which the regular pattern and structure of the myofibrils was completely destroyed. Mounted and stained samples were visually inspected with the Nikon Labophot at 100 x 2.5 microscope by Dr. James Zachary, a veterinary pathologist. Figure 7.5.4-1 displays the optical image of the intact sample and the homogenized sample. The pathological assessment of the homogenizing process was that, 1) all well defined unidirectional arrangement and structure due to the myofibrils had been destroyed, 2) there was a high degree of muscle nucleus cell trauma and destruction, and 3) the extent of the destruction was continuous throughout the homogenized sample [Zachary, 1996].

7.6 Anisotropy of the Ultrasonic Propagation Properties from Skeletal Muscle

Materials containing oriented structures display a directional dependence of the ultrasound properties; this effect should be accounted for in this examination of skeletal muscle tissues. The objective of this section is to determine the anisotropic effect on the ultrasonic propagation properties at high and low frequencies due to the fiber orientation of skeletal muscle, specifically bovine semitendinosis. To accomplish this task, the following procedure has been developed.

- (§7.6.1) Determine the attenuation coefficient and speed for 8 samples of bovine semitendinosis using the SLAM @ 100 MHz as a function of the angle of insonification of the muscle fibers.
- (§7.6.2) Determine the attenuation coefficient and speed for 8 samples of bovine semitendinosis using the DES @ 3 MHz as a function of the angle of insonification of the muscle fibers.

7.6.1 Ultrasonic Propagation Properties as a Function of the Angle of Insonification at 100 MHz

Several samples of bovine semitendinosis were used to determine the effect of anisotropy on the acoustic propagation properties using the SLAM. Ultrasonic propagation properties at insonification angles of 90, 80, 35, 45, 55, and 10 degrees with respect to the fiber orientation were obtained. The 90° and 10° angles of insonification were previously defined in Section 7.3 as the perpendicular and parallel fiber orientation with respect to the propagating ultrasound from the SLAM stage, respectively, and the attenuation coefficient and speed results at 90° and 10° were previously presented in Section 7.3. Table 7.6.1-1 lists the mean attenuation coefficient and speed along standard deviations as a function of the insonification angle. Figure 7.6.1-1 graphs the mean and standard deviation of the attenuation coefficient results and Figure 7.6.1-2 is a graph of the mean and standard deviation speed results. A significant effect between the 90° and 10° angles of insonification for the attenuation coefficient and speed has been shown in Section 7.3. A linear regression of the attenuation coefficient and speed data in Figure 7.6.1-1 and Figure 7.6.1-2, respectively, yields two equations in Table 7.6.1-2 for the attenuation coefficient and speed, respectively, as a function of the insonification angle at 100 MHz from 10 to 90°. The correlation coefficient (r) at the right of both linear equations ($r = 0.94$ for the attenuation coefficient and $r = 0.98$ for the speed) indicates a strong correlation between the angle and the acoustic propagation properties.

7.6.2 Ultrasonic Propagation Properties as a Function of the Angle of Insonification at 3 MHz

Eight samples of semitendinosis were used with the DES at 3 MHz to determine the effect of anisotropy on the attenuation coefficient and speed. Figure 7.6.2-1 is a graph of the mean of the attenuation coefficient as a function of the angle of insonification for the 8 semitendinosis samples. The angle of insonification is from 0° to 180° in 5° steps. The attenuation coefficient for the parallel and perpendicular orientation at 3 MHz are 3.84 ± 0.03 and 2.82 ± 0.01, respectively. The mean speed and standard deviation as a function of the angle of insonification for 8 semitendinosis samples is graphed in Figure 7.6.2-2. For the parallel orientation the mean speed and standard deviation was 1616 ± 9, and 1607 ± 5 for the perpendicular orientation.

Table 7.6.2-1. Interpolation of the attenuation coefficient and speed data in Figure 7.6.2-1 and Figure 7.6.2-2, respectively, by a fourth order polynomial yields two equations for the attenuation coefficient and speed as a function of the insonification angle at 3 MHz from 0 to 180° in Table 7.6.2-1. The correlation coefficient (r) at the right of the

fourth order polynomials (r = 0.97 for the attenuation coefficient and r = 0.99 for the speed) indicate a strong correlation described by the equations between the angle and the acoustic propagation properties.

7.6.3 Comparison Between the DES and SLAM Results

A comparison of the slope of the attenuation coefficient (i.e. the ration of the attenuation coefficient to the frequency expressed as dB/cm/MHz) results from the SLAM and the DES reveals results within an order of magnitude as seen in Table 7.6.3-1. Table 7.6.3-1 lists the slope of the attenuation coefficient at similar angles of insonification for the DES and the SLAM. The anisotropy effect for the slope of the attenuation coefficient was 1.33 for SLAM results and 1.48 for the DES results. For the speed, the anisotropic effect was measured to be 1.02 using the SLAM and 1.01 using the DES.

8. DISCUSSION

Previously researchers have examined the relationship between ultrasonic propagation properties and one tissue constituent [Sarvazyan et. al, 1987; Suzuki et. al., 1992] such as water or fat. Because of the non-invasive diagnostic capabilities of ultrasound, the area of acoustic tissue characterization should be extended to examine the relationship between acoustic properties and the tissue's architecture and the major tissue constituents. Recently researchers have started to examine the relationship between the acoustic parameters and diseased tissue such as dystrophic muscle, [Hete and Shung, 1994], liver fibrosis [van der Steen et al., 1994] and diseased cardiac muscle [Davidson et al., 1995]. Ultrasonic tissue characterization plays an important role as a non-invasive method to follow the progression of these diseases in order to assist a physician in predicting when clinical intervention is necessary.

The major aim of this research was to determine whether a series of empirical models could be derived which would enable the physical properties of tissue to be determined via their ultrasonic properties. This would allow non-destructive chemical analysis to be performed, and could ultimately be used in medical diagnostic ultrasound. The ultrasound properties which were studied were attenuation, speed of sound, and heterogeneity. These properties were obtained at different temperatures and different orientations of the sample with respect to the ultrasound beam. A sufficient number of samples were used for each experiment to enable rigorous statistical analysis to be carried out. The specific conclusions of this research are summarized below.

8.1 Uncertainty Measurements on the SLAM and DES

Table 7.3 lists a summary of the uncertainty assessment for the SLAM and the DES. Steiger (1986) previously determined the accuracy and precision of the ultrasonic speed for the SLAM to be ± 2.9 % and ± 0.4 %, respectively. Steiger also determined the accuracy and precision of the attenuation coefficient to be ± 12 % and ± 15 %, respectively. A possible reason for the improvement of the accuracy can be attributed to the improved data acquisition system whereby the acoustic and interference images are digitized by high resolution frame grabber and processed by software that performs frame averaging, convolutions for filtering and histograms for determining dynamic range [Nicozisin, 1989]. Meanwhile, this is the first reporting of accuracy and precision for the speed and attenuation coefficient for the DES.

8.2 Tissue Constituents and Sarcomere Length Predictions using the SLAM

The prediction model for estimating tissue constituents and sarcomere length at 100MHz is remarkably accurate, with very low errors in estimating the %water, %protein and sarcomere length. Although the percentage error for fat estimation is high, it should be noted that the absolute percentage of fat in tissue is extremely low and therefore the absolute error in fat determination is only a few percent. Overall, this newly obtained model is able to determine tissue constituents using ultrasound to within 5%, and determine sarcomere lengths with an accuracy of less than half a micron.

Although %water and sarcomere length exhibited a positive interaction ($\rho = 0.86$, Fsig < 0.01) in Table 7.3.3-2, there is actually little correlation between sarcomere length and %water and the results are due to the examination of only three types of muscle tissue. Using sarcomere length and %water results of 13 bovine muscle types listed in Table 3.3.5-2 from McKeith et al. (1985), the correlation was determined to be $\rho = 0.041$ which indicates little correlation between sarcomere length and water.

Overall, there is excellent agreement between the empirical models developed, and the chemical and physical composition of "blind" samples which were investigated. Typical errors were less than 10% in the determination of %water, %fat, %protein and sarcomere length. These results represent the first demonstration of determining both accurate chemical composition and molecular structure dimensions in the tissue being studied.

The regression equations can be directly compared with results from previous studied listed in Table 4.2-1. For example, Yao (1995) made attenuation coefficient and speed measurements at 100 MHz on 18 longissimus dorsi samples at 20°C. Regression equations were derived, but not tested, relating the attenuation coefficient and speed to the %water, fat and protein. Effects of the muscle architecture, i.e. the sarcomere length, were not included. The results presented were considerably different from those determined by this more sophisticated model. Comparison with Table 7.3.4-1 shows considerable differences in the equations derived. However, it should be noted that both models give similar absolute valued for both attenuation coefficient and speed. Moreover, close examination shows that both models predict very similar speed and attenuation coefficient dependence on the tissues constituents for both parallel and perpendicular orientation.

It is also worth comparing and contrasting these results with Tervola et al. (1985). In this the authors use the SLAM at 100 MHz to investigate the effects of fat concentration from 3-17% on the acoustic propagation properties of rat liver. Regression analysis was then used to derive the attenuation coefficient and speed as a functions of the fat concentration. While it is clear that absolute values cannot be directly compared for the two

different tissue types particularly since muscle acoustic are so orientation dependent, the following should be noted.

(1) For all of the muscle types studied, the attenuation coefficient increases with increasing fat concentration (Table 7.3.4-1) as did the attenuation coefficient in rat liver.

(2) The correlation values, r, reported in Table 7.3.4-2 for the correlation between fat concentration and attenuation coefficient are very similar to those reported by Tervola et al.

(3) In contrast to the results in rat liver, the speed was found to increase with increasing fat concentration for the three samples for both parallel and perpendicular orientation.

Muscle exposed to cold (approximately 0-15°C) before rigor mortis is called cold shorting whereby the myofibril shortens 60% of its original length. However muscle or meat that is stretched before rigor mortis tends to be more tender. Using bovine sternomandibularis muscle, Woods (1985) compared the attenuation coefficient of cold-shortened (short sarcomere length) and non-cold shortened (long sarcomere length) muscle with the sound beam perpendicular to the muscle fiber. Woods found the attenuation coefficient for cold-shortened muscle to be higher than the non-cold shortened muscle. These results aggree with the attenuation coefficient versus sarcomere length results in Table 7.3.4-1(d). In contrast, May (1987) found the attenuation coefficient higher for stretched sternomandibularis muscle (long sarcomere length) higher than cold-shortened (short sarcomere length) muscle. However the p-value of an ANOVA his results did not indicate a significant difference between the stretched and cold-shortened attenuation coefficient data ($p = 0.25$) and no actual measurements of the sarcomere length were performed.

8.3 Temperature-Frequency Dependent Acoustic Propagation Properties: Tissue Constituents and Sarcomere Length Predictions using the DES

Overall, the empirical model developed for predicting tissue constituents and sarcomere length using the DES was not as good as the ability of the SLAM in forecasting tissue constituents and sarcomere length. Results obtained at lower temperatures (4°C) are consistently better then those at higher temperatures, with all parameters within 10%. The water percentage, in particular, is very accurately predicted for all temperatures.

The ability of the prediction equations to determine the sarcomere length using the DES falls short of the design because of the operating frequency of the DES. The SLAM which operates at a frequency of 100 MHz and has a wavelength of 15 μm therefore is far better for resolving the acoustic changes in the sarcomere length. The DES, on the other hand, has a wavelength range of 1.5-0.15 mm which is much larger than the length of a sarcomere.

The slope of the attenuation coefficient (SAC) and speed (c) are influenced by temperature. The slope of the attenuation coefficient decreases as a function of temperature (T) for the parallel and perpendicular muscle according to:

$$SAC\ (dB/cm/MHz) = 2.9 - 3.2 \times 10^{-2} \bullet (T) \qquad (8.3\text{-}1)$$

and

$$SAC\ (dB/cm/MHz) = 1.7 - 1.7 \times 10^{-2} \bullet (T), \qquad (8.3\text{-}2)$$

respectively. The speed (c) increases as a function of temperature for the parallel and perpendicular muscle according to:

$$c\ (m/s) = 1524 + 4.1 \bullet (T) \qquad (8.3\text{-}3)$$

and

$$c\ (m/s) = 1511 + 4.1 \bullet (T), \qquad (8.3\text{-}4)$$

respectively.

In spite of some drawbacks such as the inability for the DES to make sarcomere length predictions, the DES is good at predicting the %water and %protein with worst case predictions of 5.9% and 22%, respectively.

8.4 Structural Contribution to the Acoustic Propagation Properties

Destruction of the regular myofibril architecture of the muscle allows for the determination of the ultrasonic propagation properties due to macromolecular level interaction without the influence of the structure of the myofibril. The mean attenuation coefficient for parallel, perpendicular and homogenized samples was 87 , 45 and 28 dB/mm, respectively. For the speed, the parallel, perpendicular and homogenized results were 1619, 1599 and 1582, respectively. The results for the attenuation coefficient and speed were found to be significantly different for the orientations. These results indicate the destruction of the muscle architecture plays a critical role in the propagation of ultrasound through tissue.

Acoustic propagation properties of biological tissues such as the attenuation coefficient, absorption coefficient and speed of sound are largely influenced at the macromolecular level by specific tissue constituents. Pauly and Schwan (1971) concluded that two-thirds of absorption occurs at the macromolecular level and one-third caused by physical structure using intact and homogenized bovine liver at 1-7 MHz. These results were confirmed for homogenates of bovine skeletal muscle (Woods 1985, Table 4.2-1)

who determined that the attenuation by myofibrils caused 64% of the attenuation. Parker et al., (1987) found this component to be smaller in homogenized rat liver. Results presented in this research showed that for bovine skeletal muscle, the ratio of the parallel to homogenized and perpendicular to homogenized attenuation coefficient results was 3.1% and 1.6%, respectively. The results from this study indicated for the first time that the myofibril structural influence on the attenuation coefficient at 100 MHz has a range from approximately 33-66% depending on the orientation. This agrees with the results of other researchers at low frequencies. Wood and Miles (1986) determined that 40-64% of the attenuation coefficient in bovine skeletal muscle homogenates was caused by the myofibrils at 1.5-7 MHz and that the remaining component was caused by viscous losses.

8.6 Anisotropy of the Ultrasonic Propagation Properties from Skeletal Muscle

Materials containing oriented structures display a directional dependence of the ultrasound properties and thus this effect should be accounted for in this examination of skeletal muscle tissues. Previous researchers have seen the effects on anisotropy of the acoustic propagation properties of cardiac muscle and Achilles tendon [Verdonk et al., 1992; Kumar and Mottley, 1994; Hoffmeister et al., 1994]. Research by Hoffmeister et al., (1994) using bovine Achilles tendon with a well defined unidirectional arrangement of fibers found a variation in the attenuation and speed with small angular rotations of the tendon fibers.

The large correlation coefficients of the equations which describe the relationship between the acoustic propagation and insonification angle indicate that the acoustic propagation properties as function of angle can be confidently modeled using the linear equation for the SLAM (from 10 to 90°) and 4th order polynomial for the DES (from 0 to 180°).

The results from this study revels the anisotropy of the ultrasonic propagation properties relative to the muscle fiber orientation at high (100 MHz) and low (3 MHz) frequencies. Higher values of the attenuation coefficient were measured when the ultrasound traveled parallel then when it traveled perpendicular to the fibers. From Figures 8.4.2-1 and 8.4.2-2, the attenuation coefficient and speed behave in a sinusoidal manner as the fibers were rotated from 0 to 180°.

A comparison of the slope of the attenuation coefficient results from the SLAM and the DES reveal comparable results within an order of magnitude. Table 7.6.3-1 lists the slope of the attenuation coefficient at similar angles of insonification for the DES and the SLAM. The anisotropy effect for the slope of the attenuation coefficient was 1.33 for the

SLAM and 1.48 for the DES. For the speed, the anisotropic effect was measured to be 1.02 for the SLAM and 1.01 for the DES. The similarity in the speed results for the SLAM at 100 MHz and the DES at 3 MHz indicates that the dispersion effects are negligible.

8.7 Conclusions

There are a number of medical imaging techniques that are used in everyday clinical diagnosis. Ultrasound, computed tomography (CT), magnetic resonance imaging (MRI) and nuclear medicine being the most common. Each of these techniques has advantages and disadvantages in terms of cost, spatial and temporal resolution, safety and non-invasive character. Ideally, an imaging modality should be able not only to give spatial information, but also specific information about the physical and chemical structure of the tissue being imaged. In MRI, for example, it is very easy to distinguish between fat and water using standard imaging protocols, since the signal from fat is much brighter. Quantitative evaluation of the relative amounts of fat and water, however, is very difficult. Determination of protein content can only be measured indirectly and qualitatively using specialized imaging sequences. Structural information likewise relies on indirect measurements of the water self-diffusion coefficient, which is again a non-standard procedure. While information on specific metabolites such as lactate and adenosine triphosphate (ATP) can be obtained, these localized spectroscopy methods have extremely low spatial (1-5 cc) and temporal (5-60 minutes) resolution.

Diagnostic ultrasound shows considerably more promise for tissue characterization within a clinical setting. It has high temporal and spatial resolution, and has the option of operating over a variable frequency range, rather than being fixed at a given frequency. Measurements of the speed and attenuation coefficient can be made relatively easily. Therefore, the "holy grail" is to be able to combine high structural and physical informational content with standard scanning procedures, in much the same way as Doppler flow methods can be interleaved with B-mode scans. Such an aim relies on the accurate modeling of the ultrasonic properties related to tissue structure and chemical components, in particular %water, %fat, and %protein. Many investigations have been published in the literature, but these have largely been incomplete, or have concentrated on either the chemical composition or the tissue structure, but not both. In addition, other factors which could be used, such as temperature, have not been widely studied. The novel aspect of this research is to hypothesize that by introducing a fourth element, the sarcomere length, which is integral to an accurate model of the physical, as opposed to chemical, structure of the muscle, accurate mathematical relationships can be developed. This

research represents one of the first examples of a complete treatment of the subject, with the derivation of multiple regression equations which can be used to predict the chemical composition and sarcomere length for an unknown sample. Necessarily, all of the initial work has been carried out in-vitro, and the models developed in this thesis need to be tested *in-vivo*.

APPENDIX A

FIGURES

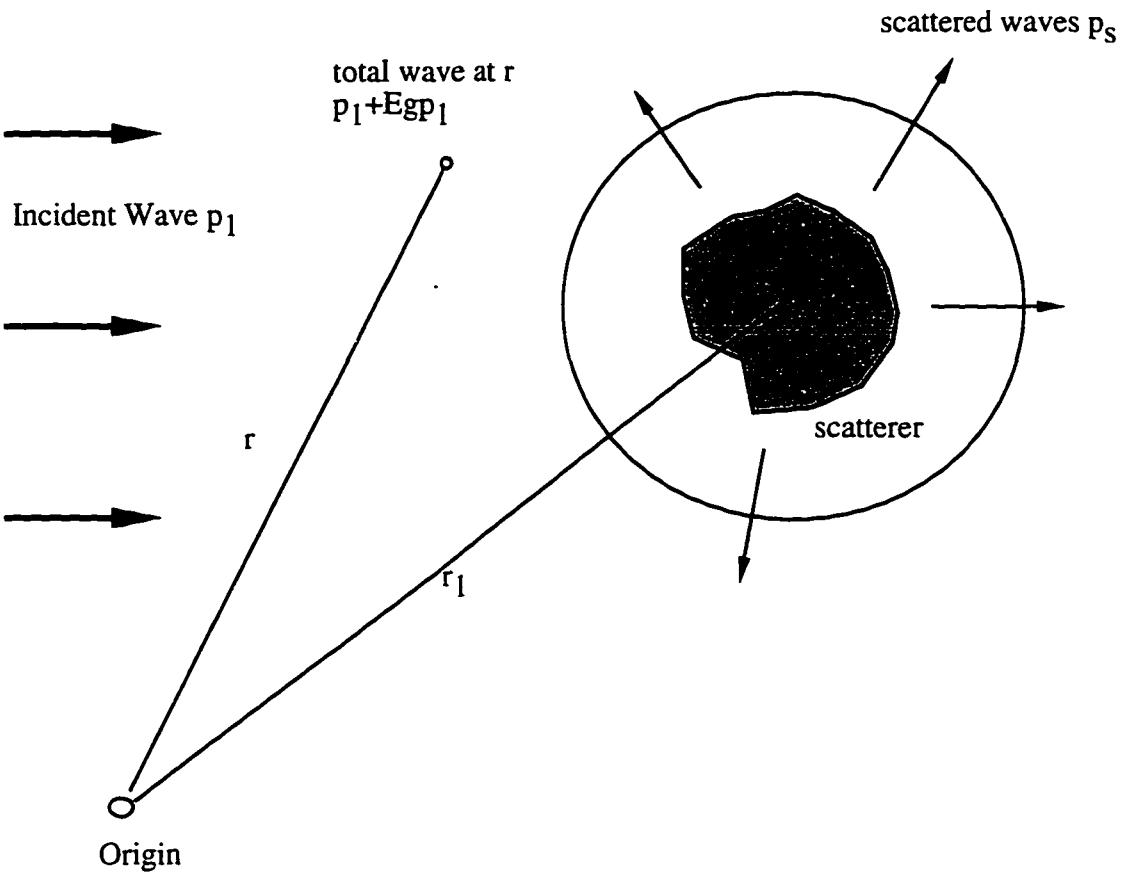

Figure 2.8-1 Scatter from a single scatter characterized by the scattering function.

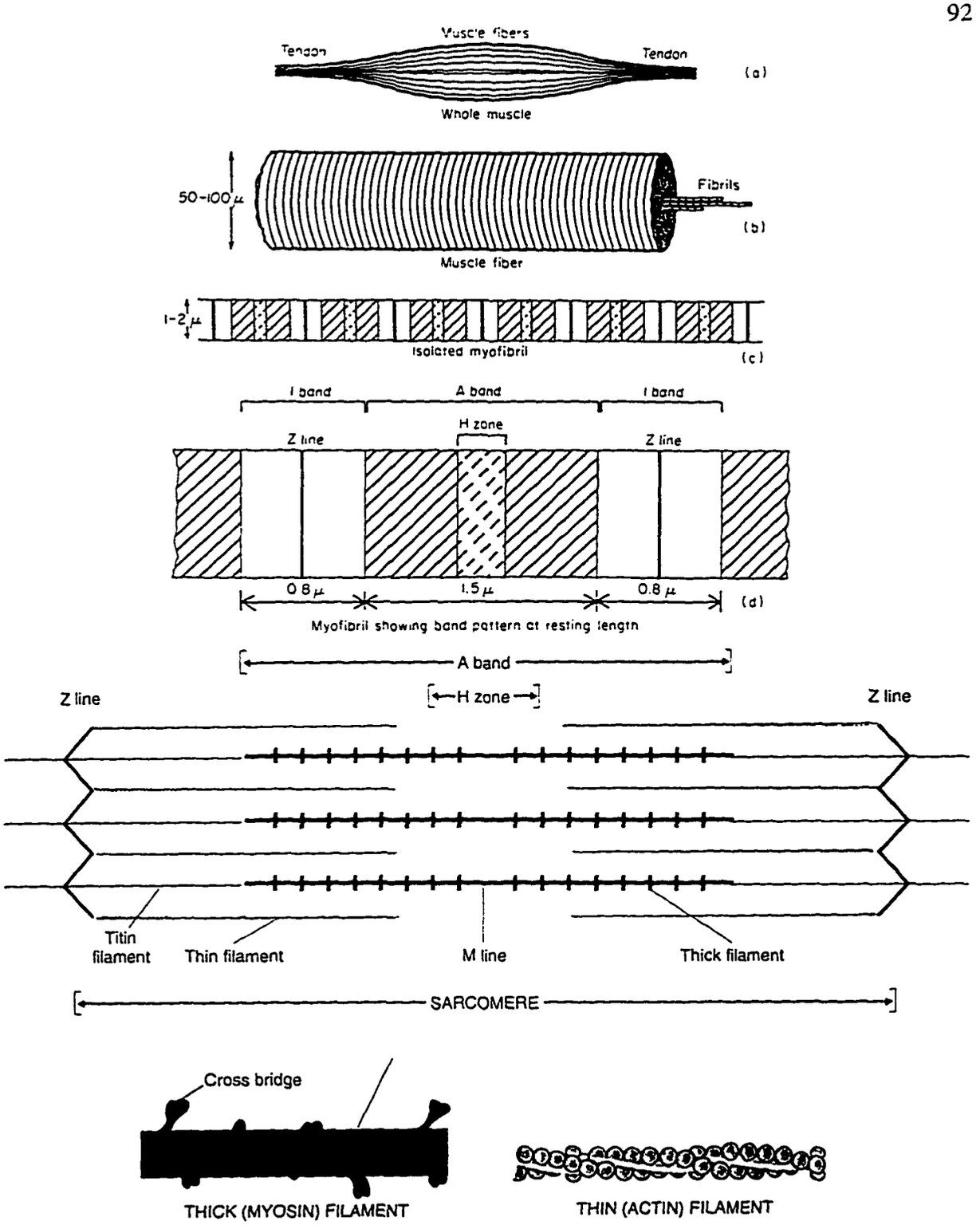

Figure 3.1-1 Diameters and arrangement of filaments in skeletal muscle fiber that produce the striated banding pattern along with arrangement of the thick and thin filaments in the single sarcomere [Huxley, 1973; Vander et al., 1994].

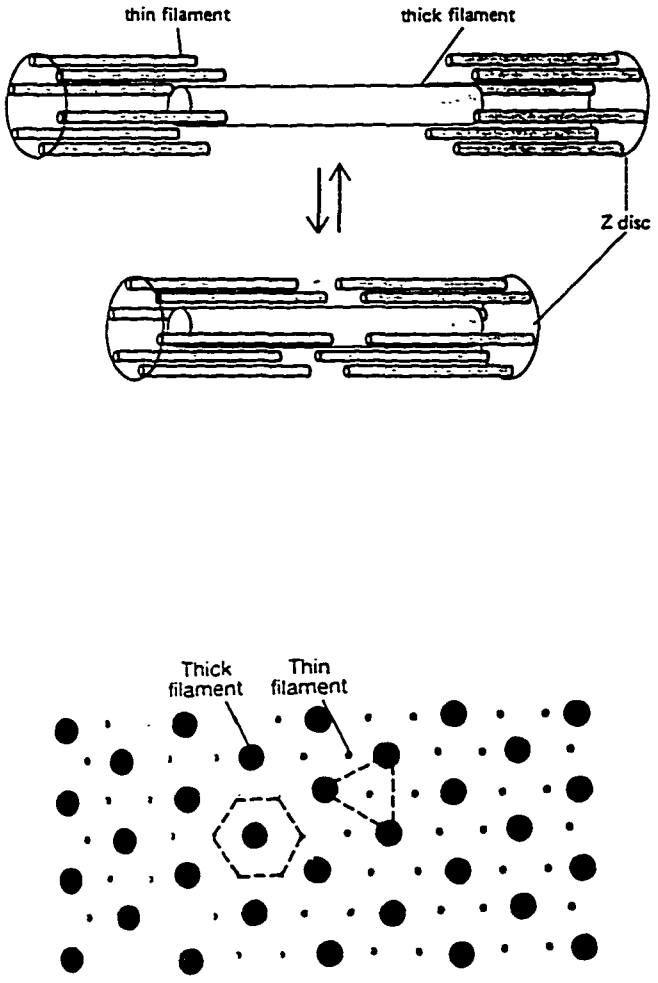

Figure 3.1-2 The top figure shows the sliding filaments model of muscle contraction in which the thin and thick filaments slide past one another. The bottom figure shows a cross section through the A band of adjacent myofibrils show the regular arrangement of the thick and thin filaments. [Alberts et al., 1989; Vander et al., 1994].

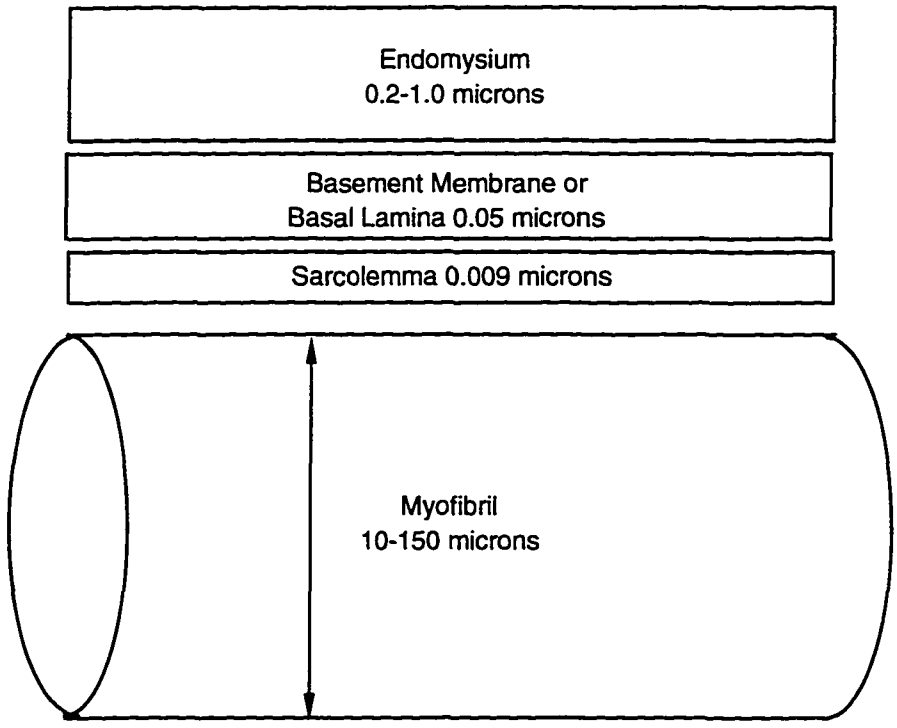

Figure 3.1-3 The endomysium surrounds each myofibril (10-150 μm diameter) with a connective tissue matrix. The myofibrils are surrounded by a 0.009 μm thick plasma membrane known as the sarcolemma. Around the sarcolemma is a 0.05μm thick protein polysaccahride cover known as the basal lamina. The 0.20-1.0 μm thick endomysium surrounds the basal lamina.

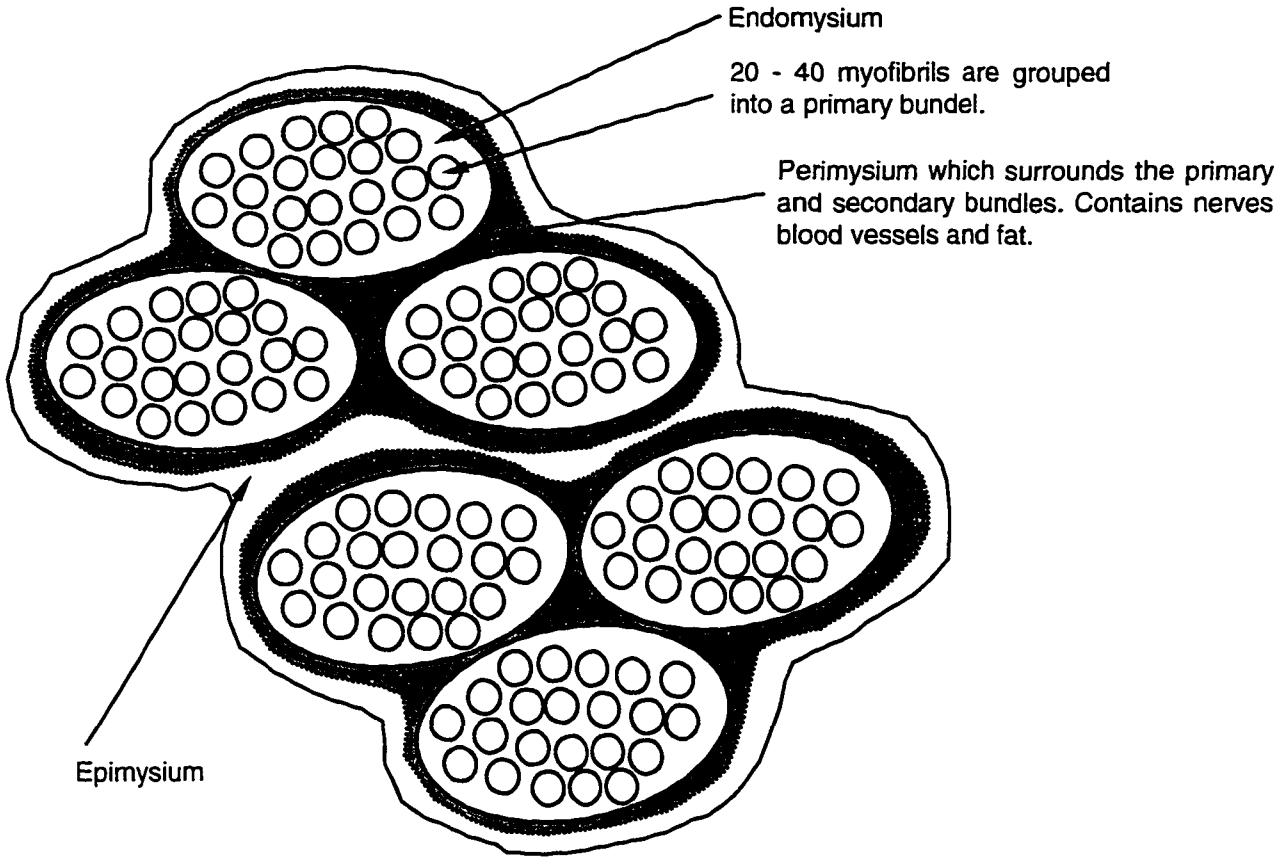

Figure 3.1-4 A cross section through the myofibrils and the connective tissue which binds the muscle fibers together into bundles. The endomysium surrounds each myofibril with a connective tissue matrix. Approximately 20 to 40 myofibrils are bundled together into a primary bundle which are grouped into secondary bundles surrounded by another connective matrix called the perimysium. Surrounding the entire muscle is the connective tissue matrix known as the epimysium.

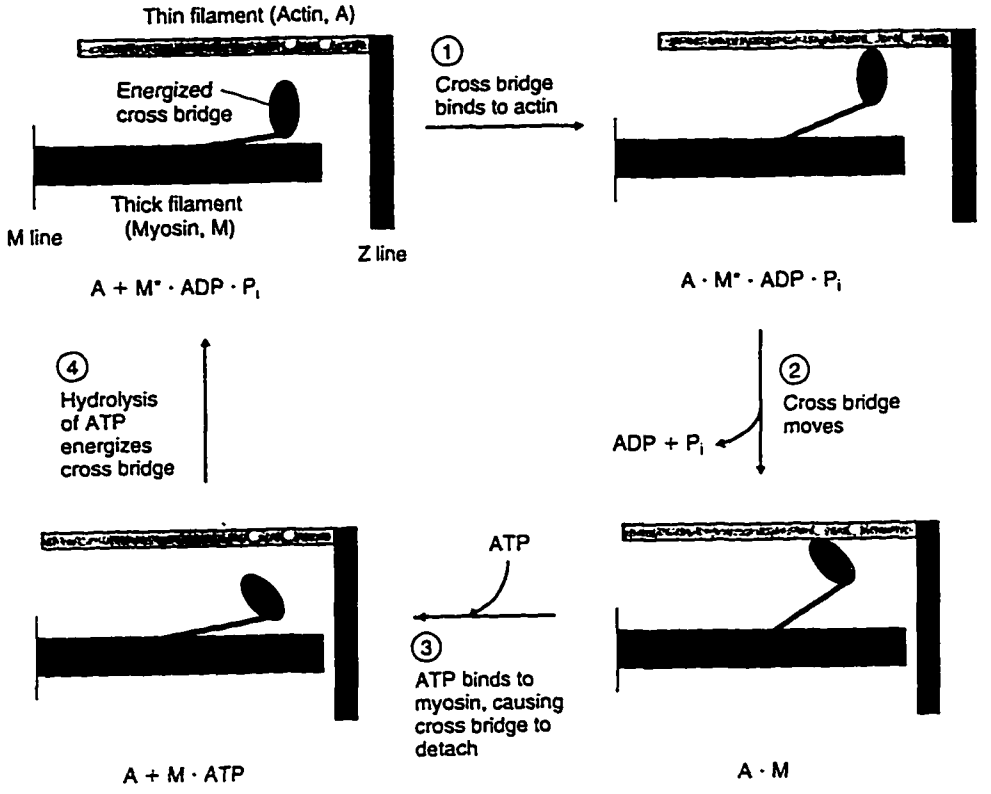

Figure 3.2-1 During the four stages of a cross bridge cycle the thick and thin filaments undergo chemical and mechanical changes. In step 1 contraction begins with the binding of the cross bridge to actin in the thin filament in a resting muscle [Vander et al., 1994].

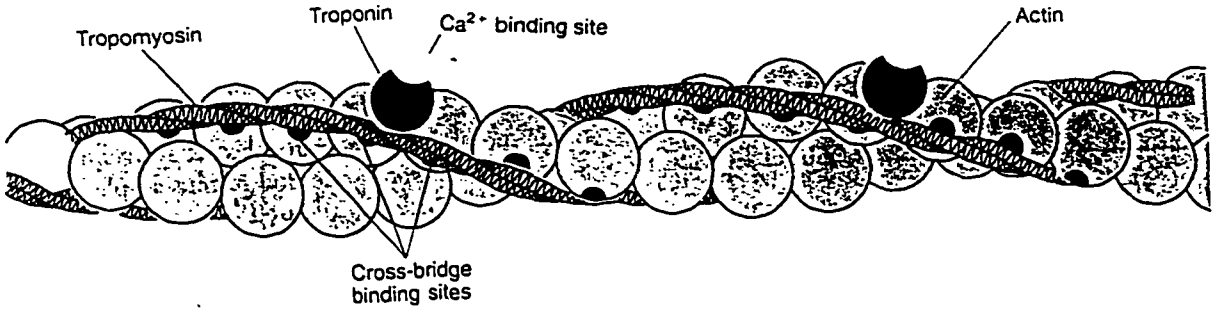

Figure 3.2-2 The cross bridge binding site on actin is regulated by the two chains of tropomyosin. The troponin molecule is bound to the tropomyosin molecule [Vander et al., 1994].

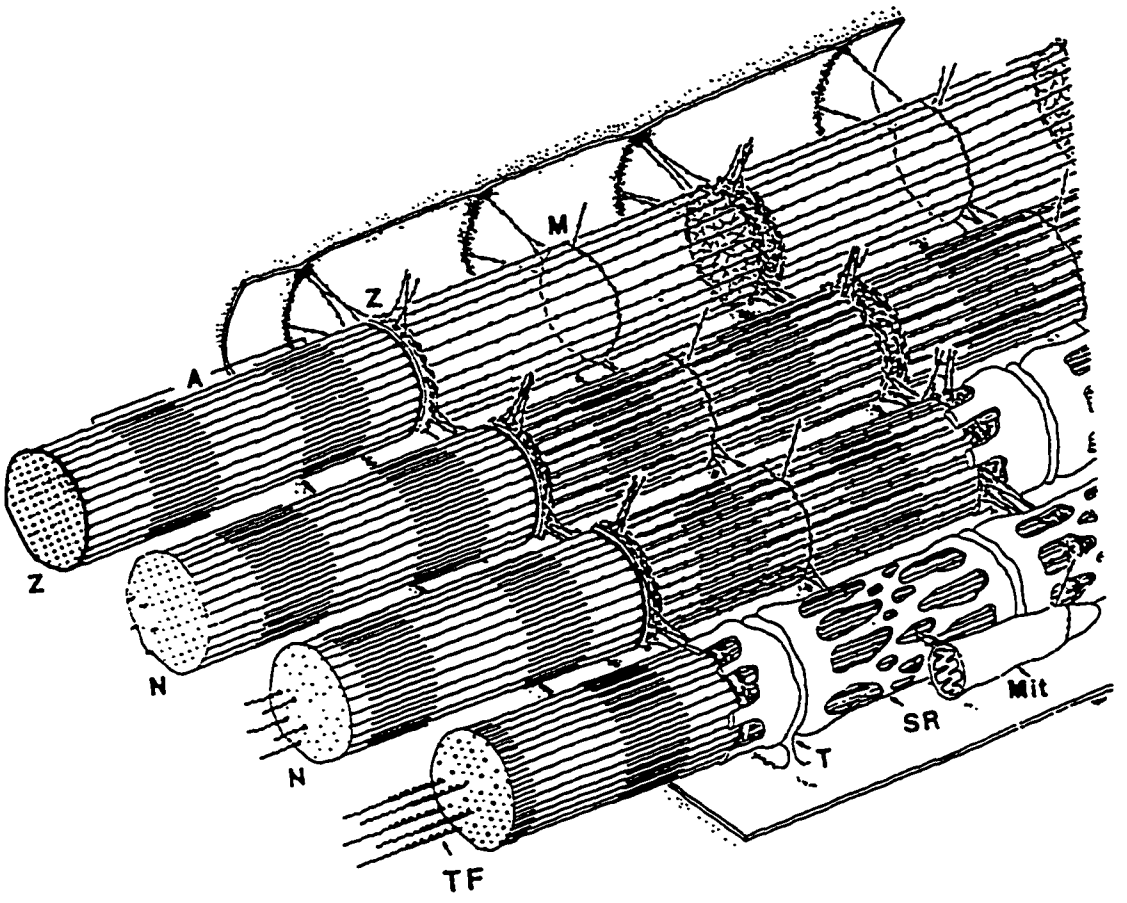

Figure 3.3.4-1 Model of the organization of the cytoskeletal filaments in skeletal muscle. Depicted are the Z-disks (Z), sarcoplasmic reticulum (SR), T-tubules, (T), M-Line (M), A-zone (A), titin-nebulin containing filaments (TF), mitochondria (Mit) and nebulin filaments (N) [Wang, 1985].

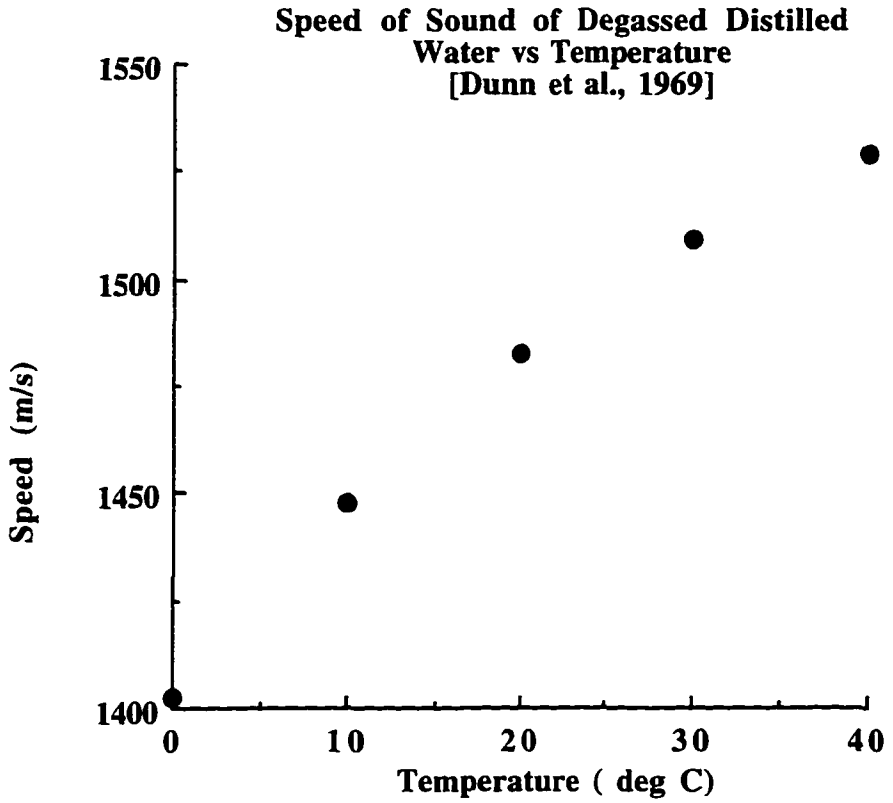

Figure 4.1-1 Speed of sound in water as a function of temperature plotted from data published from Dunn et al., 1969. The speed of sound in water increases for increasing temperatures.

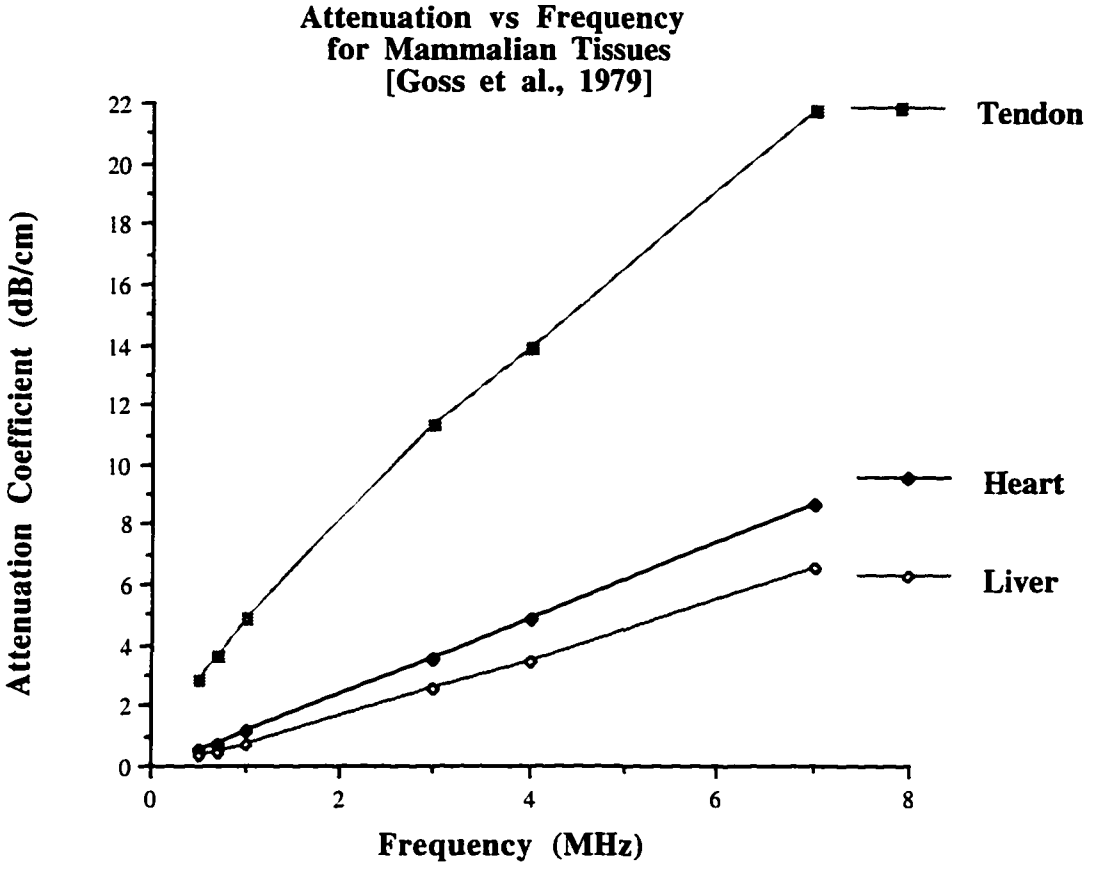

Figure 4.1-2. Graph of the attenuation coefficient versus frequency (0.5-7 MHz) for mammalian tendon, heart and liver. Measurements were made at 37.0°C. These data indicate that high collagen content (tendon) exhibits a high attenuation coefficient and low collagen content (liver) exhibits a low attenuation coefficient [Goss et al., 1979].

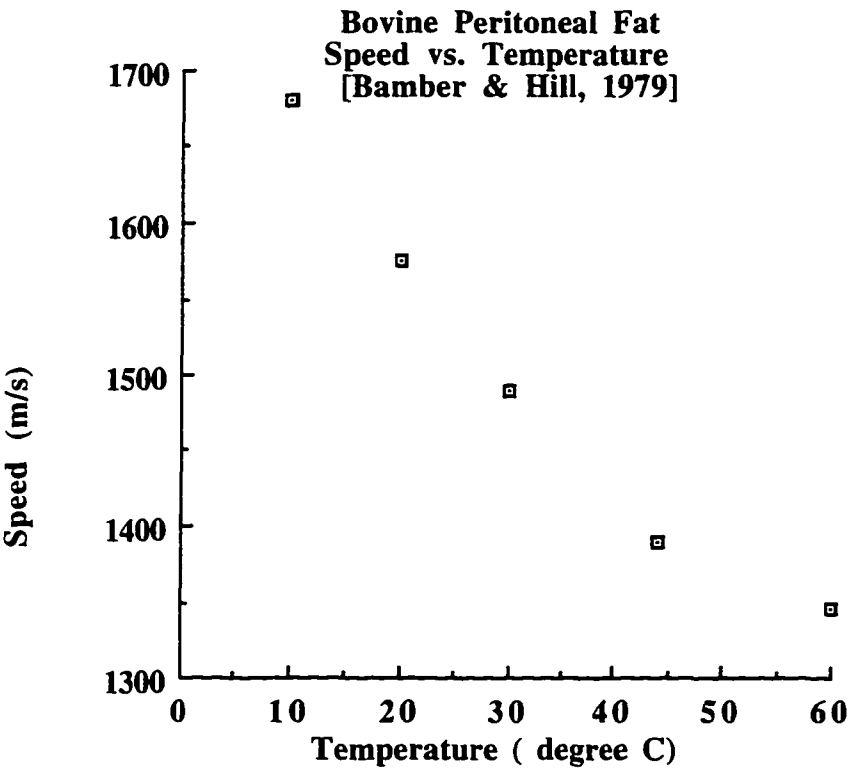

Figure 4.1-3 Plot of the speed of sound versus temperature for bovine peritoneal fat (consisting of mesothelium and a thin layer of irregular connective tissue that lines the abdominal cavity and covers most of the viscera). Bamber and Hill (1979) found a decrease in the ultrasonic speed with increasing temperature.

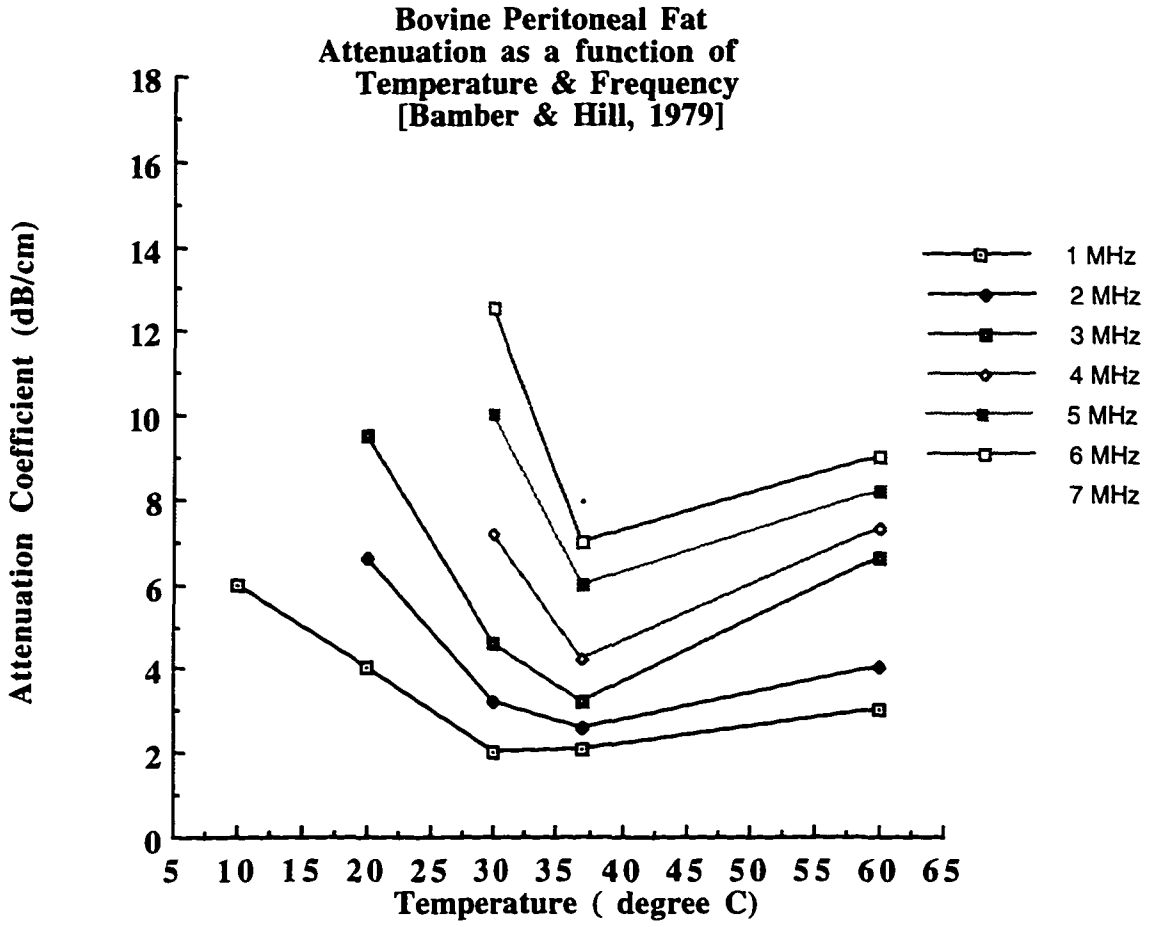

Figure 4.1-4 Plot of the attenuation coefficient as a function of temperature and frequency for bovine peritoneal fat. The error in the data was reported to be no greater than ±10%.

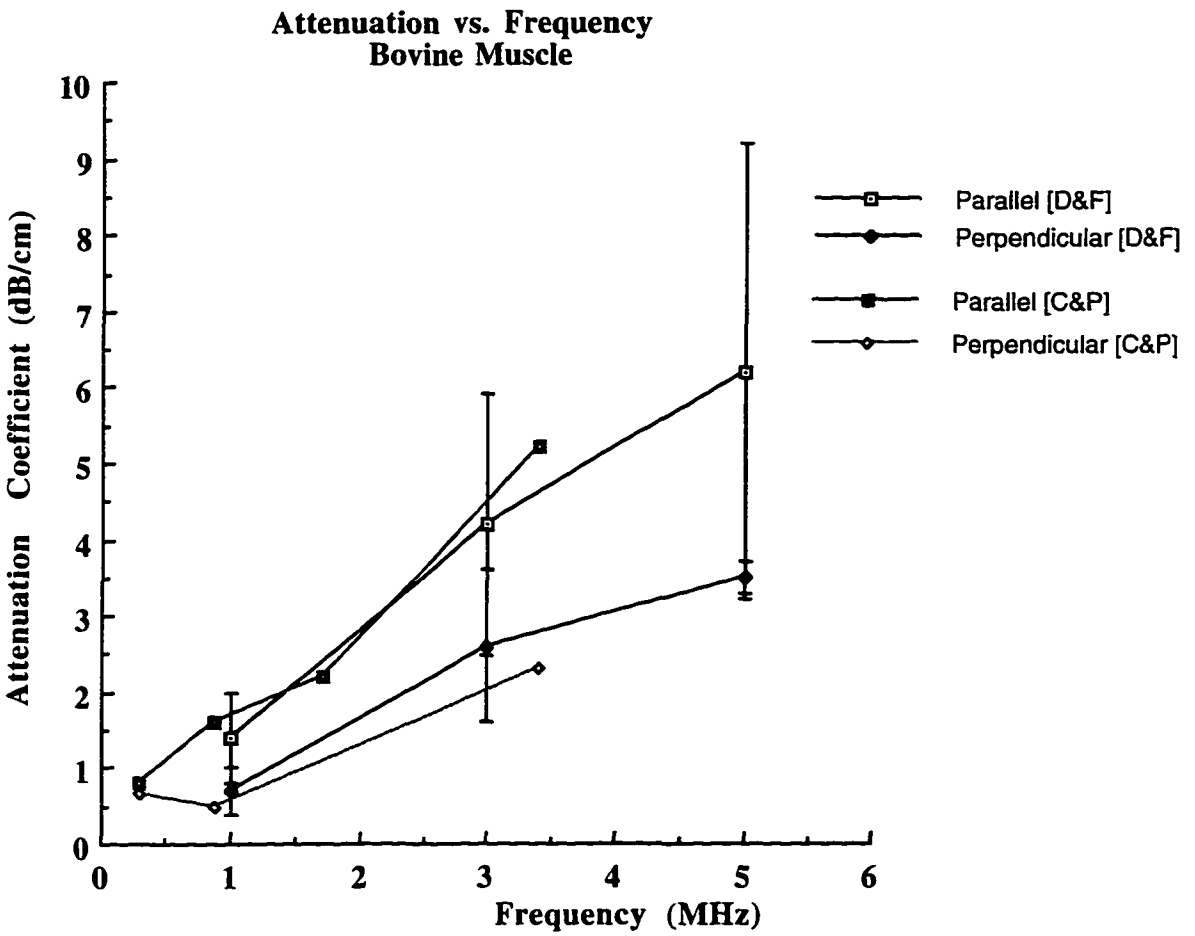

Figure 4.2-1 Comparison of attenuation coefficient versus frequency as a function of fiber orientation (i.e. ultrasound parallel perpendicular to muscle fibers) for bovine tissue from two different papers. The [D&F] in the legend represents work done by Dussik & Fritch, 1956, and the [C&P] represents work by Colobati & Pertlia, 1950.

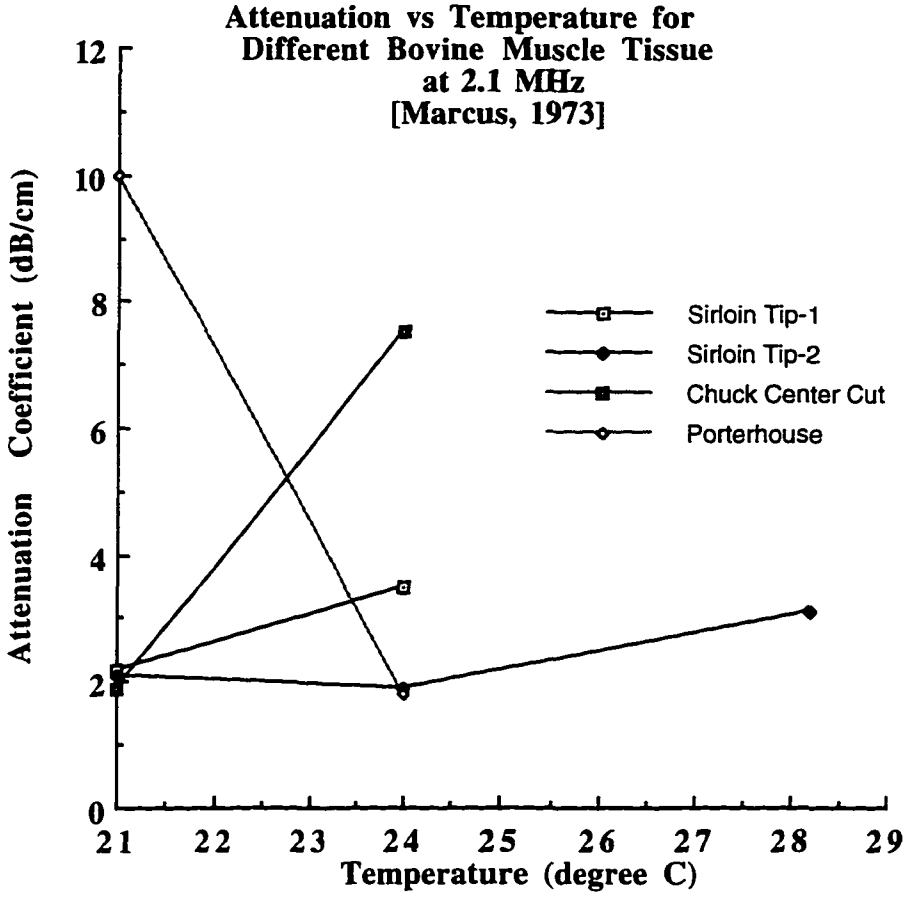

Figure 4.2-2 Attenuation coefficient versus temperature for different bovine muscle types. Sirloin tip-1, center cut and porterhouse had all been kept refrigerated before exposure. Sirloin tip-2 was the same sample as sirloin tip-1 except frozen and thawed before the exposure.

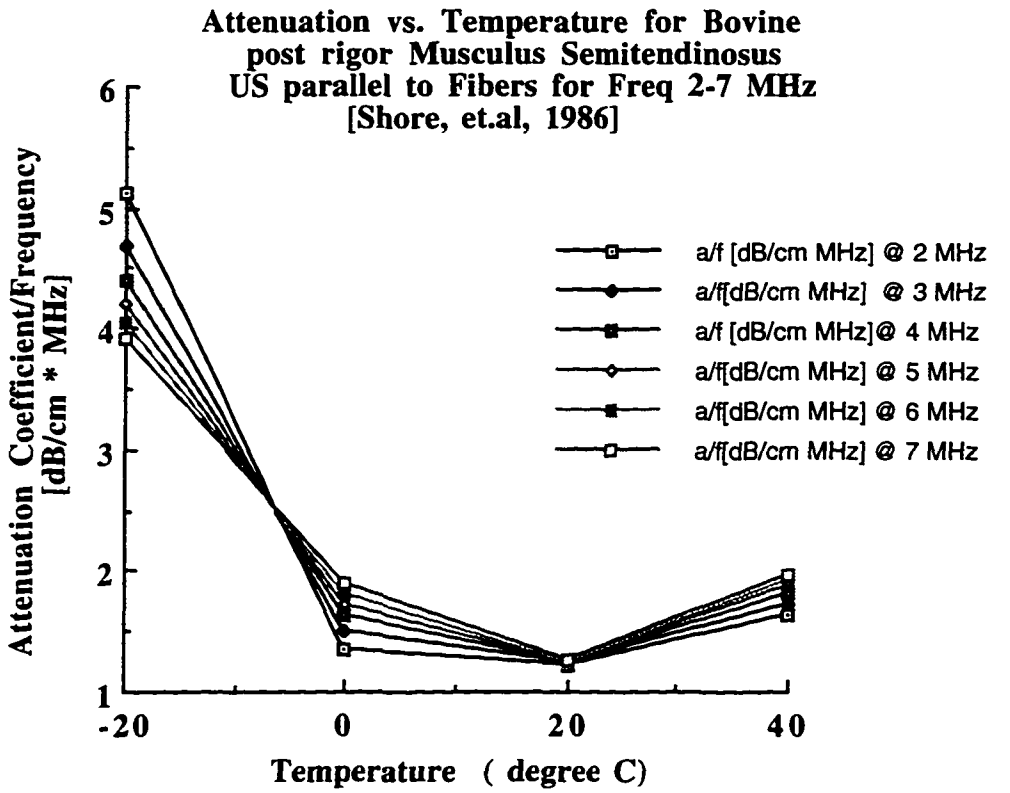

Figure 4.2-3. Attenuation coefficient versus temperature with the ultrasound parallel to the muscle fibers. The error in the attenuation measurements ranges from 0.128-0.15 dB/cm [Shore, et al., 1986].

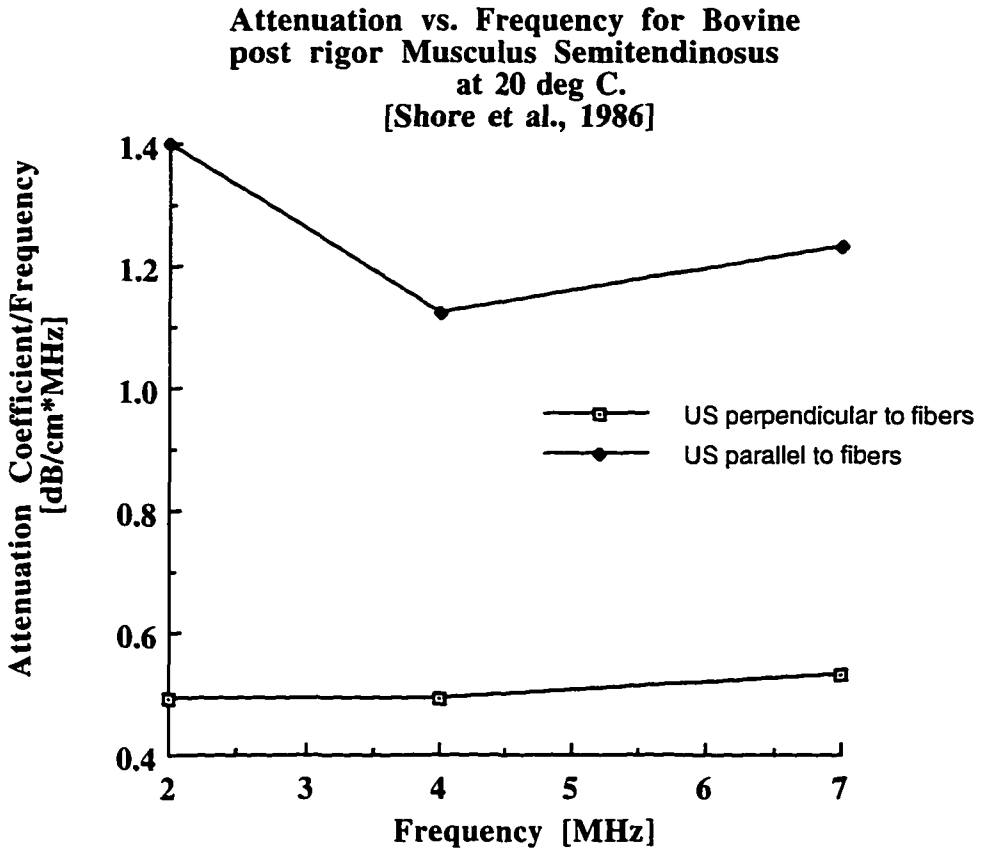

Figure 4.2-4. The attenuation coefficient of ultrasound parallel and perpendicular to the to the muscle fibers at 20°C for frequencies of 2, 4 and 7 MHz. No error is reported for these data and only 2 muscle samples were used for this experiment [Shore et al., 1986].

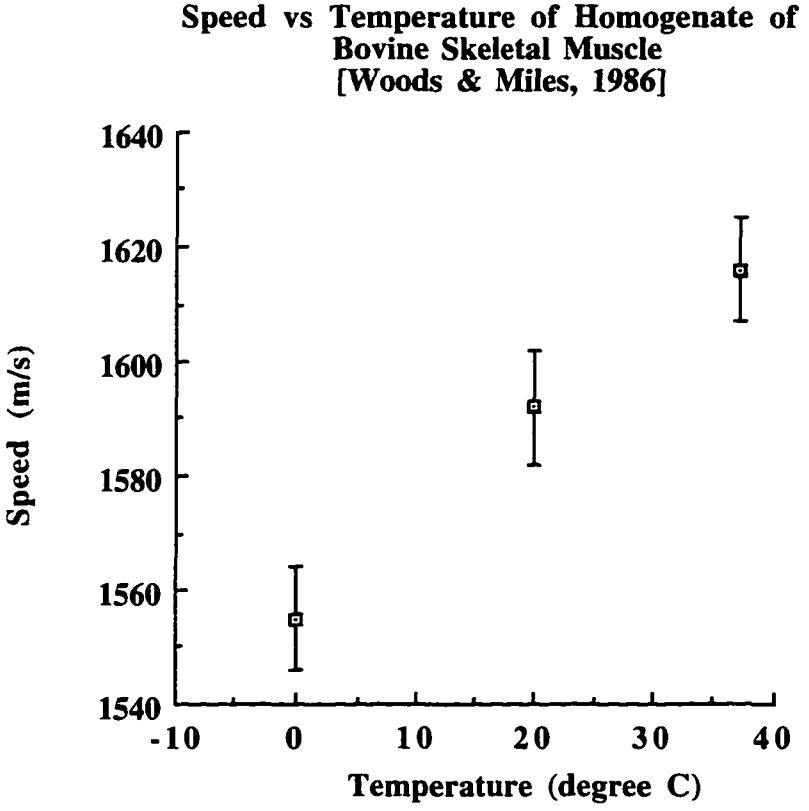

Figure 4.2-5. The ultrasonic speed versus temperatures of 0, 20 and 37°C for fat trimmed homogenates of bovine skeletal muscle is replotted from the data listed in Woods & Miles, 1986.

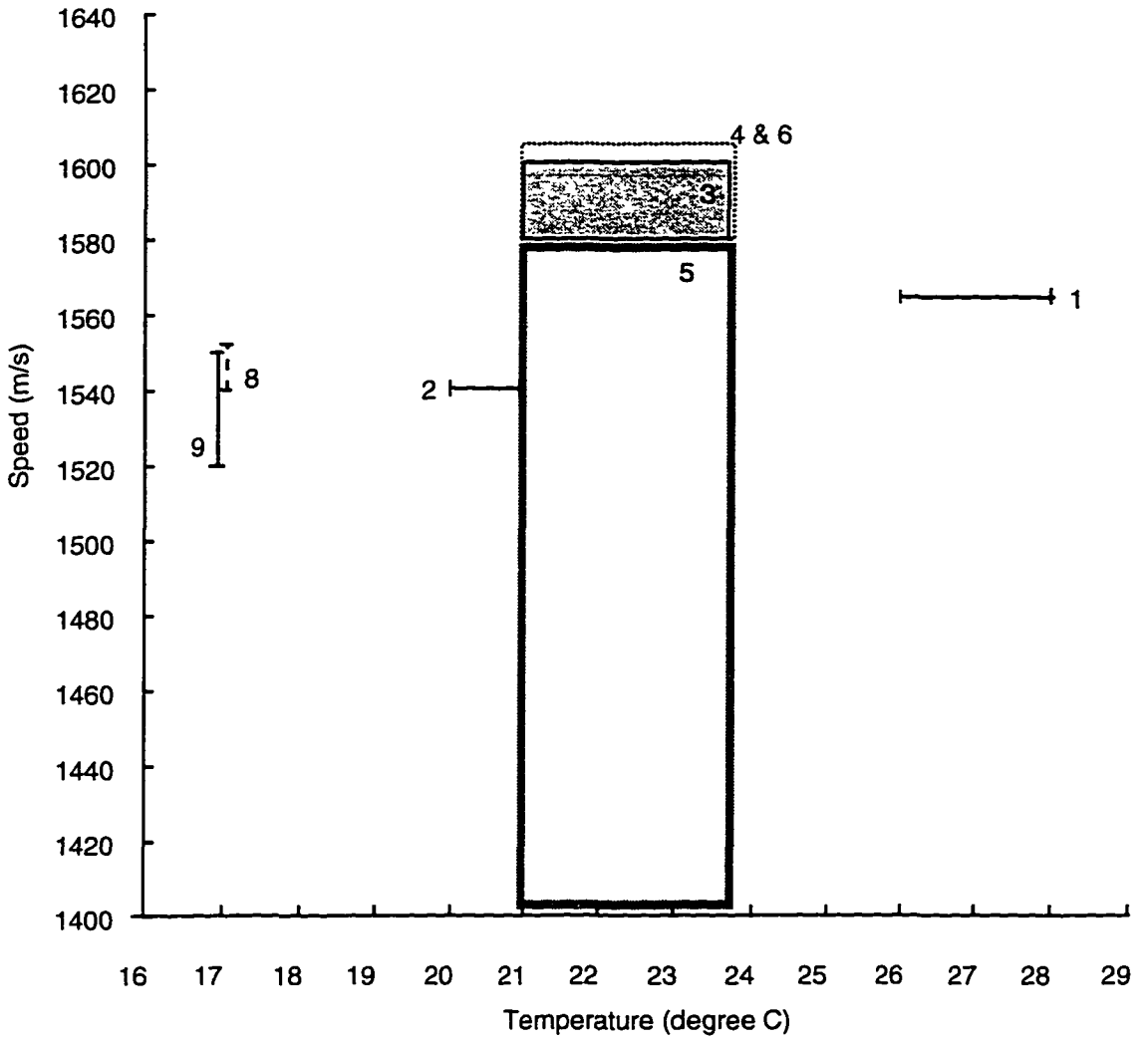

Reference No#	Muscle Type	Temperature (C)	Speed (m/s)	Reference
1	Striated, parallel	26-28	1566	Dussick & Fitch, 1956
2	*Unspecified, in vitro*	20-21	1540	Ludwig & Struthers, 1949
3	Sirloin Tip-1	21-24	1579-1600	Marcus, 1973
4	Center Cut	21-24	1579-1603	Marcus, 1973
5	Porterhouse	21-24	1401-1579	Marcus, 1973
6	Sirloin Tip-2	21-24	1579-1602	Marcus, 1973
7	Unspecified	not reported	1630	Rich, et al, 1966
8	Unspecified	17	1540-1552	Hara, et al.,1979
9	Unspecified Fatty	17	1522-1550	Hara, et al.,1979

Figure 4.2-6 Speed of sound versus temperature for different skeletal muscle types is graphed above. The number in the figure legend can be used to reference specific muscle group to a particular velocity .

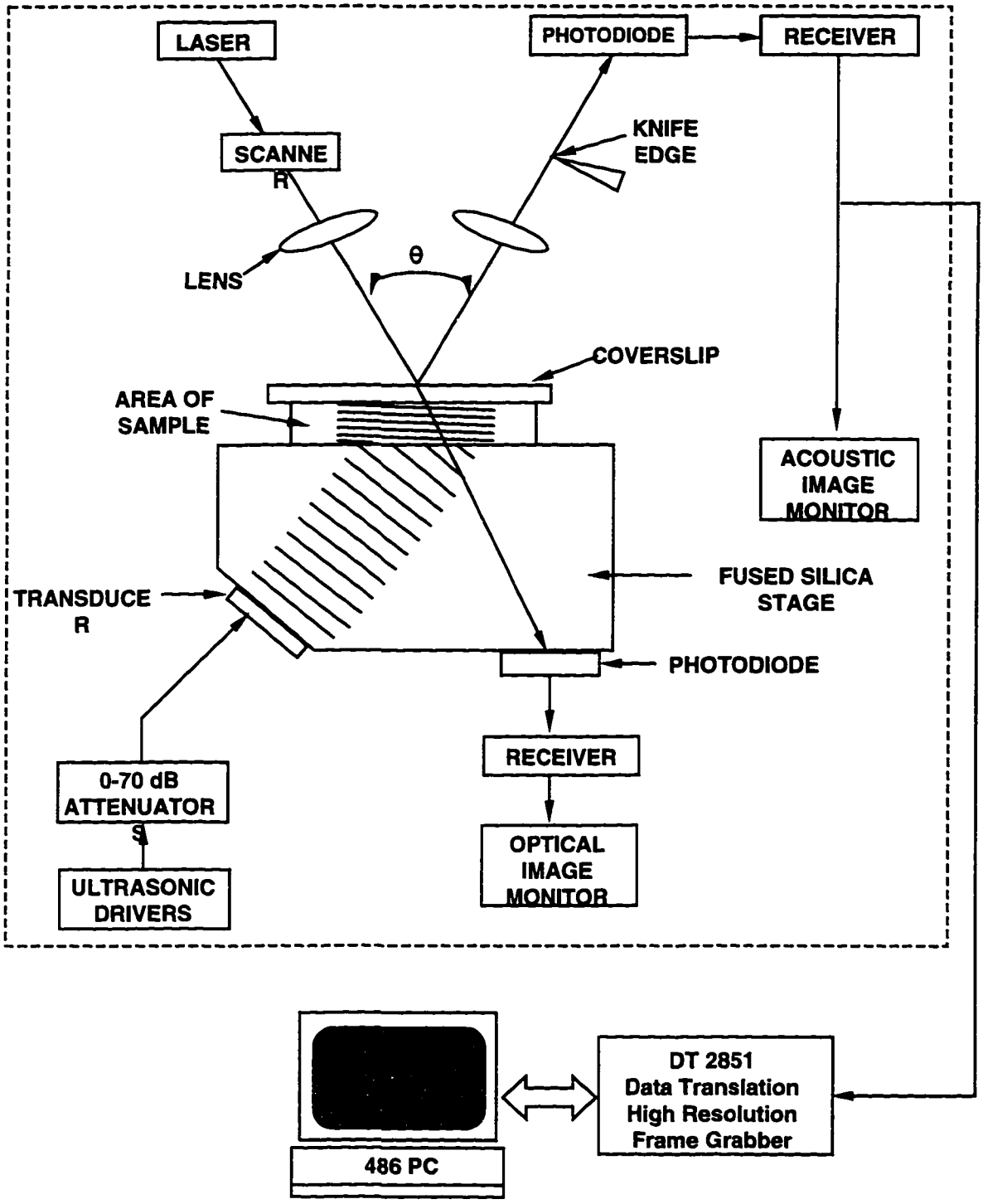

Figure 5.1-1. Block diagram of the SLAM.

(a) acoustic image

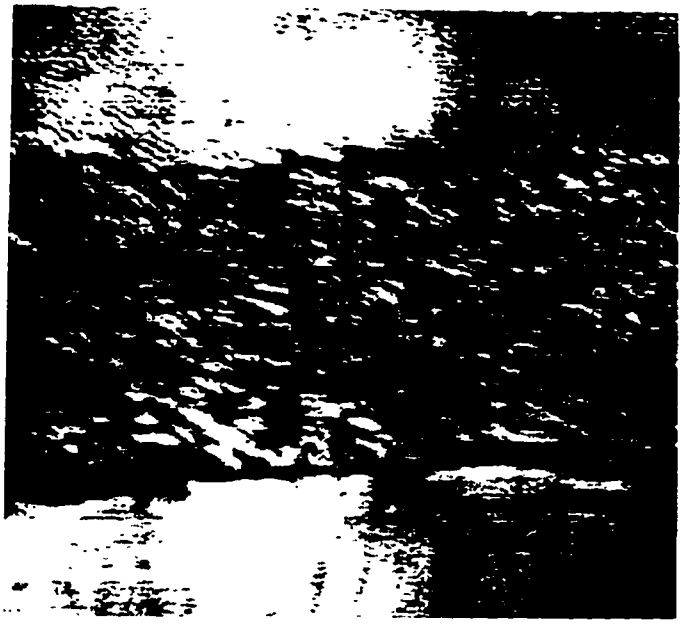

(b) interference image

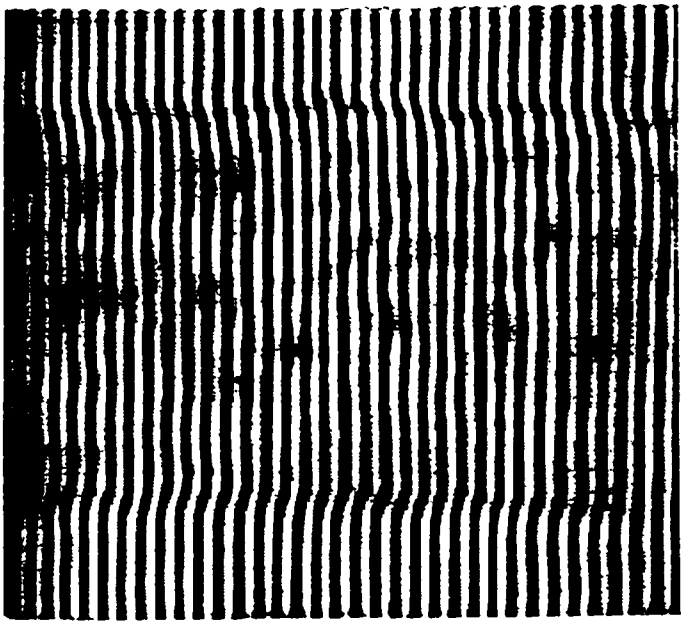

Figure 5.1-2 The SLAM provides two types of images for characterizing the bovine tissue at 100MHz. (a) The acoustic image is used for determining the insertion loss and the (b) interference image is used for determining speed.

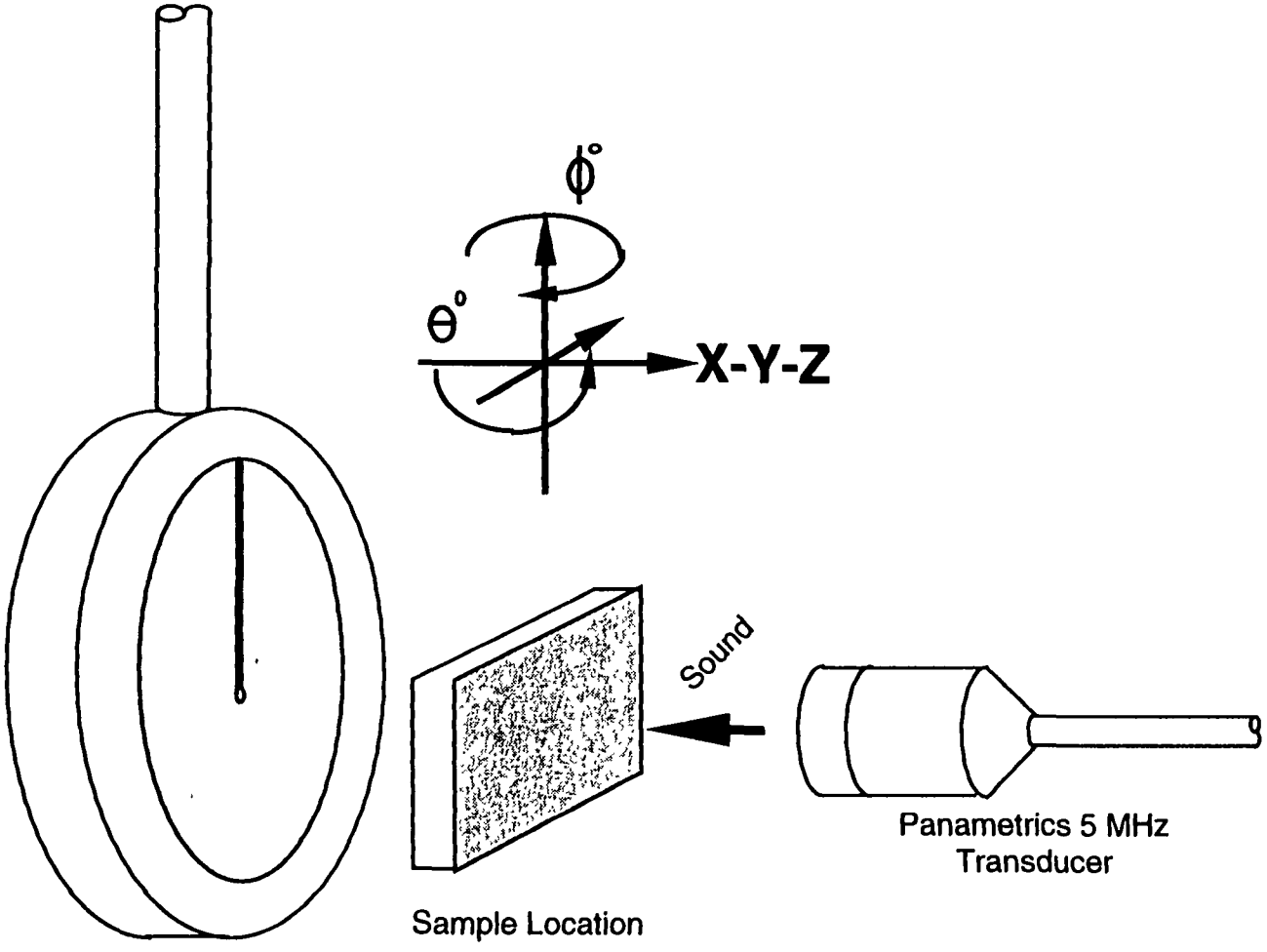

Figure 5.2-1. Information about the ultrasonic propagation properties is aquired by transmitting ultrasound through a sample material, The sample, either calibration material or a tissue sample, is attached to the moving arm of the Daedal positioning system which allows multiple data points to be aquired. The hydrophone and the transducer are held stationary. All experiments are performed in degassed water.

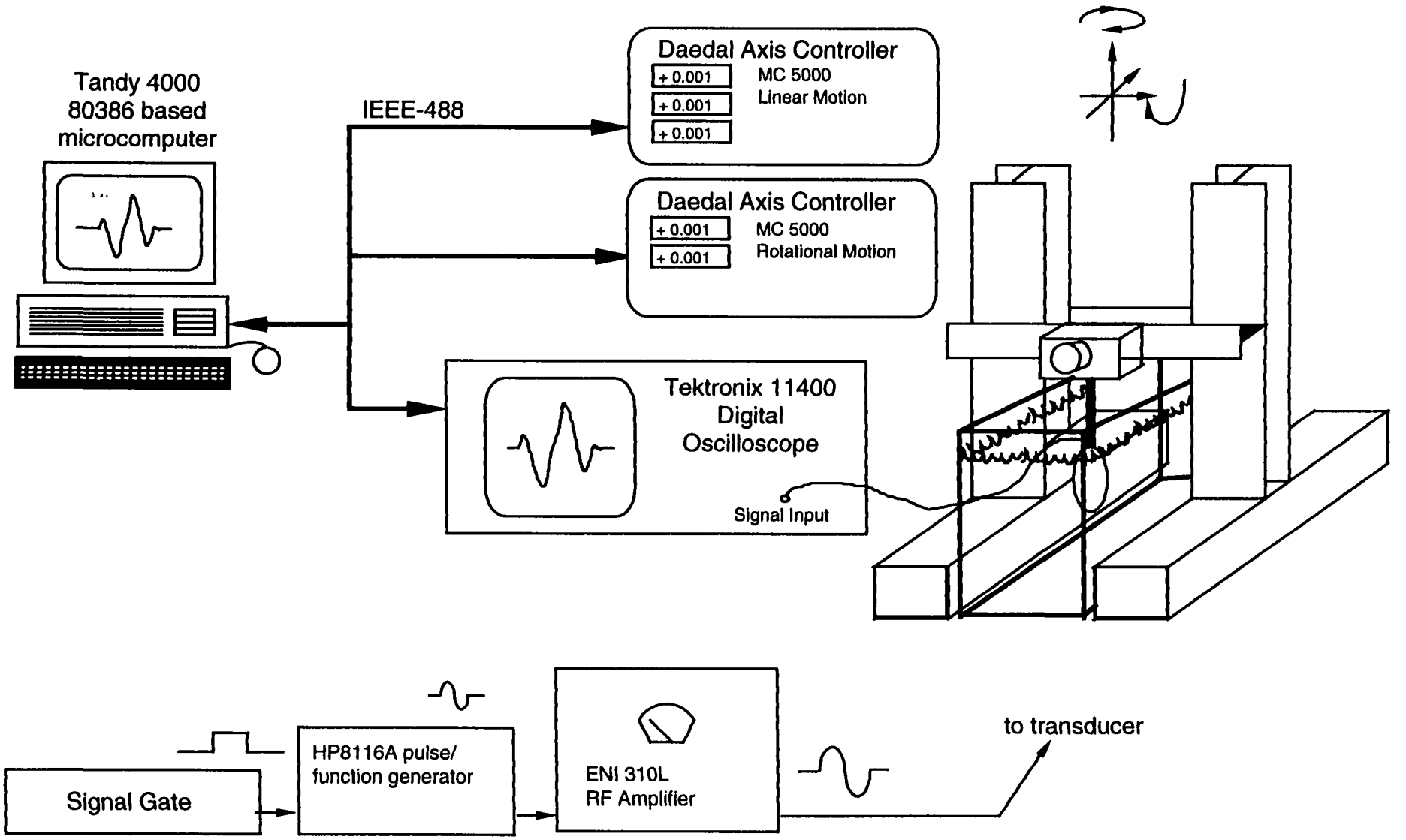

Figure 5.2-2 Block diagram of equipment used for the attenuation and speed of sound measurements. The experimental setup for measuring the attenuation and time of flight of a tissue specimen or of the calibration material with the transducer and hydrophone in the tank is not shown.

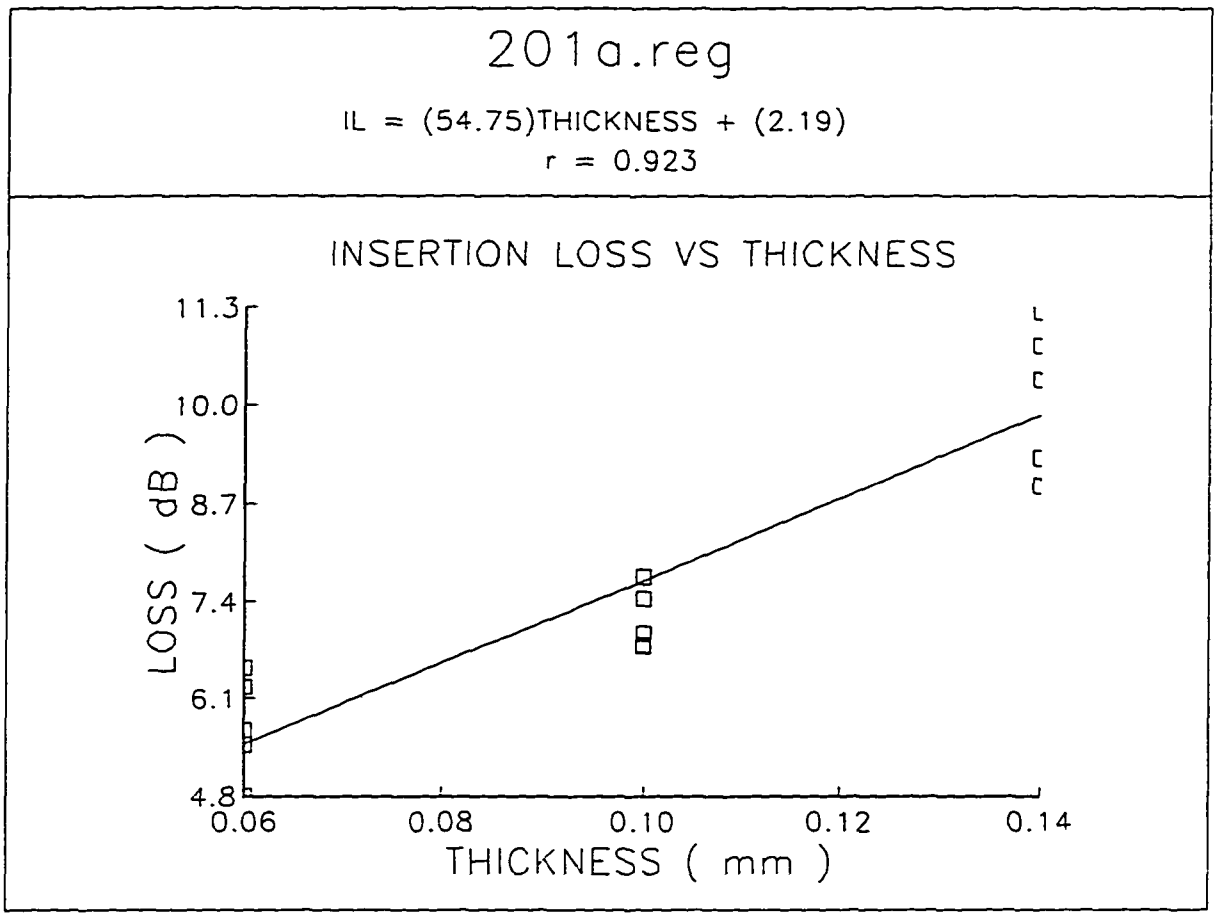

Figure 6.1.1-1 The insertion loss versus for three thicknesses is used for determining the attenuation coefficient. A linear least-squares fit utilizing the insertion loss and thickness values is used to determine the slope of insertion loss versus sample thickness yielding the attenuation coefficient. For this example the attenuation coefficient is 54.75 dB/mm, the loss (y-axis) intercept is 2.19 dB and the correlation coefficient of the least square fit is r=0.923.

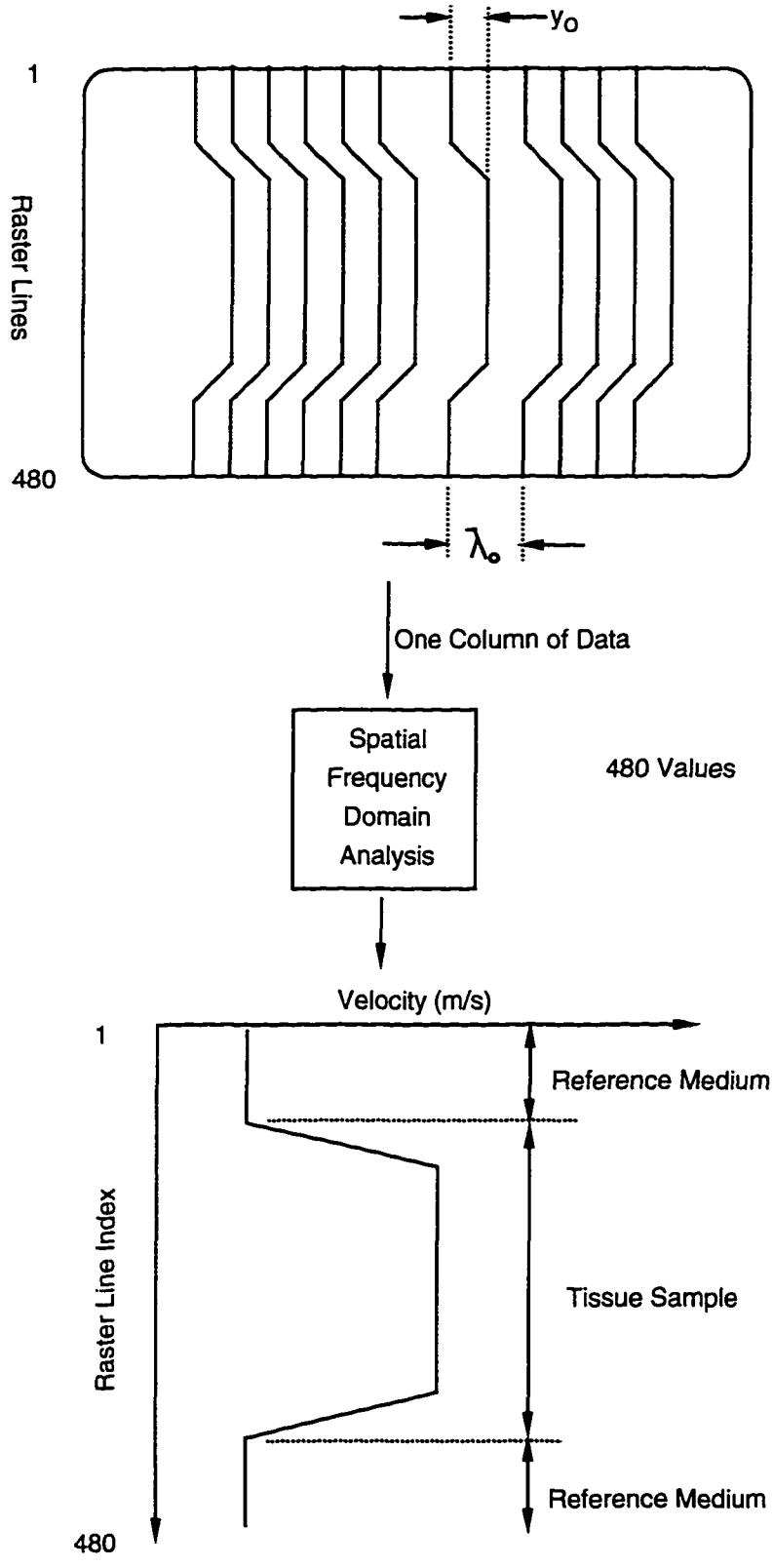

Figure 6.1.2-1 Representation of the spatial frequency domain technique used for determining the ultrasonic speed.

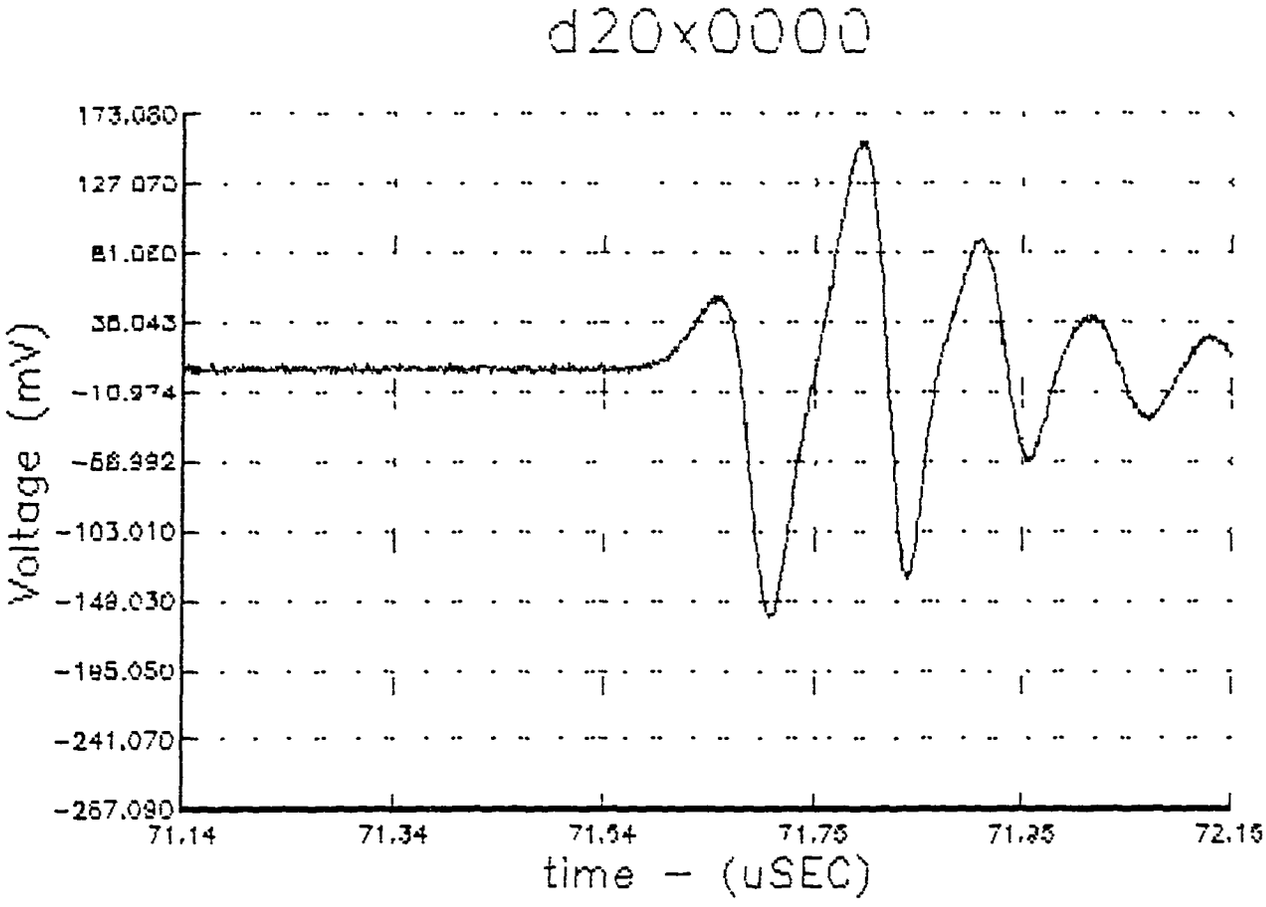

Figure 6.2.1-1. An example of a digitized pulse waveform received by the Sonic Technologies hydrophone from a Panametrics transducer and digitized by the Tektronix 11401 oscilloscope. This waveform can be stored by a the Tandy 4000 computer and recalled at a later time for processing.

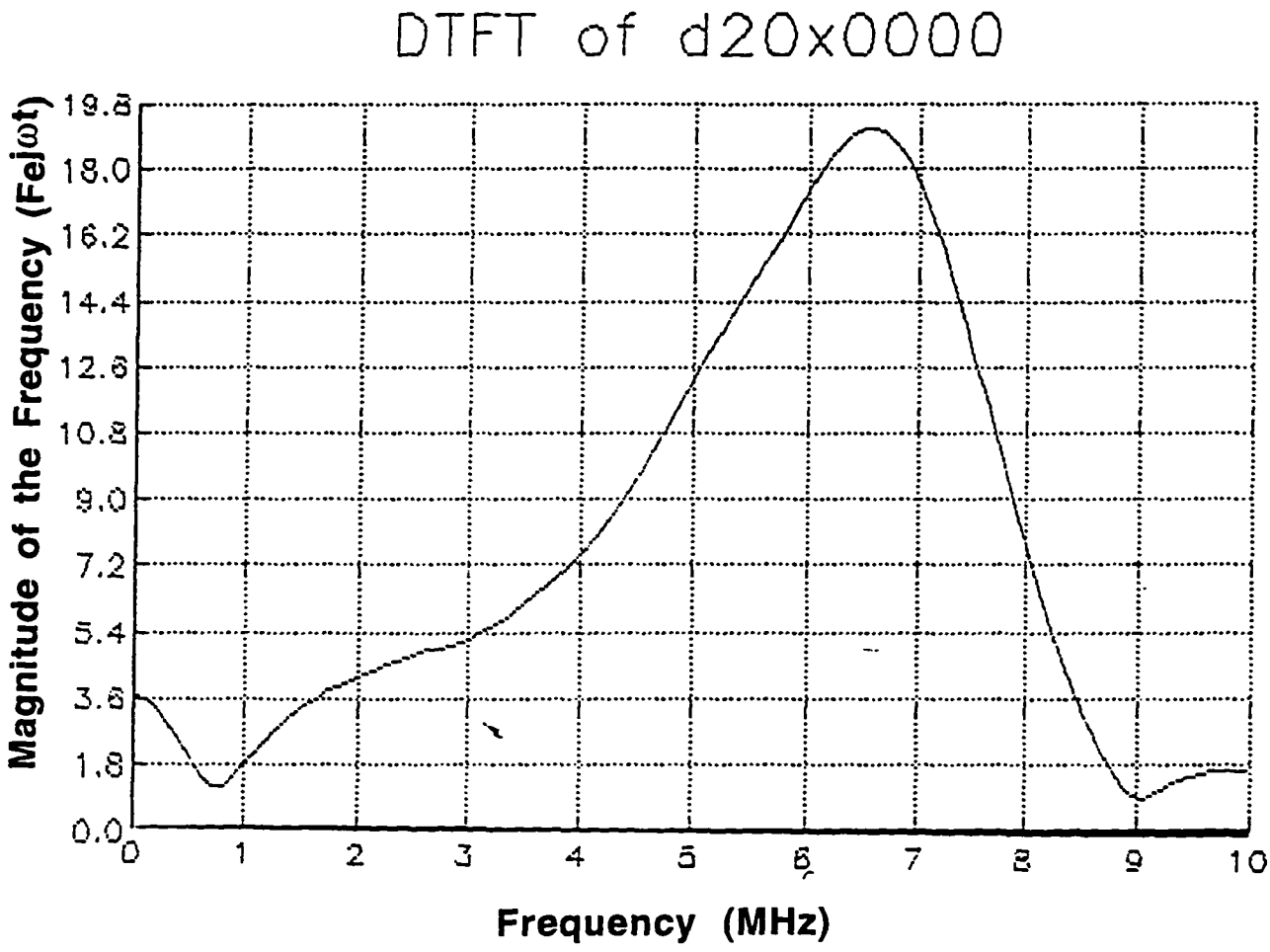

Figure 6.2.1-2. Power spectrum of a pulse waveform in the frequency range of 2-7 MHz obtained from a pulse.

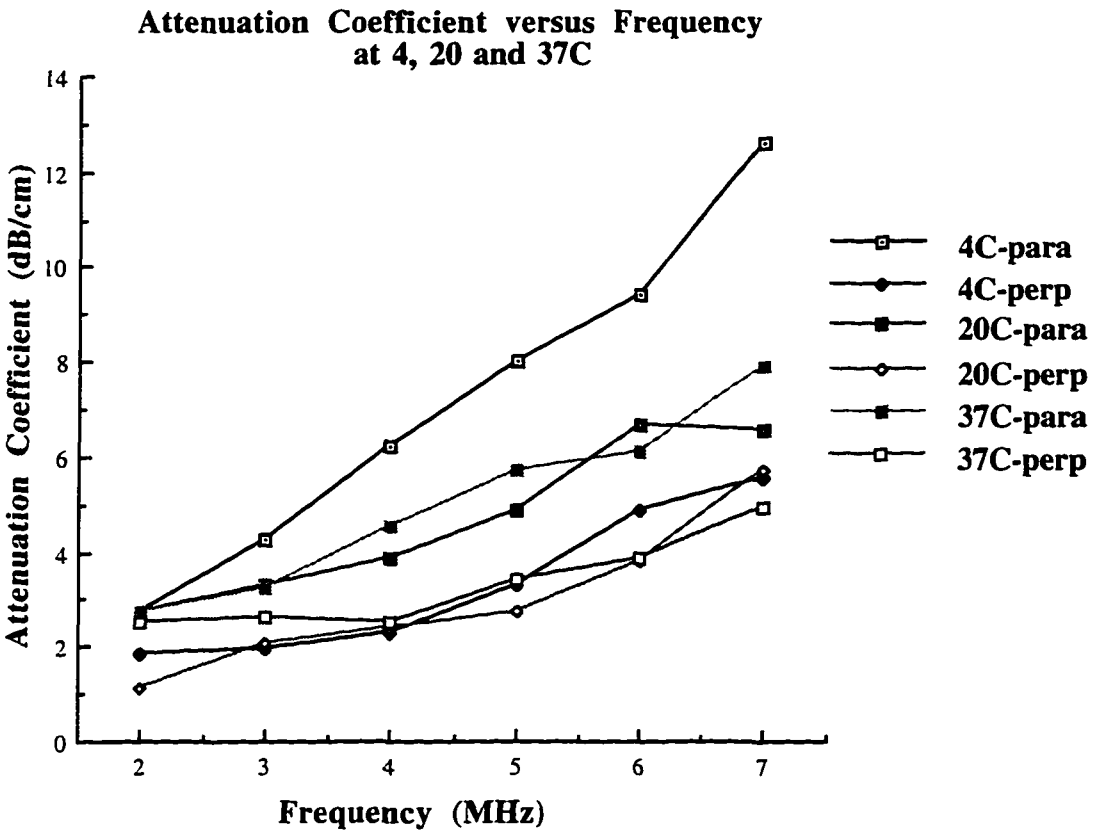

Figure 6.2.1-3 The plot is a typical example of an attenuation coefficient versus frequency curve results. The attenuation coefficient was measured at 4, 20 and 37°C over a range of 2-7 MHz with the acoustic wave insonifying the skeletal muscle tissue parallel (para) and perpendicular (perp) to the muscle fiber.

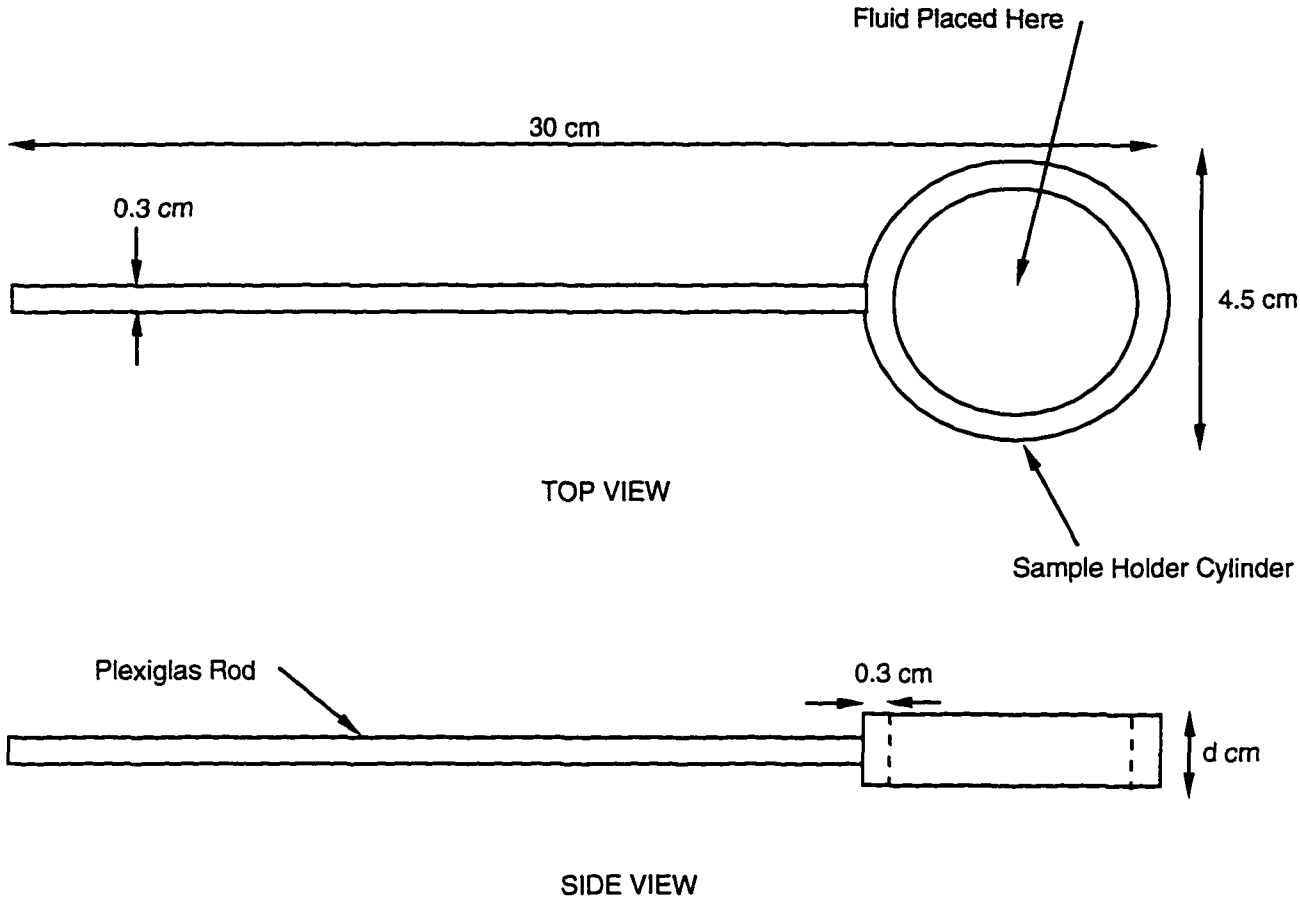

Figure 6.2.3-1 A specially made test cylinder to hold the calibration sample of Dow Corning 710. The Plexiglas rod is attached to the moving arm of the positioning system. One end of the cylinder is sealed off using Reynols 914 film and a rubber band. The calibration fluid is then poured into the cylinder and the other end is sealed off. The sample is then placed in the path of the ultrasound beam between the transducer and hydrophone. The thickness, d, of the test cylinder is either 1, 1.5 or 2.0 cm.

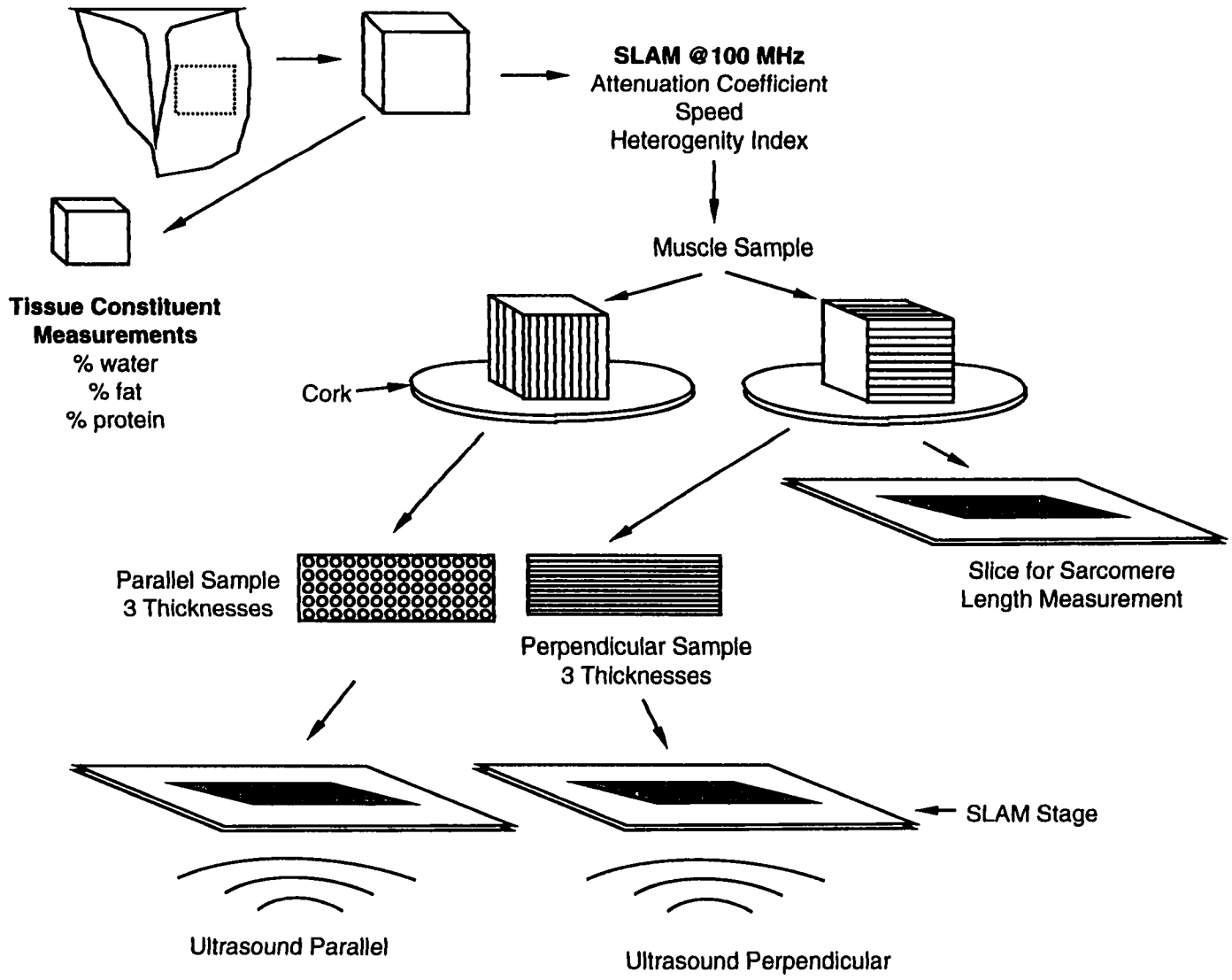

Figure 6.3-1 Diagram which indicates how a sample was divided among the experiments which determine the tissue constituents, sarcomere length and the propagation properties using the SLAM for experiment #1. Five samples of longissimus dorsi, 5 samples of psoas major, 5 samples of lobster extensor and 8 samples of semitendinosis were used for the determination of the tissue constituents using the SLAM.

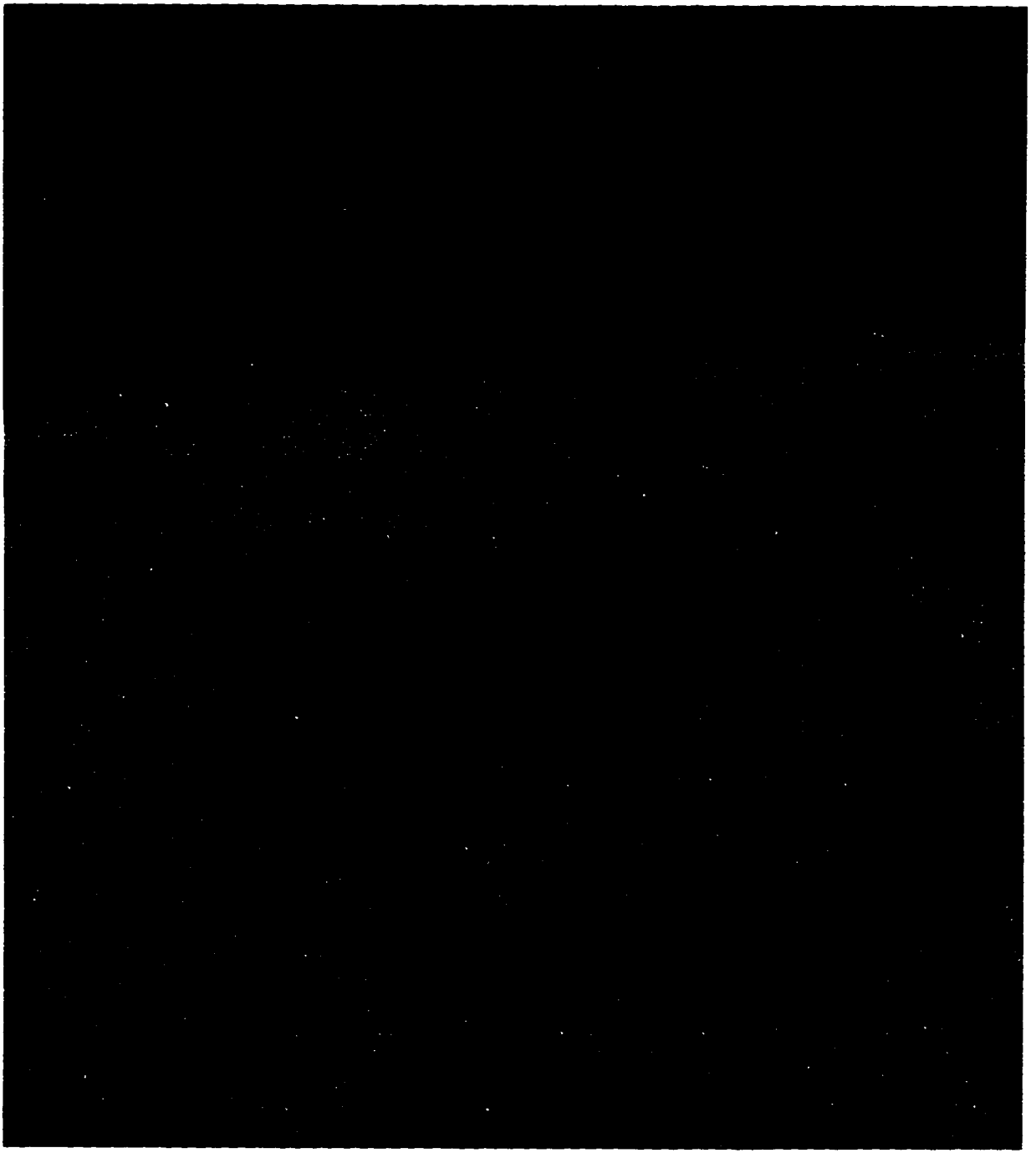

Figure 6.3.3-1 Typical myofibril used for determining the sarcomere length. Dark red lines correspond to the Z-lines.

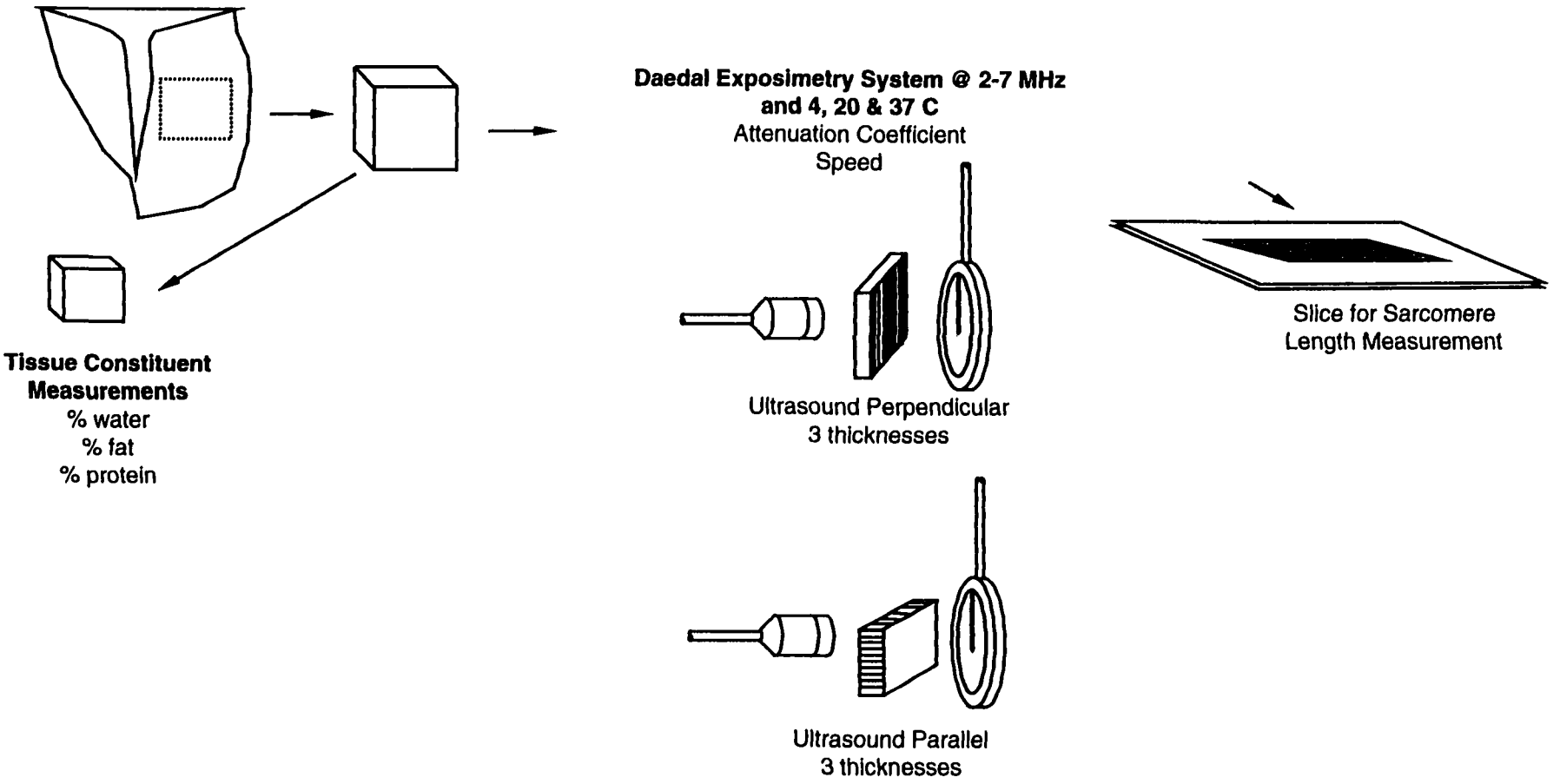

Figure 6.4-1 Experiment #2 used 30 samples of longissimus dorsi for determination of the temperature-frequency dependent acoustic propagation properties using the DES. The tissue constituents and sarcomere length were also measured to develope regression equations from the attenuation coefficient and speed.

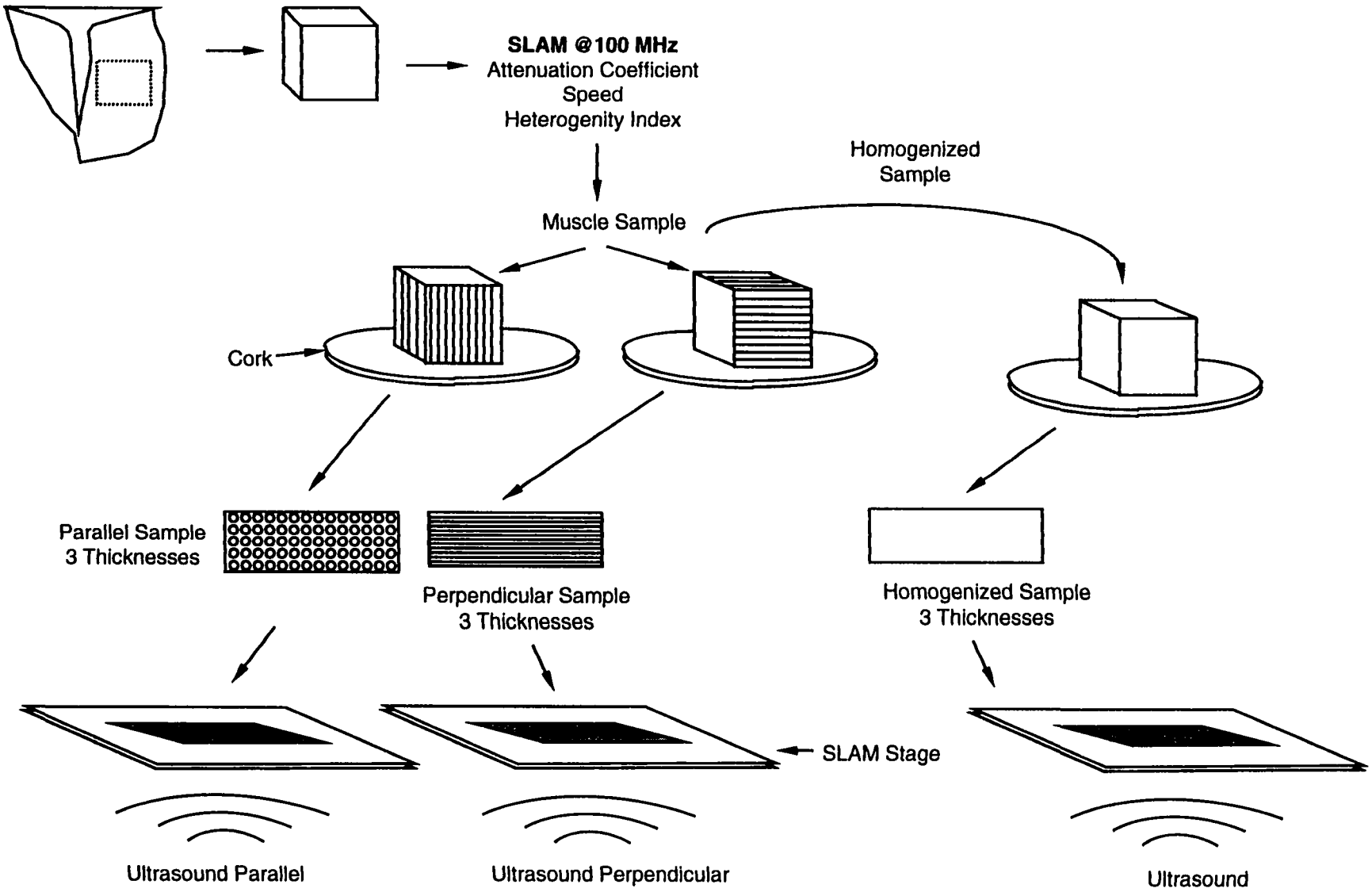

Figure 6.5-1 Experiment #3 used 18 longissimus dorsi samples for determinung the myofibrilar contribution to the acoustic propagation properties from intact and homoginized tissue.

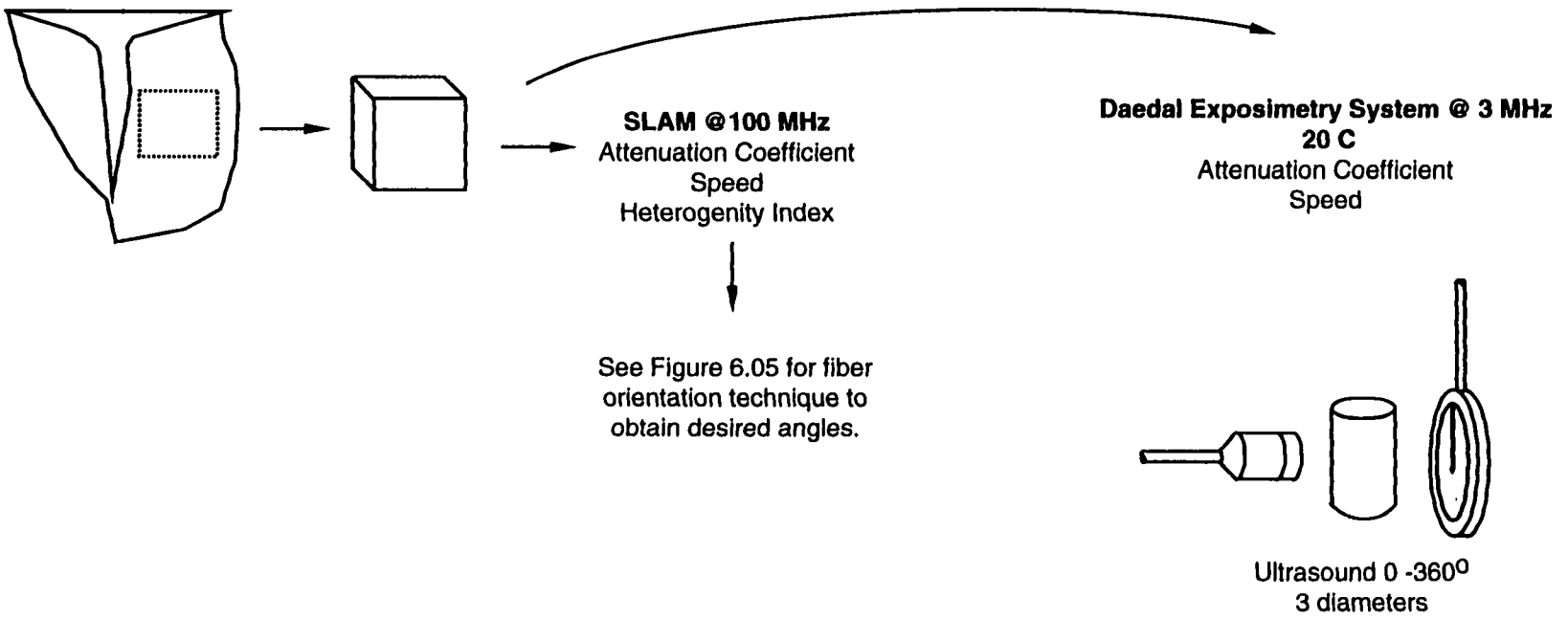

Figure 6.6-1 Eight samples of semitendinosis were exposed to ultrasound on the SLAM and the DES to determine the effect of anisotropy. The DES is capable of rotating a sample in the ultrasound field a full 360 degrees but the SLAM is limited in the fiber angles which can be obtained. Figure 6.6.1-1 demonstrates the proper technique for obtaining the angles on the SLAM.

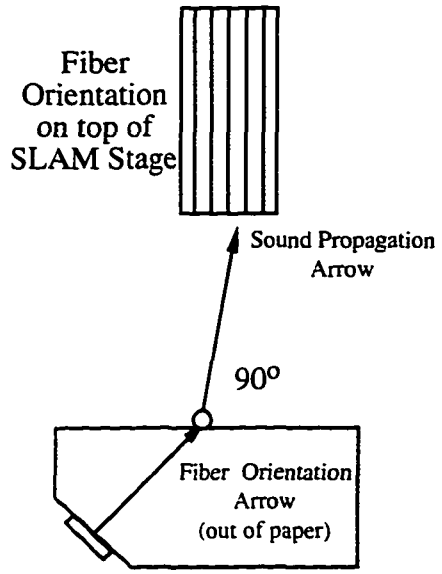

(a) Angle of sound to muscle fiber = 90°

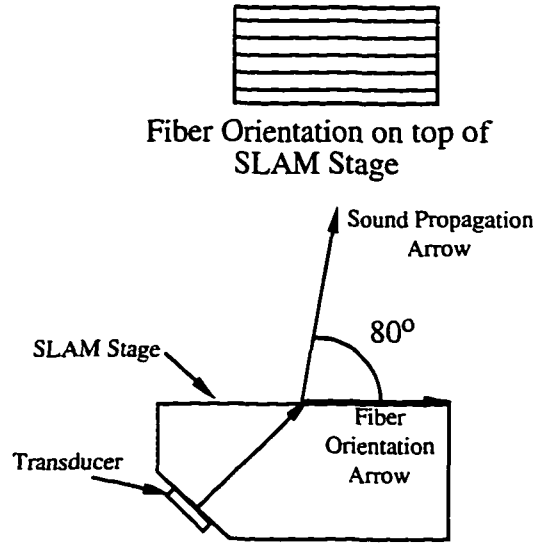

(b) Angle of sound to muscle fiber = 80°

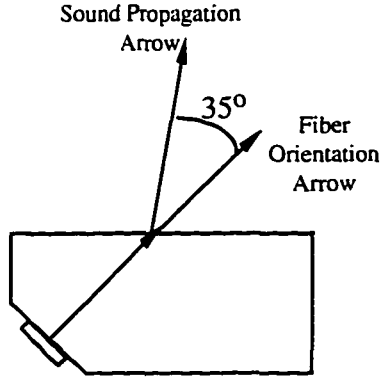

(c) Angle of sound to muscle fiber = 35°

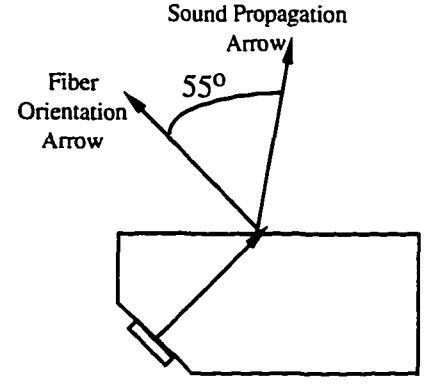

(d) Angle of sound to muscle fiber = 55°

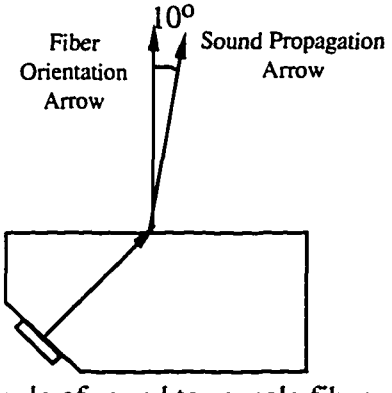

(e) Angle of sound to muscle fiber = 10°

Figure 6.6.1-1 To determine anositropic effects on the ultrasonic propagation properities, the muscle fiber was oriented on the SLAM stage at varying angles with respect to the propagating ultrasound through the fused silca stage. Angles of (a) 90° through (b) 80°, (c) 35° through (d) 55°, and (e) 10° could be obtained.

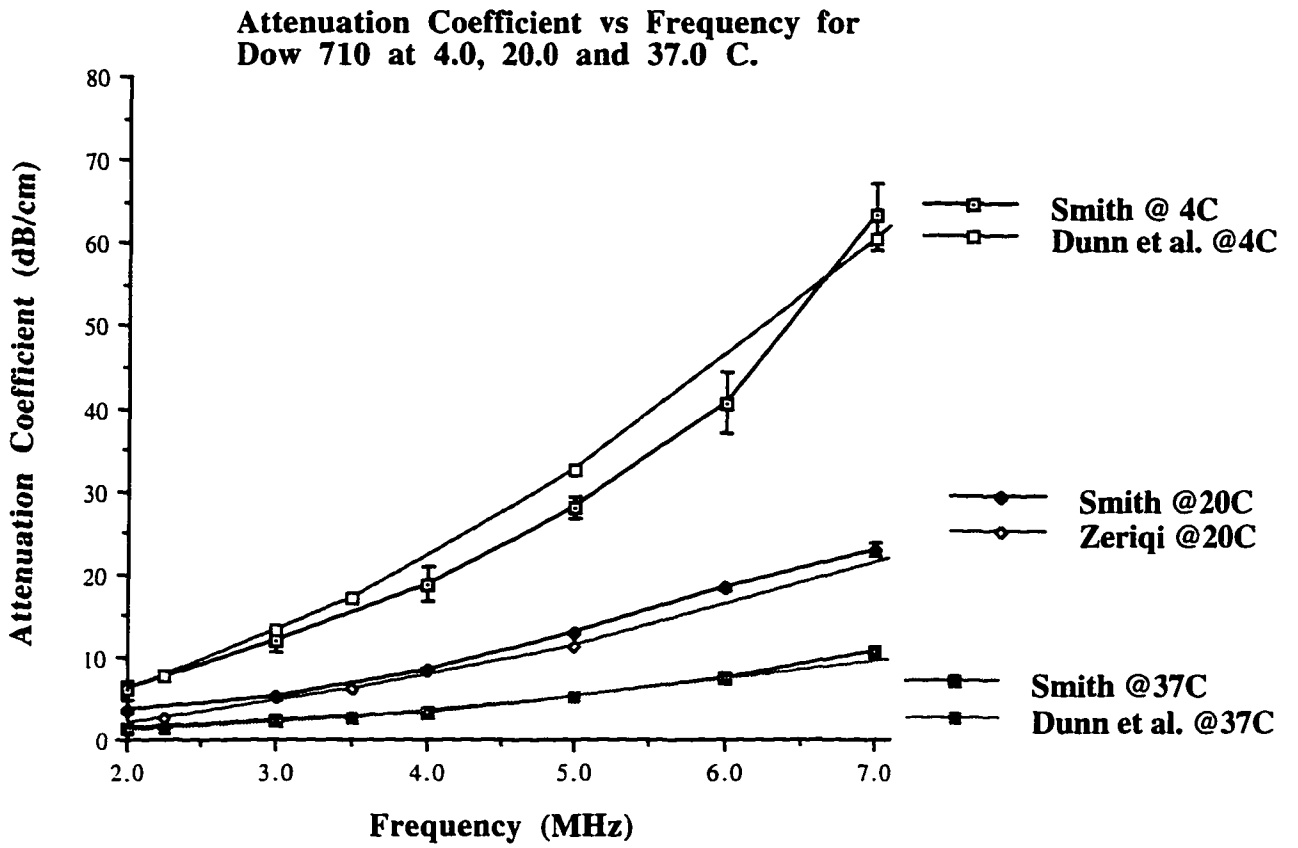

Figure 7.2.1-1. The mean attenuation coefficient and standard deviation results for Dow Corning 710 at 4, 20 and 37°C from 2-7 MHz. The results at 20°C from this experiment are plotted against the results from Zeqiri (1989) which were perform at 20°C. The expected attenuation coefficient at 4 and 37°C is calculated from information published in Dunn et al. (1969). The attenuation coefficient results from this study are plotted against the calculated results.

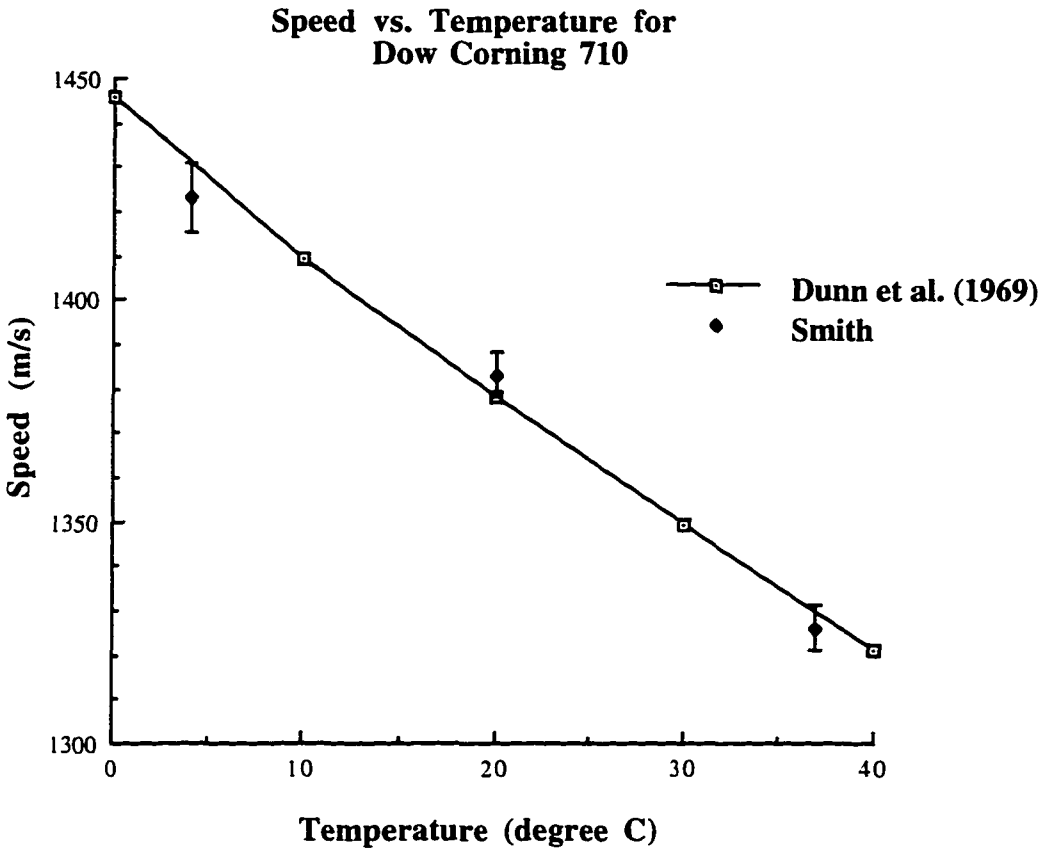

Figure 7.2.2-1 Dunn et al. (1969) reports the speed of sound as a function of temperature at 0, 10, 20, 30, 40°C for in Dow Corning 710. The linear relationship between the speed and temperature is a negative thermal dependency for speed. Thus, the speed of sound can be calculated at other temperatures using a linear regression of the data . Also graphed are the mean speed results and standard deviation bars from several independent experiments at 4, 20 and 37°C from this investigation.

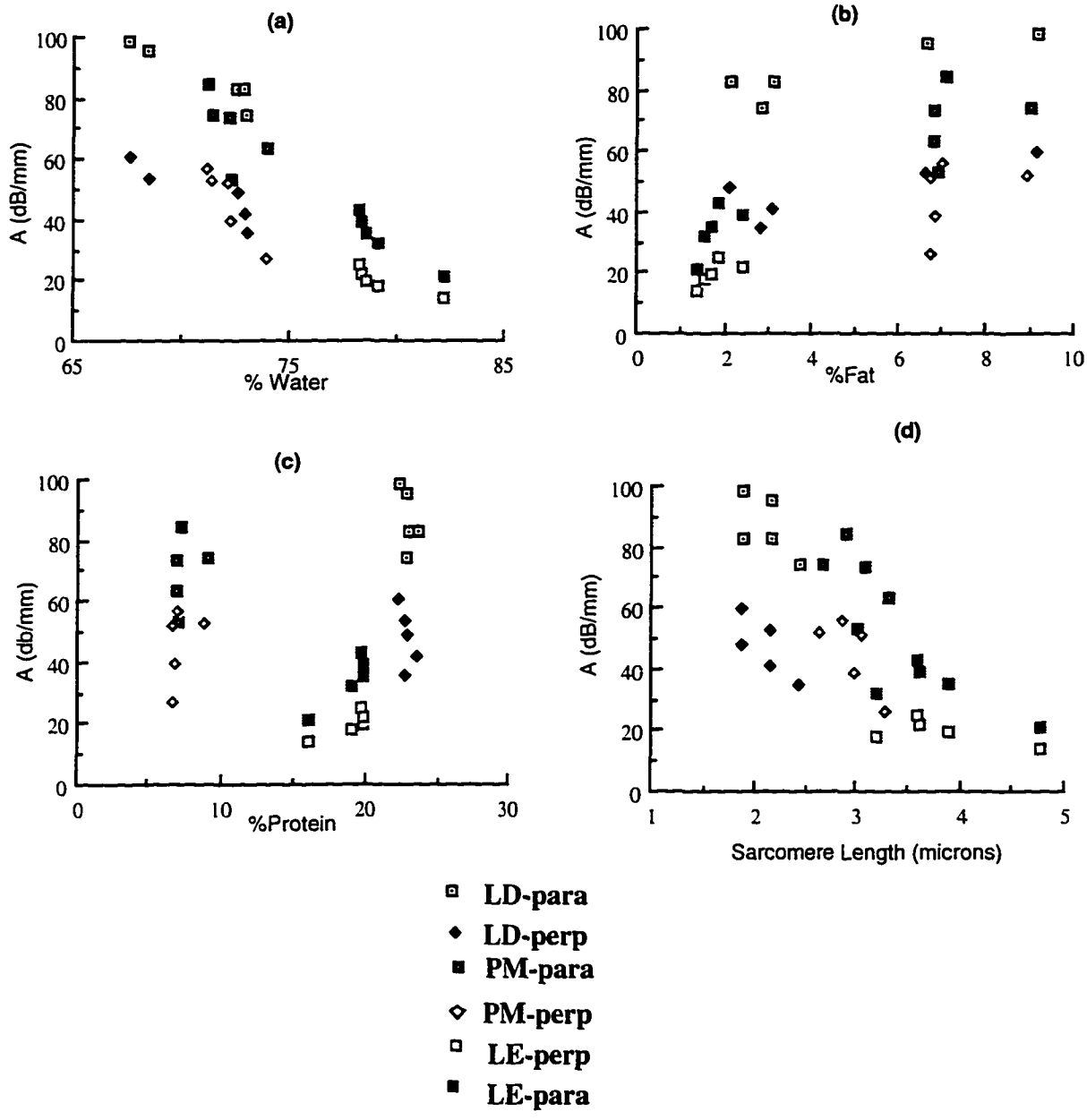

Figure 7.3.4-1 Scatter plot of the attenuation coefficient for longissimus dorsi (LD), psoas major (PM) and lobster extensor (LE) as a function of (a) %water, (b) %fat, (c) %protein and (d) sarcomere length for muscle samples parallel (para) and perpendicular (perp) to the ultrasound.

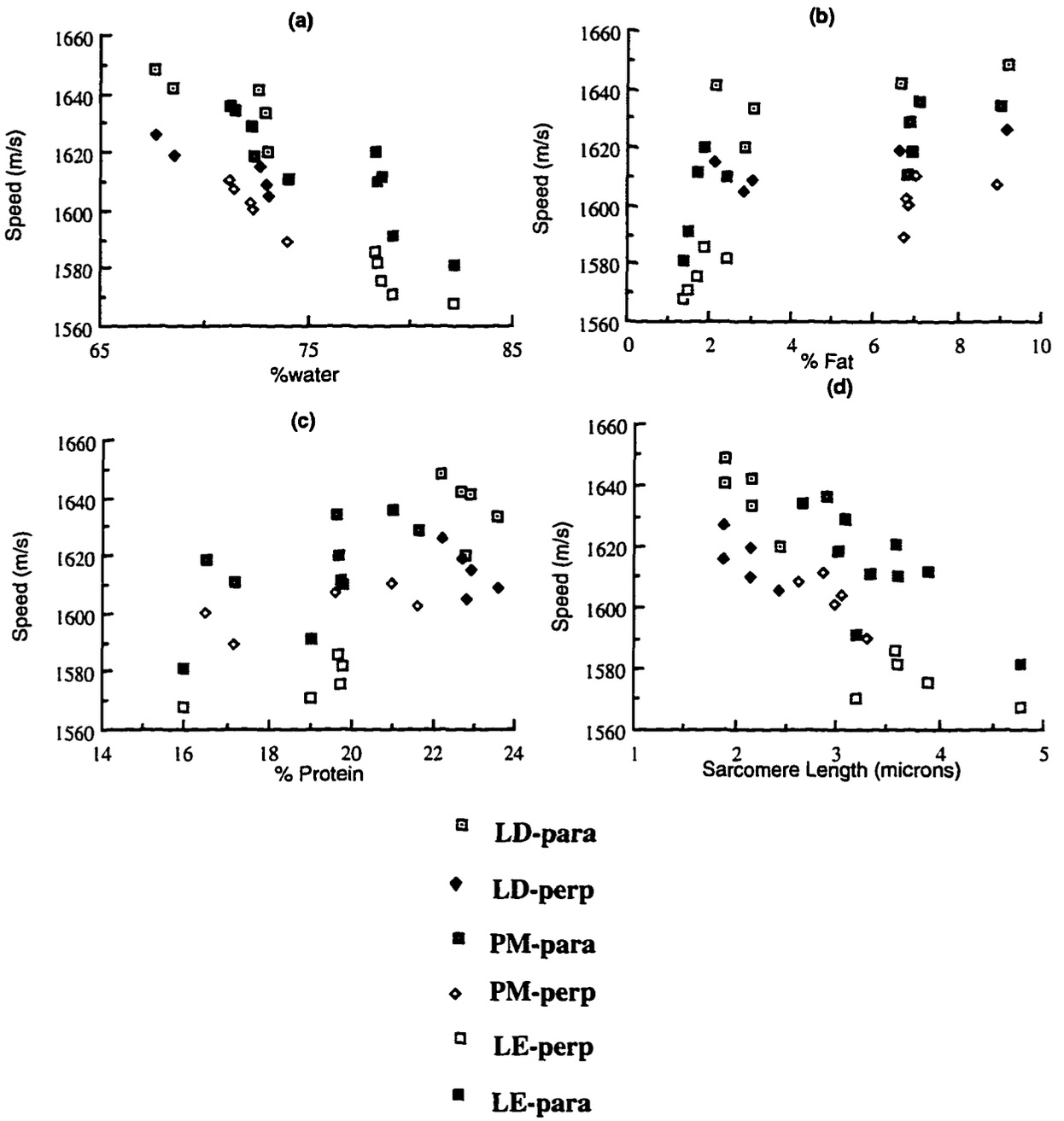

Figure 7.3.4-2 Scatter plot of the speed for longissimus dorsi (LD), psoas major (PM) and lobster extensor (LE) as a function of (a) %water, (b) %fat, (c) %protein and (d) sarcomere length for muscle samples parallel (para) and perpendicular (perp) to the ultrasound.

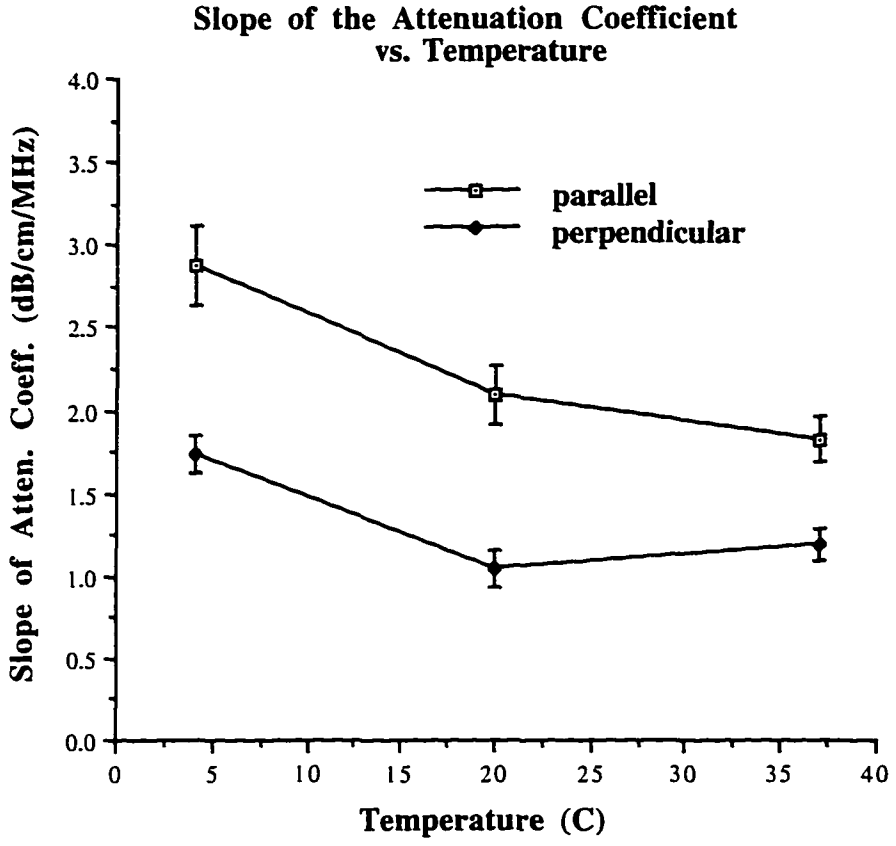

Figure 7.4.2.1-1 The mean and standard deviation of slope of the attenuation coefficient for 4, 20 and 37°C used for the ultrasound parallel and perpendicular to the fiber orientation for 30 samples are plotted above.

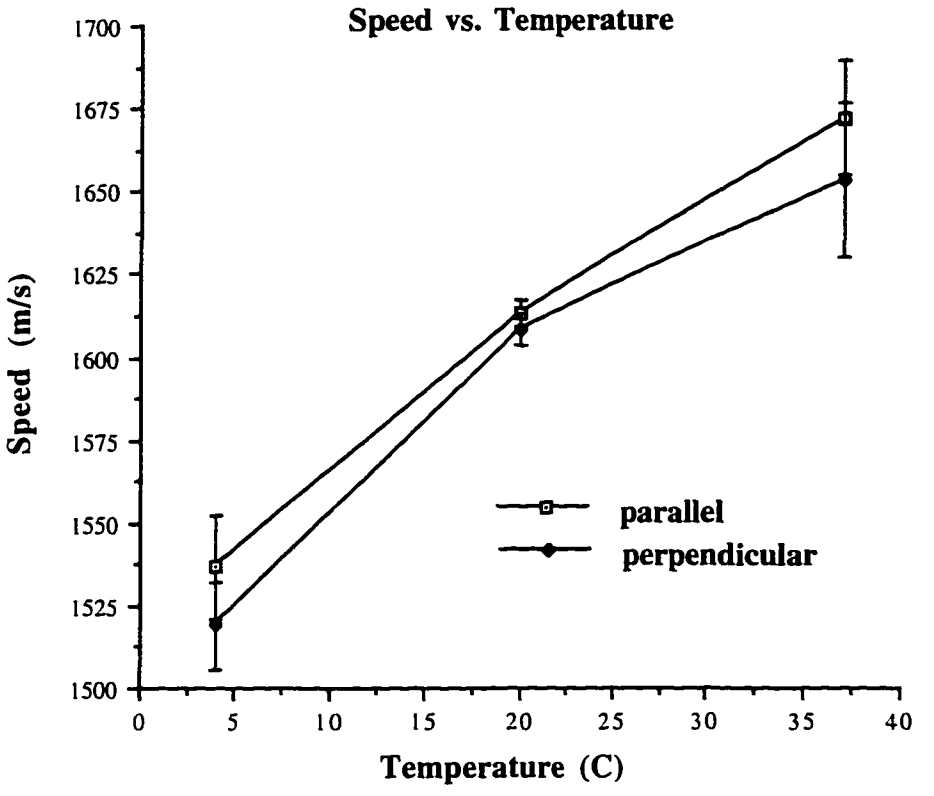

Figure 7.4.2.2-1 The mean and standard deviation of speed of sound versus for 4, 20 and 37°C used for ultrasound parallel and perpendicular to the fiber orientation for 30 samples.

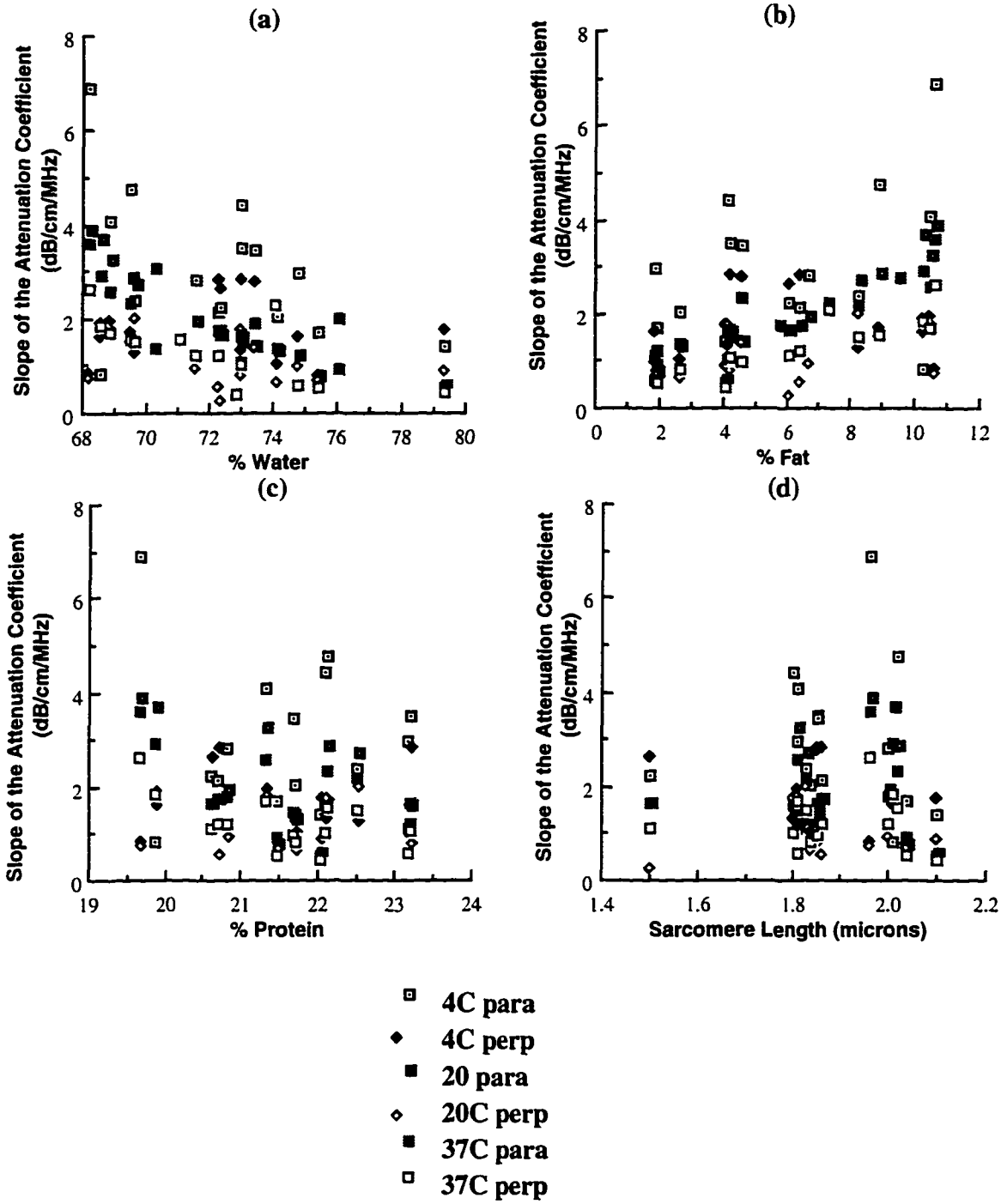

Figure 7.4.4-1 Scatter plot of the slope od the attenuation coefficient for longissimus dorsi as a function of (a) %water, (b) %fat, (c) %protein and (d) sarcomere length for samples parallel (para) and perpendicular (perp) to the ultrasound.

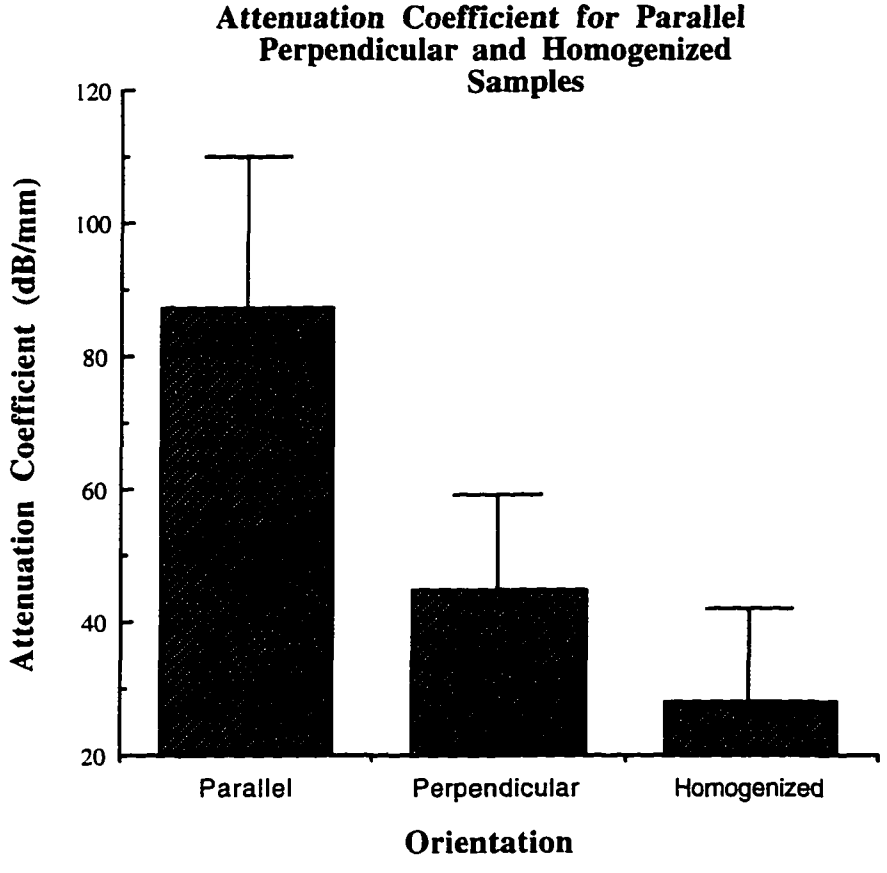

Figure 7.5.2.1-1 The mean and standard deviation of the attenuation coefficient for parallel, perpendicular and homogenized longissimus dorsi samples. The ratio of the parallel over perpendicular and parallel over homogenized attenuation coefficient results were 2.0 and 3.1, respectively.

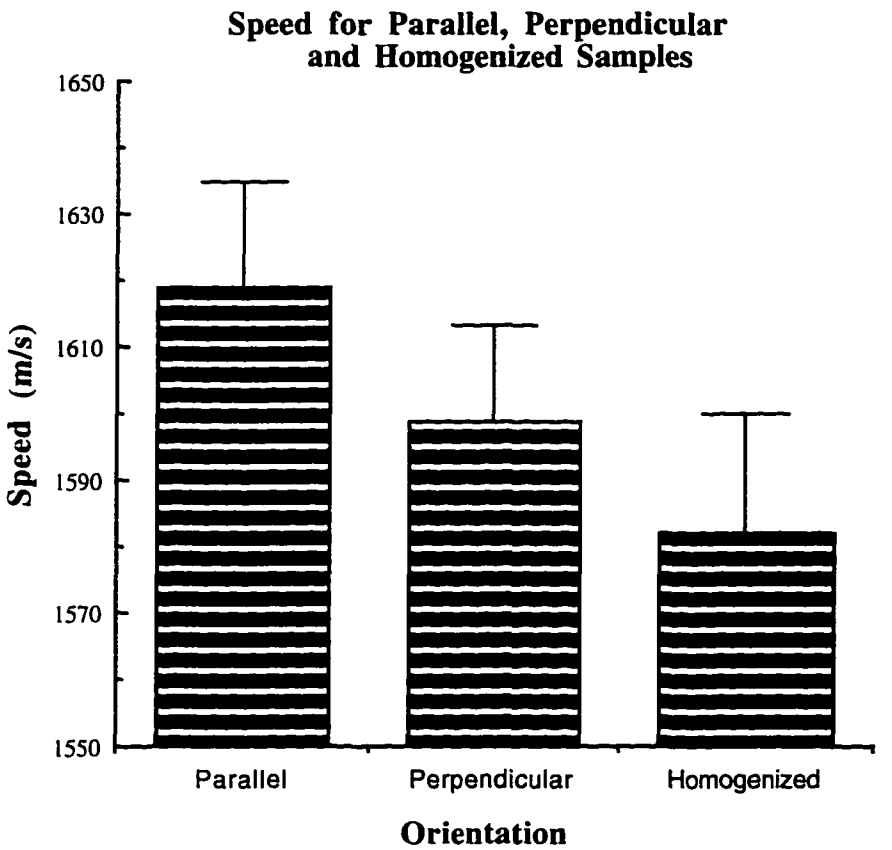

Figure 7.5.2.2-1 The mean and standard deviation of speed for parallel, perpendicular and homogenized longissimus dorsi samples. The effect of anisotropy of the tissue was measured as the ratio of the parallel to perpendicular orientation. The results of the anisotropic effect had a magnitude of approximately 1.3%.

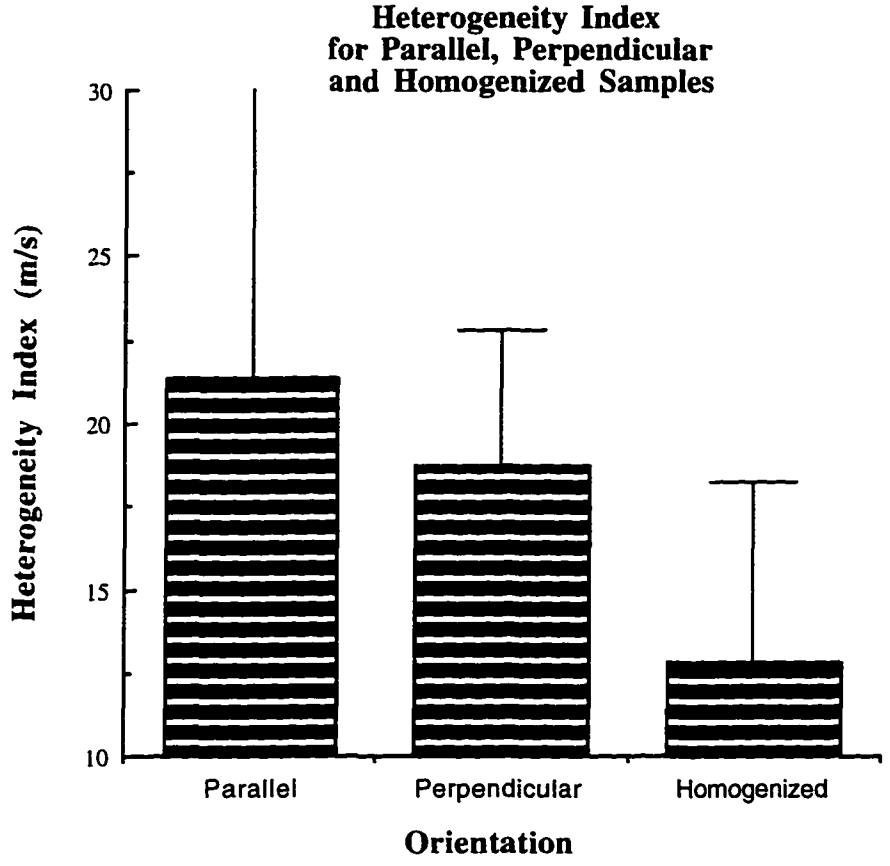

Figure 7.5.2.3-1 The mean and standard deviation of the heterogeneity index for parallel, perpendicular and homogenized longissimus dorsi samples. The results indicate that the homogenized samples are significantly more homogeneous to the acoustic signal than the parallel and perpendicular samples.

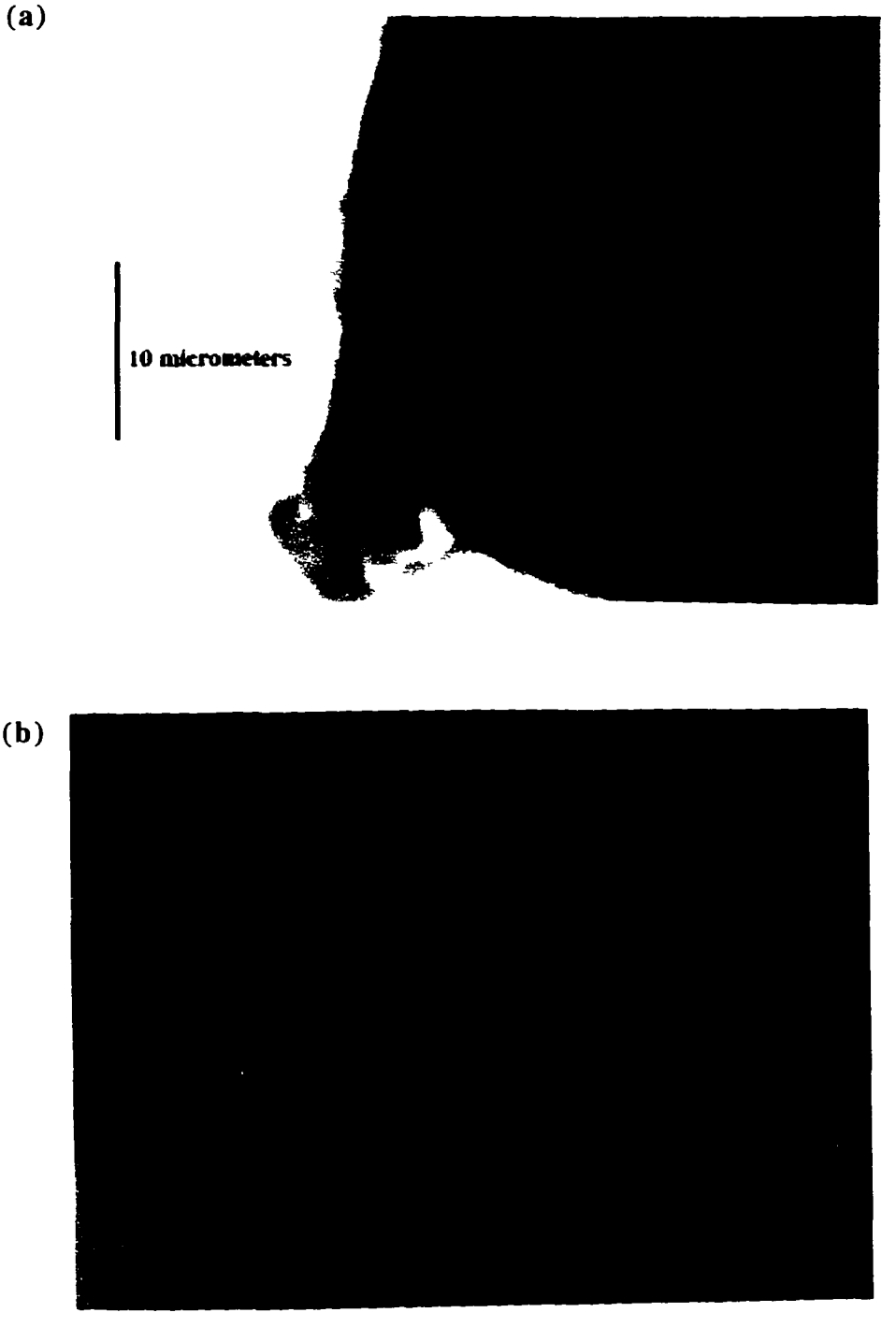

Figure 7.5.4-1 (a) Intact sample of longissimus dorsi muscle and the same sample after the (b) homogenization process (magnification = 100 x 2.5).

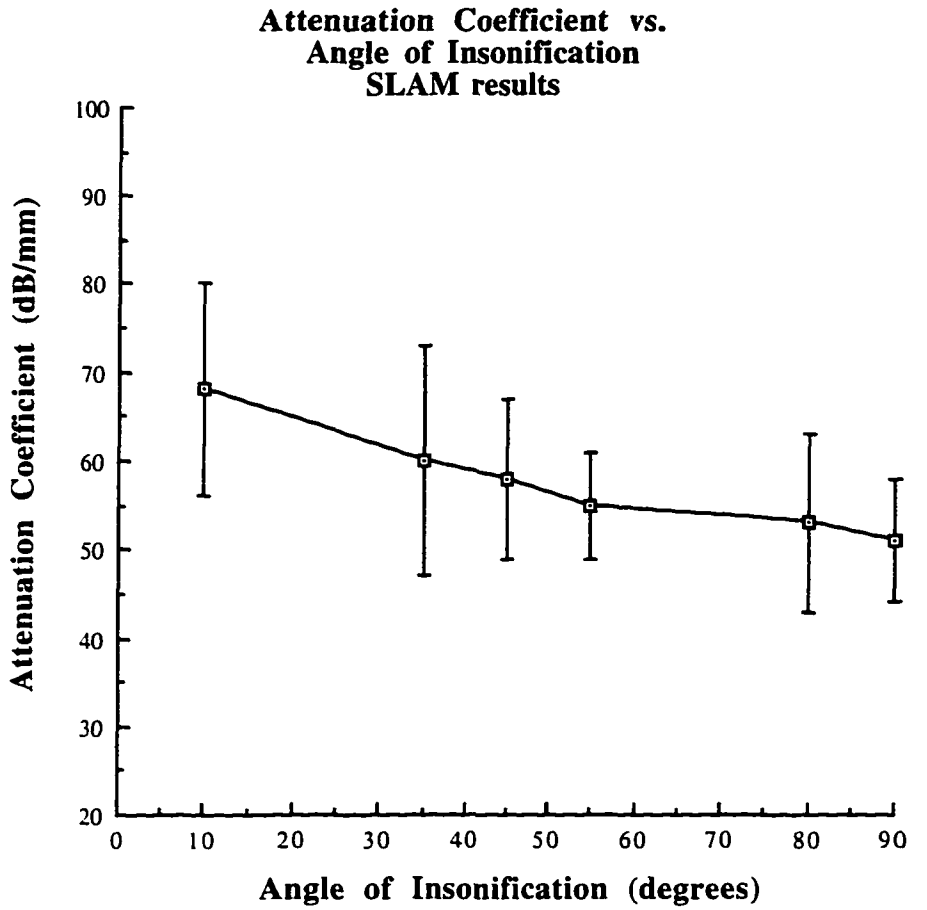

Figure 7.6.1-1 Mean attenuation coefficient and standard deviation of semitendinosis as a function of the angle of insonification from 8 samples at 100 MHz determined using the SLAM. Ten degrees corresponds to the parallel orientation while approximately 90° corresponds to the perpendicular orientation.

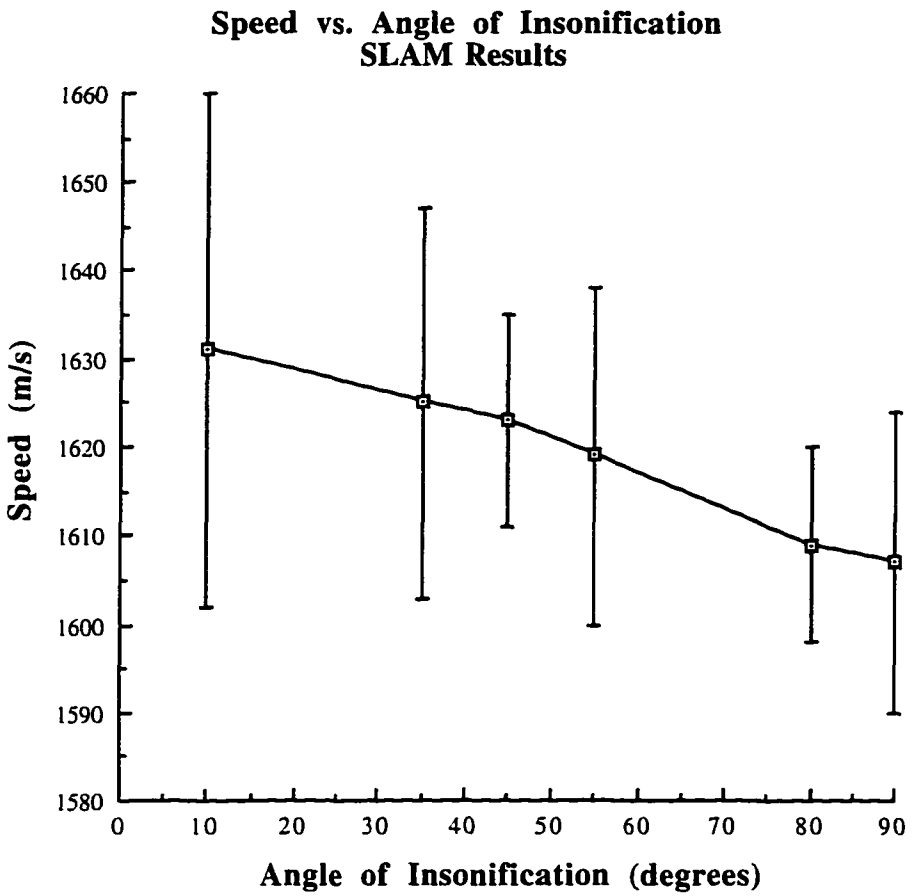

Figure 7.6.1-2 Mean speed and standard deviation of semitendinosis as a function of the angle of insonification from 8 samples at 100 MHz determined using the SLAM. Ten degrees corresponds to the parallel orientation while approximately 90° corresponds to the perpendicular orientation.

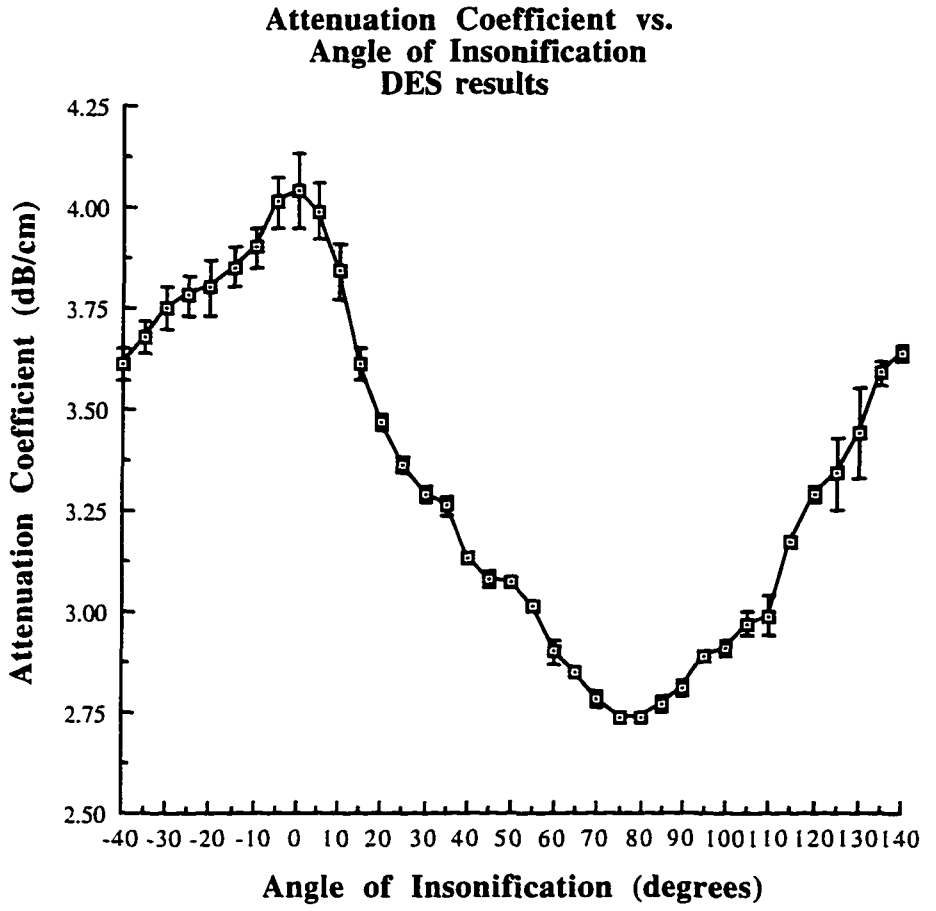

Figure 7.6.2-1 Mean attenuation coefficient and standard deviation of semitendinosis as a function of the angle of insonification from 8 samples at 3 MHz determined using the DES. Zero degrees corresponds to the parallel orientation while 90° corresponds to the perpendicular orientation.

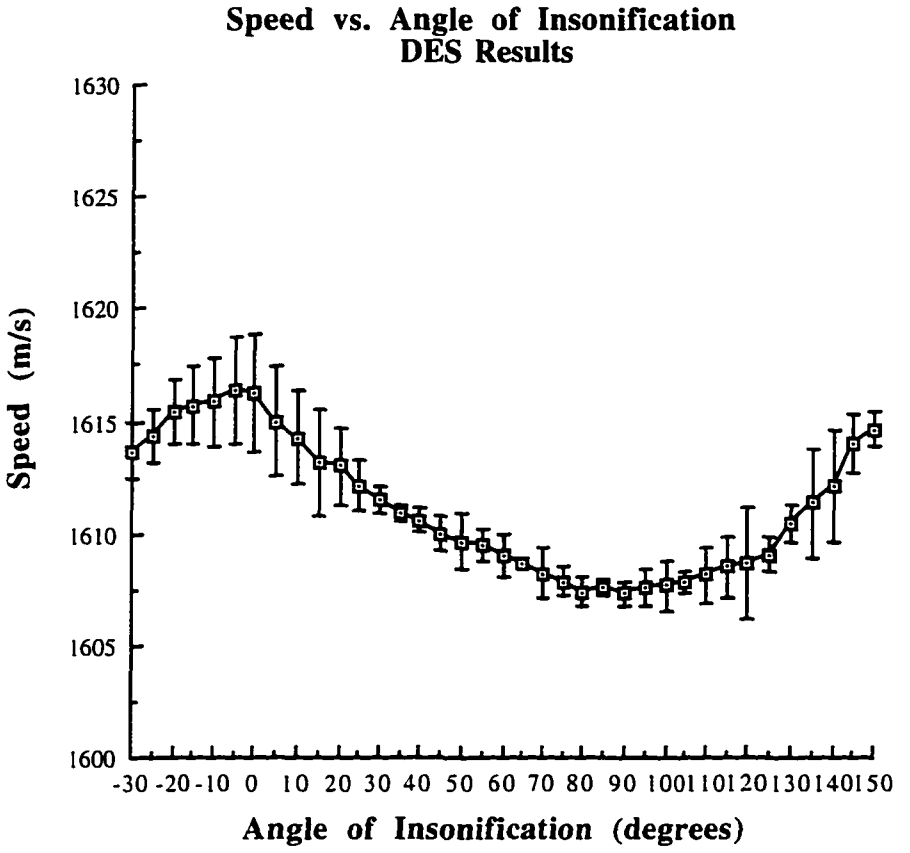

Figure 7.6.2-2 Mean speed and standard deviation of semitendinosis as a function of the angle of insonification from 8 samples at 3 MHz determined using the DES. Zero degrees corresponds to the parallel orientation while 90° corresponds to the perpendicular orientation.

APPENDIX B

TABLES

TABLE 3.3.3-1

Collagen type	Composition	Distinguishing characteristics	Tissue location	Cell types that synthesize various collagen types
I	$[\alpha1(I)]_2\alpha2(I)$	Low carbohydrate, low hydroxylation of lysine, 67-nm banded fibrils	Skin, bone, tendon, cornea	Fibroblasts, osteoblasts, smooth-muscle cells, epithelium
II	$[\alpha1(II)]_3$	>10 hydroxylysines per chain, small 67-nm banded fibrils	Cartilage, cornea, vitreous body	Chondrocytes, neural retinal cells, notochord cells
III	$[\alpha1(III)]_3$	Contains cysteine, low hydroxylation of lysine, small 67-nm banded fibrils	Fetal skin, blood vessels, organs, muscle	Fibroblasts, myoblasts
IV	$[\alpha1(IV)]_3$ $[\alpha2(IV)]_3$	Many lysines hydroxylated and glycosylated, sugars other than glucose and galactose, low alanine, high 3-hydroxyproline, nonfibrillar network	Basement membrane	Endothelial cells and epithelial cells
V	$[\alpha1(V)]_2\alpha2(V)$ (formerly αA- and αB- chains)	Elevated hydroxylysine, low alanine, contains 3-hydroxyproline, small fibers	Blood vessels, smooth muscle, most interstitial tissues	Smooth-muscle cell, chrondrocytes under certain conditions
VI	α1(VI), α2(VI), α3(VI)	Microfibrils, 100 nm banded fibrils	Most interstitial tissues	
VII	?	Dimer	Anchoring fibrils	
VIII	α1(VIII)	?	Some endothelial cells	
IX	α1(IX), α2(IX), α3(IX)	?	Cartilage	
X	α1(X)	?	Hypertrophic and mineralizing cartilage	
XI	α1(XI), α2(XI), α3(XI)	Small fibers	Cartilage	

Table 3.3.4-1 Myofibrillar Proteins of Skeletal Muscle [Wang, 1985].

Lattice	Structure	Percent Total Protein	MW (kDa)	Function
Thick Filament	Myosin	44	510	Interacts with actin filaments with hydrolysis of ATP to develop mechanical force.
	C protein	1	140	Myosin binding protein found in distance stripes on either side of the thick-filament M line.
M Line	Myomeisin	1	185	Myosin-linking protein present at the central "M Line" of the muscle thick-filament.
Thin Filament	Actin	22	42	Major component of muscle thin filaments against which muscle thick filaments slide during muscle contraction.
	Tropomyosin	5	64	Rod like protein that binds along the length of actin filaments.
	Troponin	5	78	Complex (3 subunits)protein positioned at regular intervals along actin filaments and involved in the Ca2+ regulation of muscle contraction.
Z Disk	α-Actinin	1	190	Actin-bundling protein that links actin filaments together in the region of the Z disk.
	Filamin	?	500	
Endosarcomeric Lattice	Titin	?	2500	Large complex protein that forms an elastic network linking thick filaments to Z disks.
	Nebulin	?	600	Elongated, inextensible protein attached to Z Disk, oriented parallel to the actin filaments.
Exosarcomeric Lattice	?	?	?	Scaffold for sarcomere for sarcomere and mitoconderia. Juxtaposition of the T-tubules and sarcoplasmic recticulum.

Table 3.3.5-1 Thirteen bovine skeletal muscles listed by anatomical, wholesale and retail cut name.

Anatomical	Wholesale Cut	Retail Cut
Semimembranosus	Round	Beef round top round
Adductor	Round	Beef round top round
Semitendinosus	Round	Beef round bottom round Beef round eye round
Biceps femoris	Round	Beef round bottom round
Rectus femoris	Round	Beef round tip
Gluteus Medius	Loin	Beef Loin sirloin Steak Wedge, round,flat and pin bone
Psoas major	Loin	Beef loin tenderloin
Longissimus Dorsi-Loin	Loin	Beef loin porterhouse Beef loin T-Bone Steak Beef loin Top loin steak
Longissimus Dorsi-Rib	Rib	Beef rib eye steak beef rib roast
Triceps	Chuck	Beef chuck blade roast beef chuck 7 bone pot roast Arm pot roast
Infraspinatus	Chuck	Beef chuck 7 bone pot roast Beef chuck blade roast
Pectoral	Chuck	Beef chuck arm pot roast Brisket
Supraspinatus	Chuck	Beef Chuck 7-Bone pot roast Beef chuck blade roast

Table 3.3.5-2. Rank of thirteen muscles by percent moisture, percent fat, total collagen, connective tissue and sarcomere length. Longissimus dorsi is abbreviated LD. The psoas major and the LD-Loin are highlighted in the table for comparison.

Rank	Percent Moisture	Percent Fat	Total Collagen (mg/g wet weight)	Connective Tissue Amount	Sarcomere Length (μm)
1	Supraspinatus (76.4)	Infraspinatus (7.7)	Infraspinatus (17.81)	**Psoas major (7.37)**	**Psoas major (3.46)**
2	Triceps (74.4)	LD-Rib (6.8)	Rectus femoris (13.96)	LD-Rib (6.74)	Pectoral (2.81)
3	Adductor (74.1)	**LD-Loin (6.1)**	Triceps (10.45)	**LD-Loin (6.43)**	Triceps (2.55)
4	Semimembranosus (73.4)	**Psoas major (5.9)**	Biceps femoris (9.60)	Infraspinatus (6.23)	Infraspinatus (2.45)
5	Semitendinosus (73.4)	Rectus femoris (5.7)	Pectoral (8.79)	Gluteus medius (5.75)	Rectus femoris (2.37)
6	Pectoral (73.3)	Biceps femoris (5.6)	Supraspinatus (8.72)	Rectus femoris (5.75)	Semitendinosus (2.21)
7	Biceps femoris (72.6)	Pectoral (5.6)	Semitendinosus (8.32)	Semitendinosus (5.60)	Adductor (2.17)
8	Infraspinatus (72.6)	Gluteus medius (5.1)	Gluteus medius (8.13)	Triceps (5.55)	Supraspinatus (2.11)
9	Rectus femoris (72.6)	Triceps (4.3)	Semimembranosus (7.30)	Adductor (5.34)	LD-Rib (2.10)
10	**Psoas major (72.3)**	Semimembranosus (4.0)	Adductor (5.52)	Semimembranosus (5.14)	Semimembranosus (1.96)
11	Gluteus medius (71.8)	Semitendinosus (4.0)	**LD-Loin (5.04)**	Supraspinatus (5.08)	Gluteus medius (1.90)
12	**LD-Loin (71.5)**	Supraspinatus (3.0)	LD-Rib (4.66)	Biceps femoris (4.91)	**LD-Loin (1.84)**
13	LD-Rib (71.5)	Adductor (1.5)	**Psoas major (3.23)**	Pectoral (4.02)	Biceps femoris (1.82)

Table 4.1-1 Attenuation coefficient at 1 MHz and speed of sound for tissues of various collagen content [Johnston et al., 1979].

Tissue Type	% collagen	Attenuation Coefficient (dB/cm)	Speed (m/s)
Liver	0.1-1.3	0.7-1.13	1462
Striated Muscle			
w/ fibers	0.7-1.2	1.56-2.17	1592-1603
against fibers	0.7-1.2	1.39	1576-1587
Integument	7.0 - 30.0	3.5	1498
Cartilage	10.0 - 20.0	5	1665
Tendon	32	4.7	1750

Table 4.2-1 Literature survey of ultrasonic propagation properities of bovine skeletal muscle.

Bovine Skeletal Muscle Table Legend
All Attenuation Cofficient measured parallel to the muscle fiber.
A† Attenuation Cofficient measured perpendiculat to the muscle fiber.
A Attenuation Cofficient, no fiber orientation specified.
Cll Speed measured parallel to the muscle fiber.
C† Speed measured perpendiculat to the muscle fiber.
n Number of Samples Measured
T Temperature of Sample
If only a number is listed for the speed vaule then there is no reported fiber orientation .

Biological Preparation	Ultrasonic Measurement	Attenuation Results	Speed m/s	Publication
Bovine Tongue Pre-rigor T=35C	Pulse Transmission 1.5-4.5MHz	All = 2.4 dB/cmMHz A† = 5.0 dB/cmMHz		Hueter 1948
Unspecifed, *In vitro*	Time of flight 20-21°C		1540	Ludwig & Struthers, 1949
Bovine gluteal T=15-18	Total acoustic power. 0.3-3.4 MHz	All = 1.8 dB/cmMHz A† = 1.1 dB/cmMHz		Colobati & Petralia 1950
Bovine M. adductor T=?	Pulse transmission 1-5 MHz	All = 1.58dB/cmMHz A† = 0.98 dB/cmMHz or A† = 3.11 dB/cmMHz		Dussick & Fritch 1955
Bovine Diaphram	Pulse transmission	All = 2.71dB/cmMHz A† = 3.45 dB/cmMHz or A† = 2.18 dB/cmMHz		
Bovine M. quadriceps T=?	Pulse transmission 1-5 MHz	All = 1.25dB/cmMHz A† = 0.89 dB/cmMHz or A† = 2.56 dB/cmMHz		Dussick & Fritch 1955
Bovine, Striated, parallel	Pulse transmission 26-28°C		1566	Dussick & Fritch 1956
Bovine & Human Prerigor	1-5 MHz	All = 1.3dB/cmMHz A† = 0.75 dB/cmMHz		Dussick & Fritch 1958
Unspecified	Not Reported		1630	Rich et al, 1966
1. Sirloin Tip-1 2. Sirloin Tip-2 3. Center Cut 4. Porterhouse	Acoustic Interferometry 21-24°C		1. 1579-1600 2. 1579-1602 3. 1579-1603 4. 1401-1579	Marcus 1973

Table 4.2-1 Literature survey of ultrasonic propagation properities of bovine skeletal muscle. (Continued)

Biological Preparation	Ultrasonic Measurement	Attenuation Results	Speed m/s	Publication
1. Unspecified 2. Unspecified-fatty	Pulse Echo 17°C		1. 1540-1552 2. 1522-1550	Hara, et al 1979
Fixed Bovine Post Rigor	3 MHz	All = 2.2 dB/cmMHz $A_{\dagger}$ = 1.2 dB/cmMHz		McNeely and Noordgraaf 1979
Bovine Pre Rigor	Pulse Echo 1-8 MHz 20°C	All = 2.9 dB/cmMHz $A_{\dagger}$ = 1.1 dB/cmMHz		Nassiri et .al 1979
Formalin Fixed Bovine	Pulse Echo 1-8 MHz 20°C	All = 4.1 dB/cmMHz $A_{\dagger}$ = 1.6 dB/cmMHz		Nassiri et .al 1979
Bovine M. Sternomandibularis	20 MHz	T=0°C $A_{\|\|}$ increases over time T=20°C $A_{\|\|}$ somewhat increases over time. T=37°C $A_{\|\|}$ little increases over time.		Woods 1985. PhD thesis.
Bovine M. Sternomandibularis US perpendicular. Cold =0°C Non cold=20°C	4MHz A_{non}= 0.8 dB/cm MHz A_{cold}= 0.9 dB/cm MHz	7MHz A_{non}= 1.1dB/cm MHz A_{cold}= 1.2dB/cm MHz		Woods 1985. PhD thesis.
Bovine				Woods 1985
Bovine M. Semitendinosis Post Rigor	Pulse echo 2-7 MHz T=20°C	All = 1.25 dB/cmMHz $A_{\dagger}$ = 0.5 dB/cmMHz		Shore et al. 1986

Table 4.2-1 Literature survey of ultrasonic propagation properities of bovine skeletal muscle. (Continued)

Biological Preparation	Ultrasonic Measurement	Attenuation Results	Speed m/s	Publication
Bovine. 5-3 samples for each result. Used M. sternomandibularis. M. Longissmus dorsi	Radiation force balance f=1.3, 4.2, 7.02, 9.8 MHz Cold.	M. sternomandibularis. All & stretched. 2.3, 8.6, 16.45, 25.1 A† & stretched. 0.6, 2.0, 3.8, 5.7 All & cold. 2.0, 7.9, 12.2, 17.0 A† & cold. 0.8, 2.6, 5.0, 8.04 All > A† M. Longissmus dorsi Fat 1.42 4.72 8.18 11.79 Young 1.38 4.2 7.4 10.37 Old 1.08 3.38 6.09 8.98		Joel May,1986.
Bovine M. Semitendinosis	Radiation force Balance and pulse decay (TTT).	n=3. $A < \alpha$ $A = \alpha$ $A > \alpha$		Lyons and Parker, 1988.
Semimembranosus cut into 18 cubes.	5 MHz, 20 MHz Echographic signals.	5MHz TDR: $A_{\|} = 3.1$ dB/cmMHz $A_{\dagger} = 0.9$ dB/cmMHz 20MHz TDR $A_{\|} = 3.1$ dB/cmMHz $A_{\dagger} = 1.3$dB/cmMHz		Roberjot et.al 1994.
M. Longissmus dorsi n=20	SLAM @ 100 MHz T=20°C	$A_{\|}$ =87 dB/mm $A_{\dagger}$ = 45 dB/mm	$C_{\|} = 1619$ $C_{\dagger} = 1599$	Jia Yao, 1995

Table 7.1.2-1. From the SLAM interference image, the speed of sound Dow Corning 710 is determined along with the %error determined from the reported oil's literature value of 1365 m/s [Dunn et al., 1969].

SLAM SPEED

Oil Thickness Layer (μm)	Mean (m/s)	Standard Deviation (m/s)	Error (%)
55	1348	14.4	0.6
76	1356	8.3	1.2
131	1354	13.4	1.1

Table 7.2.1-1 lists the mean attenuation coefficient and standard deviation of Dow Corning 710 from several experiments at 4, 20and 37°C from 2-7 MHz. The attenuation coefficient results are compared against the results from Zeqiri (1989) measured at 20°C and Dunn et al. (1969) determined for 4 & 37°C.

DES ATTENUATION COEFFICIENT

Temperature °C	Frequency (MHz)	Mean (dB/cm)	S.D. (dB/cm)	Error (%)
4	2	7.5	1.6	8.0
	3	12.1	2.0	8.4
	4	16.5	1.9	10.1
	5	26.0	3.1	12.3
	6	34.3	1.7	17.3
	7	57.1	5.3	10.2
20	2	2.2	0.6	8.0
	3	4.8	1.6	4.1
	4	7.3	0.7	8.4
	5	11.2	0.7	1.7
	6	15.1	1.0	7.6
	7	20.9	1.3	1.4
37	2	2.2	0.8	14.3
	3	2.7	0.5	-2.9
	4	3.3	0.5	3.6
	5	5.4	0.3	-10.8
	6	7.3	0.5	-15.3
	7	10.5	1.0	-6.4

Table 7.2.2-1 lists the mean speed of sound and standard deviation of Dow 710 from 20 independent experiments at 4, 20 and 37°C from 2-7 MHz for the DES. The speed of sound results are compared against the results from Dunn et al. (1969). The error percentage is the difference between the mean speed reported and the oil's literature value of 1365 m/s.

	DES SPEED		
Temperature °C	**Mean (m/s)**	**S.D. (m/s)**	**% Error**
4.0	1423.5	8.1	0.2
20.0	1383.5	5.2	-0.4
37.0	1326.7	5.2	-0.02

Table 7.2.2-2. Summary of the uncertainty assessment for the SLAM and DES.

	SLAM	
	Speed	**Attenuation Coefficient**
Accuracy	±2.2 %	±12.4 %
Precision	±1.4 %	±6 %

	DES	
	Speed	**Attenuation Coefficient**
Accuracy	±1.4 %	±18 %
Precision	±8 %	±5 %

Table 7.3.2-1. The factor levels for each factor included in the ANOVA .

Factor	**Levels**		
Orientation	Parallel		Perpendicular
Thickness	60	100	140

Table 7.3.2.1-1. An ANOVA was performed to assess the effect of the orientation factor on the attenuation coefficient response variable.

	Factor Orientation	
	F value	**p-value**
Longissimus Dorsi	39.17**	< 0.01
Psoas Major	11.31**	< 0.01
Lobster Extensor	12.16**	< 0.01

* if the F value exceeds the 0.05 level of significance.
** if the F value exceeds the 0.01 level of significance.

Table 7.3.2.1-2. The mean attenuation coefficient (dB/mm) and standard deviation at 100 MHz both parallel and perpendicular to the muscle fiber were determined for the three muscle types.

	Longissimus Dorsi	**Psoas Major**	**Lobster Extensor**
Parallel	87 ± 10	71 ±12	34 ± 8
Perpendicular	48 ± 10	45 ± 12	20 ± 4

Table 7.3.2.2-1 An ANOVA was performed to assess the effect of the orientation and thickness factors on the speed response variable.

Speed (m/s)	Factor Orientation		Factor Thickness	
	F value	p-value	F value	p-value
Longissimus Dorsi	12.54**	0.007	0.80	0.92
Psoas Major	11.22*	0.01	0.83	0.44
Lobster Extensor	11.22*	0.01	0.17	0.98

* if the F value exceeds the 0.05 level of significance.
** if the F value exceeds the 0.01 level of significance.

Table 7.3.2.2-2 The mean speed and standard deviation (m/s) of each thickness and the pooled values both parallel and perpendicular samples were determined for the three muscle types.

Thickness	60 μm		100 μm		140 μm		pooled	
Orientation	para	perp	para	perp	para	perp	para	perp
Longissimus Dorsi	1638 ± 19	1618 ± 6	1638 ± 8	1618 ± 26	1635 ± 31	1612 ± 11	1637 ± 11	1615 ± 8
Psoas Major	1631 ± 10	1608 ± 8	1624 ± 17	1605 ± 11	1626 ± 7	1595 ± 10	1626 ± 11	1602 ± 8
Lobster Extensor	1602 ± 17	1574 ± 12	1605 ± 21	1576 ± 9	1606 ± 11	1580 ± 9	1603 ± 4	1576 ± 7

Table Legend:
(para) Fiber orientation parallel to the ultrasound.
(perp) Fiber orientation perpendicular to the ultrasound.

Table 7.3.2.3-1 The effects of sample orientation and thickness were determined for the three muscle types by an ANOVA for the heterogeneity index.

Heterogeneity Index	Factor Orientation		Factor Thickness	
	F value	p-value	F value	p-value
Longissimus Dorsi	8.58**	0.007	4.5*	0.049
Psoas Major	5.01*	0.03	9.35**	< 0.01
Lobster Extensor	0.47	0.49	1.93	0.16

* if the F value exceeds the 0.05 level of significance.
** if the F value exceeds the 0.01 level of significance.

Table 7.3.2.3-2 The mean heterogeneity index and standard deviation of each thickness for the three muscle types in both the parallel and perpendicular orientation. These results illustrates that the heterogeneity index was negatively correlated with sample thickness.

	60		100		140	
	para	perp	para	perp	para	perp
Longissimus Dorsi	66± 6	34± 19	46± 16	27± 14	34± 19	21± 15
Psoas Major	18±4	10± 3	11± 3	10± 1	8± 1	7± 1
Lobster Extensor	17±14	25± 18	16± 17	16± 7	9± 11	11± 6

Table Legend:
(para) Fiber orientation parallel to the ultrasound.
(perp) Fiber orientation perpendicular to the ultrasound.

Table 7.3.3-1. The mean and standard deviation of the results from the biochemical analysis and sarcomere lengths measurements of the muscle samples are listed below. The tissue constituents determined by biochemical analysis were the %water, %fat and %protein.

	%Water	%Fat	%Protein	Sarcomere Length (μm)
Longissimus Dorsi	71.0 ± 2.6	4.8 ± 3.0	22.8 ± 0.5	2.1 ±0.2
Psoas Major	72.1 ±2.6	7.3 ± 1.0	19.1 ± 2.3	3.0 ± 0.2
Lobster Extensor	79.3 ± 1.7	1.8 ± 0.4	18.8 ±1.6	3.8 ±0.6

Table 7.3.3-2 Pearson correlation coefficient (ρ) and its significance (F_{sig}) among the tissue constituents and sarcomere length of the muscle.

	Water	Fat	Protein	Sarcomere Length
Water	ρ = 1 F_{sig} = 0.0			
Fat	ρ = - 0.81 F_{sig} < 0.01	ρ = 1 F_{sig} = 0.0		
Protein	ρ = - 0.56 F_{sig} = 0.028	ρ = - 0.06 F_{sig} = 0.83	ρ = 1 F_{sig} = 0.0	
Sarcomere Length	ρ = 0.86 F_{sig} < 0.0001	ρ = - 0.45 F_{sig} = 0.09	ρ = - 0.77 F_{sig} < 0.001	ρ = 1 F_{sig} = 0.0

Table 7.3.3-3 Comparisons between the sarcomere lengths, tissue constituents and propagation properties are performed with a paired Student t-test. The comparisons were considered significantly different when p-values were less than 0.05.

	Longissimus Dorsi vs. Psoas Major	**Longissimus Dorsi vs. Lobster Extensor**	**Psoas Major vs. Lobster Extensor**
% Water	0.111	< 0.001	< 0.001
%Fat	0.055	0.036	< 0.001
%Protein	0.017	0.033	< 0.001
Sarcomere Length (μm)	0.001	0.001	0.019
Atten. Coeff. Parallel	0.006	< 0.001	< 0.001
Atten. Coeff. Perpendicular	0.128	< 0.001	0.003
Speed Parallel	< 0.001	< 0.001	0.004
Speed Perpendicular	0.006	< 0.001	0.003

Table 7.3.4-1 Regression equation which elucidates the relation between the acoustic properties and the physics characteristics (tissue constituents and sarcomere length) of the three types of muscle under parallel and perpendicular orientation.

Attenuation Coefficient, dB/mm (A)

Variable	Regression Equation	r	Significance	Regression Equation	r	Significance
Longissimus Dorsi	Parallel			Perpendicular		
%Water (w)	A = 344.11 - 3.63 (w)	0.95	0.01	A = 286.31 - 3.36 (w)	0.89	0.04
%Fat (f)	A = 72.56 + 2.98 (f)	0.90	0.04	A = 34.56 + 2.73 (f)	0.84	0.08
%Protein (p)	A = 340.98 - 11.13 (p)	0.55	0.33	A = 338.92 - 12.76 (p)	0.64	0.24
Sac Leng (sl)	A = 144.1 - 27.22 (sl)	0.63	0.25	A = 119.1 - 34.0 (sl)	0.80	0.10
Psoas Major						
%Water (w)	A = 562.76 - 6.82 (w)	0.63	0.25	A = 800.76 - 10.47 (w)	0.94	0.01
%Fat (f)	A = 44.66 + 3.56 (f)	0.28	0.64	A = 8.37 + 5.03 (f)	0.39	0.51
%Protein (p)	A = -17.40 + 4.60 (p)	0.87	0.05	A = -41.82 + 4.55 (p)	0.84	0.07
Sac Leng (sl)	A = 136.9 - 22.27 (sl)	0.45	0.44	A = 158.38 - 37.3 (sl)	0.75	0.14
Lobster Extensor						
%Water (w)	A = 401.5 - 4.64 (w)	0.94	0.01	A = 191.43 - 2.17 (w)	0.87	0.04
%Fat (f)	A = 7.17 + 15.13 (f)	0.74	0.14	A = 6.50 +7.36 (f)	0.71	0.17
%Protein (p)	A = -54.41 + 4.69 (p)	0.92	0.02	A = -54.41 + 4.69 (p)	0.84	0.07
Sac Leng (sl)	A = 71.6 - 10.0 (sl)	0.71	0.17	A = 36.1 - 4.33 (sl)	0.62	0.26

Speed, m/s (c)

Variable	Regression Equation	r	Significance	Regression Equation	r	Significance
Longissimus Dorsi	Parallel			Perpendicular		
%Water (w)	c = 1863.1 - 3.19 (w)	0.76	0.04	c = 1818.9 - 3.19 (w)	0.90	0.04
%Fat (f)	c = 1625.3 + 2.47 (f)	0.68	0.20	c = 1604.1 + 2.47 (f)	0.85	0.07
%Protein (p)	c = 1859.7 - 9.75 (p)	0.44	0.45	c = 1881 - 11.67 (p)	0.69	0.19
Sac Leng (sl)	c = 1726.0 - 42.3 (sl)	0.89	0.04	c = 1675.3 - 28.5 (sl)	0.79	0.11
Psoas Major						
%Water (w)	c = 2293.0 - 9.24 (w)	0.94	0.01	c = 2144.5 - 7.51 (w)	0.99	0.0003
%Fat (f)	c = 1585.3 + 5.65 (f)	0.50	0.38	c = 1573.8 + 3.94 (f)	0.45	0.44
%Protein (p)	c = 1552.1 + 3.89 (p)	0.81	0.08	c = 1554.8 + 2.50 (p)	0.67	0.20
Sac Leng (sl)	c = 1726.0 - 42.3 (sl)	0.81	0.09	c = 1688.7 - 28.97 (sl)	0.84	0.07
Lobster Extensor						
%Water (w)	c = 2262.1 - 8.32 (w)	0.87	0.03	c = 1856.7 - 3.54 (w)	0.77	0.12
%Fat (f)	c = 1555.1 + 27.12 (f)	0.68	0.20	c = 1510.6 + 14.72 (f)	0.77	0.12
%Protein (p)	c = 1443.7 + 8.45 (p)	0.84	0.06	c = 1510.6 + 3.49 (p)	0.73	0.15
Sac Leng (sl)	c = 1652.3 - 12.9 (sl)	0.47	0.42	c = 1599.1 - 6.0 (sl)	0.46	0.43

Table 7.3.4-2 The propagation properties, sarcomere length and tissue constituents results of the three muscle types are pooled and a linear regression is performed on the pooled data. The predictive ability of these linear regression equations is stronger due to the larger data set as indicated by the correlation coefficient (r) and the significance.

Attenuation Coefficient, dB/mm (A)

Variable	Regression Equation Parallel	r	Significance	Regression Equation Perpendicular	r	Significance
%Water (w)	A = 483.6 - 5.6 (w)	0.95	<0.01	A = 299.3 - 3.5 (w)	0.95	<0.01
%Fat (f)	A = 37.50 + 5.7 (f)	0.66	<0.01	A = 18.1 + 4.1 (f)	0.76	<0.01
%Protein (p)	A = - 41.8 + 3.9 (p)	0.72	<0.01	A = -86.1 + 7.3 (p)	0.60	0.02
Sac Leng (sl)	A = 144.7 - 27.3(sl)	0.89	<0.01	A = 83.2 - 15.4 (sl)	0.90	<0.01

Speed, m/s (c)

Variable	Regression Equation Parallel	r	Significance	Regression Equation Perpendicular	r	Significance
%Water (w)	c = 1924.6 - 4.1 (w)	0.90	<0.01	c = 1911.5 - 4.2 (w)	0.95	<0.01
%Fat (f)	c = 1603.6 + 4.0 (f)	0.61	0.01	c = 1578.5 + 4.2 (f)	0.66	<0.01
%Protein (p)	c = 1507.2 + 5.7 (p)	0.72	<0.01	c = 1491.5 + 5.3 (p)	0.68	<0.01
Sac Leng (sl)	c = 1680.7 - 19.7 (sl)	0.84	<0.01	c = 1658.8 - 20.5 (sl)	0.89	<0.01

Table 7.3.5-1 Multiple linear regression equations for the tissue constituents and the sarcomere length from the attenuation coefficient and the speed under parallel and perpendicular orientation. The F-value and its probability level (F_{sig}) for each equation are listed at the right of each equation. Below the each coefficients of the equation is the T_{sig} value which indicates the significance of that coefficients to the dependent variable.

Regression Equations		**F**	**F_{sig}**
(Parallel)			
%w	$= (-0.14 \cdot A) + (-0.03 \cdot c) + 131.2$	63.2	< 0.01
	$T_{sig} = 0.03$ $T_{sig} = 0.67$		
%f	$= (0.08 \cdot A) + (0.001 \cdot c) - 3.2$	4.8	0.030
	$T_{sig} = 0.25$ $T_{sig} = 0.98$		
%p	$= (0.04 \cdot A) + (0.050 \cdot c) - 62.0$	7.1	< 0.01
	$T_{sig} = 0.44$ $T_{sig} = 0.44$		
SL	$= (-0.0249 \cdot A) + (-0.006 \cdot c) + 14.4$	24.0	< 0.01
	$T_{sig} < 0.01$ $T_{sig} = 0.54$		
(Perpendicular)			
%w	$= (-0.08 \cdot A) + (-0.15 \cdot c) + 315.9$	73.1	< 0.01
	$T_{sig} = 0.15$ $T_{sig} < 0.01$		
%f	$= (0.25 \cdot A) + (-0.10 \cdot c) + 151.2$	10.1	0.027
	$T_{sig} = 0.02$ $T_{sig} = 0.27$		
%p	$= (-0.08 \cdot A) + (0.15 \cdot c) - 218.4$	5.9	0.016
	$T_{sig} = 0.45$ $T_{sig} = 0.09$		
SL	$= (0.03 \cdot A) + (-0.062 \cdot c) + 101.3$	31.4	< 0.01
	$T_{sig} = 0.23$ $T_{sig} = 0.02$		

Table Legend

%w	%water
%f	%fat
%p	%protein
SL	sarcomere length
A	attenuation coefficient (dB/mm)
c	speed (m/s)

Table 7.3.5.1-1. An ANOVA was performed to assess the effect of the orientation factor on the attenuation coefficient response variable for the semitendinosis samples.

	Factor Orientation	
	F value	**p-value**
Semitendinosis	12.2**	< 0.001

* if the F value exceeds the 0.05 level of significance.
** if the F value exceeds the 0.01 level of significance.

Table 7.3.5.1-2. The mean attenuation coefficient (dB/mm) and standard deviation both parallel and perpendicular to the muscle fiber were determined for bovine semitendinosis.

	Parallel	**Perpendicular**
Attenuation Coefficient	68 ± 12	51 ± 7

Table 7.3.5.1-3. An ANOVA was performed to assess the effect of the orientation and thickness factors on the speed response variable.

Speed (m/s)	**Factor Orientation**		**Factor Thickness**	
	F value	**p-value**	**F value**	**p-value**
Semitendinosis	12.5**	< 0.001	0.60	0.55

* if the F value exceeds the 0.05 level of significance.
** if the F value exceeds the 0.01 level of significance.

Table 7.3.5.1-4. The mean speed and standard deviation (m/s) of each thickness and the pooled values both parallel and perpendicular samples were determined for the semitendinosis samples.

	Parallel	**Perpendicular**
60 μm	1628 ± 28	1600 ± 15
100 μm	1641 ± 34	1607 ± 16
140 μm	1623 ± 25	1613 ± 20
pooled	1631 ± 29	1607 ± 17

Table 7.3.5.1-5. The effects of sample orientation and thickness were determined for semitendinosis by an ANOVA for the heterogeneity index.

Heterogeneity Index	Factor Orientation		Factor Thickness	
	F value	p-value	F value	p-value
Semitendinosis	7.7**	< 0.01	7.0**	< 0.01

* if the F value exceeds the 0.05 level of significance.
** if the F value exceeds the 0.01 level of significance.

Table 7.3.5.1-6. The mean heterogeneity index and standard deviation of each thickness for semitendinosis in both the parallel and perpendicular orientation. These results illustrates that the heterogeneity index was negatively correlated with sample thickness.

	Parallel	Perpendicular
60 μm	64 ± 29	41 ± 25
100 μm	34 ± 21	22 ± 13
140 μm	36 ± 19	15 ± 4

Table 7.3.5.2-1. The mean and standard deviation of the results from the biochemical analysis and sarcomere lengths measurements of semitendinosis are listed below. The tissue constituents determined by biochemical analysis were the %water, %fat and %protein.

	%Water	%Fat	%Protein	Sarcomere Length (μm)
Semitendinosis	72.2 ± 1.9	7.1 ± 2.7	20.7 ± 1.1	2.7 ± 0.3

Table 7.3.5.2-2 Pearson correlation coefficient (ρ) and its significance (F_{sig}) among the tissue constituents and sarcomere length of semitendinosis.

	Water	**Fat**	**Protein**	**Sarcomere Length**
Water	$\rho = 1$ $F_{sig} = 0.0$			
Fat	$\rho = -0.9$ $F_{sig} < 0.01$	$\rho = 1$ $F_{sig} = 0.0$		
Protein	$\rho = 0.5$ $F_{sig} = 0.19$	$\rho = -0.8$ $F_{sig} = 0.019$	$\rho = 1$ $F_{sig} = 0.0$	
Sarcomere Length	$\rho = 0.5$ $F_{sig} = 0.19$	$\rho = -0.4$ $F_{sig} = 0.32$	$\rho = 0.1$ $F_{sig} = 0.9$	$\rho = 1$ $F_{sig} = 0.0$

Table 7.3.5.3-1. The acoustic, biochemical and sarcomere length results of semitendinosis are compared against the results of the muscle used to develop the multiple linear regression equations (i.e. longissimus dorsi, psoas major and lobster extensor) to determine if semitendinosis comes from the same group using the Student t-test. The comparisons were considered significantly different when p-values were less than 0.05.

	Semitendinosis vs.Longissimus Dorsi	**Semitendinosis vs. Psoas Major**	**Semitendinosis vs. Lobster Extensor**
% Water	0.15	0.48	< 0.001
%Fat	0.06	0.41	< 0.001
%Protein	< 0.001	< 0.05	< 0.01
Sarcomere Length (μm)	< 0.001	< 0.05	< 0.001
Atten. Coeff. Parallel	0.09	0.17	< 0.001
Atten. Coeff. Perpendicular	< 0.05	0.36	< 0.001
Speed Parallel	< 0.01	0.15	< 0.001
Speed Perpendicular	0.25	0.14	< 0.001

Table 7.3.5.3-2. The mean and standard deviation of the results from the biochemical analysis and sarcomere lengths measurements of semitendinosis are listed below "biochemical analysis". Also listed are the predicted tissue constituent and sarcomere length results based on the parallel and perpendicular model.

	Parallel Predicted Results	Perpendicular Predicted Results	Biochemical Analysis
%Water	72.7 ± 1.9	70.9 ± 1.5	72.2 ± 1.9
%Fat	3.9 ± 1.0	3.2 ± 1.2	7.1 ± 2.7
%Protein	22.3 ± 0.8	18.5 ± 0.6	20.7 ± 1.1
Sarcomere Length	2.9 ± 0.3	3.2 ± 0.3	2.7 ± 0.3

Table 7.3.5.3-3 lists the %error for the parallel and perpendicular prediction model compared against the actual biochemical and sarcomere length results.

	Parallel Model %Error	Perpendicular Model %Error
%Water	0.7	1.8
%Fat	45.1	50
%Protein	7.7	10.6
Sarcomere Length	7.4	18.5

Table 7.4.2-1. The factor levels for each factor included in the ANOVA .

Factor	**Levels**		
Orientation	Parallel		Perpendicular
Thickness (cm)	0.5	1.0	1.5
Temperature (°C)	4	20	37

Table 7.4.2.1-1. An ANOVA was performed to assess the effect of the orientation factor and temperature on the slope of the attenuation coefficient response variable for the 30 samples of longissimus dorsi.

	Factor Orientation		**Factor Temperature**	
	F value	**p-value**	**F value**	**p-value**
Slope of the Attenuation Coefficient (dB/cm/MHz)	47.8**	< 0.001	12.8**	< 0.001

* if the F value exceeds the 0.05 level of significance.
** if the F value exceeds the 0.01 level of significance.

Table 7.4.2.1-2. The mean slope of the attenuation coefficient (dB/cm/MHz) and standard deviation both parallel and perpendicular to the muscle fiber were determined. These data are plotted in Figure 7.4.2.2-1.

	Slope of the Attenuation Coefficient (dB/cm/MHz)		
	4°C	**20°C**	**37°C**
Parallel	2.9 ± 1.3	2.1 ±1.0	1.8 ± 0.8
Perpendicular	1.7 ± 0.6	1.0 ± 0.6	1.2 ± 0.5

Table 7.4.2.2-1. An ANOVA was performed to assess the effect of the orientation, thickness and temperature factors on the speed response variable.

	Factor Thickness		Factor Orientation		Factor Temperature	
	F value	**p-value**	**F value**	**p-value**	**F value**	**p-value**
Speed (m/s)	0.38	0.49	3.9*	0.048	54.9**	< 0.001

* if the F value exceeds the 0.05 level of significance.
** if the F value exceeds the 0.01 level of significance.

Table 7.4.2.2-2 The mean speed and standard deviation (m/s) of each thickness and the pooled values of both parallel and perpendicular samples were determined. The ANOVA results from Table 7.4.2.2-1 indicate that there was no overall variation due to specimen thicknesses; thus the speed for 3 thicknesses can be pooled without affecting the speed results.

Thickness	**0.5 cm**		**1.0 cm**		**1.5 cm**		**pooled**	
Orientation	**para**	**perp**	**para**	**perp**	**para**	**perp**	**para**	**perp**
4°C	1541	1520	1532	1511	1535	1526	1536	1519
	±12	±20	±5	±14	±11	±6	±16	±13
20°C	1620	1604	1614	1611	1605	1609	1613	1608
	± 10	± 11	± 11	±9	± 15	± 10	± 4	± 5
37°C	1681	1644	1670	1656	1665	1659	1672	1653
	± 9	± 15	± 14	±12	± 5	± 10	± 17	± 23

Table Legend:
(para) Fiber orientation parallel to the ultrasound.
(perp) Fiber orientation perpendicular to the ultrasound.

Table 7.4.3-1. The mean and standard deviation of the results from the biochemical analysis and sarcomere lengths measurements of the muscle samples are listed below. The tissue constituents determined by biochemical analysis were the %water, %fat and %protein.

	%Water	%Fat	%Protein	Sarcomere Length (μm)
Longissimus Dorsi	72.2 ± 2.7	5.87± 2.9	21.8 ± 1.0	1.93±0.2

Table 7.4.3-2 Pearson correlation coefficient (ρ) and its significance (F_{sig}) among the tissue constituents and sarcomere length of the muscle.

	Water	Fat	Protein	Sarcomere Length
Water	ρ = 1 F_{sig} = 0.0			
Fat	ρ = - 0.91 F_{sig} < 0.01	ρ = 1 F_{sig} = 0.0		
Protein	ρ = - 0.50 F_{sig} < 0.01	ρ = - 0.64 F_{sig} < 0.01	ρ = 1 F_{sig} = 0.0	
Sarcomere Length	ρ = 0.28 F_{sig} =0.14	ρ = - 0.19 F_{sig} = 0.31	ρ = - 0.77 F_{sig} = 0.68	ρ = 1 F_{sig} = 0.0

Table 7.4.4-1 Regression equation which describes the relation between the acoustic properties and the tissue constituents and sarcomere length of longissimus dorsi under parallel and perpendicular orientation at 4, 20 and 37°C.

Slope of the Attenuation Coefficient, dB/cm/MHz (SAC)

Variable	Regression Equation Parallel	r	Significance	Regression Equation Perpendicular	r	Significance
4°C						
%Water (w)	SAC = 19 - 0.2 (w)	0.2	0.08	SAC = 0.4 - 0.1 (w)	0.0	0.8
%Fat (f)	SAC = 1.9 + 0.2 (f)	0.1	0.2	SAC = 1.8 + 0.1 (f)	0.0	0.9
%Protein (p)	SAC= 4.5 - 0.1 (p)	0.1	0.8	SAC = 0.5 - 0.1 (p)	0.0	0.6
Sac Leng (sl)	SAC = 4 - 0.5 (sl)	0.1	0.8	SAC = 6 - 2.2 (sl)	0.2	0.2
20°C						
%Water (w)	SAC = 25 - 0.3 (w)	0.8	<0.01	SAC = 7.2 - 8.4 (w)	0.2	0.08
%Fat (f)	SAC = 0.1 + 0.3 (f)	0.9	<0.01	SAC = 0.6 + 0.1 (f)	0.2	0.09
%Protein (p)	SAC = 12 - 0.5 (p)	0.2	0.05	SAC = 0.4 + 0.1 (p)	0.0	0.6
Sac Leng (sl)	SAC = 2 - 0.5 (sl)	0.0	0.9	SAC = 0.8 - 0.7 (sl)	0.0	0.7
37°C						
%Water (w)	SAC = 19 - 0.2 (w)	0.8	<0.01	SAC = 13 - 0.2 (w)	0.8	<0.01
%Fat (f)	SAC = 0.4 + 0.2 (f)	0.8	<0.01	SAC = 0.2 + 0.2 (f)	0.8	<0.01
%Protein (p)	SAC = 10 - 0.4 (p)	0.3	0.03	SAC = 8 - 0.3 (p)	0.3	0.02
Sac Leng (sl)	SAC = 2 - 0.1 (sl)	0.0	0.9	SAC = 1 + 0.1 (sl)	0.0	0.9

Speed, m/s (c)

Variable	Regression Equation Parallel	r	Significance	Regression Equation Perpendicular	r	Significance
4°C						
%Water (w)	c = 1316 - 2.8 (w)	0.01	0.78	c = 1462- 10 (w)	0.07	0.54
%Fat (f)	c = 1570 + 7.8 (f)	0.04	0.47	c = 1464 + 7.7 (f)	0.04	0.64
%Protein (p)	c = 701 + 38 (p)	0.12	0.21	c = 1761 + 12 (p)	0.11	0.92
Sac Leng (sl)	c = 1876 - 188 (sl)	0.05	0.40	c = 166 - 83 (sl)	0.02	0.61
20°C						
%Water (w)	c = 1439 - 2.5 (w)	0.25	0.05	c = 1545 - 1.1 (w)	0.01	0.64
%Fat (f)	c = 1641 + 3.4 (f)	0.48	<0.01	c = 1639 + 3 (f)	0.14	0.16
%Protein (p)	c = 1423 + 9.1 (p)	0.46	<0.01	c = 1460 + 7.5 (p)	0.10	0.23
Sac Leng (sl)	c = 1679 - 31 (sl)	0.09	0.25	c = 1665 - 23 (sl)	0.01	0.62
37°C						
%Water (w)	c = 1433 - 3.7 (w)	0.01	0.65	c = 1333 - 5.2 (w)	0.01	0.68
%Fat (f)	c = 1733 + 4.7 (f)	0.01	0.65	c = 1751 + 6.7 (f)	0.02	0.59
%Protein (p)	c = 1828 + 5.7 (p)	0.01	0.85	c = 2161 + 20 (p)	0.02	0.56
Sac Leng (sl)	c = 2419 - 378 (sl)	0.25	0.07	c = 2595 - 496 (sl)	0.25	0.06

Table 7.4.5-1 Multiple linear regression equations for the tissue constituents and the sarcomere length from the attenuation coefficient and the speed under parallel and perpendicular orientation. The F-value and its probability level (F_{sig}) for each equation are listed at the right of each equation. Below the each coefficients of the equation is the T_{sig} value which indicates the significance of that coefficients to the dependent variable.

Regression Equations at 4°C

	Parallel	**F**	**Fsig**
%w =	(−0.08 • SAC) + (−0.01 • c) + 66.3	1.24	0.32
	T_{sig} = 0.54 T_{sig} = 0.14		
%f =	(−0.08 • SAC) + (0.03 • c) + 18.2	2.21	0.15
	T_{sig} = 0.08 T_{sig} = 0.03		
%p =	(−0.04 • SAC) + (−0.01 • c) +131.2	4.31	0.03
	T_{sig} = 0.05 T_{sig} = 0.03		
SL =	(−0.01 • SAC) + (−0.001 • c) + 2.4	0.60	0.56
	T_{sig} = 0.34 T_{sig} = 0.52		
	Perpendicular		
%w =	(−0.01 • SAC) + (0.63 • c) + 79.8	0.44	0.64
	T_{sig} = 0.47 T_{sig} = 0.14		
%f =	(−0.48 • SAC) + (0.01 • c) + 18.2	0.19	0.82
	T_{sig} = 0.66 T_{sig} = 0.65		
%p =	(0.001 • SAC) + (0.31 • c) +20.5	0.32	0.72
	T_{sig} = 0.05 T_{sig} = 0.03		
SL =	(−0.01 • SAC) + (−0.07 • c) + 2.3	1.59	0.62
	T_{sig} = 0.62 T_{sig} = 0.11		

Table Legend

%w	%water
%f	%fat
%p	%protein
SL	sarcomere length
SAC	slope of the attenuation coefficient (dB/cm/MHz)
c	speed (m/s)

Table 7.4.5-1 continued.

Regression Equations 20°C

	Parallel	**F**	**F_{sig}**
%w =	(–2.94 • SAC) + (–0.02 • c) + 111	44.3	<0.01
	T_{sig} = 0.33 T_{sig} = 0.00		
%f =	(2.49 • SAC) + (-0.03 • c) + 47.5	51.6	<0.01
	T_{sig} = 0.00 T_{sig} = 0.15		
%p =	(- 0.20 • SAC) + (–0.01 • c) +131.2	6.38	0.01
	T_{sig} = 0.46 T_{sig} = 0.03		
SL =	(–0.01 • SAC) + (–0.002 • c) + 6.38	0.57	0.57
	T_{sig} = 0.34 T_{sig} = 0.52		
	Perpenducular		
%w =	(–0.01 • SAC) + (-2.4 • c) + 76.5	1.56	0.24
	T_{sig} = 0.97 T_{sig} = 0.11		
%f =	(2.02 • SAC) + (- 0.03 • c) + 57.4	2.16	0.15
	T_{sig} = 0.66 T_{sig} = 0.65		
%p =	(0.02 • SAC) + (0.60 • c) - 5.21	1.08	0.40
	T_{sig} = 0.05 T_{sig} = 0.03		
SL =	(–0.05 • SAC) + (–0.01 • c) + 2.7	0.26	0.77
	T_{sig} = 0.62 T_{sig} = 0.11		

Table Legend

%w	%water
%f	%fat
%p	%protein
SL	sarcomere length
SAC	slope of the attenuation coefficient (dB/cm/MHz)
c	speed (m/s)

Table 7.4.5-1 continued.

Regression Equations 37°C

	Parallel	**F**	**F_{sig}**
%w =	(−2.97 • SAC) + (−0.01 • c) + 78.5	7.34	<0.01
	T_{sig} < 0.01 T_{sig} = 0.93		
%f =	(2.66 • SAC) + (-0.01 • c) + 2.5	4.73	0.03
	T_{sig} = 0.03 . T_{sig} = 0.05		
%p =	(- 0.40 • SAC) + (−0.001 • c) +21.73	0.54	0.59
	T_{sig} = 0.33 T_{sig} = 0.91		
SL =	(−0.04 • SAC) + (−0.002 • c) + 6.38	2.35	0.13
	T_{sig} = 0.36 T_{sig} = 0.06		
	Perpenducular		
%w =	(−4.94 • SAC) + (-0.01 • c) + 80.56	27.5	<0.01
	T_{sig} < 0.01 T_{sig} = 0.64		
%f =	(4.94 • SAC) + (- 0.001 • c) - 0.56	27.5	<0.01
	T_{sig} < 0.01 T_{sig} = 0.64		
%p =	(−1.23 • SAC) + (0.01 • c) + 25.7	3.70	0.06
	T_{sig} = 0.05 T_{sig} = 0.03		
SL =	(−0.02 • SAC) + (-0.01 • c) + 2.86	2.07	0.16
	T_{sig} = 0.64 T_{sig} = 0.06		

Table Legend

%w	%water
%f	%fat
%p	%protein
SL	sarcomere length
SAC	slope of the attenuation coefficient (dB/cm/MHz)
c	speed (m/s)

Table 7.4.6-1 The mean and standard deviation of the results from the biochemical analysis and sarcomere length measurements of the second group of longissimus dorsi are listed along "actual results". Also listed are the predicted tissue constituent and sarcomere length results based on the parallel and perpendicular model .

	%Water	%Fat	%Protein	Sarcomere Length (μm)
Biochemical Analysis	72.1 ± 2.4	5.7 ± 2.8	22.0 ± 0.9	2.01 ± 0.09
4°C Parallel Model	72.6 ± 0.2	5.8 ± 0.3	21.8 ± 0.2	2.24 ± 0.05
4°C Perpendicular Model	72.5 ± 0.4	6.0± 0.3	22.5 ± 0.1	2.01 ± 0.10
20°C Parallel Model	72.4 ± 3.0	6.7 ± 2.4	20.9 ± 0.7	1.90 ± 0.11
20°C Perpendicular Model	74.1 ± 1.5	6.9 ± 2.2	20.7 ± 0.5	2.6 ± 0.04
37°C Parallel Model	72.8 ± 2.2	7.1 ± 2.0	21.1 ± 0.3	2.8 ± 0.10
37°C Perpendicular Model	72.5 ± 2.4	3.3 ± 2.4	25.6 ± 0.6	2.7 ± 0.05

Table 7.4.6-2 lists the percentage error for the parallel and perpendicular prediction model. The error percentage is the ratio of the mean model results (parallel or perpendicular) over the actual results.

% Error	%Water	%Fat	%Protein	Sarcomere Length
4°C Parallel	0.7	1.8	0.9	11.4
4°C Perpendicular	0.6	5.3	2.3	0
20°C Parallel	0.4	17.5	5.0	5.5
20°C Perpendicular	2.8	21.0	5.9	29.4
37°C Parallel	1.0	30.0	4.1	39.3
37°C Perpendicular	0.6	42.1	16.4	34.3

Table 7.5.2-1. The factor levels for each factor included in the ANOVA .

Factor	**Levels**		
Orientation	Parallel	Perpendicular	Homogenized
Thickness (μm)	80	100	120

Table 7.5.2.1-1 An ANOVA was performed to assess the effect of the orientation on the attenuation coefficient response variable.

	Factor Orientation	
	F value	**p-value**
Attenuation Coefficient (dB/mm)	58.5**	< 0.01

* if the F value exceeds the 0.05 level of significance.
** if the F value exceeds the 0.01 level of significance.

Table 7.5.2.1-2 The mean attenuation coefficient (dB/mm) and standard deviation both parallel and perpendicular to the muscle fiber were determined for the three muscle types.

	Parallel	**Perpendicular**	**Homogenized**
Attenuation Coefficient (dB/mm)	87 ± 23	45 ±14	28 ± 14

Table 7.5.2.2-1 An ANOVA was performed to assess the effect of the orientation and thickness factors on the speed response variable.

	Factor Orientation		**Factor Thickness**	
	F value	**p-value**	**F value**	**p-value**
Speed (m/s)	48.2**	< 0.01	3.2	0.067

* if the F value exceeds the 0.05 level of significance.
** if the F value exceeds the 0.01 level of significance.

Table 7.5.2.2-2 The mean speed and standard deviation (m/s) of each thickness and the pooled values both parallel and perpendicular samples were determined for the three muscle types.

	Orientation		
Thickness (μm)	**Parallel**	**Perpendicular**	**Homogenized**
80	1622±15	1601±14	1584±19
100	1617±15	1598 ±13	1577 ±21
120	1618±16	1597 ±13	1585 ±13
pooled	1619±16	1599 ± 14	1582 ± 18

Table 7.5.2.3-1 The effects of sample orientation and thickness were determined for the three muscle types by an ANOVA for the heterogeneity index.

	Factor Orientation		**Factor Thickness**	
	F value	**p-value**	**F value**	**p-value**
Heterogeneity Index (m/s)	40.2**	< 0.01	2.77	0.067

* if the F value exceeds the 0.05 level of significance.
** if the F value exceeds the 0.01 level of significance.

Table 7.5.2.3-2 The mean heterogeneity index and standard deviation of each thickness for the three muscle types in both the parallel and perpendicular orientation. These results illustrates that the heterogeneity index was negatively correlated with sample thickness.

	Orientation		
Thickness (μm)	**Parallel**	**Perpendicular**	**Homogenized**
80	22.7±7.1	20.9±6.4	12.0±2.8
100	19.9±6.0	18.9 ±6.0	16.5 ±5.4
120	21.2±9.8	16.8 ±6.0	9.8 ±3.5
pooled	21.4±9.8	18.7±4.1	12.8±5.4

Table 7.6.1-1. Attenuation coefficient and speed results as a function of the angle of propagation from 8 samples of semitendinosis using the SLAM @ 100 MHz.

Angle degrees	Attenuation Coefficient (dB/mm)	Speed (m/s)
10 parallel	68 ±12	1631±29
35	60 ±13	1625±22
45	58 ±9	1623±12
55	55 ±6	1619±19
80	53 ±10	1609±11
90 perpendicular	51 ±7	1607±17

Table 7.6.1-2. A linear regression of the attenuation coefficient and speed data in Figure 7.6.1-1 and Figure 7.6.1-2, respectively, yields two equations for the attenuation coefficient and speed, respectively, as a function of the insonification angle at 100 MHz from 10 to 90°. The correlation coefficient (r) for the equation is listed to the right.

$$Attenuation\_coefficient(\theta) = 68.0 - 0.2 \times \theta \qquad r = 0.94$$

$$Speed(\theta) = 1635.6 - 0.31 \times \theta \qquad r = 0.98$$

Table 7.6.2-1. Interpolation of the attenuation coefficient and speed data in Figure 7.6.2-1 and Figure 7.6.2-2, respectively, by the a fourth order polynomial yields two equations for the attenuation coefficient and speed as a function of the insonification angle at 3 MHz from 0 to 180°. The correlation coefficient (r) for the equation is listed to the right.

$$Attenuation\_coefficient(\theta) = 3.9 - 9.4 \times 10^{-3} \times \theta + 3.3 \times 10^{-3} \times \theta^2 - 3.3 \times 10^{-5} \times \theta^3 + 9.2 \times 10^{-9} \times \theta^4 \qquad r = 0.97$$

$$Speed(\theta) = 1615 - 8.2 \times 10^{-2} \times \theta + 2.7 \times 10^{-3} \times \theta^2 + 4.2 \times 10^{-7} \times \theta^3 - 4.2 \times 10^{-7} \times \theta^4 \qquad r = 0.99$$

Table 7.6.3-1. Comparison of the slope of the attenuation coefficient (ratio of the attenuation coefficient to the frequency expressed as dB/cm/MHz) and speed results from SLAM and DES.

Angle (degrees)	Slope of the Attenuation Coefficient (dB/cm/MHz)		Speed (m/s)	
	SLAM	DES	SLAM	DES
10 parallel	6.8 ±1.2	1.28±0.03	1631±29	1614±2.6
35	6.0 ±1.3	1.09±0.01	1623±12	1610±0.4
45	5.8 ±0.9	1.03±0.02	1623±12	1609±0.8
55	5.5 ±0.6	1.00±0.01	1619±19	1609±0.7
80	5.3 ±1.0	0.91±0.01	1609±11	1607±0.6
90 perpendicular	5.1 ±0.7	0.94±0.01	1607±17	1607±0.5

BIBLIOGRAPHY

Agemura, D.H., Olerud, J.E., Chun, L.E., Eyre, D.E. and O'Brien, Jr., W.D, "Ultrasonic propagation properities of articular cartilage at 100 MHz", *J. Acoust. Soc. Am.*, pp. 1786-1791, vol. 87, no.4, 1990.

Agemura, D.H., "Ultrasonic propagation properities of canine myocardium and bovine articular cartilage at 100 MHz," M.S. Thesis, Department of Electrical and Computer Engineering, University of Illinois, 1986.

Akashi, N., Kuchibiki, J., Chubachi , N., and Dunn, F., "Acoustic properties of selected bovine tissues in the frequency range 20-200 MHz," *J. Acoust. Soc. Am.*, pp. 3035-3039, vol. 98, no.6, 1995.

Alberts, B., Bray, D, Lewis, J., Raff, M., Roberts, K., and Watson, J, *Molecular Biology of the Cell* 2nd Ed., Garland Publishing Inc., New York and London, 1989.

Amin, V., Roberts, R., Wilson, D. and Rouse, G., "Tissue characterization for beef grading using texture analysis of ultrasonic images," *IEEE 1993 Ultrasonics Symposium Proceedings*, pp. 696-700, Baltomore, MD., 1993.

Bamber, J.C., "Ultrasound chacterization of structure and pathology in human soft tissue," Ph. D. dissertation, London University, 1979.

Bamber, J.C. and Hill, C.R., "Ultrasonic attenuation and propagation speed in mammalian tissue as a function of temperature," *Ultrasound in Med. & Biol.*, vol. 5, no.2, pp. 149-155, 1979.

Berger, G., Laugier, P., Fink, M., and Perrin, J., "Optimal precision in ultrasonic attenuation estimation and detetection of duchenne muscular dystropy carriers," *Ultrasonic Imaging* , vol. 9, pp. 1-17, 1987.

Bhatia, A.B., *Ultrasonic Absorption: An Introduction to the Theory of the Sound Absorption and Dispersion in Gases, Liquids and Solids*, Dover Publications, Inc. New York, 1967.

Bowen, T, Connor, W.G., Nasoni, R.L., Pifer, and Sholes, R.R., "Measurement of the temperature dependance of the velocity of ultrasound on soft tissues," NBS Special Publication 525, pp. 57-61, 1979.

Brackebusch, S.A., "The proximate composition of the major muscles of the beef carcass," M.S. Thesis, Department of Animal Science, University of Illinois, 1988.

Brackebusch, S.A., Mc Keith, F.K, Carr, T.R., Dutton, D.M., and Mc Laren, D.G., "Relationship between marbling group and major muscle controbution to the beef carcass," *J. Anim. Sci.*, vol. 69, pp. 625-630, 1991.

Brackebusch, S.A., Mc Keith, F.K, Carr, T.R., and Mc Laren, D.G., "Relationship between longissimus composition and composition of other major muscles of the beef carcass", *J. Anim. Sci.*, vol. 69, pp. 631-640, 1991.

Broadband Power Amplifier Instruction Manual Model A150. Electronic Navigation Industries, Inc., Rochester, NY, 1987.

Carstensen, E.L., Li,K.,and Schwan, H.P., "Determination of the acoustic properities of blood and its components," *J. Acoust. Soc. Am.*, vol. 25, no. 2, pp. 286-290, 1953.

Chan, J., "Quantitative characterization of carotid artheromatous plaque using ultrasonic rf A-scans data," Ultrasonics, vol. 33, no. 2, pp.163-164, 1995.

Colombati and Pretralia, 1950. See Goss et al. 1978.

Davidson, G., Hall, C.H., Miller, J.G., Scott, M. and Wickline, S.A., "Ultrasonic tissue characterization of end-stage dilated cardiomyopathy", *Ultrasound in Med. & Biol.*, vol. 21, no.7, pp. 853-860, 1995.

Dock, W., Happack, T.K., Grabenwoger, Bittner and Gruber, "Neuromuscular diseases: Evaluation with high-frequency sonography," *Radiol.*, vol.177, pp.825-828, 1990.

Dussick and Fritch, 1955. See Goss, et al. 1978.

Dussick and Fritch, 1956. See Goss, et al. 1978.

Dunn, F., and Breyer, J.E., "Generation and Detection of Ultra-High Frequency Sound in Liquids," *J. Acoust. Soc. Am.*, vol. 34, no. 6, pp. 775-778, 1962.

Dunn, F., Edmonds, P.D., and Fry, W.J., "Absorption and Dispersion of Ultrasound in Biological Media," In *Biological Engineering*, Schwan, H.P., Ed. McGraw Hill, New York, pp. 205-322, 1969.

Dunn, F. and Goss, S.A., "Definations of Terms and Measurements of Acoustical Quanities," In *Tissue Characterization with Ultrasound*, vol. I., Greenleaf, J.F.,Ed. CRC Press, 1986.

Dunn, F., and O'Brien, Jr., W.D., "Ultrasonic Absorption and Dispersion. In Ultrasound:", In *Application in Medicine and Biology*, Fry F.J., Ed. Elsevier, The Netherlands, pp. 393-439, 1978.

Dussik, K.T., Fritch, D.J., Kyriazidou, M., and Sear, R.S., "Measurements on articular tissue with ultrasound," *Am.J.Phys.Med.*, vol. 37, pp. 106-165, 1958.

Exler, J., "Nutritional Monitoring Division, Composition of Foods: Finfish and Shellfish Products," In *US Department of Agriculture, Human nutritional Information Service, Agriculture Handbook*, no. 8-15, September 1987.

Fields, S., Dunn, F., "Correlation of the echographic visualizability of tissue with Biological Composition and Physiological State," *J. Acoust. Soc. Am.*, vol. 54, no. 3, pp. 809-812, 1973.

Fischer, A.Q., Carpenter, D.W., Hartlage P.L., Carroll and Stephands, S. "Muscle imaging in neuromusclar disease using computerized real-time sonography," *Muscle Nerve*, vol.11, pp. 270-275, 1988.

Foidart, M., Foidart, J.M., and Engel, W.K., "Collagen localization in normal and fibrotic human skeletal muscle," *Arch. Neurol.*, vol. 38, pp. 152-157, 1981.

Fyke, E.F, Greenleaf, J.F. and Johnson, S.A, "Continuous wave measurements of acoustic attenuation in an oil/polymer mixture," *Ultrasound in Med. & Biol.*, vol.5 pp.87-90, 1986.

Garton, G.A., *Physiological Significance of Lipids, Meat Animals, Growth and Productivity,* Plenum Press, New York, 1976.

Goss, S.A., Frizzell, L.A. and Dunn, F., "Ultrasonic absorption and attenuation in mammalian tissues," *Ultrasound in Med. & Biol.*, vol. 5, pp.181-186, 1979.

Goss, S.A., Johnston, R.L., Dunn, F., "Comprehensive compilation of emperical ultrasonic properities of mammalian tissues," *J. Acoust. Soc. Am.*, vol. 64, no. 2, pp. 423-457, 1978.

Goss, S.A., Johnston, R.L., Dunn, F., "Comprehensive compilation of emperical ultrasonic properities of mammalian tissues II,"*J. Acoust. Soc. Am.*, vol. 68, no. 1, pp. 93-108, 1980.

Goss, S.A., O'Brien, Jr., W.D, "Direct ultrasonic velocity measurements of mammalian collagen threads," *J. Acoust. Soc. Am.*, vol. 65, no.2, pp. 507-511, 1979.

Gould, R.P., "Muscle Physiology", In *The Structure and Function of Muscle*, vol.11, Bourne, G.H., Ed., Academic Press, New York, 1973.

Glueck, R.M., Mottley, J.G., Sobel, B.E., Miller, J.G., and Perez, J.E., "Changes in ultrasonic attenuation of the muscle with state of contraction," *Ultrasound in Med. & Biol.*, vol. 11, pp. 605-610, 1985.

Hall, L., "The orgin of ultrasoinc absorption in water," *Phys. Rev.*, vol. 73, pp. 775-781, 1948.

Haney, M.J. and O'Brien, Jr., W.D, "Temperature Dependancy of Ultrasonic Propagation Properites in Biological Material" In *Tissue Characterization with Ultrasound,* vol. I. Greenleaf, J.F. Ed. CRC Press,pp. 15-56, 1986.

Hara, K., Minovra, S., Sakamoto, S., Yamamoto, E., and Motegi, R., "On the precise measurement of ultrasonic velocity by means of a forked shaped reflector," *World Federarion of Ultrasound in Medicine and Biology*, 1979.

Hatta, I., Hasegawa, M., Nakayama, H., and Tamura, "Ultrasonic elastic constants of muscle," *Japan. J. Appl. Phys.*, vol. 23, pp. 66-68, 1984.

Hete, B. and Shung, K.K., "Using RF ultrasound to monitor the progression of myscular dystrophy through passive stretching," *IEEE 1991 Ultrasonics Symposium Proceedings*, pp. 1123-1126, Honolulu, HI., 1991.

Hete, B. and Shung, K.K., "Scattering of Ultrasound of Skeletal Muscle Tissue," *IEEE Transactions on Ultrasonics, Ferroelectrics, and Frequency Control*, vol. 40, no. 4, pp. 354-365, July 1993.

Hete, B. and Shung, K.K., "A study of the relationship between mechanical and ultrasonic properties of dystrophic and normal skeletal muscle", *Ultrasound in Med. & Biol.*, vol.21, no.3, pp. 343-352, 1995.

Heckmatt, J.Z., Leeman, S. and Dubowitz V. "Ultrasound imaging in the diagnosis of disease," *J. Pediat.*, vol. 101, pp. 656-660, 1982.

Hein, I.A., Novakofski, J.A., O'Brien, Jr., W.D, "Ultrasound data acquisition system for collecting high quality RF," *IEEE 1992 Ultrasonics Symposium Proceedings*, pp. 465-469, Tucson, AZ., 1992.

Hicks, J.E., Shawker, T.H., Jones, B.L., Linzer, M.L. and Gerber, "Diagnostic ultrasound: Its use in the evaluation of muscle," *Arch. Phys. Med. Reh.*, vol.65, pp. 129-131, 1984.

Hoffmeister, B.K., Verdonk, E.D., Wickline, S.A. and Miller, J.G., "Effect of collagen on the anisotropy of quasi-longitudinal mode ultrasonic velocity in fibrous soft tissues: A comparison of fixed tendon and fixed myocardium," *J. Acoust. Soc. Am.*, vol. 96, no.4, 1994.

HP8116A Programmable Pulse / Function Generator 50 MHz Operating and Service Manual. Hewlett-Packard GPIB, Federal Republic of Germany, 1984.

Huxley, H.F., "Muscle Structure", In*The Structure and Function of Muscle*, vol. II, Bourne, G.H., Ed. Academic Press, New York, 1973.

Insana, M.F., Hall, T.J., and Fishback, J.L., "Indentifying acoustic scattering sources in normal renal and parenchyma from the anisotropy in acoustic parameters," *Ultrasound in Med. & Biol.*, vol. 17, no. 6, pp. 613-626, 1991.

Johnston, R.L.,Goss, S.A.,Maynard, V., Brady, J.K., Frizzell,L.,O'Brien, Jr., W.D., Dunn, F., "Elements of Tissue Characterization Part I," In *Tissue Characterization II*, NBS Special Publication 525, pp. 19-35, 1979.

Kessler, L.W., O'Brien, Jr., W.D. and Dunn, F. "Ultrasonic absorption in aqueous solutions of polyethlyene glycol," *J. Phys. Chem.*, vol. 74, pp. 4096, 1970.

Kessler, L.W. , "The absorption of ultrasound in aqueous solutions of bovine serum albumin and polyethylene glycol," Ph.D. dissertation, Department of Electrical Engineering, University of Illinois, Urbana-Champaign, 1968.

Kinsler, L.E., Frey, A.R., Coppens, A.B. and Sanders, J.V. *Fundamentals of Acoustics, 3rd Edition*, John Wiley & Sons, 1982.

Lamminen, A., Jaaskelainen, Rapola, J. and Suramo, I. "High frequency ultrasonography of skeletal muscle in children with neuromuscular disease," *J. Ultrasound Med.*, vol. 7, pp. 505-508, 1988.

Levinson, S.F., "Ultrasound propagation in anisotropic sfot tissues: the application of the linear elastic theory," *J. Biomechanics*, vol. 20, No 3,pp. 251-260, 1987.

Ludwig, G.D. and Struthers F.W., *Considerations Ulderlying the Use of Ultrasound to Detect Gall Stones and Foreign Bodies in Tissue*, Nav. Med. Res. Inst., Project NM 004001, Rep. no. 4., 1949.

Madsen, E.L., Zagzebski, J.A., and Frank, G.R., "Oil in gelatin dispersions for use as ultrasonically tissue mimicking materals," *Ultrasound in Med. & Biol.*, vol. 8, no. 3, pp. 277-287, 1982.

Marcus, 1973. See Goss, et al.,1978.

Marioli D., Narduzzi, C., Offelli, C., Petri, D., Sardini, E., and Taroni, A., "Digital time-of-flight for ultrasonic sensors," *IEEE Transactions on Instrumentation and Measurements*, vol. 41. no. 1, February 1992.

Mason, W.P. and Thurston, R.N., *Physical Acoustics*, Volume XVI, Academic Press, 1982.

May, J., "Attenuation of skeletal muscle," M.S. Thesis, Department of Electrical and Computer Engineering, University of Illinois, 1986.

Mc Keith, F. K., De Vol, D.L.,·Miles, R.S., Bechtel, P.J., and Carr, T.R., "Chemical and sensory properities of thirteen major beef muscles," *J. Food Sci.*, vol. 50, pp. 869-872, 1985.

Merchen, N (private communication), June 1995.

Mimbs, J.M., O'Donnell, M., Bauwens, D., Miller,J.G. and Sobel, B.E., "The dependance of the ultrasonic attenuation and backscatter on collagen content in dog and rabbit hearts," *Circ.Res.*, vol. 47, pp. 49-58, 1981.

Millero, F.J. & Kubinski, T. "Speed of sound in seawater and a function of salinity," *J. Acoust. Soc. Am.*, Vol 57, no.2, p. 312, 1975.

Mottley, J.G. and Miller, J.G., "Anisotropy of the ultrasonic attenuation in soft tissues: measurements *in vitro*," *J. Acoust. Soc. Am.*, Vol 88, no. 3, pp. 1203-1210, 1990.

Nassiri, D.K., Nicholas, D., Hill, C.R., "Attenuation of ultrasound in skeletal muscle," *Ultrasonics*, pp. 230-232, 1979.

Nicozsin, D., " An automated imagining data acquisition and analysis system for the scanning laser acoustic microscope," M.S. Thesis, Department of Electrical and Computer Engineering, University of Illinois, 1989.

O'Brien, P, O'Brien, Jr., W.D., Rhyne, T.L., Warltier, D.C. and Sagar, K.B., "Relation of the ultrasonic backscatter and acoustic propagation properities to the myofibrillar length and myocardial thickness," *Circulation*, vol.91., no.1, pp. 171-175, 1995.

O'Brien, Jr., W.D. "Absorption of aqueous solutions of biological polymers," Ph. D. dissertation, Department of Electrical and Computer Engineering, University of Illinois, 1970.

O'Brien, Jr., W.D. and Dunn, F., "Ultrasonic examination of the hemoglobin dissociation process in aqueous solutions of guanidine hydrochloride," *J. Acoust. Soc. Am.*, vol. 50, no. 4, 1971.

O'Donnell, M.O., Mimbs, J.W., and Miller, J.G., "The relationship between collagen and ultrasonic attenuation in myocardial tissue," *J. Acoust. Soc. Am.*, vol. 65, no. 2, pp. 512-517, 1979.

Official Methods of Analysis of the Association of Official Analytical Chemists, pp. 931-937, Helrich, K., Ed., 15th Edition, Association of Official Analytical Chemists, Inc., Arlington, VA., 1990.

Olerud, J.E., O'Brien, Jr., W.D., and Riederer-Henderson, M.A., "Correlation of tissue constitutes with the acoustic properities of skin and wound," *Ultrasound in Med. & Biol.*, vol. 16, pp. 55-64, 1990.

Ophir, J., Cespedes, I., Ponnekanti, H., Yazdi, Y. and Li, X., "A pulsed doppler ultrasoinc system for making non-invasive measuremens of the mechanical properities of soft tissues," *J. Rehab.Res&Dev*, Vol . 24., pp. 1-8, 1987.

Parker, K.J., Tuthill, T.A., and Baggs, R.B., "Ultrasonic attenuation of glycogen: in vitro and in vivo results", *IEEE 1987 Ultrasonics Symposium Proceedings*, pp. 993-996, Denver, CO., 1987.

Parry, R.J and Chivers R.C., "Data of the velocity and attenuation of ultrasound in mammalian tissue-a survey," In *Tissue Characterization II*, NBS Special Publication 525, pp. 343-360, 1979.

Pauly, H. and Schwan, H.P., "Mechanism of Absorption of Ultrasound in Liver Tissue," *J. Acoust. Soc. Am.*, vol. 50, no. 2, pp. 692-699, 1971.

Person, A.M. and Young, R.B., *Muscle and Meat Biochemistry,* Academic Press, Inc., Hartcourt Brace Jovanovich, 1989.

Pinkerton, J.M.M., "The absorption of ultrasonic waves in liquidsand its relation to molecular constituents," *Proc. Phys. Soc.* (London, Sec. B), vol. 62, pp.129-145, 1949.

Press, W.H., Flannery, B.P., Teukolsky, S.A., and Vetterling, W.T., *Numerical Recipies in C,* Cambridge University Press, Cambridge, 1988.

Price, J.F., Schweigert, B.S., *The Science of Meat and Meat Products,* 3rd Ed., FN Press Inc., New York, 1987.

Recchia, D., Hall,C.S., Shepard, R.K., Miller, J.G. and Wickline, S.A., "Mechanisms of the view-dependance of ultrasonic backscatter from normal myocardium," *IEEE Transactions on Ultrasonics, Ferroelectrics, and Frequency Control*, vol. 42, no.1, pp. 91-97, 1995.

Reimers, K., Reimers, C.D., Wagner, S., Paetzke, I., Pongratz, D.E., "Skeletal muscle sonography: a correlative study of echogenicity and morphology," *J. Ultrasound Med.*, vol. 2, pp. 73-77, 1993.

Rich, C., Klinik, E., Smith, R., and Graham, B., "Measurement on bone mass from ultrasound transmission time," *Proc. Soc. Exp. Biol. Med.*, vol. 123, pp. 282-285, 1966.

Riederer-Henderson, M.A., Olerud, J.E., O'Brien, Jr., W.D., Forster, F.K., Steiger, D.L., Ketterer, D.J., Odland, G.F., "Biochemical and acoustic parameters of normal canine skin," *IEEE Trans. Biom. Eng.*, vol. 35, no. 11, pp.967-972, 1988.

Rose, J.H., Kaufmann, M.R., Wickline, S.A., Hall, C.S. and Miller, J.G., "A proposed microscopic elastic wave theory for ultrasonic backscatter from myocardium tissue", *J. Acoust. Soc. Am.*, vol. 97, no. 1, pp. 656-688, 1995.

Rowe, R.W.D., "Collagen fibre arrangement in intramuscular connective tissue. Changes associated with muscle shortening and their possible relevance to raw meat toughness measurements," *J. Food Technol.*, vol.9, pp. 501-508, 1974.

Rowe, R.W.D., "The effect of pre-rigor stretch and contraction on the post rigor geometry of meat samples in relation to meat toughness," In *Meat Science* vol. 1, Applied Science Publishers, Ltd. England, 1977.

Sarvazyan, A., Lyrchikov, A.G., Gorelov, S.E.," Dependance of the ultrasonic velocity in rabbit liver on water content and structure of the tissue," *Ultrasonics*, vol. 25, pp. 244-247, July 1987.

Segal, C. and Greenleaf, J., "Diffraction of ultrasound by soft tissues: The inhomogeneous continious Model," In *Acoustical Imaging*, vol. 13, Pleum Press, New York, 1984.

Smith, N.B. and O'Brien, Jr., W.D., "The Bioacoustics Research Laboratory Ultrasonic Exposimetry System", Beckman Institute for Advanced Science and Technology Technical Report, 1996. (in progress)

Steiger, D.L., "Ultrasonic assessment of skin and wounds with the scanning laser acoustic microscope," M.S. Thesis, Department of Electrical and Computer Engineering, University of Illinois, 1986.

Stryer, L., *Biochemistry,* W. H. Freeman and Company, New York, 1988.

Shore, D., Woods, C.A., and Miles, C.A., "Attenuation of ultrasound in post rigor bovine skeletal muscle," *Ultrasonics*, vol. 24, pp. 81-87, 1986.

Streeter, D.D. and Hanna, W.T., "Enginnering mechanics of successive states in canine left ventricular myocardium.II," *Circularion Research*, vol. 33, pp. 656-644, 1973.

Strom-Jensen, P.R. and Dunn, F., "Ultrasonic absorption by solvent-solute interactions and proton transfer in aqueous solutions of peptides and small proteins," *J. Acoust. Soc. Am.*, vol. 75, no. 3, 1984.

Suzuki, K, Hayashi, N., Sasaki, Y., Kono, M.,Kasahara, A., Fusamoto, H., Imai, Y., Kamada, T., "Dependance of the ultrasonic attenuation of liver on pathologic fat and fibrosis: examination with experimental fatty liver and liver fibrosis models," *Ultrasound in Med & Biol.*, vol. 18, no.8, pp. 657-666, 1992.

Tervola, K.M.U., Grummer M.A., Erdman, Jr., J.M., and O'Brien, Jr., W.D., "Ultrasonic attenuation and velocity at a function of fat concentration; a study at 100 MHz using the scanning lazer atoustic microscope," *J. Acoust. Soc. Am.*, vol. 77, no.1, pp. 307-313, 1985a.

Tervola, K.M.U., Foster, S.G. and W. D. O'Brien, Jr., "Attenuation coefficient measurement technique at 100 MHz with the scanning laser acoustic microscope," *IEEE Trans. Sonics Ultrason.*, vol. 32, pp.259-265, 1985b.

Tervola, K.M.U. and O'Brien, Jr., W. D., "Spatial frequency domain technique: An approach for analyzing the scanning laser acoustic microscope interferogram images," *IEEE Trans. Sonics Ultrason.*, vol. 32, pp. 544-554, 1985c.

Todocman, W., Santosh, K., Carter, J.R., and Haack, E.M., "Tissue characterization of arteries with 4 MHz ultrasound", Ultrasonics, vol. 4., no. 4, pp. 331-338, 1995.

Vander, A.J., Sherman, J.H. and Luciano, D.S., *Human Physiology The Mechanism of Body Function* 6th Ed., Mc Graw-Hill, Inc., New York, 1994.

van der Steen, A.F.W., Thijssen, J.M., van der Laak, J.A.W.M., Ebben, G.P.J., de Wilde, P.C.M., "Correllation of histology and acoustic parameters of liver tissue on a microscopic scale,"*Ultrasound in Med & Biol.*, vol. 20, no. 6, pp. 177-184, 1994.

Verdonk, E.D., Wickline, S.A., and Miller, J.G. "Anisotropy of ultrasonic velocity and elastic properities in normal human myocardium," *J. Acoust. Soc. Am.*, vol. 92, no.6, 1992.

Wang, K., "Sarcomere-associated cytoskeletal lattices in striated muscle." In *Cell and Muscle Motility* , Shay, J.W, Ed., vol.6, Plenum Press, New York, pp.315-369., 1985.

Wear, K.S., Milunski, M.R., Wickline, S.A., Perez, Sobel, B.E. and Miller, J.G., "Contraction-related variation in frequency dependance of acoustic properities of canine myocardium," *J. Acoust. Soc. Am.*, vol. 86, no. 8, pp.2067-2072, 1989.

Wilson L.S., Neale, M.L., Talhami, H.E., and Appleberg, M., "Preliminary results from attenuation-slope mapping of plaque using intervascular ultrasound", *Ultrasound in Med & Biol.*, vol. 20, no. 6, pp. 529-524, 1994.

Woods, C.A., and Miles, C.A., "Ultrasound speed and attenuation in homogenates of bovine skeletal muscle," *Ultrasonics*, vol. 24, 260-267, 1986.

Yao, J., "Ultrasonic propagation properties of skeletal muscle at 100 MHz," M.S. Thesis, Department of Nutritional Science, University of Illinois, 1994.

Zachary, J (private communication), March 1996.

Zeqiri, B, "Reference liquid for ultrasonic attenuation," *Ultrasonics*, vol. 27, p. 314-315, 1989.

VITA

Nadine Barrie Smith was born 21 March 1962, in Chicago, Illinois. From 1980 to 1885 she attended the University of Illinois at Urbana-Champaign and was awarded a Bachelor of Science degree in Engineering-Computer Science and received the Bioengineering Option.

From 1985 to 1987 Ms. Smith was enrolled at the University of Hawaii at Manoa Valley in the Department of Electrical Engineering. In 1987 Ms. Smith returned to the of Illinois at Urbana-Champaign in the Department of Electrical and Computer Engineering in the Bioacoustics Research Laboratory. In 1989 she received a Masters of Science in Electrical and Computer Engineering and produced a thesis entitled "An Automated Ultrasonic Exposure System to Assess the Effects of *In Utero* Diagnostic Ultrasound".

In 1991 Ms. Smith enrolled in the Ph.D. program in Biophysics. Ms. Smith has been hired by as an exposimetry consultant for companies including Mentor H/S, Inc., Arjo Inc. and SWEN Sonic Corp. She has been a teaching assistant for numerous introductory and advanced physiology and Electrical and Computer Engineering courses. She was once voted an excellent teaching assistant and twice voted an outstanding teaching assistant by her physiology students. In 1995 she received the Panhellenic Association of the University of Illinois at Urbana-Champaign Outstanding Staff Member Award. Ms. Smith has performed several oral presentations at IEEE Ultrasonics Symposiums and co-authored several peer-reviewed papers. The most recent paper was "Experimental Verification of the Theoretical *In-Vivo* Ultrasound Heating Using Cobalt Detected Magnetic Resonance" by N.B. Smith, A.G. Webb, D.S. Ellis, L.J. Wilmes and W.D. O'Brien, Jr., in IEEE Transactions on Ultrasonics, Ferroelectrics and Frequency Control, vol. 42, no. 4, July 1995.